Enhanced Performance of Sandwich Structures by Improved Damage Tolerance

Martakos, Georgios

DOI (link to publication from Publisher):
10.5278/vbn.phd.engsci.00168

Publication date:
2016

Document Version
Publisher's PDF, also known as Version of record

ENHANCED PERFORMANCE OF SANDWICH STRUCTURES BY IMPROVED DAMAGE TOLERANCE

BY
GEORGIOS MARTAKOS

DISSERTATION SUBMITTED 2016

AALBORG UNIVERSITY
DENMARK

ENHANCED PERFORMANCE OF SANDWICH STRUCTURES BY IMPROVED DAMAGE TOLERANCE

by

Georgios Martakos

AALBORG UNIVERSITY
DENMARK

Dissertation submitted 2016

.

Dissertation submitted:	December 2016
PhD supervisors:	Prof. Ole Thybo Thomsen University of Southampton, UK and Aalborg University, Denmark
	Associate Prof. Jens Henrik Andreasen Aalborg University, Denmark
PhD committee:	Associate Professor Jørgen Kepler (chairman) Aalborg University, Denmark
	Professor Bent F. Sørensen Technical University of Denmark, Denmark
	Professor Paul Michael Weaver University of Bristol, United Kingdom
PhD Series:	Faculty of Engineering and Science, Aalborg University

ISSN (online): 2246-1248
ISBN (online): 978-87-7112-844-4

Published by:
Aalborg University Press
Skjernvej 4A, 2nd floor
DK – 9220 Aalborg Ø
Phone: +45 99407140
aauf@forlag.aau.dk
forlag.aau.dk

Printed in Denmark by Rosendahls, 2016

ENGLISH SUMMARY

The PhD thesis investigates the enhancement of the damage tolerance of sandwich structures by the embedding of a new type of core inserts that act as face/core interface crack stopping elements. The thesis presents series of experimental investigations where the new crack stopping elements are embedded in both sandwich beam and panel specimens. The experimental observations form the basis for evaluating the efficiency of the proposed crack stopping inserts. For the experiments, Digital Image Correlation (DIC) was used to characterize the measure the local strain fields and overall deformation behaviour around the new crack stopper elements. In support for the experimental investigations, a Finite Element (FE) analysis based methodology, including fracture mechanics analysis and the so-called 'cycle jump' technique, was developed to predict the progression of damage in sandwich specimens with embedded crack stoppers.

The starting point for the research was is a new design for a crack stopper, referred to as a 'peel stopper', which is proposed for foam cored sandwich structures. Initially, the ability of the peel stopper to prolong the fatigue life of sandwich structures has been demonstrated through a series of three-point bending tests. During testing an initial crack front in the sandwich beams was arrested for a limited amount of cycles until a new crack initiated in the vicinity of the peel stopper. Subsequently, the study concentrated on investigating the main parameters that govern the performance of the proposed peel stopper, i.e. the crack deflection and crack arrest capability. The ability of the peel stopper to deflect a propagating face-sheet/core interface crack was investigated through a series of sandwich beam tests. Different configurations of the peel stopper were tested and the conditions for crack deflection for all configurations were identified by application of a fracture mechanics crack kinking criterion. From this research, the most promising peel stopper configurations were identified. Following this the crack arrest capacity of the peel stopper was investigated. Through the use of strain field measurements on the surface of sandwich beams with embedded peel stoppers using Digital Image Analysis (DIC), it was shown that the ability of the peel stopper to contain an arrested crack, or to prevent re-initiation of new cracks, is related to the inducement of strain concentrations in the foam core material on the back side of the peel stopper. By use of the developed numerical fracture mechanics based modelling tools, both fatigue crack growth and crack arrest in the specimens were simulated. It was shown that the strains responsible for crack re-initiation can be accurately calculated enabling the prediction of the fatigue life of the specimens.

To demonstrate the beneficial overall effect on the damage tolerance of realistic sandwich structures, the peel stoppers were also embedded in sandwich plates (or panels). It was shown that peel stoppers in all cases were capable of effectively capturing and containing a propagating interface debond crack. The lateral

displacements of the debonded face-sheet were measured using DIC and used to identify the crack tip location inside the sandwich panel specimens. To support and further explain the experimental findings, a three-dimensional FE model was developed and used to simulate the behaviour of the debonded sandwich panel specimens. The FE model was able to predict both the fatigue crack growth and crack arrest behaviour accurately. Due to time constraints, the sandwich panel fatigue experiments were only conducted up to about 200,000 load cycles, and to assess the effect of high cycle fatigue damage propagation was simulated up to about 2,000,000 load cycles. It was demonstrated that the developed computational methodology is capable of modelling the fatigue behaviour of sandwich structures with embedded peel stoppers, and that the overall enhancement of the damage tolerance can be predicted accurately.

DANSK RESUME

Ph.d.-afhandlingen undersøger forbedring af skadestolerancen i sandwichkonstruktioner ved indlejring af en ny type af indsatser, der fungerer som revnestopperelementer for revner mellem kernemateriale og dæklag. Afhandlingen præsenterer en række eksperimentelle undersøgelser, hvor den nye revnestoppers er indlejret i både sandwichbjælker og paneler. De eksperimentelle observationer danner grundlag for at vurdere effektiviteten af den foreslåede revnestopper konstruktion. Til eksperimenterne anvendtes Digital Image Correlation (DIC), til at karakterisere og måle de lokale tøjningsfelter og deformationer omkring den nye revnestopperkonstruktion. Til at understøtte de eksperimentelle undersøgelser er en Finite Element (FE) analyse anvendt, herunder brudmekanisk analyse og den såkaldte "cycle jump"-teknik, er blevet udviklet til at forudsige udviklingen af skader i sandwich emner med indlejrede revnestoppere.

Udgangspunktet for forskningen var et nyt design til en revnestopper, kaldet en "peel stopper", som er foreslået for skumkernen i sandwichkonstruktioner. I første omgang er konstruktionens evne til at bremse delaminsringsrevner , ved at forlænge levetiden af sandwichstruktur blevet påvist gennem en række tre-punkts bøjetest. Under testen er en startrevne i sandwich bjælken blev standset for et antal cykler indtil en ny revne starter i nærheden af peel stopperen. Efterfølgende undersøgelser koncentreredes om at undersøge de vigtigste parametre, der styrer effekten af den foreslåede peel stopper, dvs. revnens afbøjning og evnen til at stoppe revnen. Peel stopperens evne til at afbøje en revne mellem kerne og dæklag blev undersøgt vha. en række sandwich bjælke test. Forskellige konfigurationer af peel stoppere blev testet, og betingelserne for revne afbøjning for alle konfigurationer blev identificeret ved anvendelse af et brudmekanisk revneafbøjningskriterium. Fra denne undersøgelse, blev de mest lovende peel stopper konfigurationer udvalgt. Efter dette blev peel stopperens evne til at stoppe revner undersøgt. Gennem brug af feltmålinger på overfladen af sandwich bjælker med indlejrede peel stopper ved brug af Digital Image Analysis (DIC), blev det vist, at peel stopperens evne til at fastholde en standset revne, eller til at forhindre re-initiering af nye revner , er relateret til tøjningskoncentrationer i kernematerialet på bagsiden af peel stopperen. Ved brug af de udviklede numeriske brudmekanisk baserede modelleringsværktøjer, blev både udmattelsesrevnevækst og revne standsning i prøverne simuleret. Det blev vist, at tøjningerne er ansvarlige for start af en ny revne, kan beregnes nøjagtigt og muliggør forudsigelse af prøvernes levetid.

For at demonstrere gavnlige effekt på skader i realistiske sandwichkonstruktioner blev peel stoppere også inkorporeret i sandwich plader (eller paneler). Det blev vist, at peel stoppere i alle tilfælde var i stand til effektivt at indfange og fastholde en revne. De laterale forskydninger af dæklagene blev målt ved brug af DIC og anvendt til at identificere positionen af revnespidsen i sandwichpanelprøverne. For at

understøtte og yderligere at forklare de eksperimentelle resultater blev en tredimensionel FE-model udviklet og anvendt til at simulere opførslen af sandwich panelprøverne. FE-modellen var i stand til at forudsige både udmattelsesrevnevækst og revnefastholdelse præcist. På grund af tidspres blev sandwich paneler kun udmattet op til omkring 200.000 lastcykler, og for at vurdere effekten af et højere antal cykler blev der simuleret op til omkring 2.000.000 belastningscykler. Det blev påvist, at den udviklede beregningsmæssige metode er i stand til at modellere udmattelse af sandwich strukturer med indlejrede peel stoppere, og at den samlede forbedring af skadestolerancen kan forudsiges nøjagtigt.

ACKNOWLEDGEMENTS

The work was sponsored by the Danish Council for Independent Research | Technology & Production Sciences (FTP) under the research grant “Enhanced Performance of Sandwich Structures by Improved Damage Tolerance" (SANTOL) (Grant 10082020).
The work has been conducted in collaboration with the Technical University of Denmark, Aalborg University, Denmark, the University of Southampton, UK, and was co-sponsored by Siemens Wind Power A/S, Denmark, and LM Wind Power Blades A/S, Denmark.

I would like to say thank you to

- DIAB A/S for providing Divinycell H100 material used in this study for free.
- Siemens Wind Power A/S for providing help with fabrication of sandwich beam and panel specimens used in this study.
- The department of Mechanical and Manufacturing Engineering, Aalborg University, Denmark.
- The department of Mechanical Engineering, Technical University of Denmark, Denmark
- The Faculty of Engineering and the Environment, University of Southampton, Highfield, Southampton, UK.

I would also like to thank,

Dr. Wei Wang for the excellent collaboration while working together in Southampton University, UK for the needs of the first published paper of this work.
Professor Janice M. Dulieu-Barton for co-supervising my research activities during my visit in Southampton University, UK and writing of the first paper of this study. I would also like to thank Janice for providing valuable feedback during the full course of this PhD study.
Associate Professor Christian Berggreen for co-supervision of my research activities during my 4-month stay in the Technical University of Denmark (DTU). Christian provided some excellent feedback and direction for this PhD study while assisting in the realization of three of published papers of this study.

My Supervisors:

Associate Professor Jens Hendrik Andreasen

Professor Ole Thybo Thomsen

TABLE OF CONTENTS

Chapter 1. Introduction 1
1.1. Background and Motivation 1
1.1.1. Sandwich Structures 1
1.1.2. Failure modes 3
1.1.3. Damage tolerant design 5
1.2. Aims and objectives 5
1.3. Novelty 6
1.4. Thesis content and structure 7
1.5. Division of work 8
Chapter 2. State of the Art 11
2.1. Fracture mechanics 11
2.2. Experimental characterisation of interface fracture 11
2.3. Finite element Analysis of INterface fracture 12
2.4. Fatigue models 13
2.5. Damage tolerance and crack arrester concepts 14
Chapter 3. Peel stopper device 17
3.1. Peel stopper in beam specimens 17
3.2. Peel stopper in panel specimens 19
3.3. Peel Stopper Fabrication 20
3.4. Fabrication of sandwich specimens WITH embedded peel stoppers 22
Chapter 4. Three-point bending tests 24
4.1. Test configuration 24
4.2. Results 26
4.3. Conclusions 28
Chapter 5. Mixed Mode Bending Test for Crack Deflection analysis of an interface crack approaching a tri-material junction (Paper #1) 30
5.1. Test configuration 31
5.2. Finite Element model 32
5.3. Results 33

5.4. Peel stopper angle effect the ability to generate crack deflection 34
5.5. Discussion and conclusions..... 38
Chapter 6. Sandwich Tear Test – Fatigue Loading (Papers #2 and #3).....39
6.1. Fatigue testing configuration ([54]) 39
6.2. Experimental results ([54]) 42
6.3. Finite Element modelling ([55])..... 46
6.4. Finite Element results ([55]) 47
6.5. Energy release rate and mode-mixity ([55])..... 47
6.6. Strain calculation ([55]) 49
6.7. Conclusions..... 51
Chapter 7. Panel Testing (Paper #4).....53
7.1. Test configuration ([56])..... 53
7.2. Test Results..... 55
7.3. Finite element analyses ([56])..... 57
7.4. Finite element results [56]..... 59
7.5. Conclusions..... 62
Chapter 8. Conclusions.....63
8.1. Novel peel stopper – implementation and validation 63
8.2. Development of experimental and numerical procedures 64
8.3. Novelty claims 66
Chapter 9. Future Work.....67
Chapter 10. REFERENCES.....69
Chapter 11. Paper #1 77
Chapter 12. Paper #2 97
Chapter 13. Paper #3 123
Chapter 14. Paper #4 145

CHAPTER 1. INTRODUCTION

1.1. BACKGROUND AND MOTIVATION

1.1.1. SANDWICH STRUCTURES

Throughout the 20th and 21st century, sandwich structures have received increasing attention because of their excellent structural properties that pioneer the lightweight construction design. Sandwich structures owe their exceptional structural performance to the "I-Beam" effect that is generated using two thin layers of a stiff and strong material (face-sheets) separated and bonded together by a light and compliant material (core), Figure 1. In this structural element, referred to as a structural sandwich or just a sandwich structure, the two face-sheets are for transferring the bending loads (through in-plane tension, compression and shear stresses in the face-sheets), while the core is carrying the transverse shear forces (though thickness shear stresses in the core),

Figure 2. The main advantage of structural sandwiches over other structural members such as conventional monolithic beams, plates or shells, as the combination of very high bending stiffness and strength with low weight (mass). This has been the main driver behind first research studies published in the nineteen forties and fifties conducted by the researchers such as Hoff et al. [1, 2], Ericksen [3], Youngquist et al. [4], Norris et al. [5], Raville [6], and Lewis [7] who investigated the behaviour of sandwich panels and beams under compression, tension, bending and shear loads. As a result a wide array of different sandwich configurations and constituent materials were investigated. Thin metal sheets of steel or aluminum and composite laminates were found to excellent candidate materials for the face-sheets due to their very high stiffness and strength properties. Honeycomb type materials, balsa wood and cellular cell plastics (foams) were introduced as core materials due to their relatively high out-of-place stiffness and low mass density.

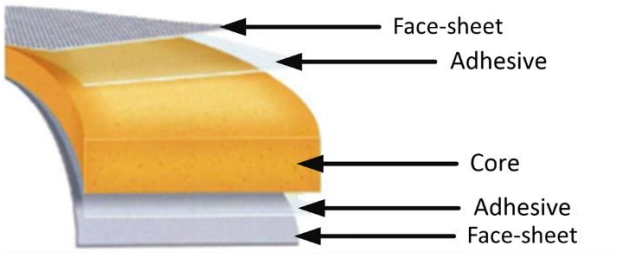

Figure 1.Typical sandwich structure constituents and lay-out.

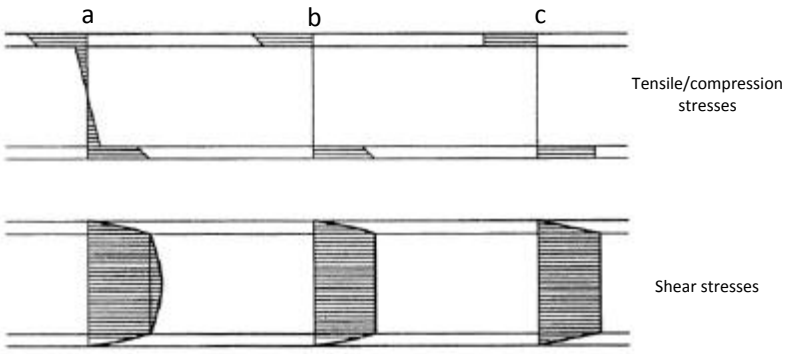

Figure 2. Sandwich structures stress caring capabilities. Levels of approximation: a) None, b) $E_c << E_f$, c) $E_c << E_f$ and $t_c >> t_{f,}$ from Zenkert [8]

The wide range of material options that can combined to achieve lightweight sandwich structures with excellent structural properties, and which allows adaptation for the requirements and environments of different applications, has led to wide spread and ever increasing use of sandwich structures in multiple industries including the maritime/ship (including naval), aeropace, rail, automotive and wind turbine industries, Figure 3. The extensive industrial application of sandwich structures fuels a growing need to understand and categorize the various failure mechanisms encountered during service.

Figure 3. Sandwich structures industries implementation

1.1.2. FAILURE MODES

Due to their layered nature sandwich structures can experience a variety of different failure modes of which some are unique in that are unique to sandwich structures not encountered in more commonly used structural elements. The stiffness and thermal mismatch between the face-sheets and core material can lead to local stress states that in some cases can lead to damaging and premature failure. Further, the bonding of the face-sheets to the core material is crucial for the structural integrity of the sandwich, and this may be compromised due to the complexity of the manufacturing process. In the case where composite materials are used as face-sheets, their layered nature where plies are separated by weak interfaces in some cases may lead to separation of the layers also known as delamination. Also, sandwich structures are sensitive to localized damage in one or more of their constituents as well as the interfaces between the face-sheets and the core, and this may lead to initiation of damage and eventually loss of structural integrity. If the face-sheets, core or the interfaces are experiencing damage, this will lead to a redistribution of the stresses in the face-sheet non-damaged parts of the structural sandwich assembly. This can result in overloading of the remaining intact structure which can lead to its collapse. Zenkert [8] provides and overview of the most commonly encountered failure mechanisms in sandwich structures, and some of these are shown in Figure 4a to 4e.

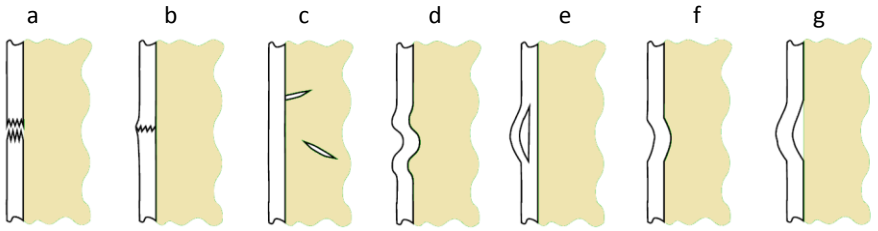

Figure 4. Sketch of failure mechanisms associated with a "simple" sandwich element [8]; a) face-sheetface-sheet tension failure, b) face-sheet compression failure, c) core shear failure, d) local wrinkling instability, e) interlaminar or delamination failure, f) indentation, g) face/core debonding (interface delamination).

Face-sheet tension and compression failure can occur as a result of in-plane tension and compression loads or due to bending loads in the sandwich structure, Fig. 4a-b. Core failure can be observed as a result of shear loads usually in the bulk of the core material, Fig. 4c. Moreover tension and compression loads could create fracture in the core close to the interface with the face-sheet which then could propagate, either in the interface or in the bulk of the core material. In cases where thin face-sheets are utilized, local instability referred to as face-sheet wrinkling can occur due to high in-plane compressive or bending loads, Fig. 4d. as a form of unstable local buckling deformation. This type of instability is strongly promoted by imperfections as e.g. waviness/wrinkles created during the manufacturing process. Interlaminar failure, Fig. 4e may occur when composite face-sheets are used and subjected to various loading condition such as compressive, out-of-plane shear or localized impact loads. In this failure mode, interlaminar peeling and shear stresses may be introduced either due to local buckling (buckling drive delamination) or impact loading that can lead to separation of the plies of the composite face-sheet. Indentation failure, Fig. 4f is usually the result of localized loads like impact loading on the face-sheet. It is most frequently observed in sandwich structures with relatively soft core materials. Finally, face/core debonding (or interface delamination), Fig 4g, may occur under similar conditions at face-sheet delamination shown in Fig. 4e. Face/core debonding could be a result of damage propagation in the core material after core failure has occurred. Face/core debonding could also be a result of the manufacturing process of sandwich structures due to poor impregnation/wetting of the face/core interfaces with resin/adhesive or the face-sheet matrix material.

Face/core debonding driven by out-of-plane loading, i.e. bending and transverse loading, will be the main failure mechanism studied and investigated in this thesis. That is because face/core debonding is one of the most commonly encountered failure modes and probably the most dangerous in sandwich structures. Since face/core debonds or delaminations can be introduced during manufacturing (manufacturing defects), the separated or debonded zones become inherent structural weaknesses of composite sandwich structures. Such debonds may expand progressively under the action of external loading (quasi-static or fatigue), and may

lead to a global failure of the component/structure that may occur with little or no prior warning. The inherent sensitivity of sandwich structures to interface debonds leads to design solutions where large safety factors are used in design to account for the presence of damage. This leads to overdesigned structures that are often heavier and costlier than needed.

1.1.3. DAMAGE TOLERANT DESIGN

Damage tolerance is the ability of a structure to function as intended by its design while containing damage. Damage in a structure or structural assembly will nearly always affect its performance, and in some cases an acceptable degree of performance drop can be set by design [9]. The damage tolerant design approach considers damage present in the structure and focuses on characterizing damage development in the structure considering all the implications to the structural performance. Despite their sensitivity to initiation of damage, composite sandwich structures can display significant resistance to damage development and growth. For the case of face/core debonding it is often the case that progression debond damage may arrest under normal operating conditions. However, understanding and enhancing the damage tolerance of sandwich structures during the design process can lead to lighter, more reliable and also cheaper design solutions by avoiding excess use of material.

1.2. AIMS AND OBJECTIVES

The aim of this work is to introduce and develop a new type of sandwich core insert that enables suppression or delaying of face/core interface crack propagation and improves the damage tolerance of sandwich structures. This sandwich core insert will also be referred to as a ‘crack arrester’ or ‘peel stopper’ in the forthcoming. The research conducted targets the evaluation of the crack arrester with regards to its ability to confine and arrest a propagating crack under fatigue loads. The work comprises both experimental and numerical/computational work parts that complement each other. The overarching goal is to demonstrate the ability of the new core insert, the peel stopper, to confine and arrest a propagating face/core crack, and also to develop finite element (FE) analysis based numerical tools that can predict this behaviour.

With respect to the experimental part, the core insert is implemented in both sandwich beam and panel (plate) specimens. For sandwich beams the objective is to gain a better understanding of the effect of the crack arrester on the propagating interface crack and the fundamental mechanics that influence the crack arrest behaviour. The use of sandwich beams offers the advantage that the position of the interface crack front can easily be located, and quantities such as crack length and crack growth rate can easily be extracted from the experiments. The tests conducted

on sandwich panels are included in the investigation to demonstrate the capability of the crack arrester to confine and arrest propagating face/core interface cracks in a more realistic setting, and by this to demonstrate the potential for improving the damage tolerance of sandwich structures by implementing embedded crack arresters as proposed.

The numerical/computational part of the work is validated by the experiments, and it is used to predict the behaviour of sandwich specimens with embedded crack arresters. The aim is to develop and validate finite element based numerical tools that can be used in the design of sandwich structures to predict the influence of embedded crack arresters on the damage tolerance. The modelling framework is based on the assumptions of linear elastic material behaviour, small displacements and rotations (geometric linearity), and that linear elastic fracture mechanics (LEFM) can be used to describe the fundamental crack load quantities (Energy release rate and Mode-mixity angle) during the crack propagation process when the sandwich element is subjected to fatigue loading. A linear relationship will be assumed between the logarithm of the crack growth rate and the Energy release rate (i.e. a Paris' Law like relation), and this is used to model the interface crack propagation.

1.3. NOVELTY

The novelty of the conducted research resides in both the design of the proposed crack arrester concept and the methodology/ tools developed and used to evaluate the effect on the performance of sandwich structures. As will be shown in the forthcoming chapter state of the arts, the research conducted builds upon and fill in the gaps of recent research in the field of damage tolerance enhancement in sandwich structures. Moreover, state of the art interface fracture mechanics based computational methodologies in this research are being expanded to account for face/core debond kinking and propagation of the crack in a differently oriented plane.

The novelty of the presented study can be summarized by the following points:

- A new peel (crack) stopper has been developed. It is manufactured as a hybrid material of comprising polyurethane polymer resin that is reinforced with glass fibres, which in combination with its geometrical shape provides improved crack deflection and fracture toughness properties in comparison with previously proposed designs. Furthermore, the new peel stopper is of much lower weight than previous designs, thus reducing the weight penalty on the sandwich component.
- It has been demonstrated that the new peel stopper is capable of deflecting and arresting propagating face/core interface cracks under a variety of mode mixities, covering the range from Mode I to Mode II dominated

loading conditions at the crack tip. Also, the new peel stopper has been shown to be equally efficient for sandwich structures subjected to quasi-static as well as fatigue loading conditions.

- The conducted experimental investigations utilize full field measurements, through Digital Image Correlation (DIC), to characterize both crack propagation and crack re-initiation. This has enabled quantification of the strain field in the vicinity of the propagating crack tip as well as the crack stopper device. In particular, the strain states at the tip of the arrested crack, as well as in the vicinity of the crack stopper device, has provided the means to develop a thorough understanding of the post arrest behaviour as well as the efficiency of the crack stopper.
- The new peel stopper has been implemented and validated also in and validated for realistic sandwich structures in the form of sandwich panels (as opposed to sandwich beams) subjected to fatigue loading conditions.
- In support of the experimental findings, and to develop a thorough theoretical understanding as well as a computational engineering design tool, a predictive finite element methodology, based on interface fracture mechanics and the so-called 'cycle jump' technique has been developed. The methodology enables quantitative analysis of the conditions under which interface crack propagation and crack deflection occur, it can predict the fatigue life, and it can also predict under which conditions reinitiation of a new crack will occur.

1.4. THESIS CONTENT AND STRUCTURE

The PhD thesis is based on 4 scientific papers published or for publication in peer reviewed international journals. The main part of the thesis presents a summary of the research conducted and published in the 4 papers that are appended as Annexes.

The (summary) thesis comprises the following: Chapter 1 – introduction (background and motivation, aims and objectives, novelty statement, and division of work for co-authred papers); Chapter 2 – State of the art; Chapters 3 and 4 – present the information about the proposed peel stopper concept, and unpublished preliminary results addressing implementation and testing of sandwich beams with embedded peel stoppers; Chapter 5 – includes a summary of results obtained for sandwich beams with embedded peel stoppers subjected to the Mixed Mode Bending (MMB) and published in appended Paper #1; Chapter 6 – presents experimental and numerical results obtained for sandwich beam specimens with embedded peel stoppers and loaded in the so-called Sandwich Tear Test (STT) and published in appended papers Paper #2 and Paper #3; Chapter 7 – presents the experimental and numerical results obtained for sandwich panel specimens subjected to fatigue loading and published in appended Paper #4; Chapter 8 –

presents the conclusions referring to the stated aims and objectives; Chapter 9 – presents an overview of suggested future research.

The 4 journal papers published through this work are:

Paper #1

Wang. W, Martakos, G., Dulieu-Barton, J.M., Andreasen, J.H. and Thomsen, O.T., "Fracture Behaviour at tri-material junctions of crack stoppers in sandwich structures". *Composite Structures*, 133, 2015, 818-833. http://dx.doi.org/10.1016/j.compstruct.2015.07.060

Paper #2

Martakos, G., Andreasen, J.H, Berggreen, C. and Thomsen, O.T., "Experimental Investigation of Interfacial Crack Arrest in Sandwich Beams Subjected to Fatigue Loading using a Novel Crack Arresting Device". *Journal of Sandwich Structures and Materials*, accepted for publication.

Paper #3

Martakos, G., Andreasen, J.H, Berggreen, C. and Thomsen, O.T., "Interfacial Crack Arrest in Sandwich Beams Subjected to Fatigue Loading using a Novel Crack Arresting Device – Numerical modelling". *Journal of Sandwich Structures and Materials*, accepted for publication.

Paper #4

Martakos. G., Andreasen, J.H, Berggreen, C. and Thomsen, O.T., "Interfacial Crack Arrest in Sandwich Panels with Embedded Crack Stoppers Subjected to Fatigue Loading". *Applied Composite Materials*, accepted for publication. DOI: 10.1007/s10443-016-9514-3

1.5. DIVISION OF WORK

The division of work between the co-authors of the appended papers, which form the basis for this thesis, is presented below:

Paper #1

Wang, W.: 40 % of total work. The author contributed during the scoping and concept phase for the paper. He was responsible for choosing and applying all the experimental techniques as well as post processing of the captured images used for the study in the paper. Further, he was responsible for conducting the experimental tests documented in the paper. Finally, he was the lead for the writing of the paper.
Martakos, G.: 35 % of total work. The author contributed during the scoping and concept phase for the paper. He was responsible for the original ideas fir the

proposed peel stoppers, and he was responsible for their manufacturing. He was further responsible for choosing and developing all the numerical tools used for the work presented in the paper. Finally, he was responsible for reaching the conclusions made from the numerical part of the work. Finally he contributed to the writing of the paper.

Dulieu-Barton, J.M.: 10 % of total work. The author had the role of supervisor and provided guidance and support with regards to the experimental techniques used in the paper. She contributed significantly to the writing of the paper.

Andreasen, J.H.: 5 % of total work. The author had the role of supervisor and provided guidance and support with regards to the fracture mechanic analyses conducted. He contributed to the editing of the paper.

Thomsen, O.T.: 10 % of total work. The author had the role of supervisor and provided guidance and support with regards to the stress analysis conducted in the paper. He contributed significantly to the writing of the paper.

Paper #2

Martakos, G.: 80 % of total work. The author was the lead for the scoping and concept phase for the paper. He was responsible for choosing and applying all the experimental techniques as well as post processing of the captured data. Further, he was responsible for conducting all the experimental work documented in the paper. Finally, he had the lead role in the writing of the paper.

Andreasen, J.H.: 5 % of total work. The author had the role of supervisor and provided guidance and support with regards to the fracture mechanic analyses conducted in the paper. He contributed to the editing of the paper.

Berggreen, C.: 5 % of total work. The author contributed during the scoping and concept phase of the paper. He provided guidance and support with regards to the sandwich structure testing set-up presented in the paper. He contributed to the editing of the paper.

Thomsen, O.T.: 10 % of total work. The author had the role of supervisor and provided guidance and support with regards to the mechanics and analysis of sandwich structures. He contributed significantly to the writing of the paper, and provided key input to the final presentation and narrative.

Paper #3

Martakos, G.: 80 % of total work. The author was the lead for the scoping and concept phase for the paper. He was responsible for choosing and developing all the numerical tools presented. He was responsible for reaching the conclusions drawn from the numerical part of the work. Finally, he had the lead role in the writing of the paper.

Andreasen, J.H.: 5 % of total work. The author had the role of supervisor and provided guidance and support with regards to the fracture mechanic analyses conducted in the paper. He contributed to the editing of the paper.

Berggreen, C.: 5 % of total work.
The author contributed during the scoping and concept phase of the paper. He provided guidance and support with regards to the sandwich structure testing set-up presented in the paper. He contributed to the editing of the paper.
Thomsen, O.T.: 10 % of total work.
The author had the role of supervisor and provided guidance and support with regards to the mechanics and analysis of sandwich structures. He contributed significantly to the writing of the paper, and provided key input to the final presentation and narrative.

Paper #4

Martakos, G.: 80 % of total work.
The author was the lead for the scoping and concept phase for the paper. He was responsible for choosing and developing all the experimental techniques and numerical tools used for conducting the research. He was responsible for reaching the conclusions drawn from experimental observations and numerical analyses. Finally, he had the lead role in the writing of the paper.
Andreasen, J.H.: 5 % of total work. The author had the role of supervisor and provided guidance and support with regards to the fracture mechanic analyses conducted in the paper. He contributed to the editing of the paper.
Berggreen, C.: 5 % of total work. The author contributed during the scoping and concept phase of the paper. He provided guidance and support with regards to the sandwich structure testing set-up presented in the paper. He contributed to the editing of the paper.
Thomsen, O.T.: 10 % of total work.
The author had the role of supervisor and provided guidance and support with regards to the mechanics and analysis of sandwich structures. He contributed significantly to the writing of the paper, and provided key input to the final presentation and narrative.

CHAPTER 2. STATE OF THE ART

2.1. FRACTURE MECHANICS

Several parameters that characterize crack growth like the stability of the crack growth or the angle of crack propagation inside a sandwich structure greatly depend on the material configuration and the imposed loading conditions. Identifying the rules that govern crack propagation is a complex task due to the highly anisotropic behaviour of composite sandwich structures. Originally a crack loaded under mixed mode conditions will tend to kink in the direction where it is loaded under pure mode I. However, for the case of a crack that is positioned between two dissimilar materials, the interface fracture resistance of their interface could be weaker than those of the individual materials. Then the crack will continue growing in that interface under mixed mode conditions without kinking. Debonds between the face-sheet and core material of sandwich structures can be considered such cracks, usually referred to as bi-material or interfacial cracks. Several studies have addressed the bi-material crack propagation and characterization problems. The earlier works of Erdogan [10] and Dundur [11] provided the theoretical background for examining crack behaviour in dissimilar materials. Later, Hutchinson and Suo [12], He and Hutchinson [13], Suo [14], and Wang [15] described the conditions for crack propagation and kinking of an interface crack for isotropic and orthotropic material constituents. Suos formulation [14] used in this Thesis to describe the behaviour of interfacial cracks is given in APPENDIX-A.

2.2. EXPERIMENTAL CHARACTERISATION OF INTERFACE FRACTURE

New testing methods have been developed to characterize interface cracks in sandwich structures. The sandwich Single Cantilever Beam test (SCB), Cantwell et. al. [16-17], and the Double Cantilever Beam (DCB), Prasad and Carlsson [18-19], was developed to apply pure mode I crack loading conditions in sandwich beam specimens. The Cracked Sandwich Beam test (CSB) by Carlsson et. al. [20] was used to apply a pure mode II loading scheme. Several tests have been developed to apply a mixed mode loading to the cracks in sandwich beams. The Mixed Mode Bending test (MMB), Quispitupa et. al. [21-22], the modified Tilted Sandwich Debond test (TSD), Berggreen et.al. [23], and also the sandwich DCB loaded by uneven moments (DCB-UBM), Lundsgaard-Larsen et. al. [24], were used to apply different loading conditions to cracked sandwich beams. From the mentioned tests the MMB and DCB-UBM set-ups are special in regards to that the mode-mixity is independent of the crack length and remains constant as the crack propagates. However, for fatigue characterization purposes the DCB-UBM is not ideal since it requires very long specimens and the use of a long pretension cable to apply the loads. The relatively limited size of the MMB test, and the fact that the mode-mixity

applied can be constant and independent of the crack length, is making this test well suited for fatigue crack growth characterization. Figure 5 shows the boundary conditions of some of the most important test set-ups used for the experimental characterization of fracture processes in sandwich.

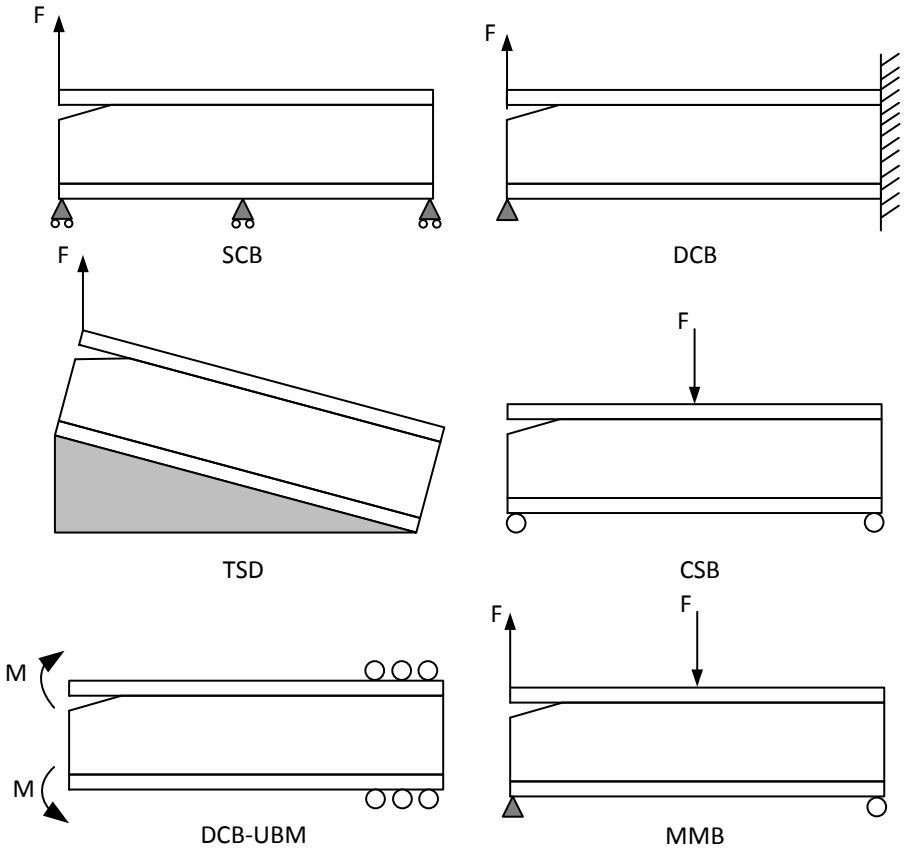

Figure 5. Cracked sandwich specimens test set-ups. Single Cantilever Beam test (SCB), Double Cantilever Beam test (DCB), Tilted Sandwich Debond test (TSD), Cracked Sandwich Beam test (CSB), Double Cantilever Beam Uneven Bending Moment test (DCB-UBM), Mixed Mode Bending test (MMB).

2.3. FINITE ELEMENT ANALYSIS OF INTERFACE FRACTURE

Within the framework of the Finite Element Method several techniques have been developed to determine the energy release rate and the mode-mixity of a crack tip. Several commercially available FEM packages include internal routines that are

used to implement the different techniques. Berggreen [25] gave a comprehensive summary of the most commonly used methods that are adopted and utilized within the FEM frame work. The most important ones are the J-Integral method introduced by Rice [26], the Virtual Crack Extension method (VCE), Matos [27], the Virtual Crack Closing Technique (VCCT), Rybicki and Krueger [28-29], the Crack Surface Displacement method (CSD) by Smelser [30], and the Crack Surface Displacement Extrapolation method (CSDE) introduced by Berggreen and Jolma [31-32]. From these methods only the CSDE method was used in this study.

The Crack Surface Displacement Exrapolation CSDE method is taking the node displacement output from the Finite Element Analysis solution and applies it to Suo's formulation [14] as presented in equations (1)-(7), of APPENDIX-A, to calculate the energy release rate and mode-mixity. The principle of the method is shown in Figure 6. In Suo's formulation an oscillation zone can be identified in the solution as an artifact induced by the bi-material oscillation index. The CSDE method is utilized as shown in Figure 6 (b) to avoid the numerical oscillation zone appearing very close to the crack tip. The method calculates the energy release rate and mode-mixity over a region of the crack surface and identifies the sub-region where the oscillation is not affecting the results. Then by using an outer and inner limit value of the quantities identified by an algorithm (see Figure 6 (b)) the technique uses linear extrapolation to calculate the values at the crack tip.

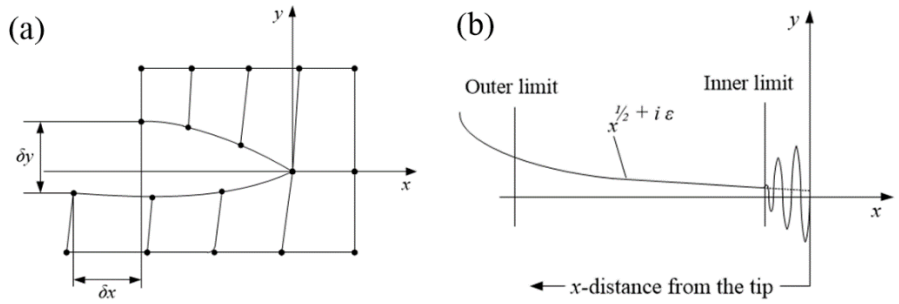

Figure 6. (a) Displacement extraction from the local coordinate system in FE and (b) Schematic representation of CSDE method.

2.4. FATIGUE MODELS

Crack propagation under fatigue loads is usually described by the relation between crack growth rate, da/dN, and the stress intensity factor range ΔK=K_max-K_min. This relation can also be transformed to use the energy release rate range ΔG instead of the stress intensity factor range. In many cases the energy release rate can easily be determined by using analytic closed form solutions for many fatigue characterization test configurations. The linear relation of the log-values of crack growth rate and the energy release rate can be expressed by a power law, as expressed by Paris [33]:

$$\frac{da}{dN} = m\,\Delta G^c \tag{2.1}$$

where m is the slope and c is the crack growth rate for $\Delta G = 1$.

To simulate fatigue crack growth Moslemian [34] introduced the cycle jump technique in combination with the CSDE method. As its name suggests the technique is used to reduce the number of simulated cycles in a fatigue crack propagation analysis by "jumping" cycles. After simulating at least three consecutive loading cycles of crack propagation, crack growth in the subsequent cycles can be calculated (estimated) by linear extrapolation without running the respective iteration of calculations, Figure 7. This allows for saving time when simulating long fatigue experiments with many loading cycles. Moslemian [35] also studied the sensitivity of the method to the "jump distance" showing that up to 90% of the calculations during a fatigue analysis could be avoided without significant sacrifice of the accuracy. The recommendations regarding the choice of "jump distance" from [35] were used in this study.

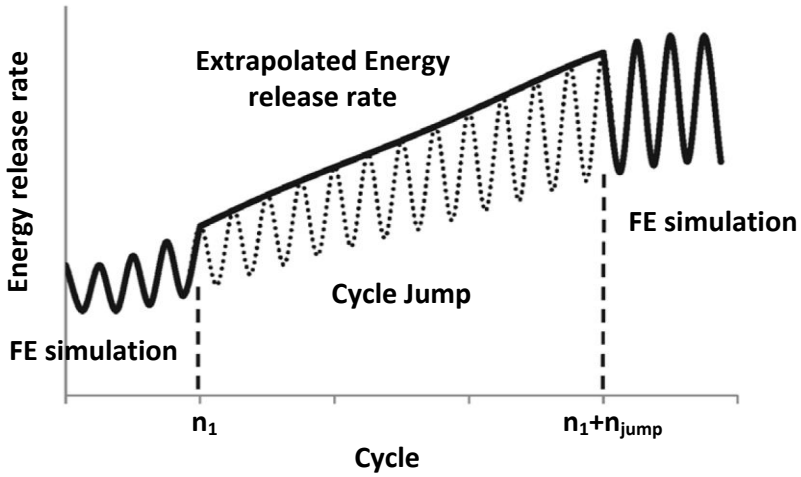

Figure 7. Schematic of Cycle jump technique method on energy release rate calculation, from Moslemian [34-35].

2.5. DAMAGE TOLERANCE AND CRACK ARRESTER CONCEPTS

Considerable efforts have been directed towards predicting and controlling the propagation of debonds in sandwich structures. Using both experimental and numerical means several approaches of damage tolerance were proposed, tested and evaluated. The need to develop propagation models under mixed-mode conditions was addressed in [36-38]. An approach for achieving enhanced damage tolerance has been suggested that encourages nonlinear behaviour by developing large-scale

fibre bridging, and also stitching of the face sheet layers was used as a means to prevent the crack from kinking into the face sheet area. Several techniques that utilize through thickness stitching of sandwich structures have been developed to enhance their face/core interface fracture properties. Kim et al [39] and Raju et al [40] investigated the effect of stitching in the strength and energy absorption capacity of sandwich composites. They demonstrated a considerable increase in the respective properties and damage tolerance of the tested components. Wallace et al [41] showed that pin reinforced sandwich structures have significantly higher resistance to axial compression failure that initiates delamination due to buckling instabilities. A limitation of stitching techniques is that they can often affect negatively the strength of the composite face-sheets especially when unidirectional (UD) fibre face-sheets are used. Pins that are stitched through the face-sheet fabrics will alter the orientation of the fibres that are wrapped around them. This drastically decreases the axial in plane strength of UD face-sheets that can lead to premature failure of the sandwich component.

Besides stitching and other interfacial fracture enhancement techniques, several studies have investigated the arrest of propagating interfacial face/core cracks by the use of special embedded crack stopping inserts (or devices). Rinker [42] introduced two types of carbon fibre reinforced composite (CFRP) inserts loaded using the Sandwich Cantilever Beam (SCB) and Cracked Sandwich Specimen (CSB) tests to examine crack arrest under mode I and mode II loadings, respectively. It was shown that the embedded crack stopper devices/elements could arrest a propagating interface crack for a considerable amount of loading cycles, especially under mode II loading conditions. The reason for this effect is the much higher fracture toughness of the CFRP compared to conventional core materials as well as the geometry of the CFRP crack arresters. Hirose et al. [43-47] demonstrated that crack arrest can be achieved by using either a semi-circular CFRP rod glued into the face/core interface, or by using a splice-type crack arrester connecting the two face-sheets through CFRP layers. In both cases stress release at the crack tip was observed as the crack approached the tip of the arresters. The reduction of stresses at the crack tip resulted in a reduction of the energy release rate and a deceleration of the crack. Common for all of these studies is that the structure/element introduced into the core was made from fibre reinforced composites materials with stiffness properties that are significantly different (stiffer) than typical sandwich core materials, such as e.g. PVC or other structural foams. The use of a high stiffness material for the crack stopper induces an abrupt stiffness change around the crack stopper, which leads to the inducement of stress concentrations that can potentially act as crack initiators.

Jakobsen [45-51] proposed and tested a new type of crack arrester (referred to as a peel stopper), Figure 8. The peel stopper, which is configured as a core insert made from a compliant/soft material bonded to both the face sheets and the sandwich core, was shown to be capable of re-directing propagating cracks away from the face/core interface and subsequently arresting the cracks somewhere near the centre of the

peel stopper. The peel stopper has been shown to be able to deflect and arrest propagating interface cracks in sandwich beams subjected to both quasi-static and fatigue loading conditions, where the stress field near the crack tip is Mode II dominated [47, 50-51].

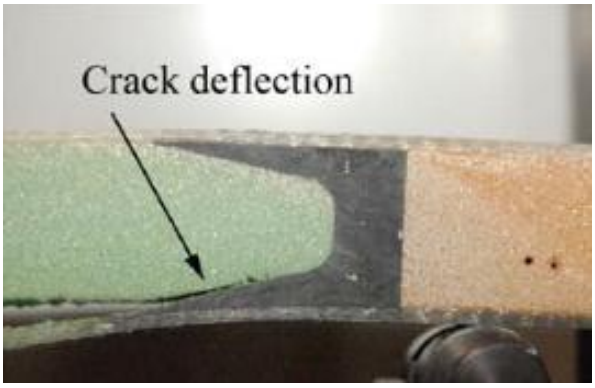

Figure 8. Peel stopper concept implemented in sandwich beams, Jakobsen et al. [45].

CHAPTER 3. PEEL STOPPER DEVICE

The starting point of this work is the peel stopper concept proposed by Jakobsen et al [45]. The overall aim of the work is to improve the initial peel stopper proposed in [45,47] by developing and validating a significantly lighter design that is capable of resisting both low and high cycle fatigue loading over a range of mode-mixities. The goal was to improve the crack arrest capability with emphasis on fatigue crack arrest, while reducing the added mass to the structure. The weight reduction of the peel stopper, compared with original design [45], has been achieved by reducing the overall thickness of the component down to 1 mm by giving it the form of a thin strip of compliant and tough Polyurethane (PU) polymer resin material, Figure 9. To enhance the crack stopping ability further, glass fibres were used to reinforce the PU material. The glass fibres increase the fracture toughness of the peel stopper, which dictates its overall resistance to crack propagation. The improved peel stopper design, which is shown in Figure 16, was initially proposed and documented in Martakos et al [52].

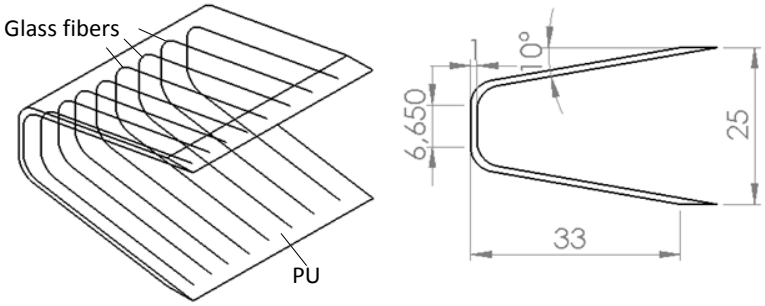

Figure 9. New glass reinforced peel stopper design concept according to Martakos et al [52].

3.1. PEEL STOPPER IN BEAM SPECIMENS

The new peel stopper concept was implemented in series of sandwich beam specimens as illustrated in Figure 10. The testing of the peel stoppers in beams has several advantages over the implementation and testing in panel or plate like sandwich structures. The main advantage is that face/core interface crack propagation in sandwich beams can be easily inspected and measured just by visually observing the condition of the specimen. This is ideal for initial conceptual tests of the peel stopper where it is difficult to predict the crack growth around the peel stopper. Moreover, sandwich beam specimens can be easily produced in large

quantities by fabrication of one large panel and subsequent cutting. This enables a large number of repetitions of the same test to be conducted, which proved crucial when developing the new peel stopper concept.

In chronological order, the beam tests conducted for the needs of this work are as follows:

- Three-point bending test – ICCM19 Proceedings [52]
- Sandwich Mixed Mode Bending test (MMB)-Paper#1, Wang et al [53]
- Sandwich Tear Test (STT) -Paper#2, Martakos et al [54]

The different sandwich beam test configurations were used to demonstrate the potential of the new peel stopper design as a crack arrester, to investigate and quantify the conditions under which interface crack deflection occurs, and finally to describe the physics behind crack arrest mechanism.

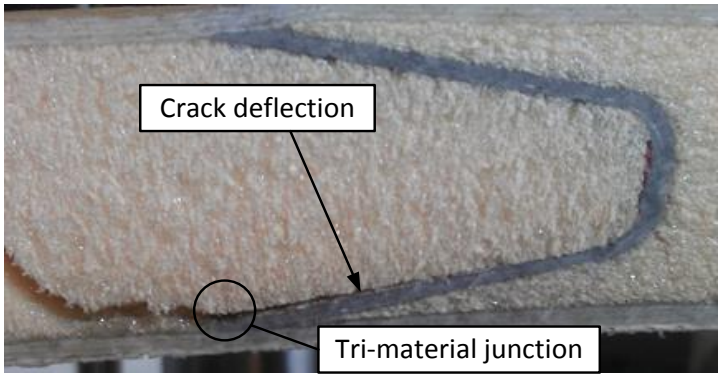

Figure 10. New peel stopper concept according to Martakos et al [52] implemented in a sandwich beam specimen.

Apart from the significant weight reduction when compared to Jakobsen's original design, the new peel stopper was significantly enhanced in the work by Wang et al [53] by improving the crack deflection capability at the tri-material junction at the peel stopper tip, Figure 10. This was achieved by increasing the the face-sheet / PU interface fracture resistance at the tip of the peel stopper by the introduction of glass fibres that connect the peel stopper and the face-sheet.

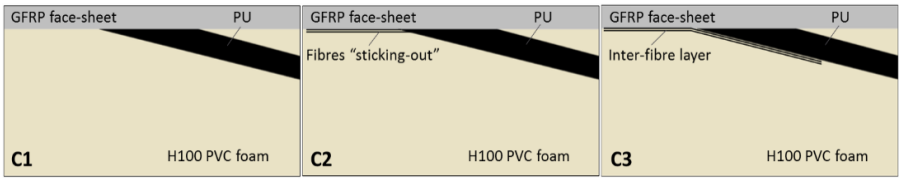

Figure 11. *Peel stopper with 3 different configurations at the tri-material junction, Wang et al. [53].*

In

Figure ***11***, in accordance with Wang [53], Configuration 1 (C1) represents the original design of the non-enhanced peel stopper tip where the face-sheet and PU materials are bonded during the sandwich specimen infusion. In Configuration C2 the fibres running inside the peel stopper are made longer in order to "protrude" from the peel stopper tip. The fibres are then joined with the face-sheet during the infusion of the sandwich beams. Finally in configuration C3 a layer of glass fibre is inserted between the peel stopper and the foam core material that is also infused together with the face-sheet. In configurations C2 and C3 the crack deflection ability of the peel stopper is greatly enhanced as will be shown.

3.2. PEEL STOPPER IN PANEL SPECIMENS

The implementation of the new peel stopper design into foam cored sandwich panels (plate like structures) is documented in Martakos et al. [56]. To achieve this some alterations of the concept as discussed above were required, to account for cracks that may be propagating from either side of the peel stopper. The sandwich panel peel stopper concept is in practice two original peel stoppers, as implemented in sandwich beams, placed "back-to-back". The concept is named the dual faced peel stopper and is sketched in Figure 12. The "core area" shown in the sketch is separated from the rest of the (PVC) core material of the sandwich panel due to the peel stopper shape in the dual faced peel stopper concept. The material of the core area is not considered vital for the performance of the peel stopper and ideally for weight reduction reasons it should be made by the same low density material used in the rest of the sandwich component core (a PVC core in this work).

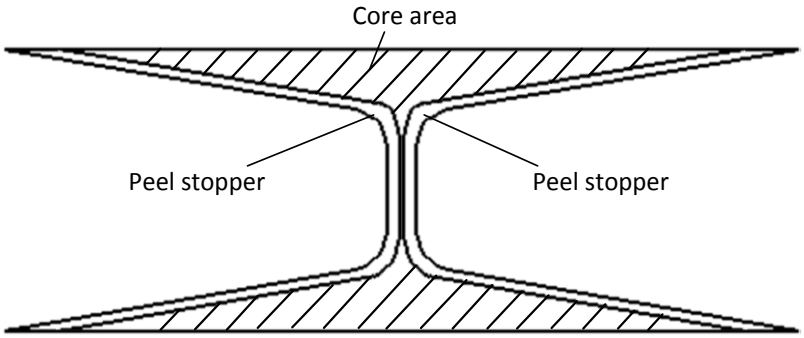

Figure 12. *Dual faced peel stopper concept*

However, to simplify both the design and the manufacturing process of the peel stopper the material of the core area in this research was selected to be the same PU resin that is used to make the rest of the peel stopper. The dual faced peel stopper was casted in a mould in one piece, while the reinforcing glass fibres were placed close to its inner faces. This design choice increased the weight of the peel stopper

significantly but simplified the manufacturing process considerably. Figure 13 shows the peel stopper implemented in the sandwich panels after the panels were cut for post-test inspection.

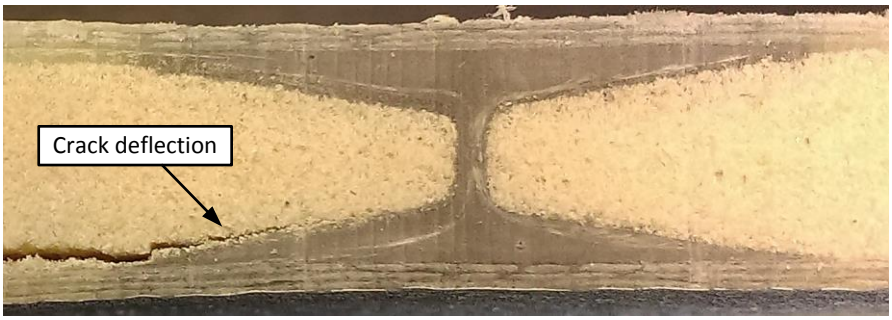

Figure 13. Dual faced peel stopper concept implemented in a sandwich panel specimens

All the dual faced peel stoppers were made based on configuration C2 (See

Figure ***11***) to improve the crack deflection capability. The peel stoppers in sandwich panels were given a circular shape such that a circular area around the centre of the panel was enclosed by the peel stoppers, Figure 14. The reason for this is that an initial interface crack of circular shape was induced in the centre of the panel specimens, and that the aim was to achieve a concentric crack pattern relative to the plate centre.

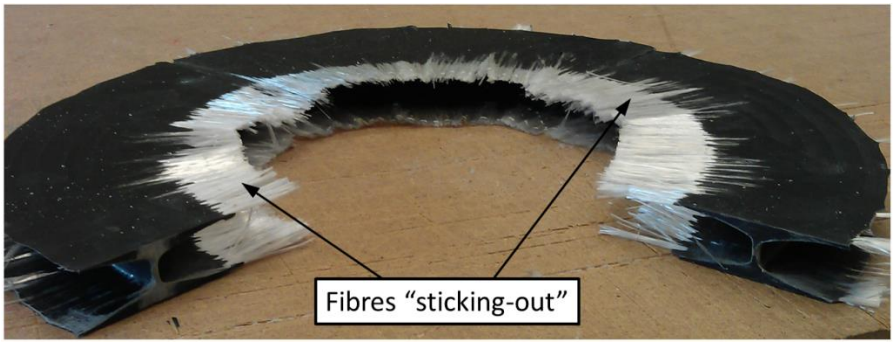

Figure 14. Circular shaped dual faced peel stoppers (Configuration C2) before they are embedded in panel specimens

3.3. PEEL STOPPER FABRICATION

The peel stoppers in this study were manufactured using the PU resin, Permalock 2K PU-9004. Using the PU/glass fibre hybrid material describe in the preceding provided peel stoppers with stiffness properties that are very similar to those of the

foam core material, but at the same time displaying a much higher fracture toughness. Depending on the configuration of the peel stopper made, the fibres running along the peel stopper (see

Figure ***11***) were either protruding from the peel stopper tip (configuration C2) or end directly at the peel stopper wedge (Configurations C1 and C3).

Two different moulds were made for the fabrication of the peel stoppers, one for the thin strip design used in sandwich beam specimens, and one for the dual faced peel stopper implemented in sandwich panel specimens. The moulds used for the fabrication of the peel stoppers are shown in Figure 15 and Figure 16. The fabrication process was very similar for the two designs and followed the same steps. First, the embedded glass fibres were inserted into the open mould. Then, the PU resin was injected in the mould in excess amount. Finally the mould was closed and the PU resin was pressed into the shape of the mould tool impregnating the glass fibres at the same time. Steel clamps were used to apply the needed pressure to close the mould, while the excess PU material was allowed to exit from holes drilled along the length of the mould. The moulds were made from Polyprolylene (PP), a material that forms neither mechanical nor chemical bonds with PU resin. Therefore no special release or demoulding agent was applied in the moulds prior to casting of the peel stoppers.

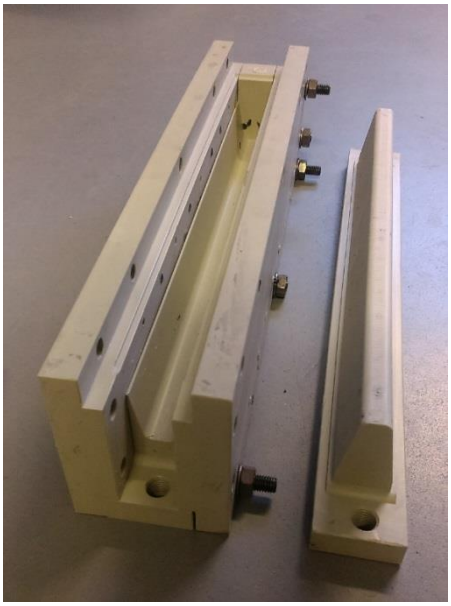

Figure 15. Peel stopper Polypropylene mould. Side view of the assembled mould showing the peel stopper shape, Wang et al. [53].

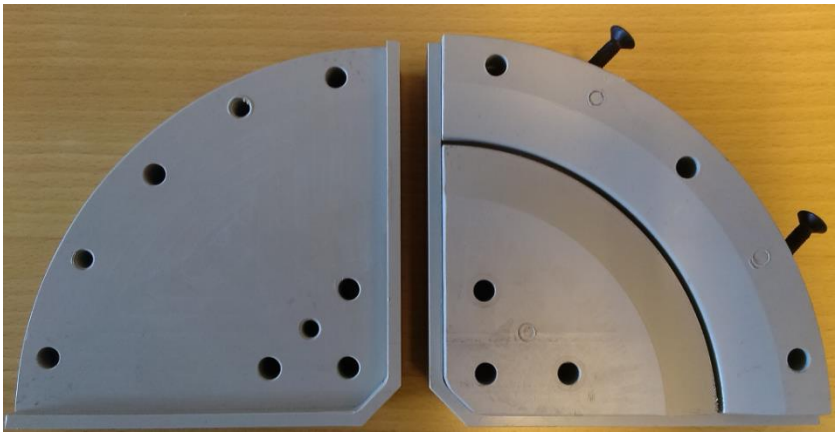

Figure 16. Dual faced peel stopper mould. The mould has the shape of a quarter of a circle.

3.4. FABRICATION OF SANDWICH SPECIMENS WITH EMBEDDED PEEL STOPPERS

The sandwich beam specimens were firstly fabricated in the form of a panel which was later cut and divided into beams. This allowed for several beam specimens to be made using one casting process, whereas the sandwich panel specimens were fabricated one at a time. The fabrication of all the specimens was achieved following similar two-step processes. In the first step, the core of the sandwich panel including the peel stoppers was assembled. This process requires the PVC foam to be milled into the shape of the peel stopper to enable assembly. Then, the peel stopper was bonded to the PVC foam using a two-component epoxy glue, Araldite 2000.

In the second step, the final assembly of the sandwich panel components was made. The face sheets and the pre-assembled core structure were placed in the right order. In all sandwich specimens a predefined crack was created by inserting a 25 μm thickness Teflon foil placed between the top face sheets and the core materials. Once the assembly of the parts was done, the core and face sheets were infused with epoxy resin using the Vacuum Assisted Resin Transfer Moulding (VARTM) technique. During the resin infusion the glass fibres protruding from the peel stoppers in configurations C2 and C3 were bonded to the face sheet glass reinforcement. Finally, in the case of sandwich beam specimens, the sandwich panel was cut into beam specimens that contained the peel stopper in the core structure.

Table 1. Material properties of sandwich specimens

Materials	In-plane Young's modulus (E_x)	Through thickness Young's modulus (E_y)	Shear modulus (G_{xy})	Poisson's ratio (ν_{xy})
DIVINYCELL H100	56 MPa (M)	128 MPa (M)	32 MPa (M)	0.3 (A)
E-glass/epoxy	18.6 GPa (M)	9.2GPa (A)	2.7 GPa (M)	0.4 (M)
PU	100 MPa (A)	100 MPa (A)	34.2 MPa (A)	0.45 (A)

where (M) stands for "measured" and (A) stands for "assumed".

The PU material properties were derived by Jakobsen [51]. The E-glass/epoxy through thickness Young's modulus is assumed based on commonly used values in literature [22]. For consistency reasons the same materials were used in all sandwich specimens made for the needs of this study.

CHAPTER 4. THREE-POINT BENDING TESTS

The purpose of the initial 3-point bending tests was to observe the propagation of a crack under fatigue loading conditions when it meets the peel stopper tip using a simple and well-established test set-up. This was seen as a preliminary investigation to obtain insight about the behaviour of the new peel stopper design. Fatigue crack propagation in sandwich specimens subjected to 3-point bending has been studied experimentally and numerically by Zenkert [57]. A similar test set-up was used in this study with the initial crack being positioned at the same location in the sandwich specimen. The predefined crack in the face/core interface was introduced at one side of the sandwich beam specimen between two peel stopper devices, Figure 17. To avoid indentation damage at the load application points a stiffer PVC foam Dyvinycell H200 [58] (H100 was used for the centre core of the specimens) was used locally. The loading and boundary conditions of the 3-point bending test set-up are shown in Figure 17.

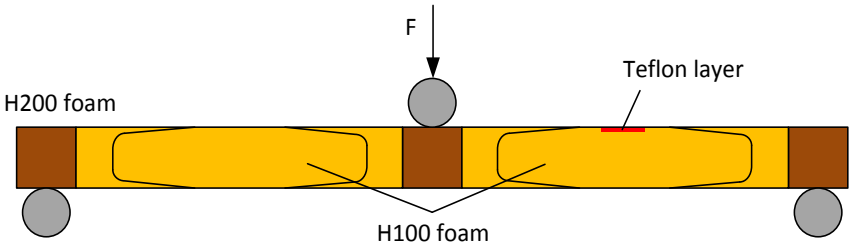

Figure 17. Test set-up schematic

4.1. TEST CONFIGURATION

A total of six specimens were tested under displacement controlled fatigue loading conditions. The displacement control scheme results in stable crack growth as the energy release rate is reducing with increasing crack length. This behaviour can frequently lead to self-crack arrest in specimens when the crack length has increased to a point where the energy release rate is too small compared to the fracture toughness of the materials. In this test after the crack had propagated a certain distance, the displacement amplitude was increased to increase the energy release rate at the crack tip. The initial maximum displacement fatigue load was chosen as 80% of the quasi-static load limit (failure) obtained in quasi-static tests on similar sandwich beam specimens. In the second load step the maximum displacement was increased to 90% of the quasi-static load limit. The second displacement magnitude

was applied when the crack reached the peel stopper boundary (tip). The increased displacement amplitude was applied to enable observation of the post arrest behaviour of the crack, particularly whether the crack would propagate into the peel stopper material. **Error! Reference source not found.** gives an overview of the test loading parameters.

Table 2. Prescribed displacement amplitudes during fatigue loading.

Fatigue test data	Initial fatigue load (Until arrest point)	Second fatigue load (After arrest point)
Fatigue maximum displacement [mm]	6.8	7.5
Fatigue minimum displacement [mm]	0.68	0.75
Load Ratio, R	0.1	0.1
Frequency, f	3 Hz	3 Hz

The tests were conducted in the lab of the Technical University of Denmark (DTU) using a 25 kN capacity MTS servo-hydraulic test machine. The test set-up is shown in Figure 18.

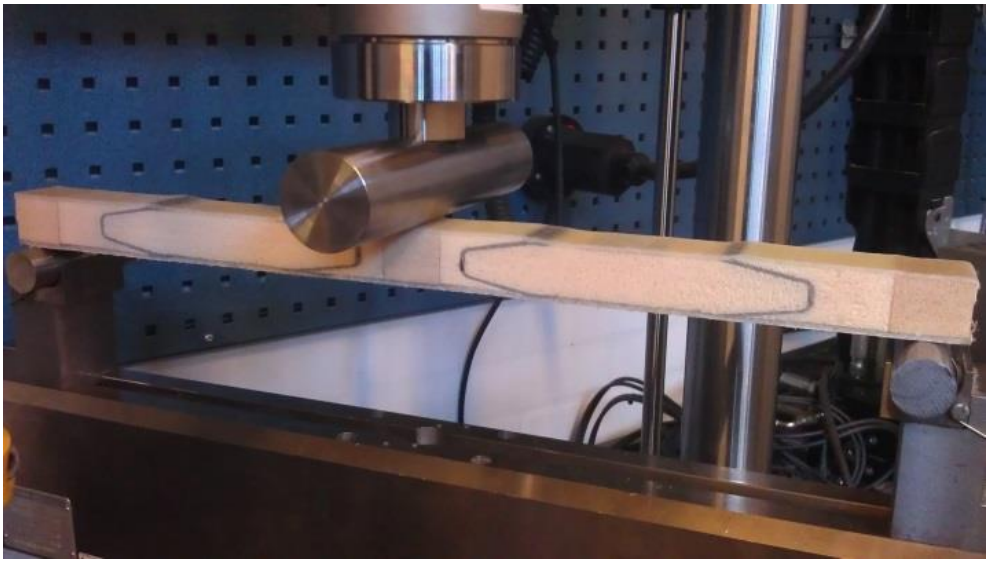

Figure 18. Sandwich beam specimens in 3-point bending testing rig.

4.2. RESULTS

During the fatigue tests, the initial crack induced in the upper face-sheet of the specimens propagated towards the lower face-sheet by kinking directly into the foam core material. The crack propagated under pure mode I conditions until it reached the lower face /core interface. Thereafter the crack reached the peel stopper where is was deflected away from the interface. Finally the crack reached the end of the peel stopper/core interface, hereinafter referred to as the "arrest point", where the crack propagation stopped. It was observed that the crack was not able to penetrate the peel stopper body, and instead a new crack initiated in the foam material on the back side of the peel stopper, Figure 19. It is believed that the new crack was initiated due to the strain concentration developing on the back side of the peel stopper. This assumption is investigated thoroughly later in this thesis. The observations reveal that the new peel stopper concept with fibre reinforcement can resist crack penetration through the peel stopper and arrest the initial crack.

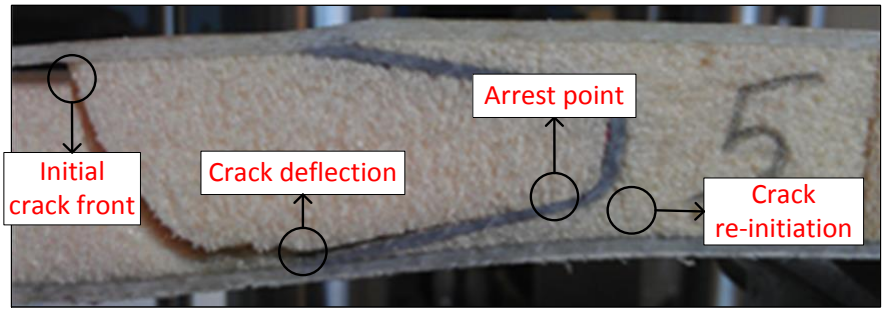

Figure 19. Crack propagation in 3-point bending sandwich beam specimen embedded with peel stoppers.

The number of cycles during the 3-point bending tests was recorded and used to make a preliminary evaluation of the crack arresting ability of the new peel stopper. The number of cycles for three different propagation events: a) when the crack was deflected by the peel stopper, b) when it reached the arrest point and, c) when a new crack initiated on the opposite side of the peel stopper are given in Table 3. Furthermore the change in the compliance of all the specimens during the tests in relation to the number of loading cycles is given in Figure 20. The compliance which is the ratio of the applied displacement to the resulting force is plotted in Figure 20 as the actual load and the applied displacement are increased during the tests. The compliance of the specimens provides valuable information about the accumulated effect of level of damage in the specimens, and it relates directly to the crack length of the delamination. It is important to note here that from a structural integrity point of view the sandwich beams have failed completely at a very early stage of the experiments. Thus, a crack extending through the thickness of the core would render the sandwich beams incapable of transferring shear loads, and the bending stiffness of sandwich assembly will reduce to the sum of the bending

stiffnesses of the 2 face-sheets. However, this focuses on the crack propagation behaviour in the sandwich beam rather than the overall structural performance.

Table 3. 3-point bending fatigue test results.

Specimen	Crack deflection cycles, n_d	Crack arrest cycles, n_a	Crack re-initiation cycles, n_r	Crack arrest duration, n_a-n_r
Beam 1	640	6750	21800	15050
Beam 2	520	9300	29700	20400
Beam 3	440	4700	14000	9300
Beam 4	740	9500	35100	25600
Beam 5	250	400	5100	4600
Beam 6	510	7500	25000	17500

The crack arrest duration shown in Table 3 is the difference between the number of cycles to crack re-initiation (back side of peel stopper) and the number of cycles to initial crack arrest. During the crack arrest duration the initial crack did not propagate in the foam core and the peel stopper material. It was observed that the peel stopper in all cases was able to limit crack propagation for a considerable number of cycles, see 5th and 3rd columns of Table 3. Figure 20 shows the behaviour of all the specimens during the experiments. The points of crack arrest and crack re-initiation are highlighted, although it is difficult to clearly see the effect of the peel stopper from the compliance plots. That is because the crack introduced in the specimens had two propagation fronts, one that kinked into the lower face/core interface and which was arrested by the peel stopper, and another crack that that remained in the upper face/core interface. The second crack front started propagating under high mode II loading, while the first crack was arrested by the peel stoppers. The propagation of the second crack led to an increase of the compliance of the specimens, even though the investigated crack front did not propagate.

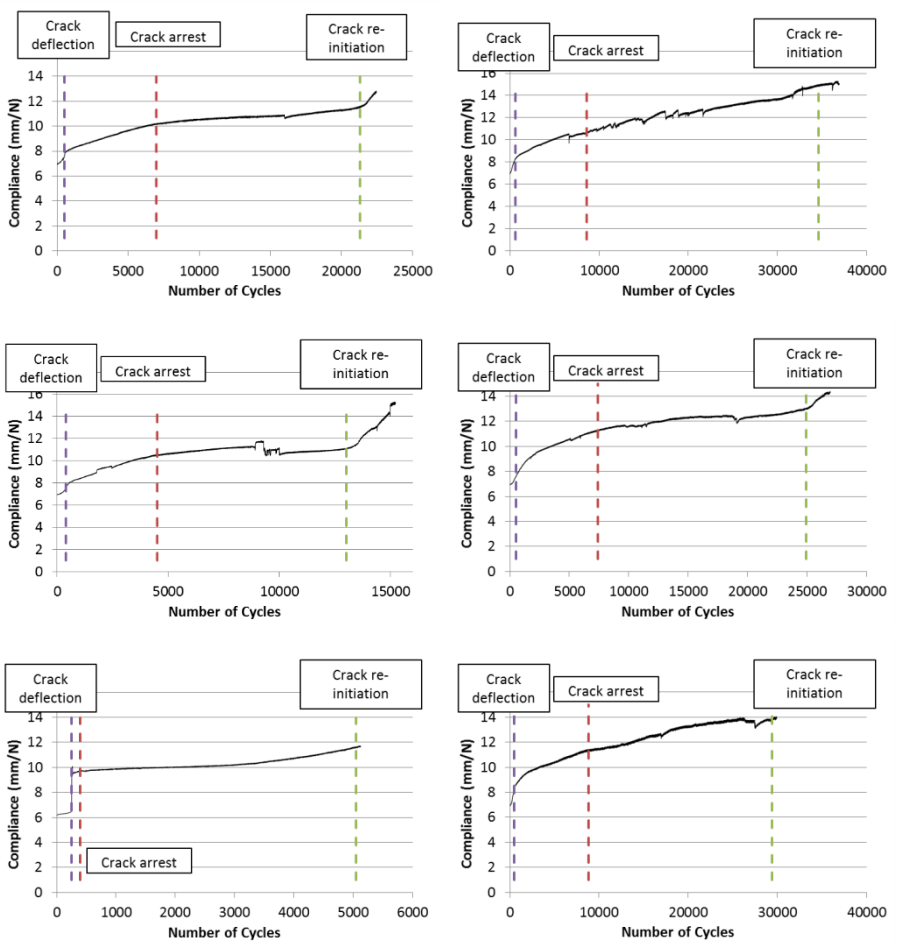

Figure 20. Compliance vs. Number of cycles for the six beams loaded in fatigue. The inserted dashed lines identify three different stages of life cycle of the sandwich beam specimens. The compliance of the specimens increases even though the crack is arrested at one end.

4.3. CONCLUSIONS

The 3-point bending tests have shown that the new peel stopper design in all cases has been able to deflect and arrest propagating interface cracks for a large/significant number of fatigue load cycles. These observations made act as a preliminary evaluation that encourages a more in depth investigation of the behaviour/performance of the new peel stopper design. From the conducted tests it was concluded that all future cracked/damaged sandwich specimens should ideally

should exhibit only one crack front, since it is very difficult to extract firm conclusions due uncertainties with respect to the crack propagation behaviour.

CHAPTER 5. MIXED MODE BENDING TEST FOR CRACK DEFLECTION ANALYSIS OF AN INTERFACE CRACK APPROACHING A TRI-MATERIAL JUNCTION (PAPER #1)

The work presented in this chapter has been published in Wang et al. [53] which is appended as Paper #1 in the appendix of this thesis.

The Mixed Mode Bending test (MMB) was chosen for the investigation of the behaviour of a face/core interface crack approaching the peel stopper wedge (tip). The aim was to develop an understanding of the conditions under which the crack deflects away from the interface using both experimental and numerical methods (FE), and further to establish a design solution for the peel stopper that ensures crack deflection. Three different configurations of the peel stopper tip were evaluated as presented in Chapter 3,

Figure ***11***, and as proposed by Wang et el [53], on their ability to deflect a crack away for the face/core interface. The MMB test was selected since it is possible to control the energy release rate for a range of fixed mixed mode conditions at the crack tip [21-22]. The crack propagation magnitudes at a given crack length can be determined by use of either FE analysis or analytical closed form solutions. In this study FE analysis was selected for determining the crack loading conditions, since the presence of the peel stopper cannot be easily accounted for in an analytical solution. The MMB test set-up with a specimen with an embedded peel stopper is shown in Figure 21, and the test parameters are given in **Error! Reference source not found.**.

Table 4. MMB test set-up and specimen parameters [53].

Parameter	Description	Value (mm)
a_0	Initial crack length	17-20
d	Crack tip distance to peel stoppers tip	32-35
L	Half beam span length	90
c	MMB set-up lever arm	75

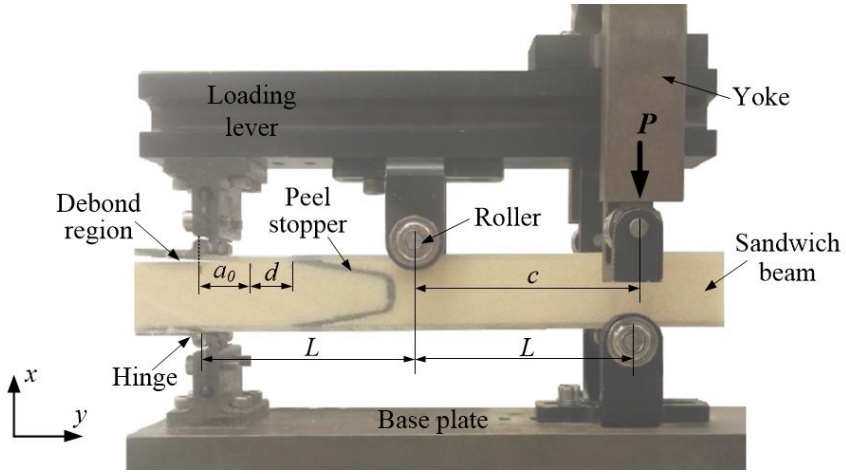

Figure 21. Sandwich beam specimen loaded in the MMB test rig, [53].

5.1. TEST CONFIGURATION

A total of nine sandwich beam specimens were tested under fatigue loading conditions, three from each configuration shown in

Figure ***11***. The tests were conducted under displacement control to achieve stable test conditions and promote a stable crack growth. A displacement ratio ($\delta_{min}/\delta_{max}$) of $R = 0.2$ and a testing frequency of $f = 3\ Hz$ were used. To ensure that the three different configurations were tested under similar crack loading conditions, the displacement amplitude of the tests was increased step wise as the crack propagated. By increasing the displacement amplitude multiple times, the energy release rate of the crack tip was kept at a level close to 450 J/m^2, Figure 22. FE analysis was used to determine the crack length to displacement amplitude relation which was used as input to impose the correct displacement amplitudes during the tests. This indirect energy release rate control scheme ensured that the crack tip would experience similar crack loading conditions in terms of energy release rate and mode-mixity angle when it reached the peel stopper tip for all three test specimen configurations.

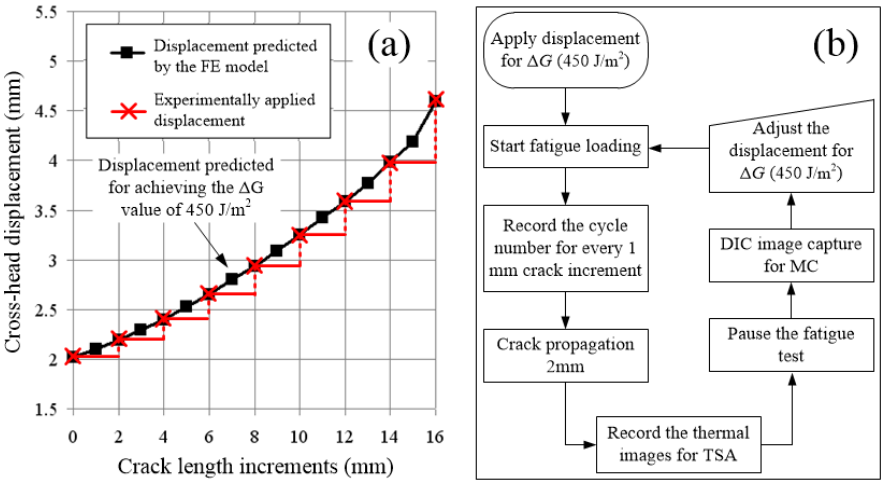

Figure 22. (a) Fatigue control method, and (b) Flowchart of the fatigue test procedure [53].

During the tests the crack was driven up to the peel stopper tip and afterwards it was allowed to propagate a distance of approximately 10 mm. The post deflection behaviour and crack arrest were out of the scope of the MMB tests conducted. This is mainly because the MMB test is ideal for crack propagation characterization purposes, but has limited usefulness as a structural component evaluation test. The crack propagation length was limited in all MMB tests by the distance between the upper hinge pulling the face-sheet and the roller in the middle of the specimens (L, see Figure 21). Furthermore, the applied displacement at the yoke reached the maximum allowable magnitude before the yoke stroke the lower roller. These limitations mean that the crack propagation length is limited in the MMB setup, which in turn makes it inappropriate for crack arrest assessment of the peel stoppers which involve large crack lengths.

5.2. FINITE ELEMENT MODEL

The FE model of the set-up and test specimens used to derive the displacement to crack length relation was developed using the commercial FE package ANSYS 15.0 [59]. The analysis used 8-node 2D plain strain plane elements (PLANE 183) with an average element size of 0.5 mm. At the crack tip, between 36 and 144 elements of size 5 to 10 μm were used. Mesh sensitivity analysis was used to ensure that a sufficient number of elements was used in the FE model to obtain a converged solution for the CSDE method so that that the numerical errors would be sufficiently small as to not influence the calculated fracture mechanics quantities. Figure 23 shows the sandwich beam model and the different crack path scenarios around the tri-material corner for each configuration. In configurations C2 and C3 an extra layer of elements (the element with orange colour) was used to simulate the fibres sticking

out and the inter-fibre layer, respectively, as shown in images b and c in Fig. 30. The thickness of the additional layer is 0.1 mm.

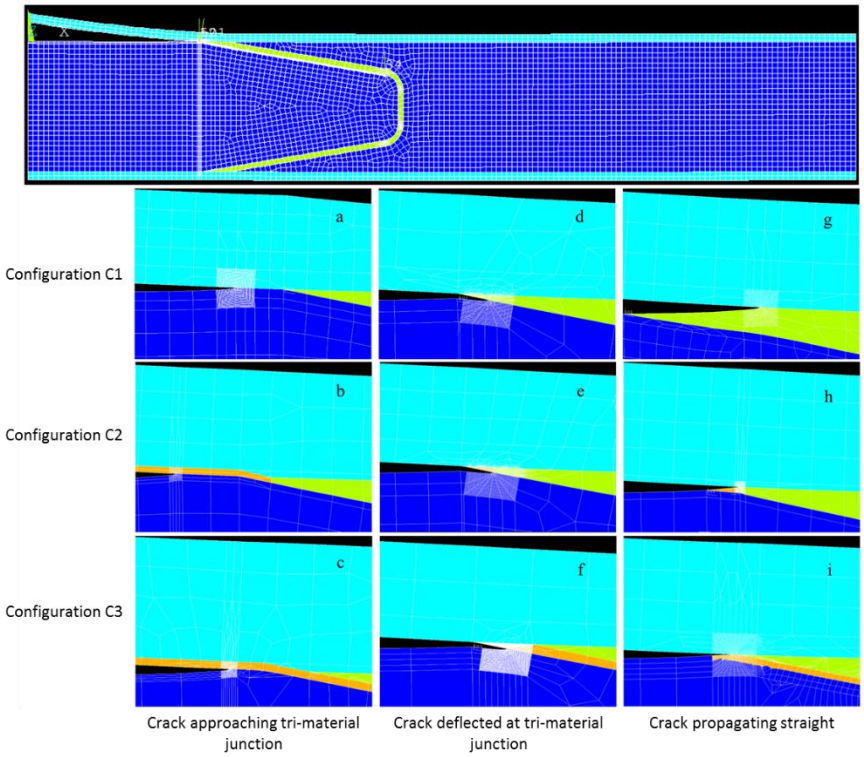

Figure 23. Crack tip modelled for all crack propagation cases. In the images: light blue colour represents the main face-sheet material, orange represents the UD fibre layer used in configurations C2 and C3, deep blue represents the core material and yellow the peel stopper material [53].

5.3. RESULTS

Table 5 summarizes the results of the MMB deflection test for all nine specimens. Only configurations C2 and C3 showed consistent behaviour with regards to crack deflection. For configuration C1 only one specimen achieved crack deflection, while the two other specimens failed to do so. This shows that the unreinforced tip of the peel stopper was incapable of deflecting the propagating interface crack consistently.

To understand the mechanisms and conditions that lead to crack deflection two approaches were used [53]; one based on full field stress measurement and the other on finite element analysis. The full field measurement technique used was Thermoelastic Stress Analysis (TSA) which is based on Infrared (IR) imaging. The parts of the investigation that include TSA, post processing of thermal images and

mapping of the state of stress in the vicinity of the peel that led to crack deflection were planned and conducted by Dr. Wei Wang, University of Southampton University, UK, as part of his PhD project. The details of this work are given in Wang et al. [53].

Using the Finite Element model (Figure 23) the conditions for crack kinking to occur as well as the influence of the peel stopper angle were investigated for all the considered specimen configurations.

Table 5. Crack propagation paths of different specimens [53].

Specimen	Crack paths before the tri-material junction	Crack path after the tri-material junction
C1_f1	Foam	Deflected
C1_f2	Foam	Not deflected
C1_f3	Foam	Not deflected
C2_f1	Interface, foam	Deflected
C2_f2	Interface, foam	Deflected
C2_f3	Interface, foam	Deflected
C3_f1	Interface	Deflected
C3_f2	Interface	Deflected
C3_f3	Interface, foam	Deflected

5.4. PEEL STOPPER ANGLE EFFECT THE ABILITY TO GENERATE CRACK DEFLECTION

The FE model presented in Figure 23 was used to derive and compare the energy release rate and mode-mixity values for each of the experimentally observed crack paths. The paths consisted of the "horizontal path" (or straight path) for the crack penetrating the peel stopper, and the "deflected path" for crack deflecting and propagation along the peel stopper into the core, see Figure 24. The aim was to evaluate the influence of the peel stopper angle on the propensity for achieving crack as well as the differences in performance of the 3 different configurations. The peel stopper angle, θ was chosen to vary between 5^o to 30^o in steps of 5^o with a kinked crack length of 0.5 mm away from the corner as depicted in Figure 24. A peel stopper angle of 10^o was used for the sandwich beam specimens that were investigated experimentally.

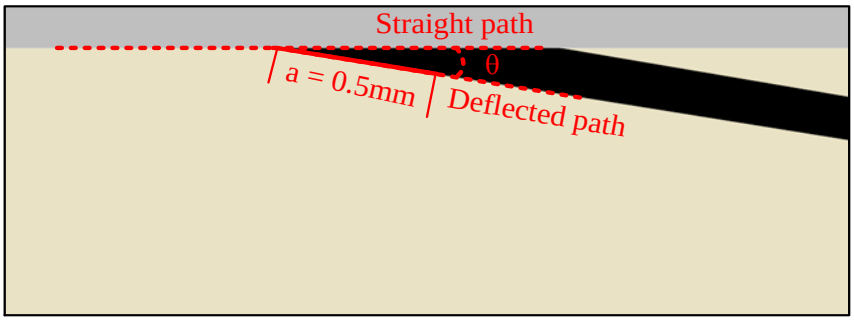

Figure 24. Crack paths investigated around the tri-material junction, [53].

In Figure 25, the energy release rate and mode-mixity of the two crack paths are plotted against the peel stopper angle for each of the investigated configuration. From plots to the left it is seen how the energy release rate changes for the two crack paths as the peel stopper angle increases. It is observed that the energy release rate for crack "straight" (or horizontal) crack propagation is not influenced significantly by variation of the peel stopper angle. For configurations C2 and C3 however, it is seen that energy release rate increases significantly with increasing peel stopper angle, as the protruding glass fibres and the inter fibre layer, respectively, are also following the changing angle, θ. The change of θ of influences the local stiffness around the crack tip, which directly affects the energy release rate. For the deflected crack, it is seen that for configurations C1 and C2 the change in energy release rate is very small, but for that for C3 a significant decrease is observed as the angle increases.

The right plots in Figure 25 show the mode-mixity variation. For the horizontal crack path the influence of the angle θ is small for all three configurations, albeit the mode-mixity for C2 and C3 increases slightly with increasing θ. Opposed to this, it is observed the mode-mixity decreases with increasing θ along the deflected crack path for configurations C1 and C2, while the mode-mixity along the deflected path is hardly influenced for C3. Further, for C1 and C2 the mode misty changes from positive to negative as θ increases, while for C3 the mode-mixity remains positive. It should be noted that even though the mode-mixity changes for the deflected crack, the shear component (Mode II) only becomes significant for very high deflection angles. For small deflection angles the mode-mixity is such that the crack tip experiences Mode I dominated conditions for both possible crack paths.

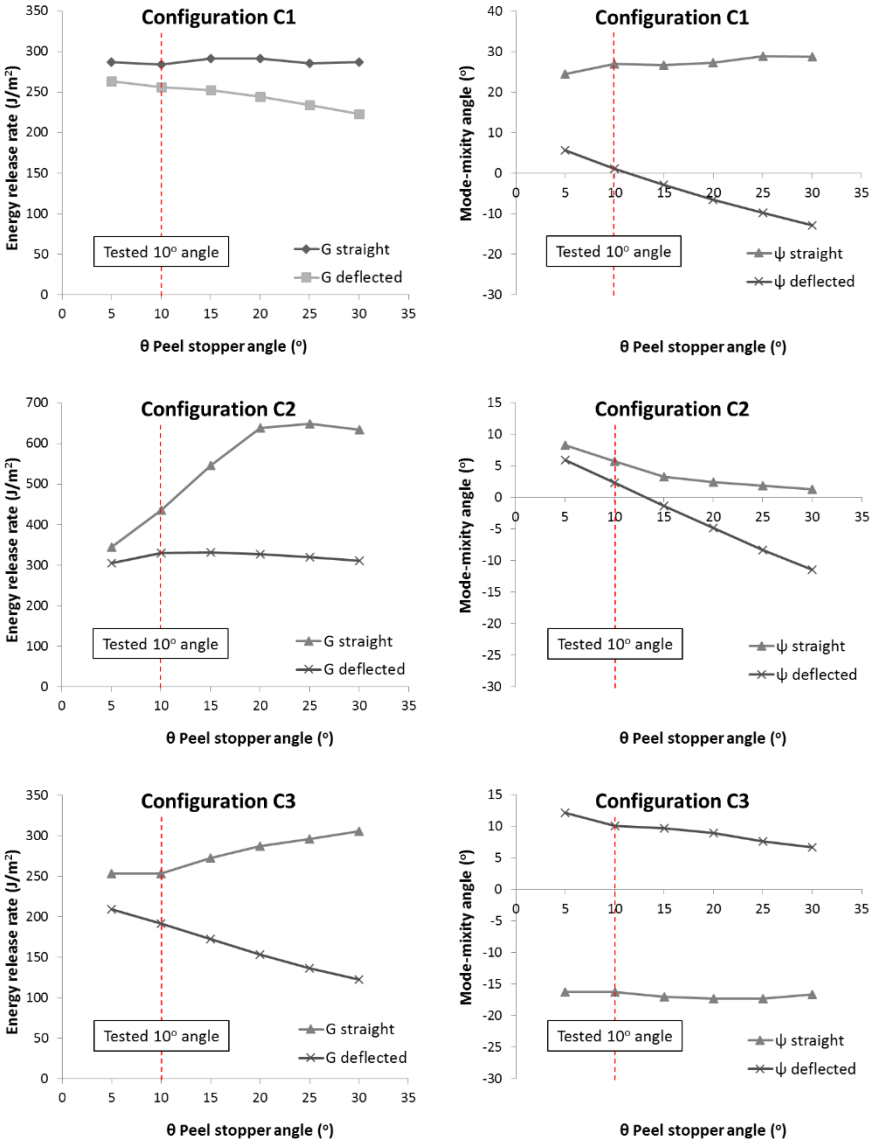

Figure 25. Plot on the left: Energy release rate vs. stopper angle for the three configurations. Plots on the right: mode-mixity vs. peel stopper angle for the three configurations, [53].

The crack kinking criterion suggested by He and Hutchinson [13] has been applied to the numerical results shown in Figure 25 to explain the crack deflection behaviour of the three different peel stopper configurations. According to [13], the condition for crack kinking out of an interface can be expressed as:

$$\frac{G_{straight}}{\Gamma(\psi)_{straight}} < \frac{G_{deflected}}{\Gamma(\psi)_{deflected}} \quad (5.1)$$

,where $G_{straight}$ is the calculated energy release rate at the face/core interface (i.e. for a crack growing at the straight path) and $G_{deflected}$ refers to the energy release rate at the respective deflection angle, θ, which is also the peel stopper angle. $\Gamma(\psi)$ represents the material and interface fracture toughnesses values at a given mode-mixity angle, ψ. In this study, since the fracture toughness values are unknown (and difficult to determine), the considerations made are based only on the calculated energy release rate and mode-mixity values. This is achieved by reformulating the inequality given by Eq. (5.1), and proposing the crack kinking (or deflection) criterion at the peel stopper tip as follows

$$\frac{G_{deflected}}{G_{straight}} > \frac{\Gamma(\psi)_{deflected}}{\Gamma(\psi)_{straight}} \quad (5.2)$$

The new crack kinking criterion (5.2) predicts that crack kinking is highly dependent on the ratio of the interface fracture toughnesses $\Gamma(\psi)_{deflected}$ and $\Gamma(\psi)_{straight}$. The fracture toughness values for the straight and deflected interfaces are unknown for all the configurations, but experience can give some insight as to what is their relative magnitude would be along the interfaces. From Figure 25 the ration $\frac{G_{deflected}}{G_{straight}}$ for the different deflection or peel stopper angles can be calculated, see Figure 26. To satisfy the crack deflection/kinking criterion suggested by the inequality (5.2), the fracture toughness ratio $\frac{\Gamma(\psi)_{deflected}}{\Gamma(\psi)_{straight}}$ must be smaller than energy release rate ratios shown in Figure 26 for the 3 configurations.

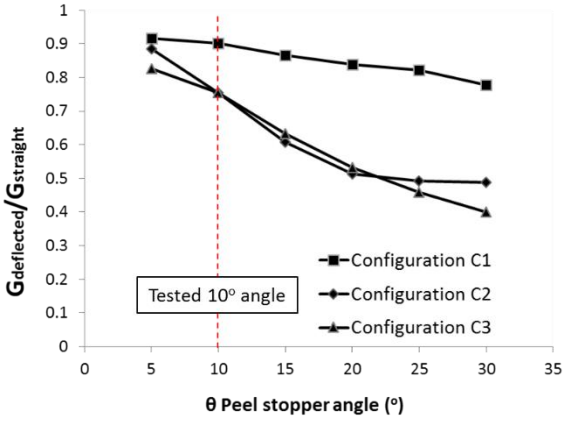

Figure 26. $\frac{G_{deflected}}{G_{straight}}$ values vs. peel stopper angle θ, [53].

5.5. DISCUSSION AND CONCLUSIONS

The behaviour observed for the C1 specimens can be explained by Figure 26. Since the required fracture toughness ratio must be smaller than the energy release rate ratio, interface fracture toughness ($G_{straight}$) along the straight (horizontal) crack path must be larger than the interface toughness of the deflected path. It may be assumed that the material systems of the two interfaces possess comparatively similar fracture properties since the bonding was achieved by vacuum infusion of epoxy resin and bonding with epoxy adhesive, respectively. From Figure 25 it is seen that the energy release rate ratio is just slightly lower than 1 for small peel stopper angles, and since the fracture toughness ratio will also be close to 1 as argued above, , this can explains why only one of the C1 tests resulted in crack deflection at the tri-material junction (peel stopper tip), while it did not occur for the two other tests. Accordingly, and based on the numerical results it is concluded that crack deflection may occur only occasionally for configuration C1 since the energy and fracture toughness ratios are close to being equal.

Configurations C2 and C3 represent an effort to increase the straight (horizontal) path interface fracture toughness by inserting/embedding glass fibres reinforced with epoxy resin in the interface between the peel stopper and the face-sheet. The aim of this was to reduce the fracture toughness ratio $\frac{\Gamma(\psi)_{deflected}}{\Gamma(\psi)_{straight}}$. . For a crack to propagate along the horizontal path at the peel stopper tip it has to first break the glass fibres at the straight path interface. In both configurations C2 and C3 the increase of fracture toughness is local, i.e. it only occurs around the peel stopper tip where the fibres are sticking out or placed in front of the peel stopper. Even though, from Figure 26, the energy release rate ratio is $\frac{G\_deflected}{G\_straight} = 0.75$ at the tested peel stopper angle of 10°, the Mode I fracture toughness of the fibres is several times higher than that of the epoxy resin [60].

Finally, it can be seen that by increasing the peel stopper angle crack kinking at the tri-material junction (peel stopper tip) becomes more difficult, especially for configurations C2 and C3. For the case of $\theta = 10^o$ investigated experimentally in this research, the fracture toughness ratio needed for achieving deflection is similar for configurations C2 and C3, while for configuration C1 the required fracture toughness ratio is higher. Figure 25 shows that the mode-mixity remains highly Mode I dominant, which means that the interface fracture toughness of each crack path is close to its Mode I fracture toughness

Based on the results of this study the peel stoppers used in subsequent tests are made using configuration C2. Even though configuration C3 demonstrated the same level of efficiency in promoting crack deflection as configuration C2, it is a far more complex solution to fabricate and implement.

CHAPTER 6. SANDWICH TEAR TEST – FATIGUE LOADING (PAPERS #2 AND #3)

The work presented in this chapter has been published in the papers by Martakos et al [54,55], which are appended as Papers #2 and #3 in the appendix of this thesis.

As explained in a previous chapter, the MMB test does not allow for testing interface crack propagation for very large crack lengths. In the previous study, this prohibited the crack from advancing until (and beyond) the physical boundary of the peel stopper. To circumvent this problem, in this study the STT set-up (Sandwich Tear Test [54]) was chosen due to its ability to allow for very large crack lengths. A drawback (or rather a validation challenge) of the STT test, when comparing with numerical simulation results, is that the physical crack propagation parameters, i.e. the energy release rate and mode-mixity, cannot be specified independently during the testing. Thus, when using the STT test, the crack is allowed to propagate freely without any control over the energy release rate or mode-mixity being possible.

The performance of the peel stopper has been evaluated based on its ability to achieve crack arrest for a high number of loading cycles. Insight from the initial 3-point bending tests (described in chapter 4) that showed that the post arrest behaviour of the interface crack leads to a new crack initiation behind the peel stopper has been used to design the test procedure such that a deeper understanding of the peel stopper behaviour can be obtained. The assess the crack arrest and post arrest behaviour quantitatively Digital Image Correlation (DIC) was used to link the strain distribution on the sandwich specimen in the vicinity of the crack arrest directly to the performance of the peel stopper. The STT test set-up and specimen are sketched in Figure 27 showing specimen dimensions, as well as the applied force in the middle, and the boundary conditions imposed at the edges of the sandwich beam specimens. In the STT set-up the initial debond is covering half the specimen length, and initial debond was generated using a thin Teflon foil on half of the face sheet/core interface as shown in Figure 27.

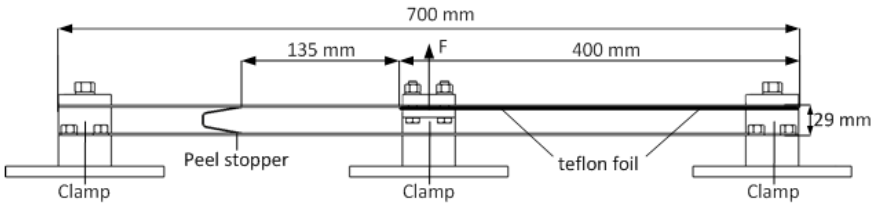

Figure 27. STT specimen dimensions and test setup, [54].

6.1. FATIGUE TESTING CONFIGURATION ([54])

A four-column 100 kN MTS 319.25 with a T-slot table operated by a MTS FlexTest 60 controller and equipped with a 10 kN load cell was used to mount and load the

STT specimens for both quasi-static and fatigue load testing. At the edges of the sandwich beam specimen Divinycell H100 foam (which was used for the previous tests) was replaced by wooden inserts to enable the imposing of appropriate clamping conditions (Figure 28). Two digital cameras were placed on one side of the STT beam specimens to monitor the crack tip region of interest using DIC. The DIC system ARAMIS 4M from GOM Gmbh was used to track crack propagation and strain evolution through the fatigue experiments. In Figure 28, the STT setup and DIC system are shown. Images of the area of interest were taken with an interval of 60s for the entire duration of the experiment.

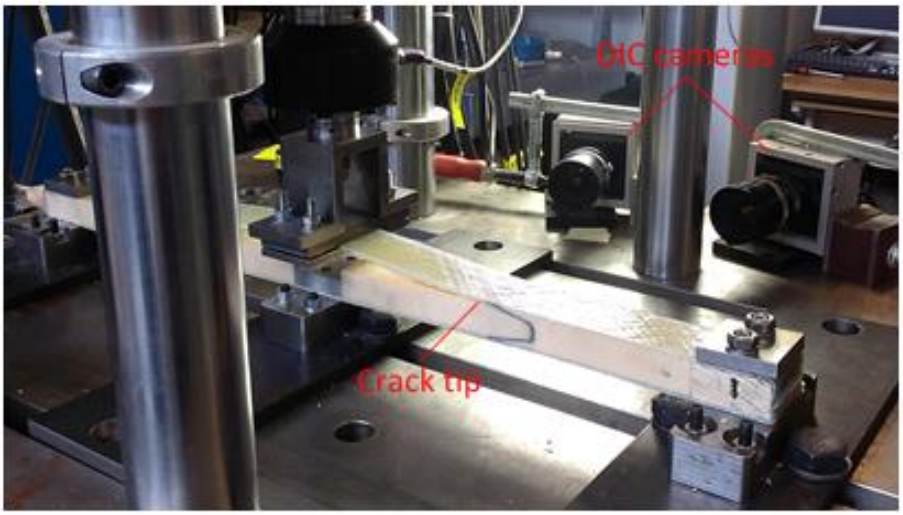

Figure 28. DIC camera set-up and STT test setup, [54].

The STT crack growth behaviour makes it difficult to test under displacement controlled fatigue loading conditions due to the large increase in displacement that occur as the crack length increases. Due to this, load control was chosen for the fatigue testing. Since the load required to propagate the face/core interface crack changes significantly during the test, the propagation of the crack in fatigue was conducted using two different fatigue load amplitudes. The initial fatigue load sequence (Sequence A) corresponds to the average minimum load needed to propagate the crack under quasi-static loading conditions. The second fatigue load sequence (sequence B) corresponds to the average load that caused initiation of a new (and second crack) behind the crack stopper when the initial crack had been arrested. The fatigue load sequences were chosen such that they represented approximately 80% of the imposed quasi-static loads through most of the duration of the experiments. Prior to the fatigue tests quasi-static tests were conducted to identify the loads required to achieve crack propagation, Figure 29.

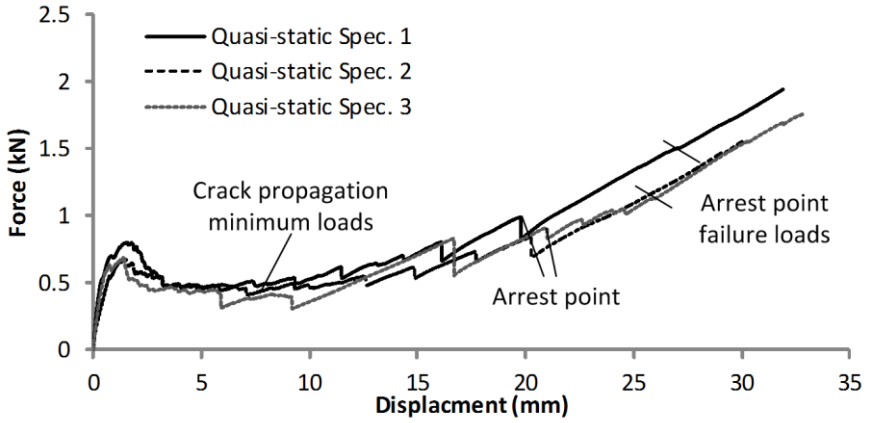

Figure 29. Quasi-static test results for fatigue load identification. Force-displacement relation, [54].

The fatigue tests were conducted at a load ratio of *R=0.2* and a frequency *f=2 Hz*. Table 6 summarizes the observed loads from the quasi-static tests and the chosen fatigue load amplitudes, load ratios and loading frequencies. A total of 3 quasi-static and 4 fatigue tests were conducted. The manufacturing of the peel stoppers and the test specimens is described in chapter 3 of this thesis.

Table 6. STT Quasi-static and fatigue test configuration, [54].

	Crack propagation minimum load (N)	Arrest point failure load (N)
Quasi-static Specimen 1	437	1120
Quasi-static Specimen 2	457	1040
Quasi-static Specimen 3	452	1410
Static average	448	1190
Fatigue test data	Initial fatigue load Sequence (A)	Second fatigue load Sequence (B)
Fatigue maximum load	380	950
Fatigue minimum load	76	190
Load Ratio	0.2	0.2
Frequency	2 Hz	2 Hz

6.2. EXPERIMENTAL RESULTS ([54])

The observed crack propagation path in the sandwich specimens is shown in Figure 30 (a-d). The crack propagated along the face sheet/foam core interface immediately below the resin rich layer just below the face sheet, until it reached the peel stopper tip, Figure 30 (c). After this point the crack continued to propagate in the PU/foam interface after it was deflected by the peel stopper. Finally, the crack was arrested towards the end of the peel stopper, Figure 30 (d).

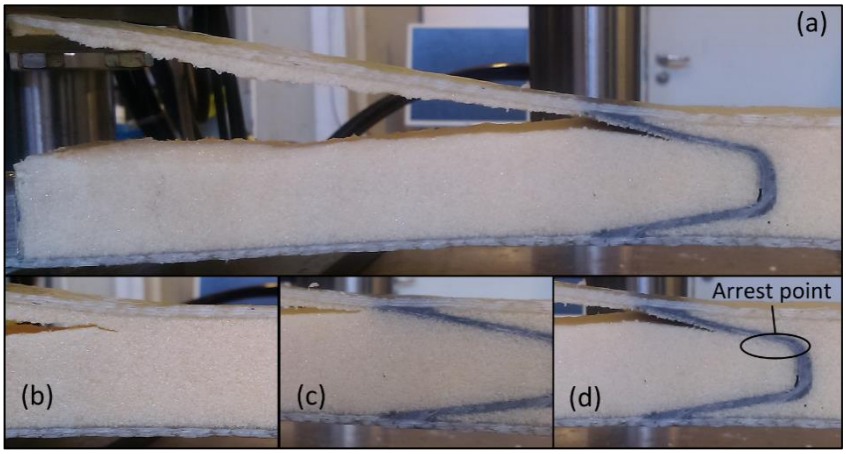

Figure 30. (a) Crack propagation in STT specimen and peel stopper. (b) Crack propagation in/near the face-sheet/foam core interface. (c) Crack propagation close to the peel stopper tip. (d) Crack propagation in the PU-foam interface near the crack arrest point, [54].

The vertical face sheet displacement during the fatigue experiment is plotted against the number of loading cycles for all four specimens in Figure 31. When the propagating interface crack reached the peel stopper tip the load was increased which led to an abrupt change of specimen displacement. The number of cycles until occurrence of crack arrest was identified from the recorded images (used for DIC) to assess the effect of the peel stopper. From Figure 31 is observed that, as opposed to the 3 point bending tests (chapter 4 of this thesis), the compliance of the specimens did not change much during the time (cycles) where the crack was arrested. This is attributed to the fact that only one crack front, namely the one that was arrested, existed in the specimens.

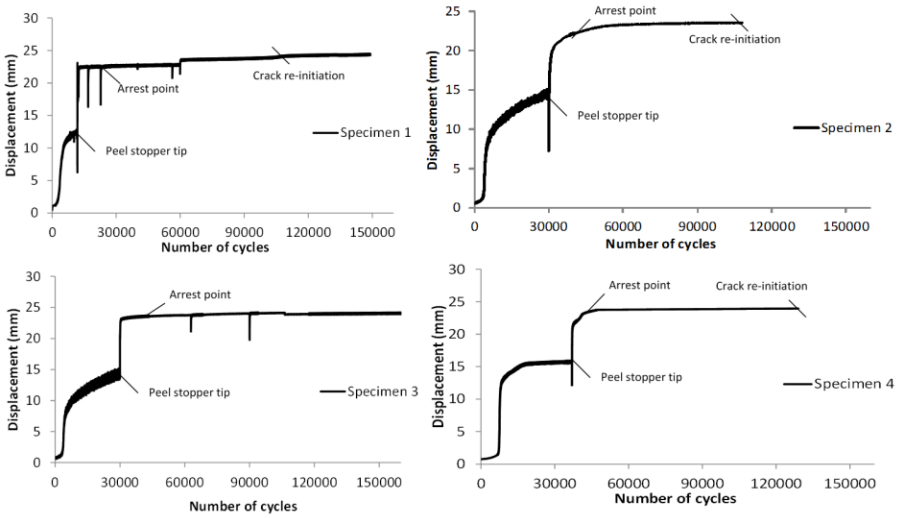

Figure 31. Vertical displacement vs. number of loading cycles obtained for the four STT specimens, [54].

A summary of the observations made from Figure 31 is given in Table 7. The number of cycles to crack arrest, crack re-initiation and total number of cycles are given for all specimens in order to assess the peel stopper efficiency.

Table 7. Observed number of cycles at the arrest point, [54].

Specimen	Number of cycles to crack arrest point	Number of cycles until crack re-initiation	Total number of cycles	$\frac{\text{Cycles to arrest}}{\text{Total life}}$ %
Specimen 1	22,136	81,432	103,568	78,62
Specimen 2	42,905	65,197	108,102	60,31
Specimen 3	46,000	< 114,000	160,000	< 71,25
Specimen 4	51,547	77,489	129,036	60,05

From the 3rd column in Table 7 it is seen that the lowest number of loading cycles to crack arrest observed was 65,197. This represents at least 60% of the total test duration, which includes propagation of the crack in the both face sheet/core and the PU/core interfaces. Thus, it is evident that the peel stopper increases the overall fatigue life of the tested sandwich beams significantly. In Figure 32, the major principal strain field is plotted for all four specimens at the loads and number of cycles corresponding to crack arrest after the crack has been deflected away from the

face/core interface. It is observed that a strain concentration appears on the back side of the crack arrester corresponding to the arrest point in the core material. It is hypothesized that this strain concentration (which is linked to a corresponding stress concentration) is causing the initiation of a new crack in the foam core material behind the crack arrester.

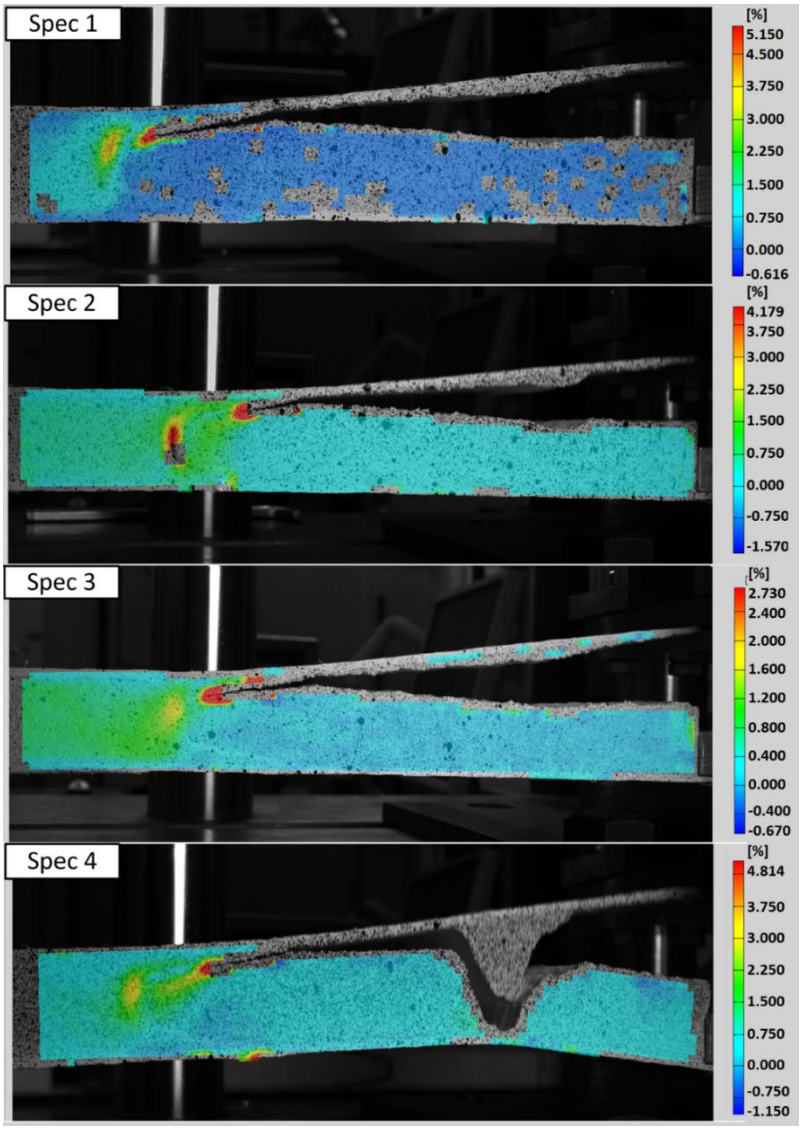

Figure 32. Major principal strain fields corresponding to crack arrest in STT specimen surfaces measured using DIC. In addition to the strain concentrations near the crack tip, a strain concentration appears behind the peel stopper, [54].

Table 8 summarizes the largest values of the major principal strains observed at the crack re-initiation point behind the peel stopper when the peak fatigue load was applied to each specimen.

Table 8. Maximum major principal strain at crack re-initiation point extracted from the DIC measurements, [54].

Specimen	Major principal strain %
Specimen 1	4.037
Specimen 2	4.225
Specimen 3	1.910
Specimen 4	4.819

Figure 33 shows an S-N curve obtained from four-point bending of sandwich beam specimens investigating the fatigue behaviour of H100 PVC foam core material subjected to shear loading [61].

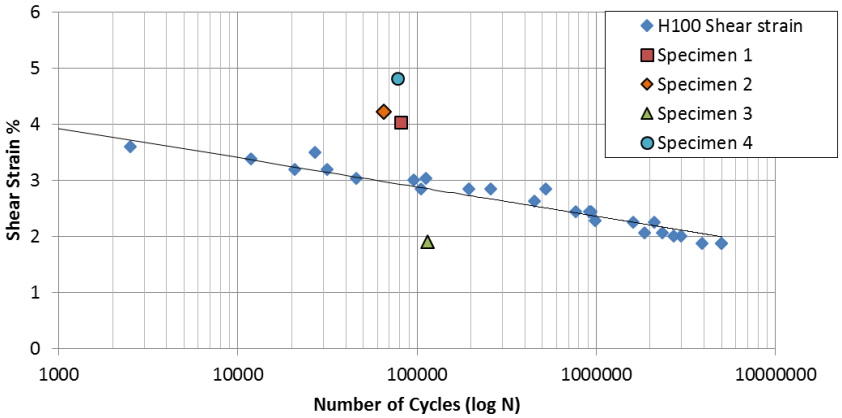

Figure 33. Fatigue data (shear strain vs. number of cycles) for Divinycell® H100 foam core material [61] and major principal strains vs. number of cycles when the crack was arrested before initiation of a new crack for sandwich beam specimens tested using the STT setup, [54].

The maximum major principal strains measured using DIC at the crack re-initiation point behind the peel stopper for test specimens 1, 2, 3 and 4 are also plotted in Figure 33. From Tables 7 and 8 and Figure 33 it is observed that the interval of loading cycles where the crack remains arrested is higher than suggested by the pure shear fatigue data for specimens 1, 2 and 4. For specimen 3, crack re-initiation was not observed at all, and therefore the interval of load cycles where the initial crack remained arrested before crack re-initiation is higher than observed for specimens 1,

2 and 4. The comparison of the shear and major principal strains is meaningful since the shear strain fatigue data for the Divinycell H100 foam were derived from sandwich beam four-point bending tests where damage initiated at the centre of the core [61]. The major principal strain at this location in a sandwich beam loaded in four-point bending is identical to the shear strain.

6.3. FINITE ELEMENT MODELLING ([55])

The finite element modelling was conducted using the commercial FE package ANSYS 15.0 [59]. The FE model was used to predict the crack loading conditions including the energy release rate (ERR) and the mode-mixity phase angle as functions of the crack length. To simulate fatigue crack growth in the face sheet/foam and PU/foam interfaces a re-meshing algorithm was used. Since the crack in all the experiments propagated along the face sheet/core interface until it reached the peel stopper tip, after which the crack was deflected along the PU/core interface, the debonded area in the FE simulations follows the path of the peel stopper angle (see Figure 34 a). The FE model represents the STT setup without including the unloaded specimen region below the debonded face sheet on the left side of the specimen, see Figure 34 a. The peel stopper was meshed in the core structure such that it shared nodes with the foam core elements. In Figure 34 b-d the crack tip elements are shown at different states of crack propagation, while in Figure 34 e-g the respective states are shown in a physical and tested STT specimen.

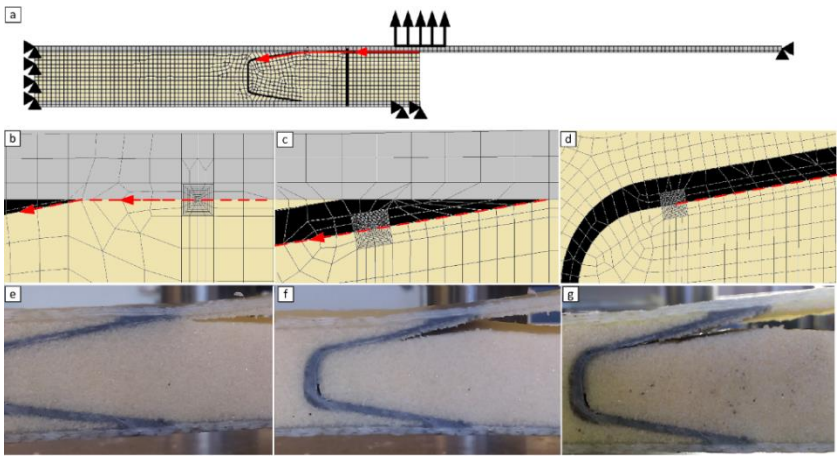

Figure 34. a) STT finite element model representation: b) and e) Crack propagating at face-sheet/foam interface; c) and f) Crack propagating at the PU/foam interface; d) and g) Crack at the arrest point, [55].

The FE mesh was created using 8-node plane strain elements (PLANE 183) with a global element size of 1 mm. The crack tip was meshed using element sizes down to

10 μm at the bi-material interfaces. The face sheet and foam materials were modelled as orthotropic, while the PU/glass fibre reinforced material of the peel stopper for simplicity was homogenised and modelled (approximated) as isotropic. Geometric nonlinear behaviour was included in the FE-models to capture the in-plane membrane stresses developed in the face sheet due to large vertical displacements.

6.4. FINITE ELEMENT RESULTS ([55])

Figure 35 shows the test machine actuator piston displacement measured for all four STT specimens, and the FE model predictions corresponding to the load application point on the debonded face-sheet plotted against number of cycles for loading sequences A (F_{max}=380 N) and B (F_{max}=950 N), respectively (corresponding to crack propagation as indicated in Figure 34 a and b). The first part (left side) of the plot (Sequence A) represents the fatigue response of the specimens during propagation in the face/core interface and the initial stage of the fatigue life of the specimens. The second part to the right (Sequence B) represents the fatigue response after deflection of the crack into the PU/core interface.

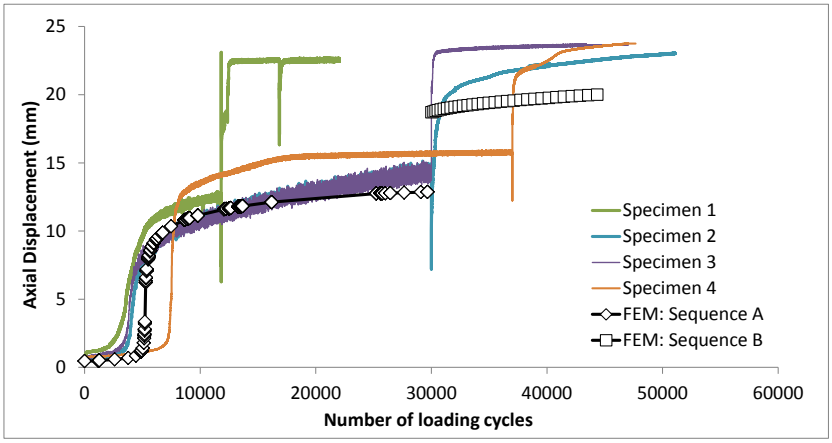

Figure 35. Vertical displacement (test machine actuator piston) vs. number of loading cycles; experimental data and FE model predictions, [55].

6.5. ENERGY RELEASE RATE AND MODE-MIXITY ([55])

Figure 36 and Figure 37 show the evolution of the ERR and mode-mixity phase angle as function of the crack length (Figure 36) and number of loading cycles (Figure 37). It is observed that the ERR increases considerably with increasing crack length until it reaches a maximum. Past this point the vertical displacements of the debonded face sheet have become so large compared to the face-sheet thickness that

the in-plane membrane forces in the face sheet become dominating and thus affect the load response. Effectively the induced membrane forces stiffen the face sheet and specimen response significantly (geometrically nonlinear effect) and consume the majority of the strain energy in the specimen, and consequently reduce the resulting ERR at the crack tip. This is the reason why it was decided to increase the imposed load at stage b (see Figure 34– corresponding to load Sequence B), when the crack propagated into and along the PU/foam interface. The higher load counteracts the increased resistance to out of plane displacements of the face-sheet due to the membrane forces. If the load amplitude had been kept constant as per Sequence A, the crack would arrest due to the continuously decreasing ERR. The observed abrupt change in ERR, seen from both the FE results and the experimental observations, is a result of this sudden increase of the imposed load. It is further observed that the ERR decreases again until the crack arrest point is reached.

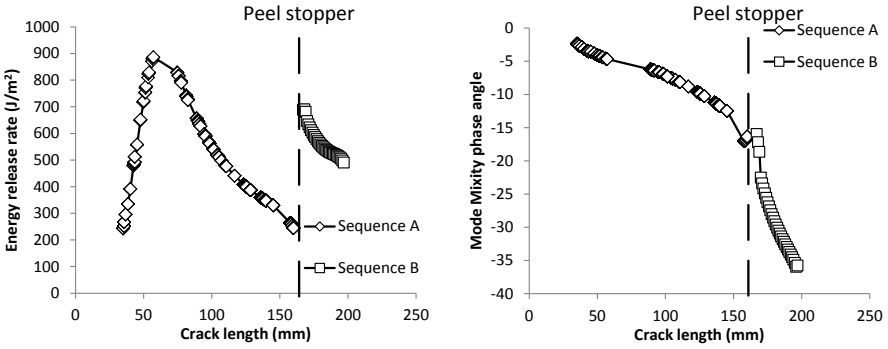

Figure 36. Energy release rate and mode-mixity phase angle vs. Crack length for loading sequences A and B, [55].

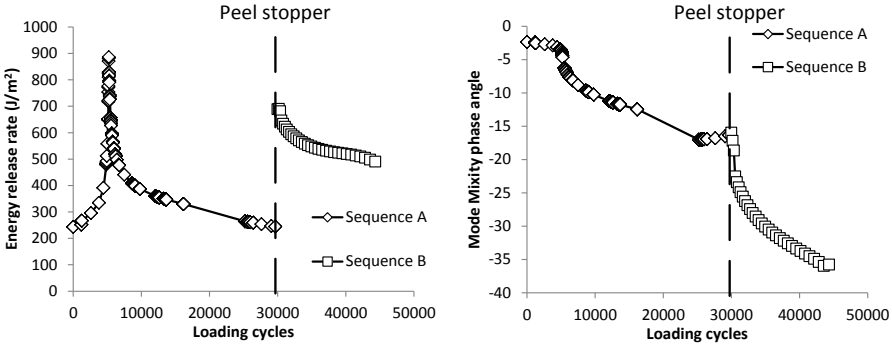

Figure 37. Energy release rate and mode-mixity phase angle vs. Number of loading cycles for loading sequences A and B, [55].

6.6. STRAIN CALCULATION ([55])

The major principal strains in the core material behind the peel stopper have been derived from the FE analysis of the STT specimen with the crack located at the arrest point, i.e. stage c (cf. Figure 34). Figure 38 shows the field of major principal strains obtained from the DIC measurements for specimens 1-4 during the fatigue tests, and the corresponding field of major principal strains predicted using the FE model. It is observed that the characteristic strain concentration observed in the core material on the back side of the peel stopper in the experiments is also observed from the FE simulation results. Moreover, the FE model predicts principal strain values that are close to the average of the values measured using DIC. In all cases the observed strain concentrations are caused by local bending of the peel stopper and are not the result of the stress concentrations at the crack tip.

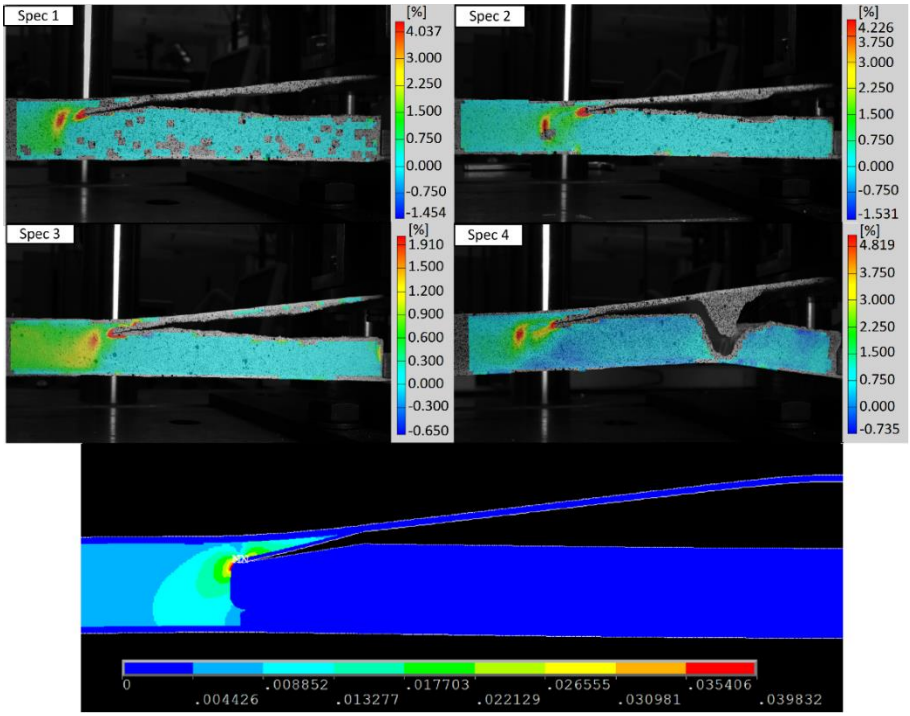

Figure 38. Comparison of FE predictions and measured major principal strain fields (DIC) at crack re-initiation behind the peel stopper, [55].

To predict the crack arrest time, i.e. the number of cycles between crack arrest and crack re-initiation behind the peel stopper (i.e. number of cycles where the crack remains at stage (c), Figure 34), it is necessary to relate the peak strain values to the occurrence of crack re-initiation. Since the development of a crack re-initiation modelling algorithm was not part of this work, the estimation of the remaining

fatigue life has been conducted through the use of fatigue data obtained for the Divinycell® H100 PVC foam material (see Figure 33), [58], [61]. The FE model was used to predict the major principal strain field, as depicted in Figure 39, for several different crack lengths extending between the peel stopper tip and the crack arrest point.

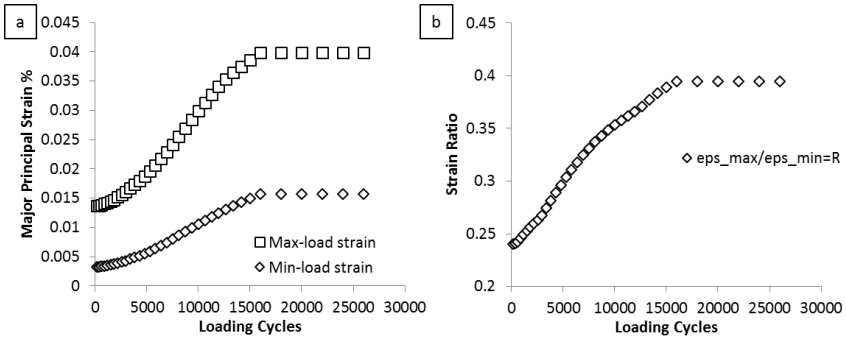

Figure 39. Major principal strains and the strain ratio at the crack re-initiation point corresponding to the maximum and minimum fatigue load levels during fatigue testing vs. number of load cycles, [55].

To estimate the total time of crack arrest (or the number of cycles between crack arrest and crack re-initiation) based on the calculated strains, shear strain fatigue data for H100 Divinycell PVC foam derived from four-point bending tests were considered according to [58], [61]. The stress ratio, or equivalently the strain ratio, during the fatigue tests was defined at R=0.1. To account for the effect of the strain ratio on the fatigue damage accumulation in the foam, and to effectively compare the strains calculated from the FE analyses with the H100 fatigue data, the maximum to minimum strain difference (or strain range) was calculated:

$$\Delta\varepsilon = (1 - R) * \varepsilon_{max} \quad (1)$$

,where ε represents the shear strain obtained from the fatigue data, as well as the major principal strains obtained from both the DIC measurements and the FE analyses. Figure 40 shows observed strain range vs. the number of cycles (observed experimentally using DIC and predicted using FE analysis) when the crack was arrested (between crack arrest and re-initiation) in comparison with the H100 shear fatigue data. The shear fatigue data curve in combination with the calculated FE model strain have been used to predict the number of cycles before crack re-initiation at the crack arrest point, and this is also shown in Figure 40 (orange circle).

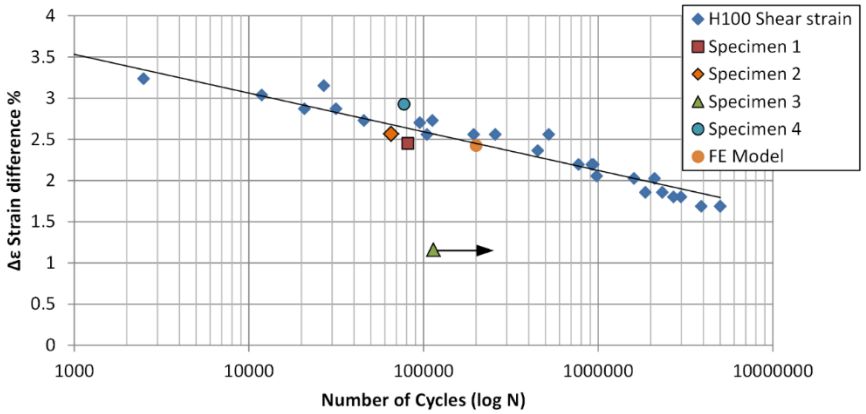

Figure 40. Strain range vs. Number of cycles while the crack is arrested; measurements, FE model results and comparison with H100 shear fatigue data, [55].

6.7. CONCLUSIONS

The Sandwich Tear Test (STT) together with DIC was used to evaluate the crack arrest effect of the peel stopper, as well as the identification of the mechanisms of crack re-initiation on the back side of the peel stopper. The proposed peel stopper was found to perform well under fatigue loading conditions. The observed crack propagation paths can be divided into 3 phases: (1) Firstly the propagating initial face sheet/core interface crack was deflected away from the face sheet/core interface when reaching the peel stopper tip; (2) the crack was arrested inside the peel stopper and remained arrested for more than 67% (average of 4 tests) of the total duration of the fatigue experiments; (3) finally a new crack was initiated in the core material behind (backside) the peel stopper. Investigation of the strain distribution in the vicinity of the crack arrest area suggests that the post-crack arrest behaviour was determined by the fatigue properties of the foam core material used in the STT specimens. This further suggests that the efficiency and overall performance of the proposed peel stopper are highly dependent on the local strains developed in the core material on the back side of the peel stopper behind the arrest point.

From Figure 40 it is observed that according to the FE model predictions the average STT (sandwich) specimen could be expected to withstand a total of approximately 200,000 load cycles in the crack arrested state before crack re-initiation would occur. This corresponds to almost 3 times the number of cycles to crack arrest, and this effectively implies that the embedded peel stopper has almost doubled the expected fatigue life of the specimens in comparison with sandwich specimens without embedded peel stoppers. The four sandwich beam specimens tested experienced between approximately 65,000 and 114,000 load cycles at the crack arrest state, and this implies that FE-model in combination with the H100 fatigue data overestimates the number of load cycles to crack re-initiation. The likely reason

for this is that the fatigue shear data for the H100 PVC that was used together with the FE model was obtained from a four-point shear test, and this test configuration does not provide an accurate representation of the stress/strain state at the crack re-initiation point behind the peel stopper. This demonstrates that the performance and efficiency of the peel stopper concept proposed is very sensitive to the actual strain state developing at the crack re-initiation point. Accordingly, a small change (reduction) of the peak strains developing behind the peel stopper, which can be achieved by careful design optimisation of the peel stopper geometry/configuration, has the potential of increasing the expected fatigue life considerably.

CHAPTER 7. PANEL TESTING (PAPER #4)

The work presented in this chapter has been published by Martakos et al. [56], which is appended as Paper #4 in the appendix of this thesis.

The implementation of the new peel stopper in sandwich panels (plates) represent the last step of this study. The double-sided peel stopper has been embedded in sandwich panels as specified in Chapter 3, Figure 13 and Figure 14 in order to examine the ability to prolong the fatigue life of sandwich plate/panel structures that are much more realistic in a practical engineering design context than sandwich beams as investigated in this study in three-point bending, MBB and STT configurations (chapters 4, 5 and 6 of this thesis). In this study quadratic and simply supported sandwich panel specimens with embedded peel stoppers were loaded in bending by a single force applied at the panel/plate centre. A quadratic sandwich panel configuration, a concentric circular peel stopper and a central external load was selected to achieve a nearly axisymmetric strain and stress field in the vicinity of the plate centre and the peel stopper. The sandwich panel/plate dimensions were chosen such that edge effects from the four straight edges did not influence the strain and stress fields near the crack stopper.

Figure 41 shows the sandwich panel specimen including concentric peel stopper. An initial debond/crack was induced into the centre of the panel specimens around the steel insert that was imbedded to apply the external loading, see Figure 41. The concentric debond/crack was introduced to promote propagation from the centre towards the boundaries of the specimen.

7.1. TEST CONFIGURATION ([56])

The tests were conducted using a Schenck 400 kN servo-hydraulic test machine with an Instron 8800 controller. A 10 kN load cell was mounted in the machine to improve the load control accuracy during the tests. Figure 42 shows the test set-up, including load application through a central insert and the square shaped steel test rig providing the simply supported boundary conditions imposed along the panel edges. As indicated in Figure 42, the sandwich panels were simply resting on the square shaped steel test rig, providing approximate simple support conditions along the four panel edges. Rubber strips were attached to the supporting flat steel surfaces of the test rig, and the specimens rested on these rubber strips to avoid indentation damage during testing. The mounted test rig was placed as high as possible to maximize the distance between the hydraulic actuator at the bottom of the test frame and the underside of the panel specimen. This was done to maximize the viewing area of the 2 digital cameras facing upwards towards the panel specimens and used for DIC measurements.

The self-similar crack propagation behaviour in all the tested specimens allowed for high consistency and repeatability throughout the tests, and thus reduced the number of test repetitions required. Three tests were conducted under load controlled fatigue conditions with an R-ratio of R=0.1; two specimens with embedded peel stoppers (PLP1 and PLP2), and one specimen without a peel stopper (PLT2). In addition, one sandwich panel specimen was tested subject to quasi-static loading in order to derive the appropriate load amplitudes imposed in the fatigue tests. Table 9 summarizes the fatigue loading conditions applied to the 4 sandwich panel specimens.

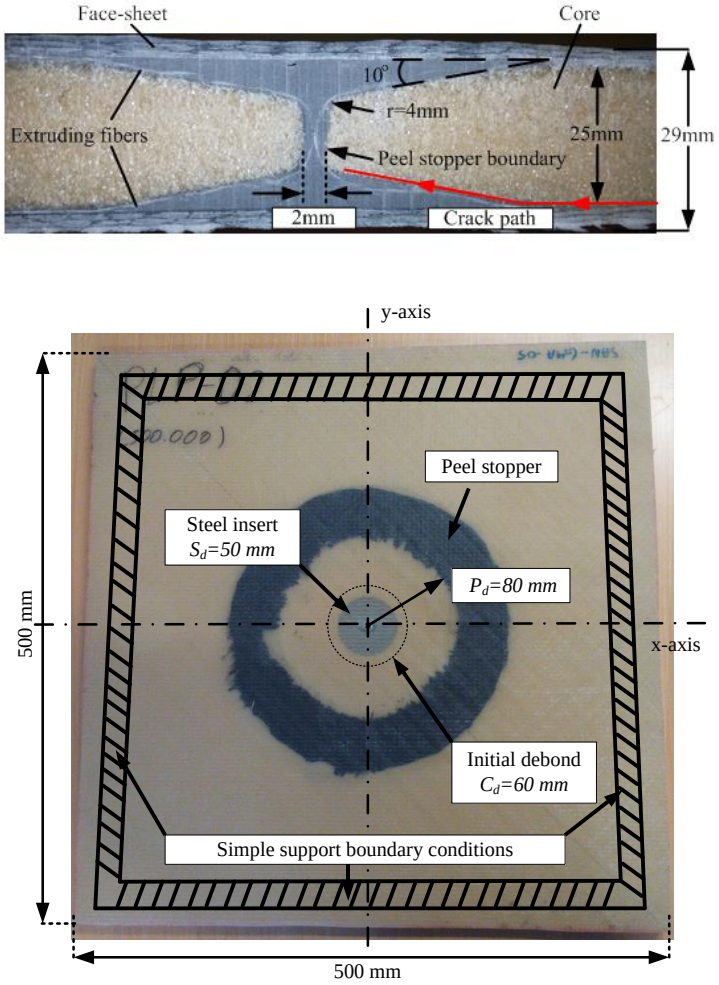

Figure 41. Layout and dimensions of foam cored sandwich panel test specimens with embedded PU peel stopper, [56].

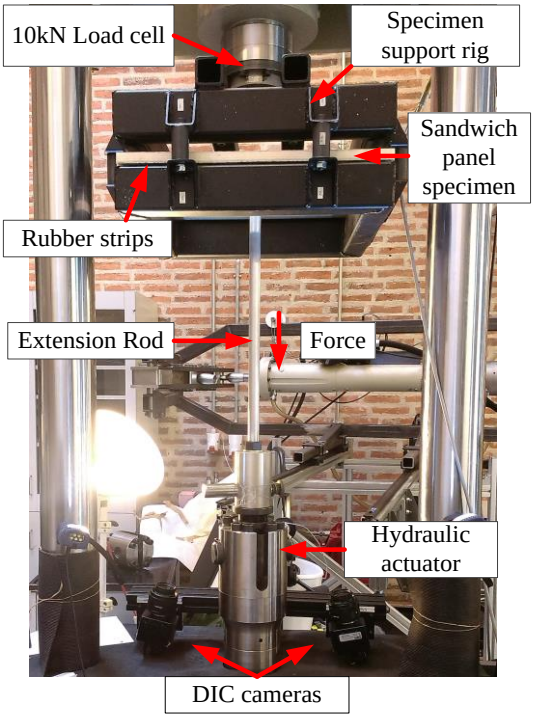

Figure 42. Sandwich panel testing setup and DIC setup of the tested sandwich panels, [56].

Table 9. Fatigue loading configuration, [56].

Fatigue test data	Fatigue load
Fatigue maximum load	3800 N
Fatigue minimum load	380 N
Load Ratio	0.1
Frequency	2 Hz

7.2. TEST RESULTS

The specimen without embedded peel stoppers was tested up to 250,000 cycles, while the specimens including peel stoppers were tested up to 500,000 cycles. This was done to demonstrate the crack arrest ability of the peel stopper, and further to show the ability to contain damage under high cycle fatigue loading conditions. The evolution of the displacements during the tests has been recorded and plotted against the number of loading cycles in Figure 43. Since the applied force was of constant

amplitude, the resulting displacement could be directly linked to the compliance of the specimens and thus the damage growth inside the sandwich panel structure.

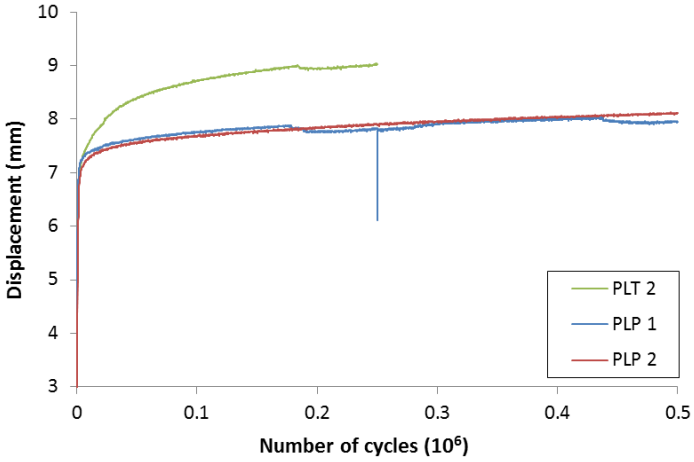

Figure 43. Measured piston displacement vs. number of cycles for the three fatigue tested sandwich specimens, [56].

Since it was not possible to observe the crack length (or radius) inside the sandwich panels during the actual tests, displacement profiles observed by DIC during the tests was used to track the crack front after the experiments were finished. Thus, by extracting the out-of-plane displacements, the crack front location was estimated. Reference is made to [56] for the details about how this was achieved. Figure 44 shows the crack length to number of cycles relation as calculated based on the images captured by the DIC system.

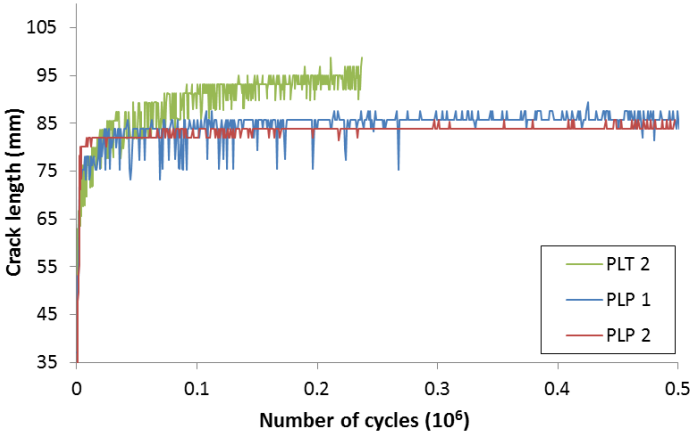

Figure 44. ”Corrected” interface crack length (radial direction) vs. number of load cycles, [56].

From Figure 43 and Figure 44 it is observed that the interface crack growth was significantly influenced (delayed) by the presence of a peel stopper. To verify the experimental observations, the sandwich panel specimens were cut up after the tests to inspect the crack paths. Figure 45 shows two section cuts from specimens PLP2 (below - with peel stopper) and PLT2 (top - without peel stopper). The two cut sections are aligned so that the loading points of the two specimens are coinciding. For specimen PLT1 it is observed that no crack deflection occurred, while it is observed that crack deflection occurred for specimen PLP2. The interface cracks in both specimens were measured and compared with the crack lengths extracted from the DIC data. For both cases the DIC measurements were very close to the crack lengths observed from the cut specimens. The crack in the panel without a peel stopper (PLT2) propagated up to about 100 mm during 250,000 loading cycles, thus exceeding the peel stopper boundaries (96 mm). For the panel with an embedded peel stopper (PLP2) the interface crack was measured to be about 87 mm long after a total of 500,000 loading cycles.

Figure 45. Post mortem sections of sandwich panel specimens PLT2 (above – no peel stopper) and PLP2 (below - with embedded peel stopper), [56].

7.3. FINITE ELEMENT ANALYSES ([56])

A three dimensional (3D) Finite Element (FE) model was developed in the commercial software package ANSYS 15.0 [59]. The model was developed to simulate crack growth in the sandwich panel specimens with and without peel stoppers subjected to fatigue loading conditions. To capture the 3D nature of the problem, the crack propagation in the face/core and core/PU interfaces were modelled by means of a 3D crack front. By using the mesh at the crack tip, the CSDE mode-mixity method (described in Chapter 2) was used to extract the energy release rate and mode-mixity along the crack tip front. Each nodal point was able to move independently in a direction perpendicular to the crack front depending on the

energy release rate and mode-mixity values, respectively. As shown in Figure 46 the crack front always propagated along the x-axis of the local coordinate system, i.e. always perpendicular to the crack front curvature. By the use of a re-meshing algorithm, the 3D crack propagation inside the sandwich panels was simulated.

Figure 46 and Figure **47** show the detailed 3D FE models for both the specimens with and without peel stoppers. Only one quarter of the sandwich plate specimens were modelled due to double-symmetry of the test specimens. The main panel model consisted of 8.000-14.000 20-node solid elements, depending on the radius of the crack front modelled. Geometrical non-linear analyses were conducted to accurately account for the large displacements and rotations of the debonded face-sheet during the experiments, as well as the significant membrane effects that developed in the debonded face-sheet during the fatigue sequence.

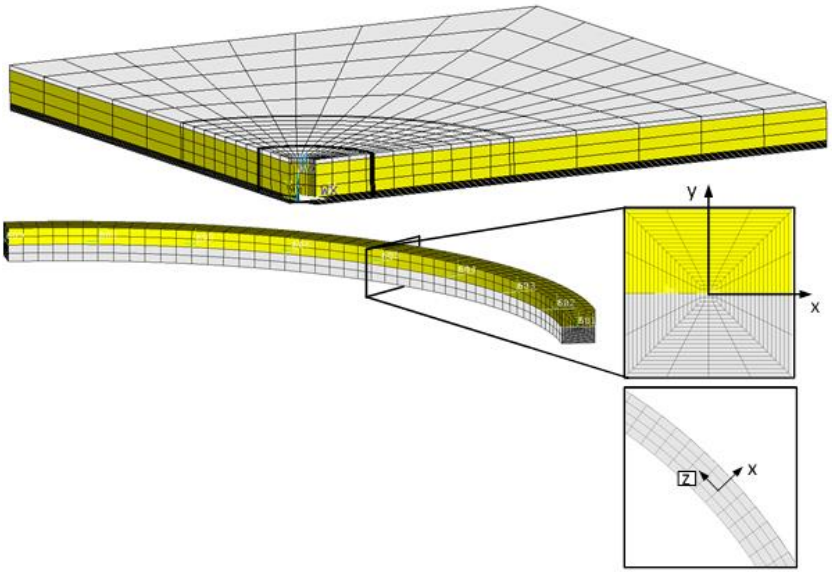

Figure 46. Global FE model of a sandwich panel specimen without a peel stopper (left), and FE sub-model and crack tip mesh along the crack front (right), [56].

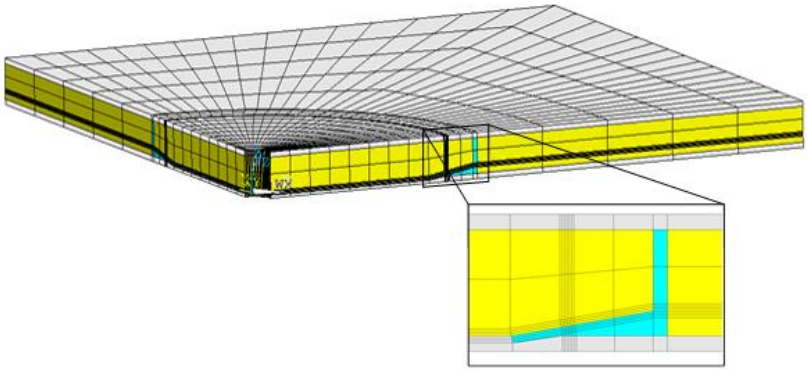

Figure 47. Global FE model of a sandwich panel specimen with an embedded peel stopper, and detailed meshing around the peel stopper, when the interface crack has been deflected, [56].

7.4. FINITE ELEMENT RESULTS [56].

The predicted loading point (vertical) displacement and the interface crack length evolution during the fatigue testing are shown in Figure 48 and Figure 49 for sandwich panels with and without embedded peel stoppers. The crack length data have been extracted from the FE model at the location of the crack front nodal points parallel to the x-axis (see Figure 41). Figure 48 shows that the FE modelling was able to capture the initial steep rise in displacement as well as the plateau that was reached at the final stages of the fatigue experiment. In a similar manner it is observed from Figure 49 that the FE model was capable of predicting the crack propagation rate with reasonable accuracy during the entire fatigue experiment for the specimens with embedded peel stoppers. However, for the panel specimen without peel stoppers the FE model over-predicted the crack growth. The likely explanation for this is the large geometrically non-linear effects that may not be captured accurately at very large crack lengths (i.e. large radial crack extensions).

The fatigue testing was limited to 500,000 loading cycles (for specimens PLP1 and PLP2 with embedded peel stoppers). To develop a further understanding of the effect and performance of the embedded peel stoppers, the FE simulation of the fatigue process together with the fatigue crack propagation algorithm has been used to extrapolate beyond 500,000 loading cycles. Figure 50 and Figure **51** show the predicted ERR and mode-mixity against number of cycles and crack length, respectively. The fatigue experiments were simulated up to 2 million loading cycles, which is considered to be a realistic expected fatigue life for many foam cored composite sandwich structures.

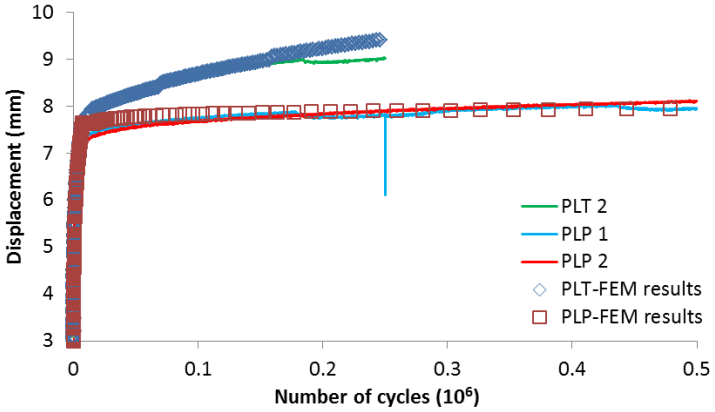

Figure 48. Central displacement for specimens PLP1, PLP2 (with embedded peel stoppers) and PLT2 (without peel stopper) vs. number of loading cycles; FE model predictions and experimental results (piston displacement of test machine), [56].

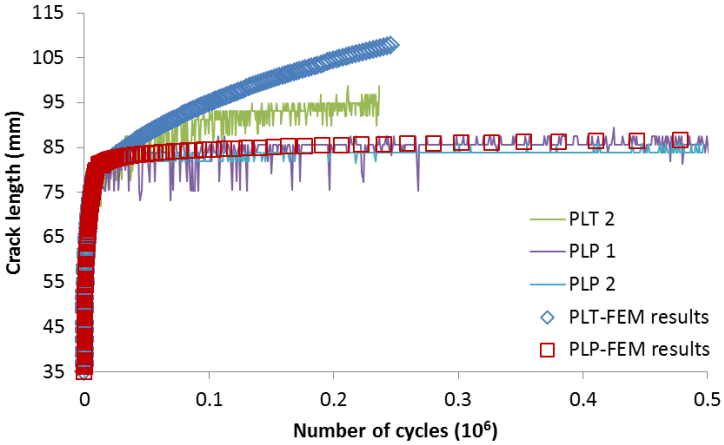

Figure 49. Interface crack length evolution vs. number of loading cycles; FE predictions and experimental results for specimens PLP1, PLP2 (with embedded peel stoppers) and PLT2 (without peel stopper), [56].

From Figure 50 and Figure 51 it is observed that the ERR drops significantly after the propagating interface crack has been deflected by the peel stopper, whereas the mode-mixity increases. Figure 50 shows that the ERR reaches a plateau which is associated with a drastic decrease in crack growth rate, when the propagating interface crack reaches the peel stopper (corresponding to approximately 25,000 cycles and a crack length of 80 mm). It is further seen that the mode-mixity increases continuously at a very low rate throughout the fatigue process. Figure 51 provides further information about the behaviour of the sandwich panel specimens in the earlier stages of the fatigue process. Thus, it is observed that the ERR is very high for small interface crack lengths, and that it decreases considerably as the crack

propagates. This explains the very high propagation rate observed at the beginning of the fatigue process, as well as the crack arresting effect when the radial extension of the crack (the crack length) becomes larger. It is further observed that the mode-mixity increases slightly during crack propagation in the face/core interface, and that the mode-mixity increases significantly, when the interface crack deflects into the core at the peel stopper tip. This can be explained by the change in the angle of crack propagation, as the interface crack is forced to propagate at an angle of 10^{o} relative to the face-sheet. This increases the shear component (mode II) of the propagating crack front, since the crack naturally tends to propagate towards the lower face-sheet under such loading conditions.

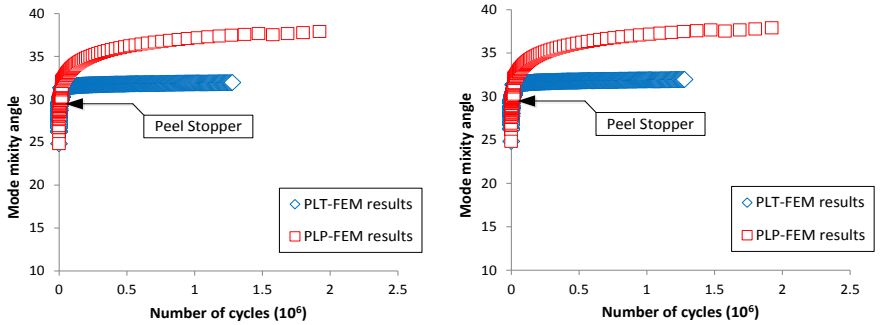

Figure 50. FE simulation of the fatigue process in the sandwich panel specimens with (PLP) and without peel stoppers (PLT): ERR and mode-mixity vs. number of loading cycles for up to 2×10^{6} cycles, [56].

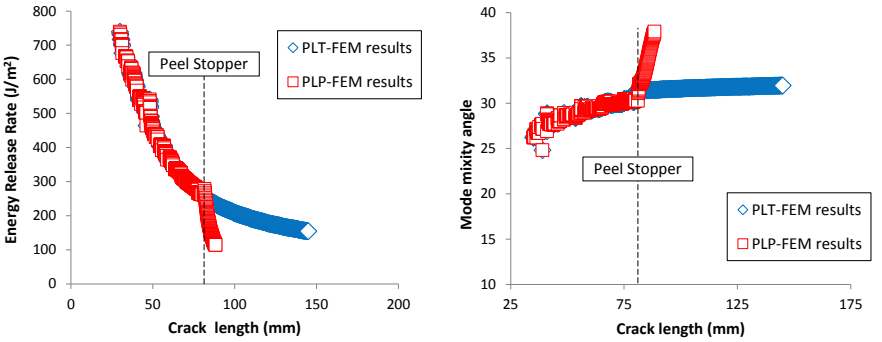

Figure 51. FE simulation of the fatigue process in the sandwich panel specimens with (PLP) and without peel stoppers (PLT): ERR and mode-mixity vs. crack length, [56].

7.5. CONCLUSIONS

From the experimental and numerical results it can be concluded that the proposed dual faced (or double-sided) peel stopper device can successfully limit the propagation of a crack in the face/core interface of sandwich panels and provide a significant improvement of their fatigue life time.

The experimental results have shown that sandwich panels with embedded peel stoppers displayed a far greater resistance to crack propagation in comparison to the panel without peel stoppers. In both panel types crack propagation was eventually arrested as the crack front expanded in size, but for the case of the panel with embedded peel stoppers the crack arrest was achieved at a mush earlier stage of the fatigue life of the specimen. In addition the crack arrested at a much lower crack radius compared to the specimen without peel stoppers. Since the crack never reached the physical boundaries of the sandwich panel specimens, a quantitative evaluation of the improvement of the fatigue life of the specimens is not possible. It is nevertheless evident from the experimental observations alone that the peel stoppers enhance the crack growth resistance of the sandwich panel specimens and therefore their damage tolerance.

FE analyses were conducted to further substantiate the conclusions made from the fatigue experiments. The fatigue crack growth data that were extracted from the FE model simulations explains the experimental observation of a marked deceleration of the crack front as it propagated and expanded into the panel specimens. More importantly it has been shown that the peel stopper and the crack deflection achieved greatly influences the energy release rate and mode-mixity angle of the crack front at short crack lengths. In this case crack arrest has been shown to be achieved even before the crack reached the “crack arrest point” of the peel stopper encountered in the previous sandwich beam experiments. Finally, the numerical calculations indicate that the potential of the peel stopper is far greater than evidenced from the physical experiments conducted which only extended to 500,000 load cycles, since the FE analyses suggest that the proposed peel stopper concept will be capable of arresting propagating interface cracks for as much as 2×10^6 cycles.

CHAPTER 8. CONCLUSIONS

8.1. NOVEL PEEL STOPPER – IMPLEMENTATION AND VALIDATION

The goal of this PhD project was to validate a new crack arrest concept (peel stopper) that can be embedded into foam cored composite sandwich structures to arrest propagating face/core interface cracks and therefore improve the damage tolerance. The crack arrester concept considered in this work is based on a significantly redesigned and improved version of crack arresting introduced in [45-51]. The new peel stopper was enhanced by glass fibres extending along its surface to improve its fracture toughness as well as a significant reduction of thickness to reduce the weight. Both experimental investigations and FE analyses have been used to study and understand the behaviour of the new peel stopper. A FE analysis framework has been developed in which Liner Elastic Fracture Mechanics (LEFM) was integrated to develop and thorough understanding of the effect of the peel stopper on the interface crack growth behaviour. The final goal was to propose a set of tools with which the fatigue life of sandwich components including peel stoppers can be simulated and predicted. This is considered as an essential step towards introducing the new peel stopper concept into the design of foam cored sandwich structures to enhance their damage tolerance.

In the course of this PhD project the new peel stopper was implemented into sandwich beams and evaluated for its ability to deflect a propagating crack away from the face/core interface, and further to arrest the crack in the interior of the core material.

Initially, a series of 3-point bending sandwich beam tests were conducted to gain insight about the behaviour new peel stopper concept. From the tests it was shown that the peel stopper could arrest the crack for a period of time and also resist further crack growth. It was observed that the peel stopper was forcing a new crack to initiate in the sandwich structure behind the peel stopper.

Subsequently the Mixed Mode Bending (MBB) test was used to investigate crack deflection at the peel stopper tip. Three different peel stopper configurations were investigated, and it was found that two of these were capable of deflecting the face/core interface crack consistently. From these two the configuration, both using glass fibres running inside the peel stopper to enhance the crack deflection capability, the one that was assessed to be the most robust and practical was chosen as a candidate to be used in the subsequent peel stopper implementations.

Based on the observations and results from the first two sandwich beam test campaigns the chosen peel stopper concept was implemented into Sandwich Tear Test (STT) specimens aiming to evaluate and validate its ability to deflect and arrest propagating face/core interface cracks. The crack arrest behaviour was examined by

use of DIC to capture the face-sheet deflections and the strain evolution in the face-sheet and core areas around the crack tip and adjacent to the tip of the peel stopper. The results showed that the proposed peel stopper was capable of enhancing the fatigue life of the tested sandwich beams considerably. Furthermore, the crack re-initiation behaviour was linked to the strain evolution behind (on the back-side) of the peel stopper arrest area. It was shown that by using the strains measured by DIC in combination with FE analyses the crack arrest time could be estimated.

Finally the peel stopper was embedded into sandwich panels/plates to investigate its ability to extend the fatigue life of the more realistic sandwich structures. It was shown that the peel stopper was able to completely arrest the propagating crack front in the 3D sandwich panel/plate environment and further to deflect the propagating face/core interface crack away from the interface. A comparison between panels embedded with peel stoppers and panels without peel stoppers showed that the peel stoppers were not only capable of extending the fatigue life but also to completely stop the crack propagation. In the panel specimens, the arrested crack never reached the peel stopper boundaries. This means that the crack would be able grow further in size before reaching the crack arrest point as was observed for the sandwich beam specimens. This observation indicates that the full potential of the peel stopper to enhance the damage tolerance of sandwich panels has not demonstrated during the fatigue experiments conducted in this research. Since the crack was arrested before reaching the peel stoppers allowable growth limit (arrest point), a new crack did not initiate as a result of the first, as in the case of the beam specimens. This is interpreted as if the peel stopper completely halted the propagation of the interface crack.

8.2. DEVELOPMENT OF EXPERIMENTAL AND NUMERICAL PROCEDURES

DIC was successfully used to record the displacement and strain fields in the sandwich specimens. This full field deformation data were used to develop a detailed understanding of the behaviour and performance of the proposed peel stopper as embedded in both the STT and sandwich panel specimens. For the sandwich beam tests conducted using the STT set-up the images taken using DIC were used to estimate the crack length during the fatigue experiments. Moreover, the strain evolution on the surface of the specimens was captured and related to the post crack arrest behaviour of the specimens. It was shown that crack re-initiation was directly related to the strain field induced (strain concentration) in the foam core on the back-side of the peel stopper. For the sandwich panel tests, DIC was used to extract the out-of-plane displacement field of the loaded face-sheet. From the out-of-plane displacements, the crack location inside the panels was identified and the crack propagation was tracked throughout the fatigue experiments. The developed method is has proven robust and may be of use in future research, since it has been shown to provide a good estimation of the debond damage inside the sandwich

panels without requiring the specimens to be removed from the test set-up. In comparison, other non-destructive techniques which may be used to identify debond damage inside sandwich panels/structures, such as ultrasound P or C scanning or computerized X-ray tomography, require special equipment and deemed to be both expensive and cumbersome to use.

In parallel with the experimental investigations, a suite of FE based numerical tools were developed to derive the magnitude the energy release rate and the mode-mixity angle of interface cracks in the tested specimens, and further to simulate the fatigue crack growth during the experiments. The aim was to develop, implement and validate generic techniques that can be used in the future to design and predict the behaviour of sandwich structures with embedded peel stoppers. Initially a FE model of the Mixed Mode Bending (MMB) test set-up was developed and used to provide the relation of applied displacement to crack length for a predefined energy release rate. By following the resulting curve, Figure 22 and by stepwise increasing the prescribed displacement amplitude as the interface crack increased in length, the energy release rate applied at the crack tip was controlled at the desired level. Moreover, the crack behaviour around the peel stopper tip (tri-material junction) was related to the energy release rate and mode-mixity angle for all three configurations of the peel stopper. The efficiency of the different peel stopper configurations was assessed based on the assumed fracture toughnesses of the face/core and face-sheet/PU interfaces in combination with a criterion proposed for crack kinking (deflection) at the peel stopper tip.

A FE model for the Sandwich Teat Test (STT) set-up was developed to enable simulation of the complete fatigue experiment. The analysis used the Crack Surface Displacement Extrapolation (CSDE) method to derive the energy release rate and mode-mixity angle of the crack at each loading cycle. By use of the cycle jump technique the number of cycles that were analyses was reduced to a fraction (approximately 10%) of the number of cycles that were simulated for the entire fatigue sequence. The FE model predictions were validated were shown to correlate well with the experimental observations, thus showing that it is possible to simulate fatigue interface crack growth and crack kinking/deflection caused by the peel stopper. Moreover, the strain distributions in the vicinity of the peel stopper that were predicted by the FE analyses were shown to correlate well with the DIC measurements. Crack re-initiation was predicted based on fatigue damage analysis using the strains calculated in the vicinity of the peel stopper and fatigue damage data for the Divinycell PVC foam used as core material.

Finally, FE analysis procedures for the sandwich panel/plate configuration with and without embedded peel stoppers was developed following the principles and techniques used for the STT beam test set-up. The predicted interface crack propagation and crack deflection/kinking behaviour were compared with experimental observations and a good match was found. Finally, the FE model was used to simulate interface crack growth for a significantly larger number of cycles than was carried out in the physical experiments. The predictive have demonstrated

the efficiency of the dual faced peel stopper that was implemented in the sandwich panel specimens. In particular, it was shown that even after 2 million cycles the interface crack remained arrested inside the physical boundaries of the peel stopper, thus suggesting that the proposed peel stopper can significantly improve the damage tolerance and fatigue life of forma cored sandwich panels/plates.

8.3. NOVELTY CLAIMS

The novelty claims stated in the introduction of the Thesis were supported by the work presented in the chapters above. In detail,

- The new lightweight design proposed for the peel stopper was found to be capable of ensuring crack arrest under both quasi-static and fatigue loading conditions, as well as for varying mode mixities. Moreover the material combination proposed ensured that the fracture toughness of the peel stopper would be high while the stiffness remains almost unchanged.
- Digital Image Correlation was used to capture the strain fields in the vicinity of the peel stopper, and the measured peak strains were used to predict the remaining lifetime of the specimens. The results were validated against real fatigue data for the same type of (PVC) core material that was used for the specimens in this work.
- The new crack stopping elements were successfully implemented in sandwich panels, and it was shown that peel stoppers were able to enhance their damage tolerance under fatigue load conditions. A novel method to locate the crack inside the panel specimens was developed and validated.
- 2D and 3D FE Models were developed capable of predicting crack growth under fatigue loads, and also able to predict the effect of the peel stopper on the lifetime of the specimens. The tools presented in this work can effectively be used to design sandwich structure components with embedded peel stoppers and predict the overall improvement of their damage tolerance.

CHAPTER 9. FUTURE WORK

The results of this study showed shown that the proposed peel stopper concept has significant potential to improve the damage tolerance of sandwich structures subjected to fatigue loading conditions. To further develop and validate the proposed concept, topics for further research would encompass investigation of the peel stopper/core interface fatigue properties (a Paris law relation), development of further improvements of the peel stopper concept, as well as the application of the peel stopper in sandwich components/structures subjected to different loading conditions.

Crack propagation along the PU/core interface was simulated in this work by using fatigue crack growth data derived from the STT experiments. To model the crack propagation in the peel stopper/core interface properly it is necessary to determine the e fatigue crack growth rate data for the relevant interfaces accurately (Paris law). Ideally, the investigation should include a multitude of crack loading conditions with regards to energy release rate and mode-mixity combinations, as it was shown that these parameters change drastically as the crack propagates in the PU/core interface. In addition to the fatigue growth data, the quasi-static fracture toughness of the interfaces should be determined, as this will enable applying the proposed crack kinking criterion to determine whether the peel stopper configuration is able to deflect a propagating crack. The fracture properties of the interfaces can be determined by extensive testing using well established test set-ups such as the MMB and the Modified Tilted Sandwich Debond test (TSD) [23]. The fracture properties of the interface for quasi-static and fatigue loading are of crucial importance from a design standpoint, as they represent the key inputs to the FE based simulation tools developed in this study.

From the experimental and numerical investigation of the STT configurations, it was concluded that the strain distribution in the vicinity of the peel stopper in state where the crack was arrested state was responsible for the crack re-initiation and the post crack arrest behaviour. A study focusing on the shape optimization of the peel stopper, aiming to reduce the magnitude of the local strain concentrations that are responsible for crack re-initiation, could improve the crack arrest performance by increasing the number of loading cycles where the crack would remain at the crack arrest point. From the PVC foam fatigue data used in this study (see Figure 52 and Refs [58], [61]) it is seen that a small decrease of the strain amplitude could improve the fatigue performance of the peel stopper significantly.

Finally, an investigation of the effect of the peel stopper on the damage tolerance of sandwich structures subjected to different test and loading conditions could be the focus of a new study. Test set-ups that are more representative of real structure loading conditions including buckling and impact loads would be highly relevant for further experimental investigations. The sandwich panel configuration and test used

for the evaluation of the peel stopper behaviour in this PhD project cannot be considered representative for typical sandwich structures seen in practical applications. Thus, the self-arrest behaviour of the crack front propagating in the panels observed in this work makes it difficult to test for longer crack lengths and also to assess the full potential of the peel stopper. This is because it is very difficult to conduct "run-out" tests where the specimens including peel stoppers fail completely. Testing of sandwich panels subjected to compressive loads introducing buckling driven delamination would be of high relevance to assess the peel stopper and its effect on the damage tolerance of realistic sandwich structures.

CHAPTER 10. REFERENCES

[1] Hoff, N.J. and Mautner, S.E., "The Buckling of Sandwich-Type Panels". *Journal of Aeronautical Sciences*, 12, 1945, 285-297.

[2] Hoff, N.J. and Mautner, S.E. "Bending and Buckling of Sandwich Beams". *Journal of Aeronautical Sciences*, 15, 1948, 707-720.

[3] Ericksen, W.S., "The Bending of a Circular Sandwich Plate Under Normal Load". *FPL Report 1828,* 1953.

[4] Youngquist, W.G. and Kuenzi, E.W., "Stresses Induced in Sandwich Panel by Load Applied at an Insert". *FPL Report 1845,* 1955.

[5] Norris, C.B. and Boller, K.H., "Transfer of Longitudinal Load From one Facing of a Sandwich Panel to the Other by Means of Shear in the Core". *FPL Report 1846,* 1955.

[6] Raville, M.E., "Deflection and Stresses in a Uniform Loaded, Simply Supported, Rectangular Sandwich Plate". *FPL Report 1847,* 1955.

[7] Lewis, W.C., "Deflection and Stresses in a Uniform Loaded, Simply Supported, Rectangular Sandwich Plate – Experimental Verification of Theory". *FPL Report 1847-A,* 1956.

[8] Zenkert, D., "An introduction to sandwich construction". *London: Chameleon Press Ltd*, 1995.

[9] Hayman, B., "Approaches to Damage Assessment and Damage Tolerance for FRP Sandwich Structures". *Journal of Sandwich Structures and Materials*, 9(6), 2007, 571-596.

[10] Erdogan, F., "Bonded dissimilar materials containing cracks parallel to the interface". *Engineering Fracture Mechanics*, 3, 1971, 231-240.

[11] Dundurs, J., "Edge-bonded dissimilar orthogonal elastic wedges". *Journal of Applied Mechanics*, 36, 1969, 650-652.

[12] Hutchinson, J.W. and Suo Z., "Mixed Mode Cracking in Layered Materials". *Advances in Applied Mechanics*, 29, 1992, 63-191.

[13] He, M.Y. and Hutchinson, J.W. "Kinking of a crack out of an interface". *Journal of Applied Mechanics*, 56, 1989, 270–278.

[14] Suo, Z., "Singularities, interfaces and cracks in dissimilar media". *Proc. R. Soc. Lond,* A427, 1990, 331-358.

[15] Wang, T.C., "Kinking of an interface crack between two dissimilar anisotropic elastic solids". *International Journal of Solids and Structures*, 31(5), 1994, 629–641.

[16] Cantwell, W. J. and Davies, P. "A test technique for assessing core-skin adhesion in composite sandwich structures". *Journal of Materials Science Letters*, 13 (3), 1994, 203-205.

[17] Cantwell, W. J., Davies, P., "A study of skin-core adhesion in glass fibre reinforced sandwich materials". *Applied Composite Materials*, 3 (6), 1996, 407-420.

[18] Prasad, S. and Carlsson, L.A., "Debonding and crack kinking in foam core sandwich beams—I. analysis of fracture specimens". *Engineering Fracture Mechanics*, 47 (6), 1994, 813–824.

[19] Prasad, S. and Carlsson, L.A., "Debonding and crack kinking in foam core sandwich beams—II. experimental investigation". *Engineering Fracture Mechanics*, 47 (6), 1994, 825–841.

[20] Carlsson, L.A., Sendlein, L.S. and Merry, S.L., "Characterization of face/core shear fracture of composite sandwich beams". *Journal Composite Materials*, 25, 1991, 101–116.

[21] Quispitupa, A., Berggreen, C. and Carlsson, L.A. "On the analysis of a mixed mode bending sandwich specimen for debond fracture characterization". *Engineering Fracture Mechanics*, 76 (4), 2009, 594–613.

[22] Manca, M., Quispitupa, A., Berggreen, C. and Carlsson, L.A. "Face/core debond fatigue crack growth characterization using the sandwich mixed mode bending specimen". *Composites Part A: Applied Science and Manufacturing*, 43 (11), 2012, 2120–2127.

[23] Berggreen, C. and Carlsson, L.A. "A modified TSD specimen for fracture toughness characterization - fracture mechanics analysis and design". *Journal of Composite Materials*, 44 (15), 2010, 1893-1912.

[24] Lundsgaard-Larsen, C., Sørensen, B. F., Berggreen, C. and Østergaard, R. C., "A modified DCB sandwich specimen for measuring mixed-mode cohesive laws". *Engineering Fracture Mechanics*, 75 (8), 2008, 2514-2530.

[25] Berggreen, C., "Damage tolerance in debonded sandwich structures". *Technical University of Denmark*, PhD. Thesis, Department of Mechanical Engineering, 2004.

[26] Rice, J.R., "A Path Independent Integral and the Approximate Analysis of Strain Concentration by Notches and Cracks". *Journal of Applied Mechanics*, 35(2), 1968, 379-386.

[27] Matos, P.P.L., McMeeking, R.M., Charalambides, P.G. and Drory, M.D., "A method for calculating stress intensities in bimaterial fracture". *International Journal of Fracture*, 40 (4), 1989, 235-254.

[28] Rybicki, E. F., Kanninen, M.F., "A finite element calculation of stress intensity factors by a modified crack closure integral". *Engineering Fracture Mechanics*, 9 (4), 1977, 931-938.

[29] Krueger, R., "Virtual Crack Closure Technique: History, Approach and Applications", *Applied Mechanics Reviews*, 57, 2004, 109-143.

[30] Smelser, R. E., "Evaluation of stress intensity factors for bimaterial bodies using numerical crack flank displacement data". *International Journal of Fracture*, 15 (2), 1979, 135-143.

[31] Jolma, P., Segercrantz, S. and Berggreen, C., "Ultimate Failure of Debond Damaged Sandwich Panels Loaded with Lateral Pressure: An Experimental and Fracture Mechanics Study". *Journal of Sandwich Structures and Materials*, 9(2), 2007, 167-196.

[32] Berggreen, C., Simonsen, B.C. and Borum, K., "Experimental and Numerical Study of Interface Crack Propagation in Foam Cored Sandwich Beams". *Journal of Composite Materials*, 41(4), 2007, 493-520.

[33] Paris, P. and Erdogan, F., "A critical analysis of crack propagation laws". *Journal Basic Engineering Trans ASME Ser D*, 85 (4), 1963, 528–534.

[34] Moslemian, R., Karlsson, A.M. and Berggreen, C., "Accelerated fatigue crack growth simulation in a bimaterial interface". *International Journal of Fatigue*, 33 (12), 2011, 1526–1532.

[35] Moslemian, R., Berggreen, C. and Karlsson, A.M. "Application of a Cycle Jump Technique for Acceleration of Fatigue Crack Growth Simulation". *In Proceedings — NAFEMS Nordic Seminar: Simulating Composite Materials and Structures*, 2010.

[36] Quispitupa, A., Berggreen, C. and Carlsson. L.A., "Design analysis of the mixed mode bending sandwich specimen". *Journal of Sandwich Structures and Materials*, 12(2), 2010, 253-272.

[37] Lundsgaard-Larsen, C., Berggreen, C. and Carlsson. L.A., "Tailoring sandwich Face/Core interfaces for improved damage Tolerance|Part i: Finite element analysis". *Applied Composite Materials*, 17(6), 2010, 609-619.

[38] Lundsgaard-Larsen, C., Berggreen, C. and Carlsson. L.A., "Tailoring sandwich Face/Core interfaces for improved damage Tolerance|Part II: Experiments". *Applied Composite Materials*, 17(6), 2010, 621-637.

[39] Kim, J.H., Lee, Y.S., Park, B.J. and Kim, D.H., "Evaluation of durability and strength of stitched foam-cored sandwich structures". *Composite Structures*, 47, 1999, 543-550.

[40] Raju, K.S. and Tomblin, J.S., "Energy absorption in stitched composite sandwich panels". *Journal of Composite Materials*, 33(8), 1999, 721-728.

[41] Wallace, B.T., Sankar, B.V. and Ifju P.G., "Pin reinforcement of delaminated sandwich beams under axial compression". *Journal of Sandwich Structures and Materials*, 3, 2001, 117-129.

[42] Rinker, M., Zahlen, P. C., John, M. and Schäuble, R., "Investigation of sandwich crack stop elements under fatigue loading". *Journal of Sandwich Structures and Materials*, 14 (1), 2012, 55–73.

[43] Hirose, Y., Matsubara, G., Hojo, M., Matsuda, H. and Inamura, F., "Evaluation of modified crack arrester by fracture toughness tests

under mode I type and mode II type loading for foam core sandwich panel". *Proc. US-Japan conference on composite materials*, Tokyo, Japan, 2008.

[44] Hirose, Y., Matsuda, H., Matsubara, G., Hojo, M. and Inamura, F., "Proposal of the concept of splice-type arrester for foam core sandwich panels". *Composites Part A: Applied Science and Manufacturing*, 43 (8), 2012, 1318–1325.

[45] Jakobsen, J., Bozhevolnaya, E., Thomsen, O.T., "New peel stopper concept for sandwich structures". *Composite Science Technology*, 67, 2011, 3378–85.

[46] Jakobsen, J., Andreasen, J.H. and Bozhevolnaya, E., "Crack kinking of a delamination at an inclined core junction interface in a sandwich beam". *Engineering Fracture Mechanics*, 75(16), 2008, 4759–73.

[47] Bozhevolnaya, E., Jakobsen, J. and Thomsen, O.T., "Fatigue Performance of Sandwich Beams With Peel Stoppers". *Strain, An International Journal on Experimental Mechanics*, 45(4), 2009, 349-357.

[48] Jakobsen, J., Thomsen, O.T., Andreasen, J.H. and Bozhevolnaya, E., "Crack deflection analyses of different peel stopper design for sandwich structure". *Composite Science Technology*, 69, 2009, 870–5.

[49] Jakobsen, J., Andreasen, J.H. and Thomsen, O.T., "Crack deflection by core junctions in sandwich structures". *Engineering Fracture Mechanics*, 76(14), 2009, 2135–47.

[50] Jakobsen, J., Johannes, M. and Bozhevolnaya, E., "Failure prediction of in-plane loaded sandwich beams with core junctions". *Composite Structures*, 82 (2), 2009, 194-200.

[51] Jakobsen, J. "Local Effects and the Control of Face-Core Debond Failure in Sandwich Structures". *Aalborg University*, PhD Thesis, Department of Mechanical Engineering, 2008.

[52] Martakos, G., Andreasen, J.H., and Thomsen, O.T., "Preliminary Evaluation of the Performance of Novel Fibre Reinforced Peel Stopper Concept in Sandwich Structures". *In the Proceedings of International Conference of Composite Materials-19*, Montreal, 2013.

[53] Wang, W., Martakos, G., Dulieu-Barton, J.M., Andreasen, J.H. and Thomsen, O.T., "Fracture Behaviour at tri-material junctions of crack stoppers in sandwich structures". *Composite Structures*, 133, 2015, 818-833. http://dx.doi.org/10.1016/j.compstruct.2015.07.060

[54] Martakos, G., Andreasen, J.H, Berggreen, C. and Thomsen, O.T., "Experimental Investigation of Interfacial Crack Arrest in Sandwich Beams Subjected to Fatigue Loading using a Novel Crack Arresting Device". *Journal of Sandwich Structures and Materials*, accepted for publication.

[55] Martakos, G., Andreasen, J.H, Berggreen, C. and Thomsen, O.T., "Interfacial Crack Arrest in Sandwich Beams Subjected to Fatigue Loading using a Novel

Crack Arresting Device – Numerical modelling". *Journal of Sandwich Structures and Materials*, accepted for publication.

[56] Martakos. G., Andreasen, J.H, Berggreen, C. and Thomsen, O.T., "Interfacial Crack Arrest in Sandwich Panels with Embedded Crack Stoppers Subjected to Fatigue Loading". *Applied Composite Materials*, accepted for publication. DOI: 10.1007/s10443-016-9514-3

[57] Zenkert, D. "Strength of sandwich beams with interface debondings". *Composite Structures*, 17 (4), 1991, 331–350.

[58] DIAB. Divinycell H-Grade Technical data. Laholm (Sweeden) (http://www.diabgroup.com), 2014.

[59] ANSYS® Academic Research, Release 15.0

[60] Ashby, S.M., "Materials Selection in Mechanical Design", *Butterworth-Heinemann*, 2011.

[61] Burman, M. and Magnusson, B., "Fatigue testing of H60, H100 and H200". Technical report (DIAB), KTH (Sweeden), 2008.

[62] Berggreen, C., Simonsen, B.C. and Borum, K.K., "Experimental and numerical study of interface crack propagation in foam-cored sandwich beams". *Journal of Composite Materials*, 41 (4), 2007, 493–520.

APPENDICES

Appendix A. Interface Fracture Formulation [14]

Suo introduced the anisotropy parameters H_{11} and H_{22} which are implemented in the COD formulation [14]:

$$\sqrt{\frac{\boldsymbol{H_{11}}}{\boldsymbol{H_{22}}}}\,\boldsymbol{\delta_y} + \boldsymbol{i\delta_x} = \frac{\boldsymbol{2H_{11}(K_1 + iK_2)|x|^{\frac{1}{2}+i\varepsilon}}}{\boldsymbol{\sqrt{2\pi}(1 + 2i\varepsilon)cosh\pi\varepsilon}} \tag{1}$$

$$\sqrt{\frac{H_{11}}{H_{22}}}\,\sigma_{yy} + i\sigma_{xy} = \frac{K\,x^{i\varepsilon}}{\sqrt{2\pi x}} \tag{2}$$

where x represents the distance away from the crack tip (see Figure 5 (a)), and K is the complex stress intensity factor K_1+iK_2. The oscillation in the solution is created by the $i\varepsilon$ term which acts as a power of the distance away from the tip.

From trigonometry and fracture mechanics [14],

$$\begin{aligned} Kx^{i\varepsilon} = {} & [K_1 \cos(\varepsilon\, lnx) - K_2 \sin(\varepsilon\, lnx)] \\ & + i[K_2 \cos(\varepsilon\, lnx) + K_1 \sin(\varepsilon\, lnx)] \end{aligned} \tag{3}$$

$$\psi_K = \arctan\left[\frac{\Im(Kh^{i\varepsilon})}{\Re(Kh^{i\varepsilon})}\right] \tag{4}$$

$$G = \frac{H_{11}\,|K|^2}{4\cosh^2(\pi\varepsilon)} \tag{5}$$

, where G represents the energy release rate, and ψ is the mode-mixity angle of the crack tip that can be solved with regards to the relative crack displacements by substituting equation 1 and 2 into equation 4 and 5:

$$\psi_K = \arctan\left(\sqrt{\frac{H_{22}}{H_{11}}}\frac{\delta_x}{\delta_y}\right) \tag{6}$$

$$G = \frac{\pi(1 + 4\varepsilon^2)}{8\,H_{11}|x|}\left(\frac{H_{11}}{H_{22}}\,\delta_y^2 + \delta_x^2\right) \tag{7}$$

In this formulation the energy release rate and mode-mixity are functions only of the crack tip relative displacements. This formulation works well under the Finite Element Method framework where the crack tip displacements can directly be extracted from node displacements.

PAPER #1

Fracture Behaviour at Tri-material Junctions of Crack Stoppers in Sandwich Structures

W. Wang[1], G. Martakos[2], J.M. Dulieu-Barton[1], J.H. Andreasen[2], O.T. Thomsen[1,2]

[1] Faculty of Engineering and the Environment, University of Southampton, Highfield, Southampton, UK
[2] Department of Mechanical and Manufacturing Engineering, Aalborg University, Aalborg, Denmark

The paper is published in the Journal of Composite Structures, volume number: 133, page: 818-833, July 2015
DOI: http://dx.doi.org/10.1016/j.compstruct.2015.07.060

Composite Structures 133 (2015) 818–833

Contents lists available at ScienceDirect

Composite Structures

journal homepage: www.elsevier.com/locate/compstruct

Fracture behaviour at tri-material junctions of crack stoppers in sandwich structures

W. Wang [a], G. Martakos [b], J.M. Dulieu-Barton [a,b], J.H. Andreasen [b], O.T. Thomsen [a,b,*]

[a] Faculty of Engineering and the Environment, University of Southampton, Highfield, Southampton, UK
[b] Department of Mechanical and Manufacturing Engineering, Aalborg University, Aalborg, Denmark

ARTICLE INFO

Article history:
Available online 21 July 2015

Keywords:
Foam cored composite sandwich structures
Peel stoppers
Thermoelastic stress analysis
Fracture modelling
Damage tolerance

ABSTRACT

Inspired by a previously published peel stopper design for foam cored composite sandwich structures, three novel markedly lighter peel stoppers were evaluated with respect to their ability to deflect and arrest propagating face debond cracks. Of the three novel peel stopper configurations, C1, C2 and C3, C1 was similar to the previous design, whereas C2 and C3 were modified with layers of glass fibre fabric extending from the peel stopper tip into the face sheet (C2) or into the face sheet/core interface (C3). The previous peel stopper was validated under mode II dominated conditions, but the novel designs were investigated under mode I dominated crack propagation conditions, which are of higher practical relevance. Both quasi-static and fatigue loading scenarios were investigated. The mechanisms controlling crack propagation at the internal peel stopper tip were studied using thermoelastic stress analysis (TSA) and finite element (FE) analysis. The TSA has revealed significant new information about the local stress fields in the vicinity of the tri-material junction (peel stopper tip) as well as the fracture process zone. Configuration C1 was unable to deflect debond cracks consistently, albeit it did so in most cases, whereas it was incapable of achieving crack arrest. C2 and C3 both performed better in that they consistently demonstrated the ability to deflect propagating cracks, whereas only C2 could arrest the cracks consistently as well. Detailed fracture mechanics analyses confirmed and explained the experimental observations.

1. Introduction

A sandwich structure is a layered composite formed by attaching two thin but stiff face sheets to a thick but lightweight core material. Compared to monolithic structures or laminated composites, this structure is well known for its superior bending stiffness and strength to weight ratios [1]. A weakness of sandwich structures is the quality of the bonding between the face sheet and core. Debonds can initiate from manufacturing defects as well as in-service overload or impact. Propagation of the debonded area is often rapid due to the brittle behaviour of the face sheet/core interface bond, leading to face sheet detachment. The result is loss of strength and stiffness, which may lead to catastrophic failure. From a practical point of view it is desirable to suppress the debond propagation so that some of the loading carrying capacity is retained. Therefore attention has been paid to the development of inserts in the core material to suppress interfacial debonding.

In several studies sub-structural elements (i.e. crack stoppers) made from carbon fibre reinforced plastic (CFRP) were proposed and applied to foam cored sandwich components to prevent the propagation of interfacial cracks. Hirose et al. [2,3] introduced semi-circular shaped CFRP rods in the face sheet/core interface to increase the fracture toughness at the edge of the CFRP inserts. In their studies an increase of the critical load was observed as the crack tip approached the CFRP rods, which was attributed to the redistribution of the stresses between the crack tip and the CFRP rods. Rinker et al. [4] integrated a CFRP double-T joint element and a rectangular shaped CFRP element into the core. Sandwich structures with different embedded elements were investigated under fatigue loading and an increase of fatigue life was observed. Although the introduction of different CFRP inserts increases the interfacial fracture toughness, it was not possible to arrest the crack using these approaches. Moreover, the crack stoppers made from CFRP are much stiffer than the foam core material, which result in severe stress concentration that could initiate cracks.

A different concept was proposed by Jacobsen et al. [5–8], where the crack stopper was manufactured from a PolyUrethane

* Corresponding author at: Faculty of Engineering and the Environment, University of Southampton, Highfield, Southampton, UK. Tel.: +44 7770 347160.
E-mail address: o.thomsen@soton.ac.uk (O.T. Thomsen).

http://dx.doi.org/10.1016/j.compstruct.2015.07.060
0263-8223/

(PU) material with stiffness properties similar to those of the foam core materials. A key element in the design was to confine and arrest the growth of the interfacial crack. The basic principle of the so-called 'peel stopper' is to deflect the crack away from the face sheet/core interface into the core, so that the crack path follows the boundary of the peel stopper. The functionality of the crack stopper was validated experimentally using three-point bend tests in which sandwich beams with aluminium or GFRP face sheets and Divinycell H60 PVC foam core were studied [5,6]. It was shown that interfacial cracks that were initiated by core shear failure were successfully deflected and arrested by the peel stopper. The purpose of the present paper is to further explore the peel stopper concept. In particular two considerations emerge from the peel stopper design proposed in [5,6]. Firstly, the loading conditions at the debond tip in [5,6] were mixed mode with significant contribution in mode II. However, many realistic loading situations are mode I dominated, hence there is a need to assess the ability of the peel stopper to deflect propagating interfacial cracks under this condition. Secondly, the bulky design of the peel stoppers accompanied by the high density of the PU material suggests that the use of the peel stoppers described in [5,6] will incur a serious weight penalty.

The work described in the present paper investigates the mechanisms controlling crack deflection in the neighbourhood of peel stoppers experiencing mode I dominated loading. The geometry of the peel stopper is modified to reduce its weight. Three new peel stopper configurations are proposed. Thermoelastic stress analysis (TSA) [9] and finite element (FE) analysis are used to derive the crack-tip stress field and to characterise the fracture behaviour in the neighbourhood of the peel stopper to assess the conditions to achieve successful crack deflection.

TSA is based on the thermoelastic effect where a small temperature change on the surface of a material is measured using infra-red (IR) imaging of the structure under cyclic load. For isentropic conditions, the temperature change (ΔT) divided by the absolute temperature (T) is linearly proportional to the change in the sum of principal stresses [9]. Therefore, TSA is used to determine the stress state in the neighbourhood of the peel stopper and to assess the stress evolution during crack growth. As high spatial resolution data can be obtained from TSA, the aim is to investigate the local effects (local stress concentrations) introduced by the different peel stopper configurations and to understand the associated crack propagation mechanisms. A major challenge in obtaining the stress state from an interfacial crack is the large and discontinuous motion induced by the face sheet/core detachment. As the IR detector is stationary and the specimen is moving, each point on the specimen surface is detected by different elements of the detector array. This leads to erroneous measurement of the temperature change as IR detector cannot track the specimen motion. To address the complex motion expected for the mode I dominated loading of the sandwich specimen, a motion compensation technique has been developed [10]. Digital image correlation (DIC) [11] is used to track the specimen motion and incorporate the displacement field for motion correction of each pixel in the IR images.

In addition to TSA, a FE model was developed based on Suo's interfacial crack formulation [12] and implemented as a subroutine in ANSYS. The goal is to study the energy release rate and mode-mixity of a propagating crack at different locations around the peel stopper. Berggreen [13,14] developed the so called Crack Surface Displacement Extrapolation (CSDE) method and implemented it in ANSYS as a subroutine. The method has been successfully used in combination with FE analysis to investigate interface cracks in sandwich structures. The CSDE method is utilised in this work since it enables calculations close to the crack tip while avoiding the oscillations in the solution that derive from the dissimilarity of material properties.

2. Configurations of the peel stopper

Three different configurations of peel stoppers are studied. In all cases the peel stopper geometry is as shown in Fig. 1(a) which is a modification of the original design by Jakobsen et al. [5]. Here the peel stopper is moulded into a 'U' shaped geometry so that the volume of material is significantly reduced, thus reducing the mass correspondingly. The PU material used for the peel stopper is reinforced by a layer of glass fibre fabric as shown in Fig. 1(b). Comparing to the original design, the glass fibre fabric is introduced to enhance the peel stopper fracture toughness and to prevent the crack from penetrating into the peel stopper.

The peel stopper is moulded in a 'U' shape using a mould made of Polypropylene. The polypropylene does not bond with the PU material making it a good choice for the mould tool as extra coatings are not required. The mould is shown in Fig. 2(a) which includes two parts: the lower and upper parts. The fabrication firstly applies the PU material in the lower part of the mould. The PU material is in liquid form and can take the shape of the mould. The UD fibres are then attached to the upper part with the main fibre direction following the arrows as shown in Fig. 2(a). Finally, the upper part of the mould together with the fibres are pressed into the lower part containing the PU adhesive. Fig. 2(b) shows the side view of the assembled mould where the gap between the upper and lower parts are filled with the PU and fibres. The mould is closed tightly using bolts and nuts to contain the material in the desired dimensions. When the mould is fully closed, the excess PU material is driven out by holes drilled in the mould body.

The three different configurations of peel stoppers are shown in Fig. 3. In configuration 1 (C1), the PU material is directly bonded to the foam core. As the 'U' shaped peel stopper has the same wedge angle (10°) as that suggested in the original design, the configuration at the peel stopper tip of C1 remains the same as that of the original peel stopper. In configurations 2 (C2) and 3 (C3) modifications of small material features at the tri-material junction are made. The aim is to change the local effects at the tri-material junction and thereby enabling crack deflection. In C2 the PU material is also directly bonded to the foam, but the glass fibre layer inside the PU material protrudes from the peel stopper tip. The fibre layer is infused together with the face sheet during the manufacturing process. In C3 an extra fibre layer is introduced at the PU/foam interface when the PU material is bonded to the foam. The part of fibre layer behind the peel stopper is attached to the face sheet as for C2.

In the following sections, the ability of the different peel stoppers to deflect the interfacial crack is examined under both static and fatigue loading. The experimental results obtained from the static tests are used to validate FE models of sandwich specimens containing the different peel stopper configurations. The mechanisms controlling the crack propagation in the vicinity of peel stoppers are then studied using both TSA and FE analysis.

3. Test specimens

The sandwich specimens studied in the present work consist of 25 mm cross-linked PVC foam cores (Divinycell H100) and 210 gm^{-2} plain woven E-glass/epoxy composite face sheets. The core materials include two blocks of foam which have been machined to the required geometries using a CNC milling centre; the two blocks of foam are attached to the inner and outer side of the peel stopper as shown in Fig. 3. The fibre layers introduced

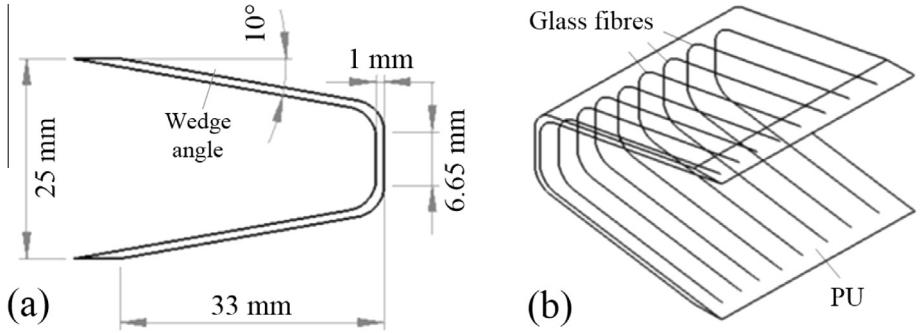

Fig. 1. (a) Peel stopper shape and fibre reinforcement alignment inside the PU material and (b) the dimension of the peel stopper.

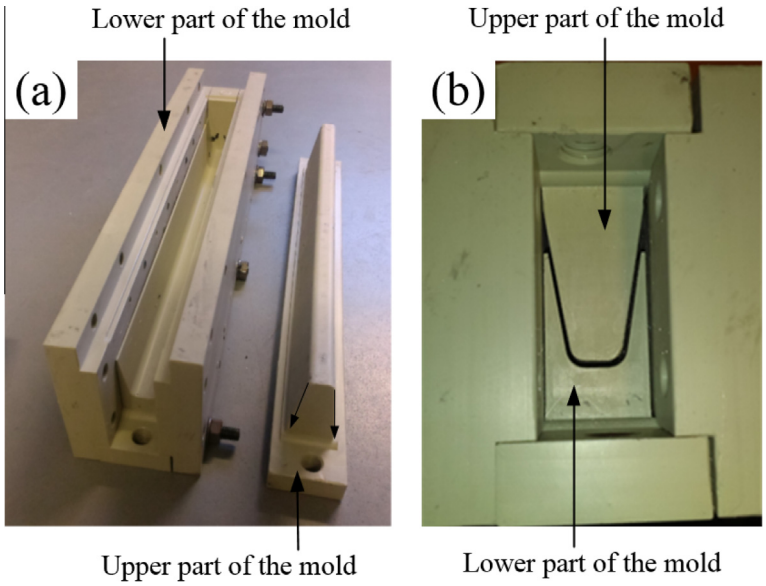

Fig. 2. (a) The lower and upper parts of the peel stopper polypropylene mould and (b) side view of the assembled mould showing the peel stopper shape.

inside the peel stopper and placed at the peel stopper/core interface in C3 are made from the same E-glass fabric that was used for the face sheet. The material properties of the sandwich constituent materials are listed in Table 1 [5,15].

The sandwich panel that incorporates the peel stopper was manufactured in a single shot resin infusion process using Prime 20 LV epoxy resin by Gurit. Three panels each containing a peel stopper configuration (i.e. C1, C2 and C3) were manufactured. To create an initial debond behind the peel stopper tip, a thin Teflon film of 25 μm thick was placed between the face sheet and the core across the width of the panel. Prior to the manufacturing, the peel stopper was adhesively boned to the foam using the Araldite 2000 epoxy adhesive as suggested in [5]. For C3, the extra fibre reinforcement layer was firstly placed on the foam (i.e. the block of foam that was attached to the inner side of the peel stopper) with the epoxy adhesive applied, and then the foam was bonded to the peel stopper.

For each configuration, four sandwich beam specimens of 210 mm length and 30 mm width were cut from the panels (one specimen was tested under static loading and the rest of the specimens were tested under fatigue loading). The specimens were loaded using the mixed mode bending test rig (MMB) as shown in Fig. 4. The MMB test rig was used because the applied loading mode at the crack tip remains the same during the crack propagation [16]. Table 2 summarises the dimensions of each sandwich specimen and its loading conditions. A long level arm distance, c, was applied in the tests to provide a mode I dominated loading. The mode-mixity, ψ, shown in the table (predicted by the FE model described in Section 4) confirms that a mode I dominated loading was applied to different specimens and configurations. As shown in Fig. 4, the distance between the initial crack tip and the peel stopper tip is relatively long (15 mm) to allow the crack to propagate before reaching the tri-material junction. This is important, as a well-defined stable crack growth must be achieved behind the peel stopper tip.

4. FE modelling

4.1. Fracture at bi-material interface

To account for anisotropy in the neighbourhood of the bi-material interface Suo's formulation was used [12]. Furthermore the Crack Opening Displacement (COD) approach is adapted for bi-material problems in a finite element analysis (FEA) framework so the required displacements at the crack tip are calculated from the predicted nodal displacements. The formulation includes material anisotropy parameters H_{11} and H_{22}, Dundur's parameters for dissimilar crack interface materials and the oscillation parameter ε [12,17–19]. The parameter ε accounts for the oscillations of mode-mixity and energy release rate in the FEA close to the crack tip.

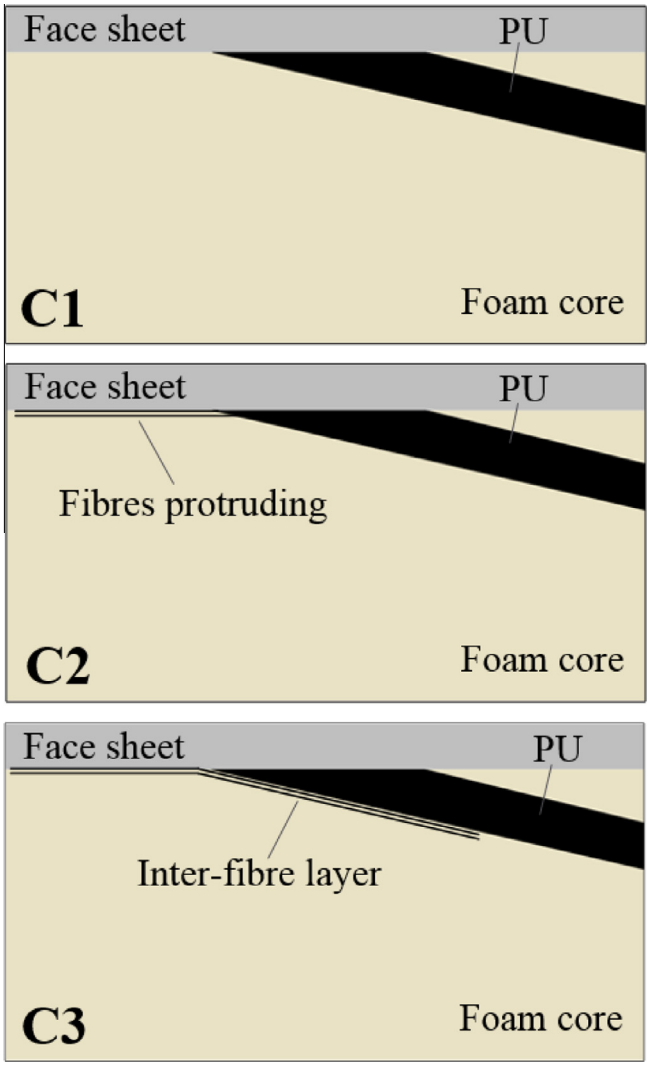

Fig. 3. The three peel stopper configurations.

The anisotropy parameters, H_{11} and H_{22}, are implemented in the COD formulation as follows [12]:

$$\sqrt{\frac{H_{11}}{H_{22}}}\delta_y + i\delta_x = \frac{2H_{11}(K_1 + iK_2)|x|^{\frac{1}{2}+i\varepsilon}}{\sqrt{2\pi}(1+2i\varepsilon)\cosh(\pi\varepsilon)} \tag{1}$$

$$\sqrt{\frac{H_{11}}{H_{22}}}\sigma_{yy} + i\sigma_{xy} = \frac{Kx^{i\varepsilon}}{\sqrt{2\pi x}} \tag{2}$$

where x represents the distance away from the crack tip (see Fig. 5(a)) and K is the complex stress intensity factor $K_1 + iK_2$. The opening and shear displacements are represented by δ_y and δ_x respectively in the local coordinate system as shown in Fig. 5(a).

Also it can be shown that [12]:

$$Kx^{i\varepsilon} = [K_1\cos(\varepsilon \ln x) - K_2\sin(\varepsilon \ln x)] + i[K_2\cos(\varepsilon \ln x) + K_1\sin(\varepsilon \ln x)] \tag{3}$$

$$\psi = \arctan\left[\frac{\Im(K\mathrm{h}^{i\varepsilon})}{\Re(K\mathrm{h}^{i\varepsilon})}\right] \tag{4}$$

$$G = \frac{H_{11}|K|^2}{4\cosh^2(\pi\varepsilon)} \tag{5}$$

where G is the energy release rate and ψ is the mode-mixity of the crack.By substituting Eqs. (1) and (2) into Eqs. (4) and (5) yields:

$$\psi = \arctan\left(\sqrt{\frac{H_{11}}{H_{22}}}\frac{\delta_x}{\delta_y}\right) \tag{6}$$

$$G = \frac{\pi(1+4\varepsilon^2)}{8H_{11}|x|}\left(\frac{H_{11}}{H_{22}}\delta_y^2 + \delta_x^2\right) \tag{7}$$

In Eqs. (6) and (7) the oscillation term, $x^{i\varepsilon}$, has been eliminated, however for very small elements the crack tip singularity may still introduce numerical instability. The CSDE method [13,14] is utilised as shown in Fig. 5(b) to suppress any numerical errors near to the crack tip. The CSDE method calculates the energy release rate and mode-mixity over a region of the crack surface and identifies the sub-region where the oscillation is not affecting the results. Then by using outer and inner limit values of the energy release rate and the mode-mixity (see Fig. 5(b)) linear extrapolation is used to calculate the values at the crack tip.

4.2. FE modelling

FE models of the test specimens were constructed using the commercial FE package ANSYS 15.0 [20]. The two scenarios of crack deflection and crack propagating along the horizontal interface (i.e. no crack deflection) at the tri-material junction were modeled for each peel stopper configuration. 8-node 2D plane stress elements (PLANE 183) with an average element size of 0.5 mm were used. Near the crack tip, the number of elements ranged from 36 to 144 with element sizes of 5 to 10 μm. Fig. 6 shows the FE meshes corresponding to the three peel stopper configurations and the geometry of the sandwich beam model. The detailed models of different crack path scenarios around the tri-material junction for each configuration are shown in the images (a)–(f) in Fig. 6. In the models of C2 and C3, an extra layer of elements of 0.1 mm thickness (shown in orange) was used to model the protruding fibre layer and the inter-fibre layer. In C2 the extra fibre layer was attached to the tri-material tip to model the fibres protruding from the peel stopper.

5. Experimental setup

Sandwich specimens mounted in the MMB rig were tested in an Instron ElectroPuls machine (E1000) with a 1 kN actuator and load cell capacity. The actuator of the test machine was connected to the loading yoke (see Fig. 4), which applied the downward force to the MMB test fixture.

The static tests were conducted with a displacement rate of 1 mm/min. To validate the FE models described in Section 4, the load–displacement data output from the test machine were recorded and compared to the FE results. The crack lengths input into the FE models were obtained from the images recorded by a camera. The images were recorded simultaneously with the load

Table 1
Mechanical properties of the constituent material in the sandwich structures [5,15].

Materials	Young's modulus (E_x)	Young's modulus (E_y)	Shear modulus (G_{xy})	Poisson's ratio (υ_{xy})
Foam	58 MPa	132 MPa	33 MPa	0.17
Composite	17 GPa*	–	6.84 GPa*	0.32*
PU	100 MPa	–	–	–

* Obtained experimentally.

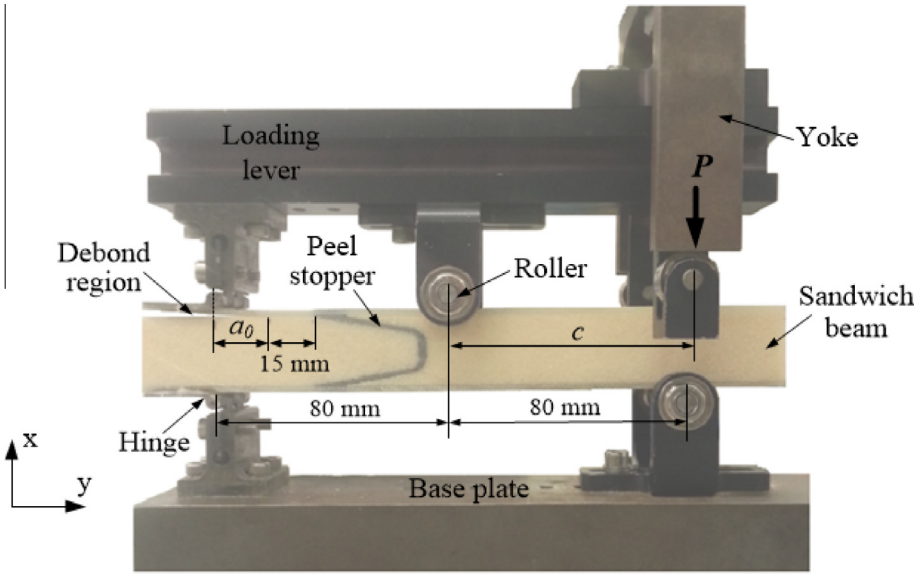

Fig. 4. Sandwich beam specimen with peel stopper loaded in the MMB test rig.

Table 2
Dimensions and the loading conditions of each sandwich specimen.

Specimen	Peel stopper configuration	Initial crack length (a_0, mm)	Face sheet thickness (t_f, mm)	Lever arm distance (c, mm)	Mode-mixity (ψ, °)
C1_s1 (static)	C1	14	1.6	60	−12.6
C1_f1 (fatigue)		17	1.6	75	−10.2
C1_f2 (fatigue)		18	1.6	75	−10.2
C1_f3 (fatigue)		18	1.6	75	−10.2
C2_s1 (static)	C2	13.5	1.7	60	−12.9
C2_f1 (fatigue)		17	1.7	75	−10.4
C2_f2 (fatigue)		19	1.7	75	−10.5
C2_f3 (fatigue)		19.5	1.7	75	−10.5
C3_s1 (static)	C3	14	1.7	60	−12.5
C3_f1 (fatigue)		15.5	1.7	75	−9.7
C3_f2 (fatigue)		19	1.7	75	−9.9
C3_f3 (fatigue)		20	1.7	75	−9.9

and displacement data, and were calibrated using a pre-applied scale on the specimen surface.

The fatigue tests were performed using displacement control as the displacement controlled tests generally offer more stable test conditions and promote stable crack growth. A displacement ratio $R(\delta_{min}/\delta_{max}) = 0.2$, and a loading frequency of 3 Hz were used. In the tests TSA was performed to determine the local effects at the tri-material junction of the face sheet, core and the peel stopper. The experimental setup for the TSA is shown in Fig. 7. The IR camera captured the thermal images for TSA with a frame rate of 383 Hz. To perform the motion compensation, images for DIC were captured by a white light camera placed behind the IR camera. To correlate the displacement field and the thermal image, both cameras were aligned perpendicular to the specimen surface [10]. The IR camera was placed on a tripod which allows the camera to be moved up and down vertically. Thus, when the white light camera captures the images, the position of the IR camera was adjusted, so the white light camera could observe the specimen. A detailed description of the fatigue test procedure is provided in Section 6.

The IR system used in this work is the FLIR SC5500 series. The system includes a photon detector, sensitive to radiation with wavelengths from 3 to 5 μm. The detector is a 320 × 256 pixel indium/antimonide (InSb) sensor array. In standard operation the detector has a sensitivity of 4.2 mK at 25 °C and a maximum frame rate of 383 Hz. The system enables the use of a magnifying lens (L0510 × 0.5) which provided a region of interest of 17.9 × 14.3 mm^2, with a spatial resolution of 0.06 mm/pixel. The white light camera used for motion compensation was a LA Vision VC-Imager E-lite digital camera with 5 mega-pixel sensor array. To achieve a similar field of view to that of the thermal data, a 105 mm lens (SIGMA) was used. The lens was set with a scale factor of 0.01 mm/pixel to provide a region of interest of 24 × 22 mm^2. Displacements of the specimen were computed from the recorded white light images using the commercial DIC software (DaVis 8) produced by LAVison.

The thermal and white light images collected in the neighbourhood of the tri-material junction are shown in Fig. 8(a) and (b) respectively. In both images the position of the peel stopper is marked by the dashed line. A small piece of foil was attached to the face sheet to help identify the position of the peel stopper tip. The position masks placed on the specimen surface was used to align the thermal and white light images so that the displacement vector corresponding to each IR pixel can be located [10]. The white rectangular area bounded by the position marks is the

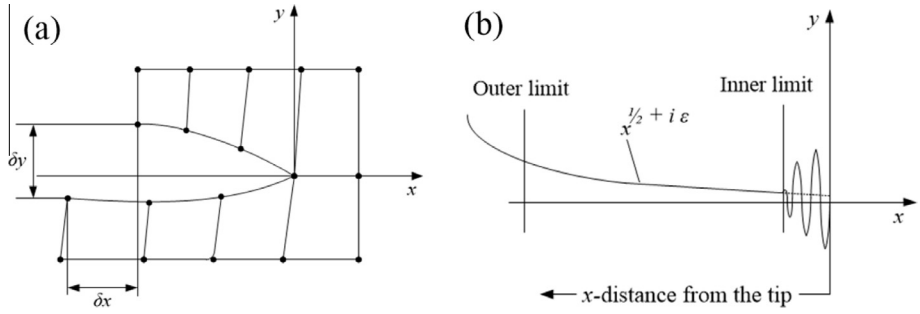

Fig. 5. (a) Extraction of displacement data from the local coordinate system in the FE model, and (b) schematic representation of CSDE method.

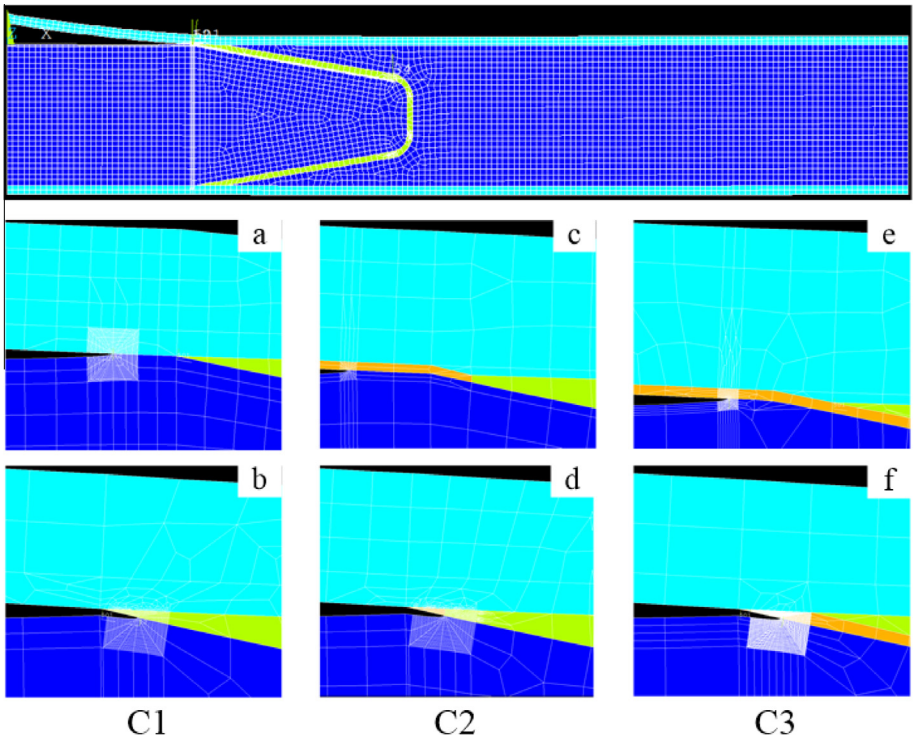

Fig. 6. FE models of the sandwich specimens corresponding to different crack path scenarios near the tri-material junction for C1 (a and b), C2 (c and d) and C3 (e and f). (For interpretation of the references to colour in this figure caption, the reader is referred to the web version of this article.)

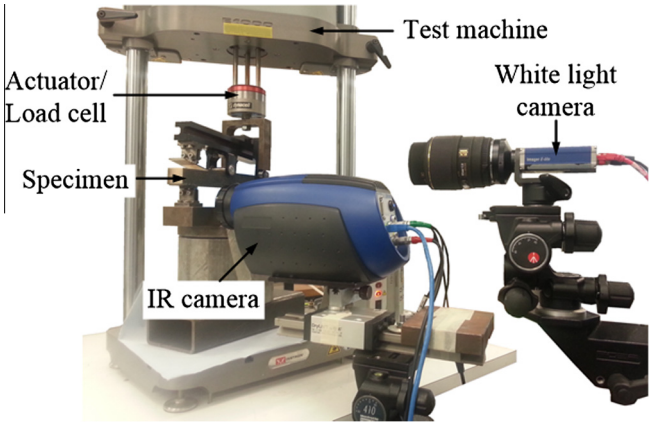

Fig. 7. Test setup for the TSA measurement in the fatigue test.

region of interest (i.e. the area where the motion compensation was applied). The grid shown in Fig. 8(b) shows the interrogation cells used for the DIC.

6. Fatigue test procedure

A disadvantage of the displacement controlled fatigue test is that the energy release rate decreases with crack growth. This means that more loading cycles are required to achieve the desired crack length. The specimens were tested until the crack length was about 25 mm, i.e. 10 mm after the peel stopper tip. During the crack propagation the energy release rate will decrease significantly, and the crack may stop growing before it has reached the peel stopper. Therefore during the tests it is necessary to change the displacement amplitude to control the ΔG at the prescribed value (see Fig. 9(a)). The 'ΔG control' is described in Fig. 9(b). Firstly the FE model described in Section 4 is used to predict the maximum displacement (δ_{max}) shown by the black line in Fig. 9(b). A ΔG of 450 J/m^2 was selected which is smaller than the interfacial fracture toughness of the sandwich specimens studied in this work [21]. For the small displacement ratio of $R = 0.2$ the difference between ΔG and G_{max} is insignificant [22]. Thus, δ_{max} can be obtained directly using the value of 450 J/m^2, so δ_{max} was calculated in increments of 1 mm (note the 0 mm crack increment

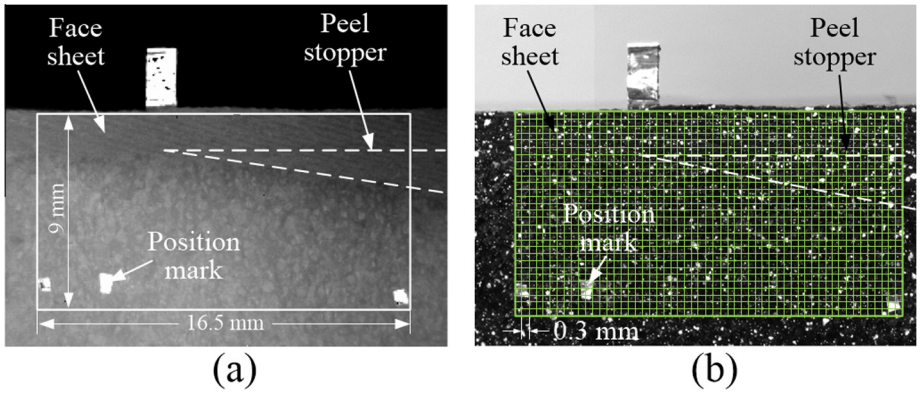

Fig. 8. (a) Thermal image and (b) white light image collected from the specimen surface in the neighbourhood of the tri-material junction. (For interpretation of the references to colour in this figure caption, the reader is referred to the web version of this article.)

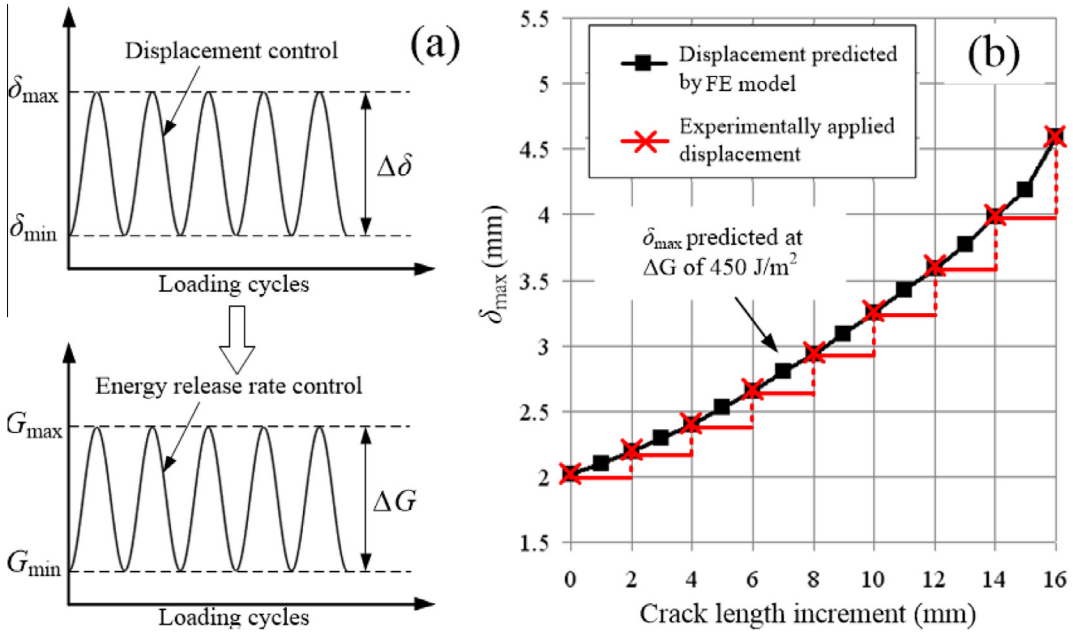

Fig. 9. (a) Displacement control and energy release rate control in the fatigue test, (b) δ_{max} against crack increment at ΔG of 450 J/m^2. (For interpretation of the references to colour in this figure caption, the reader is referred to the web version of this article.)

as shown in Fig. 9(b) corresponds to the initial crack length). The displacement amplitude (δ_{amp}) and the mean displacement (δ_{mean}) were calculated according to the δ_{max} and displacement ratio (R) as follows:

$$\delta_{amp} = \frac{\delta_{max} - R\delta_{max}}{2}$$
$$\delta_{mean} = R\delta_{max} + \delta_{amp} \quad (8)$$

The fatigue test was initially setup by using the δ_{amp} and δ_{mean} calculated at 0 mm crack increment. This allowed the fatigue test to be started with ΔG of 450 J/m^2. The δ_{mean} and the δ_{amp} were then adjusted for each 2 mm crack increment as indicated by the red line shown in Fig. 9(b). By doing this, the ΔG value was maintained close to 450 J/m^2 throughout the test.

The fatigue test procedure is described by the flowchart shown in Fig. 10. The test was started using the δ_{amp} and δ_{mean} derived at 0 mm. When the crack tip has moved by 2 mm, the test was paused. The δ_{amp} and δ_{mean} values were adjusted and the fatigue test was restarted using the new δ_{amp} and δ_{mean} values. This process was continued until the crack propagated into the neighbourhood of the tri-material junction (i.e. when the distance between the crack tip and the peel stopper tip was smaller than 6 mm). During the process, the crack tip location was determined from the live thermal images where the pixel resolution was calibrated beforehand using a pre-applied scale on the specimen surface. Once the crack tip reached the region of interest, the fatigue test was paused after a set of 1200 thermal images was recorded for the TSA, and the position of the IR camera adjusted. The images for DIC were then captured as the specimen was loaded *quasi* statically over a range equivalent to the dynamic loading range. The fatigue test was restarted using the new δ_{amp} and δ_{mean} values and the IR camera returned to its original position to observe the region of interest. For each 2 mm crack increment, the sequence of thermal and white light images capture was repeated until the crack had propagated 10 mm beyond the tri-material junction.

7. Fracture test results

Table 3 summarises the crack paths of the different specimens observed in the static tests. It was observed that the crack was

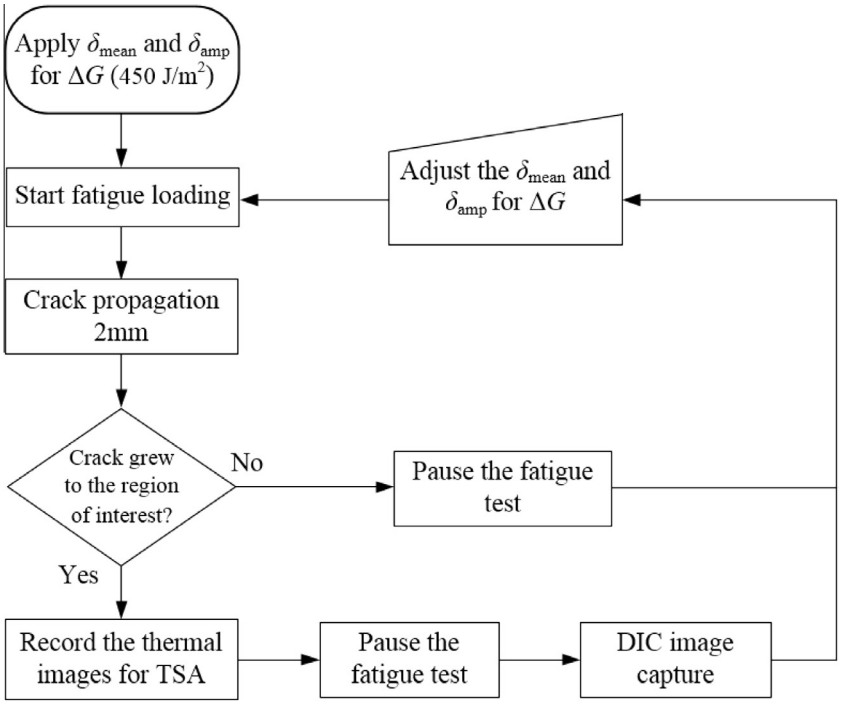

Fig. 10. Flowchart of the fatigue test procedure.

Table 3
Crack paths observed from different specimens in the static tests.

Specimen	Peel stopper configuration	Crack paths at the tri-material junction	Post crack deflection behaviour
C1_s1	C1	Deflection occurred at one side of the specimen	Debond occurred at the face sheet/peel stopper interface
C2_s2	C2	Deflection occurred at both sides of the specimen	No debond occurred
C3_s3	C3	Deflection occurred at both sides of the specimen	Debond occurred at the face sheet/peel stopper interface

Table 4
Crack paths observed from different specimens in the fatigue tests.

Specimen	Peel stopper configuration	Crack paths before the tri-material junction	Crack paths at the tri-material junction
C1_f1	C1	Foam	Deflected
C1_f2		Foam	Not deflected
C1_f3		Foam	Not deflected
C2_f1	C2	Interface, foam	Deflected
C2_f2		Interface, foam	Deflected
C2_f3		Interface, foam	Deflected
C3_f1	C3	Interface	Deflected
C3_f2		Interface	Deflected
C3_f3		Interface, foam	Deflected

successfully deflected at the tri-material junction in specimens C2 and C3. However, C1 which essentially was of the same design configuration at the tri-material junction of the original peel stopper cannot deflect the crack efficiently. After the crack passed the peel stopper tip, a debond was observed at the face sheet/peel stopper interface in specimens C1 and C3. This could be caused by defects introduced during the manufacturing process.

The crack paths of the different specimens observed in the fatigue tests are summarised in Table 4. The crack paths at the tri-material junction of different configurations are similar as those observed in the static tests. In specimens C1 the crack propagated in the foam just below the interface as it approached the tri-material junction. There are two specimens (C1_f2 and C1_f3) where the crack did not deflect at the tri-material junction. Fig. 11 shows the crack paths captured at the tri-material junction from specimens C1. In all cases the crack kinked back towards to the face sheet at the tri-material junction resulting in the crack propagating at the face sheet/peel stopper interface in specimens C1_f2 and C1_f3. In specimens C2 the crack firstly propagated at the face sheet/core interface and then grew in the foam just below the interface. In specimens C3 the crack propagated with different paths as it approached the tri-material junction. The crack propagated along the face sheet/core interface in specimens C3_f1 and C3_f2. In specimen C3_f3 the crack firstly propagated along the interface and then grew in the foam. The crack paths at the tri-material junction obtained from specimens C3_f1 (i.e. crack tip in the face sheet) and C3_f3 (i.e. crack tip in the foam core) show that the crack deflected regardless of where the crack tip was located. Additionally, in all cases there was no debonding at the face sheet/peel stopper interface, unlike the static test results.

To validate the FE models, the loads and the corresponding crack lengths (determined from white light images) recorded in the static tests were input into the models for deriving the actuator displacement (δ_{MMB}) based on the relationship given by [16]:

$$\delta_{MMB} = \delta_1 + \frac{c}{L}(\delta_1 + \delta_2) \tag{9}$$

where δ_1 is the displacement of the central 'roller' line of the sandwich beam specimen (see Fig. 4) and δ_2 is the crack tip opening displacement. δ_1 and δ_2 were obtained from the nodal displacements derived from the FE models.

Fig. 12 plots the load–displacement data obtained from the experiments and the FEA for the different peel stopper configurations. The red dashed line shown in the figures indicates the value of the actuator displacement when the crack tip passed the peel

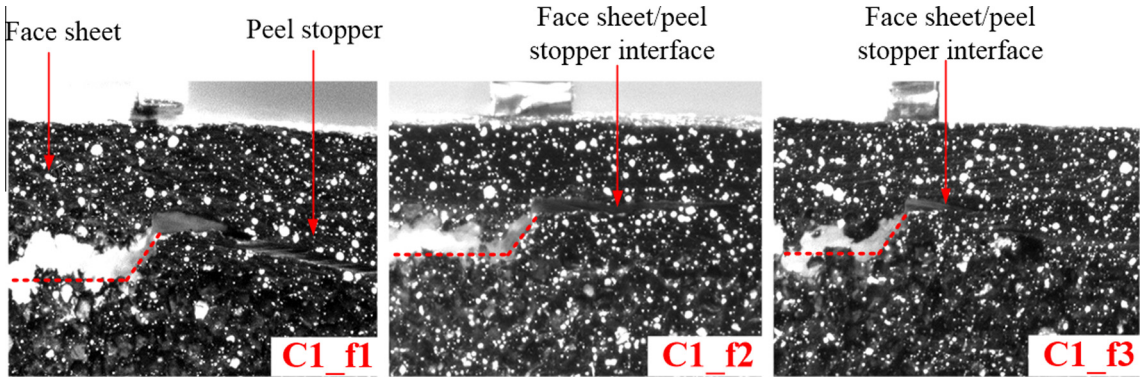

Fig. 11. Crack paths at the tri-material junction observed from specimens C1.

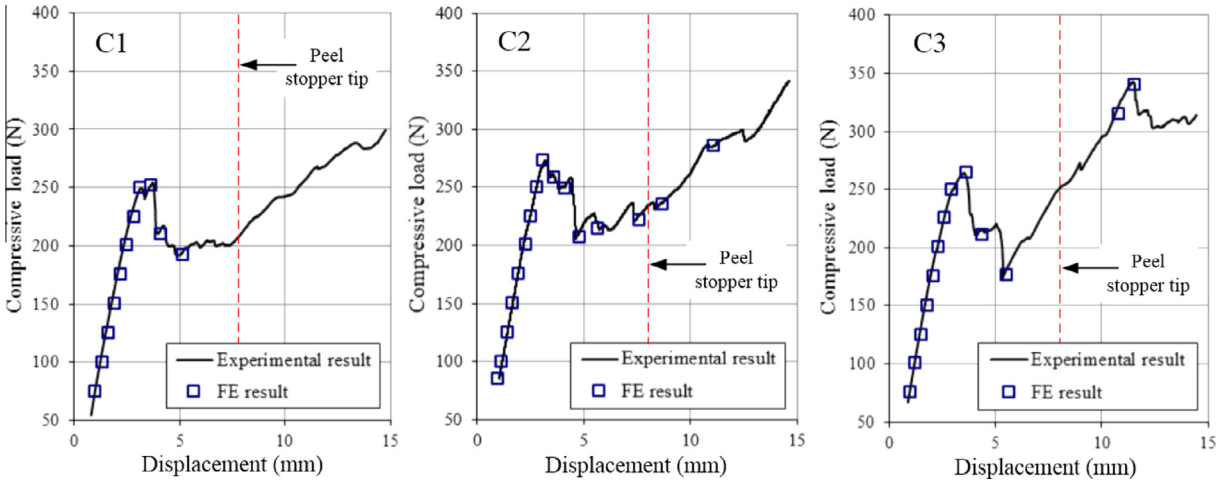

Fig. 12. Comparison of the results between the experiments and the FEA for different peel stopper configurations. (For interpretation of the references to colour in this figure caption, the reader is referred to the web version of this article.)

stopper tip, i.e. the load–displacement curve shown on the right hand side of the red line was obtained after the crack tip passed the peel stopper tip. For specimen C1, two crack paths were observed across the specimen width when the crack passed the peel stopper tip. Thus, the load–displacement data on the right hand side of the red line are not available from the FE model. For all the different peel stopper configurations, the FE results show a good agreement with the results obtained from the experiments. This indicates that the FE model can predict the specimen behaviour during the crack propagation.

8. TSA results

TSA results collected in the neighbour of the peel stopper tip are presented in the form of the non-dimensional stress metric, $\Delta T/T$, which is linearly proportional to the change in the sum of principal stresses (i.e. $\Delta\sigma_x + \Delta\sigma_y$). The thermoelastic constant, K_T, is a material parameter that defines this proportionality (i.e. $\Delta T/T = K_T(\Delta\sigma_x + \Delta\sigma_y)$). An example showing the difference in the $\Delta T/T$ data before and after applying the motion compensation is shown in Fig. 13 as the crack propagated in the foam and reached the tri-material junction. After applying motion compensation, a localised increase in $\Delta T/T$ at the tri-material junction, i.e. in the face sheet and at the crack tip, can clearly be observed in Fig. 13(b).

Fig. 14 shows the $\Delta T/T$ values obtained in the vicinity of the tri-material junction from the three C1 specimens. In Fig. 14 Images 1, Images 2 and Images 3 were obtained when crack approached, reached and passed the tri-material junction respectively. As the crack approached the tri-material junction (see Images marked as 1), the through-thickness stress gradient changes from compression to tension, as does the stress concentration in the foam just below the interface at the crack tip. As the thermoelastic constant of the foam is about 20 times higher than that of the E-glass/epoxy composites [23], this indicates that the stress produced in the face sheet is much higher than that at the crack tip. When the crack reached the tri-material junction (Images marked as 2), large $\Delta T/T$ values were obtained from the face sheet on the right hand side ahead of the peel stopper. The $\Delta T/T$ values in the face sheet ahead of the peel stopper tip are of comparable magnitude to those in the foam below the peel stopper tip (i.e. the crack tip). After the crack passed the tri-material junction, two crack paths were observed in specimens C1 as described in Section 7, Fig. 11 and Table 4. Although the crack was deflected in specimen C1_f1, an increase in $\Delta T/T$ in the face sheet close to the face sheet/peel stopper interface is seen in Image 3. This may be due to weak bonding between the face sheet and the peel stopper. In specimens C1_f2 and C1_f3, the crack was not deflected; hence large $\Delta T/T$ values are generated in the face sheets.

Fig. 15 shows the $\Delta T/T$ data obtained from the three C2 specimens. Here in all specimens the crack propagated in the foam just below the interface and was deflected at the tri-material junction. The $\Delta T/T$ values obtained as the crack approached the tri-material junction (see Images marked as 1) show similar results to specimens C1. When the crack reached the tri-material junction (see Images

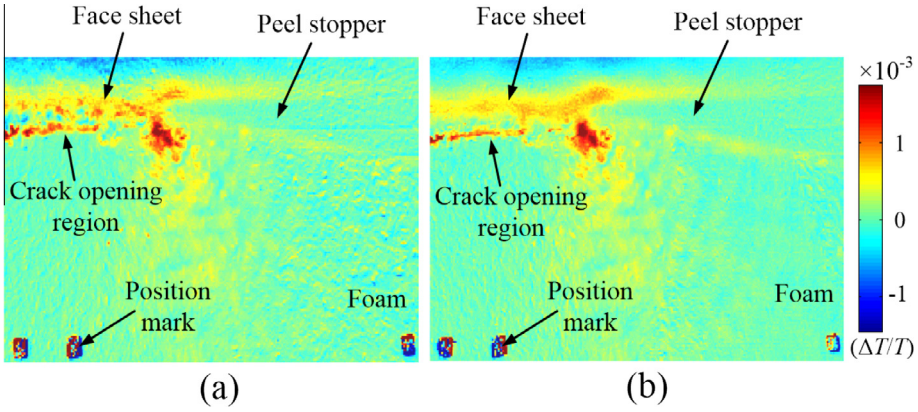

Fig. 13. Comparison of the TSA results before (a) and after (b) motion compensation.

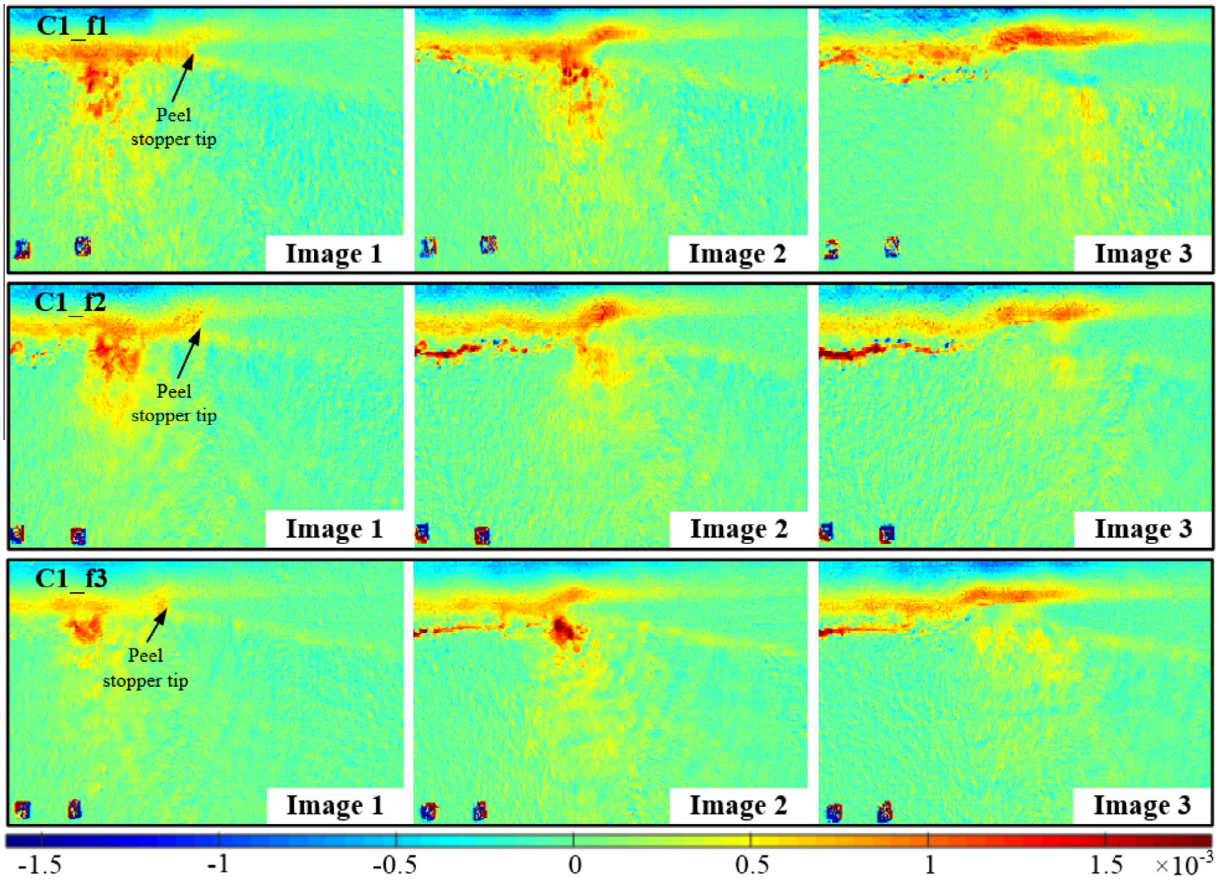

Fig. 14. $\Delta T/T$ obtained from the neighbourhood of the tri-material junction from specimens C1.

marked as 2), the $\Delta T/T$ value in the face sheet ahead of the peel stopper tip was much smaller than observed in C1. Moreover, an increase in $\Delta T/T$ occurs at the peel stopper/core interface compared to that observed for C1. After the crack passed the tri-material junction, large $\Delta T/T$ values were produced around the peel stopper/core interface. The $\Delta T/T$ values in the face sheet ahead of the peel stopper tip were much smaller than those observed in C1.

The $\Delta T/T$ values obtained from the three C3 specimens are shown in Fig. 16. When the crack approached the tri-material junction (see Images marked as 1), the $\Delta T/T$ values were similar to those obtained from specimens C1 and C2. When the crack reached the tri-material junction (see Images marked as 2), the $\Delta T/T$ fields obtained from different crack tip locations (i.e. in the face sheet/core interface or in the foam core) were comparable to those observed from C2, i.e. large $\Delta T/T$ values were only produced on the left hand side of the peel stopper tip accompanied by an increase in $\Delta T/T$ at the peel stopper/core interface. After the crack was deflected, an increase in the $\Delta T/T$ values was observed in a small area ahead of the peel stopper tip; this was not the case for C1 and C2.

The local effects introduced by different peel stopper configurations have been identified using the TSA data collected from the neighbourhood of the tri-material junctions. It was shown that the local effects are strongly dependent on the peel stopper

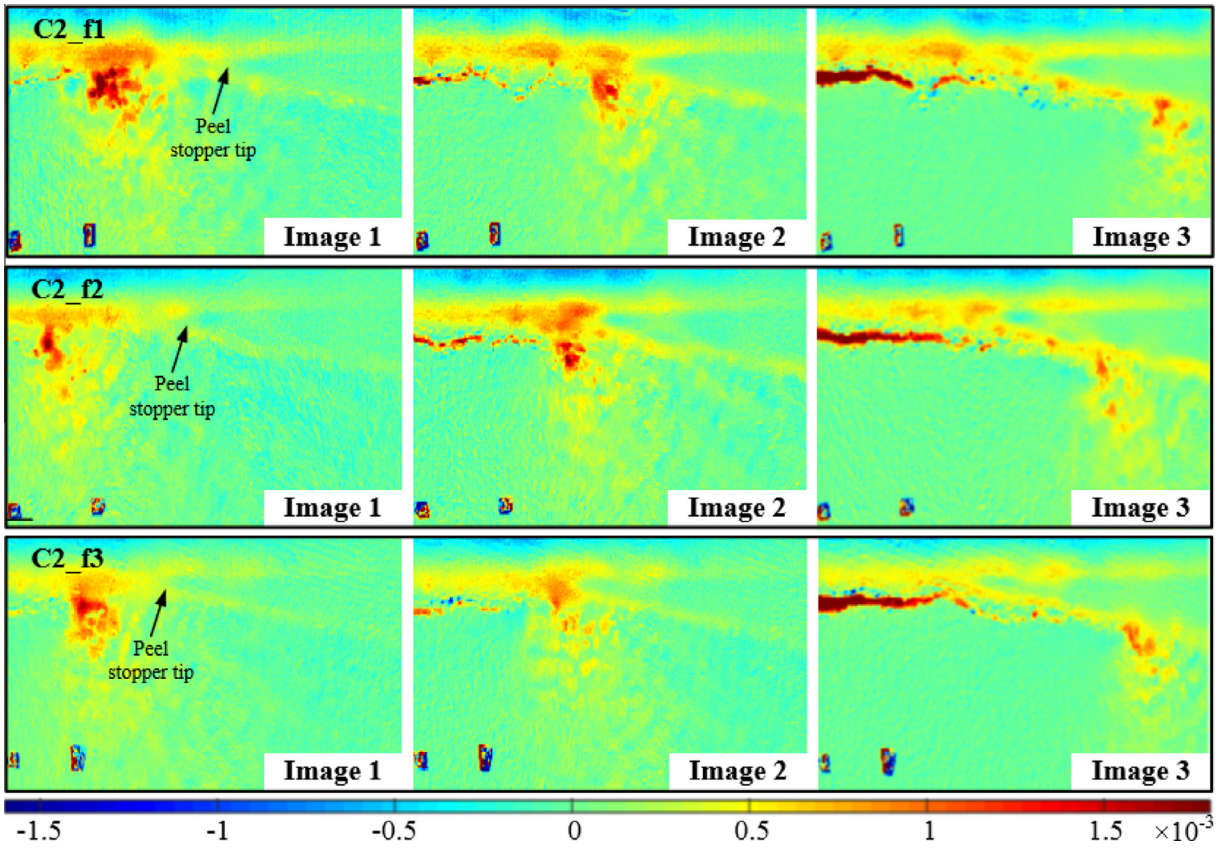

Fig. 15. $\Delta T/T$ obtained from the neighbourhood of the tri-material junction from specimens C2.

configuration, especially when the crack reached and passed the tri-material junction.

When crack reached the tri-material junction, it is shown that the increase in $\Delta T/T$ in the face sheet ahead of the peel stopper tip is more significant in specimen C1 than that in specimens C2 and C3. Furthermore, an increase in $\Delta T/T$ at the peel stopper/core interface is observed in C2 and C3. The TSA results for C1 indicate that large longitudinal stresses (σ_x) exist in the face sheet ahead of the peel stopper tip. It is important to note that the stresses in the face sheet are predominantly in plane, conversely in the foam the thermoelastic response is dominated by the transverse normal stresses. So the σ_x values in the core area below the face sheet/peel stopper interface in C1 are much smaller compared to those in the face sheet. In C2 and C3, this is not the case as an increase in $\Delta T/T$ is identified at the peel stopper/core interface (the increase in $\Delta T/T$ in the face sheet ahead of the peel stopper tip is insignificant), indicating that σ_x has influence in both the face sheet and the peel stopper. If the bending moment that produces σ_x only acts on the face sheet, it induces large peeling stresses between the face sheet and the peel stopper. Furthermore, compressive transverse normal stresses are induced across the face sheet/peel stopper interface ahead of the crack tip as shown in Fig. 17(a). This explains the crack path in specimens C1 where the crack kinked back towards to the face sheet at the tri-material junction. On the other hand, if the bending moment acts on both the face sheet and the peel stopper as in C2 and C3, peeling stresses are induced at the peel stopper/core interface as illustrated in Fig. 17(b). Hence, facilitating the crack deflection at the tri-material junction.

The specific peel stopper configuration also influences the stress state after the crack deflection has occurred. In specimens C1 large $\Delta T/T$ values can be observed near the face sheet/peel stopper interface as shown by Image 3 of Fig. 14. In C3 an increase of the $\Delta T/T$ values can be also observed around the face sheet/peel stopper interface (see Images marked as 3 in Fig. 16), but is most noticeable in the area close to the peel stopper tip. Compared to specimens C1 and C3, the increase in $\Delta T/T$ values at the face sheet/peel stopper interface is much smaller for the specimens C2 (see Images marked as 3 in Fig. 15). The reason for the relatively large $\Delta T/T$ values observed ahead of the peel stopper tip for the C3 specimens is not entirely clear, but it may be caused by defects introduced during the manufacturing, for example that the inter-fibre layer may not be bonded perfectly to the peel stopper tip and the face sheet at the tri-material junction, and also voids and a resin rich area may be introduced at the tri-material junction as sketched in Fig. 18. This may be caused by two different mechanisms: (1) the applied vacuum in combination with the atmospheric pressure, which together drives the infusion process, may not be sufficient to assure that air bubbles are not entrapped and that full wetting of the glass fabric is achieved at the tri-material junction; (2) the geometry of the peel stopper tip is imperfect (i.e. not a perfect wedge). This large $\Delta T/T$ values ahead of the peel stopper tip observed in C1 and C3 specimens indicate a weak bonding at the face sheet/peel stopper interface which can result in the debond damage. Thus, the TSA results provide a clear indication of the reasons why significant debond damage was observed for specimens C1 and C3 during the static tests.

9. FE analysis

The case of crack deflection for the crack passing the tri-material junction was analysed. The predicted energy release rate and the mode-mixity values were compared to the experimentally observed crack paths. The paths consist of the "straight path" for the crack penetrating the peel stopper, and the "deflected

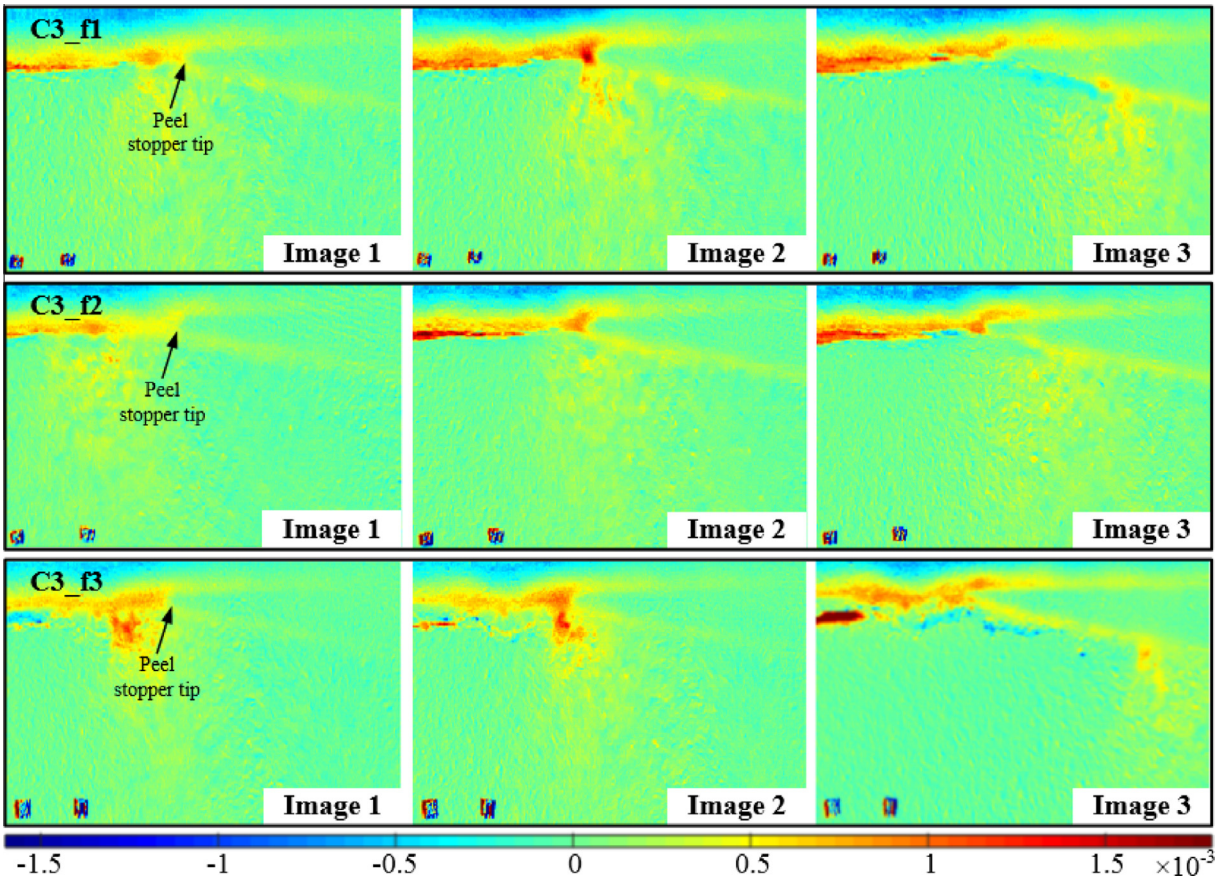

Fig. 16. $\Delta T/T$ obtained from the neighbourhood of the tri-material junction from specimens C3.

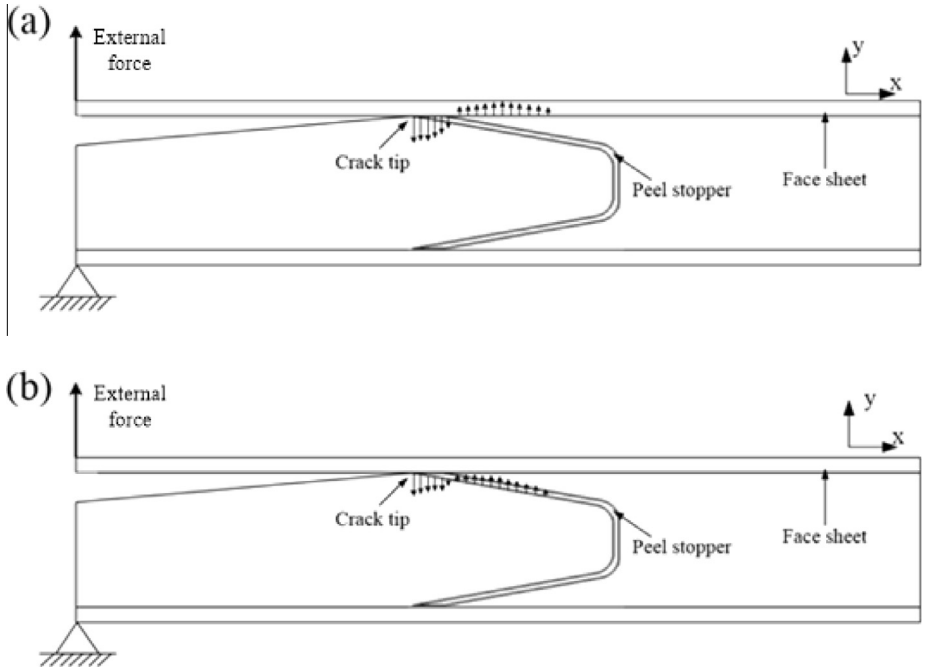

Fig. 17. Force diagram of the debonded sandwich beam specimen associated with (a) crack path at the face sheet/peel stopper interface and (b) crack path at the peel stopper/core interface.

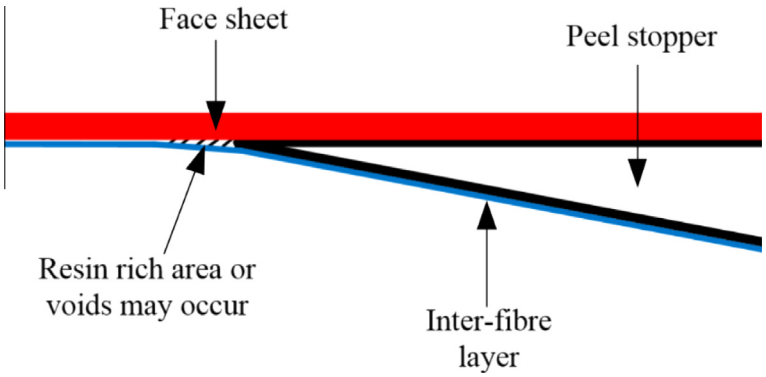

Fig. 18. Sketch of the tri-material junction for specimens C3.

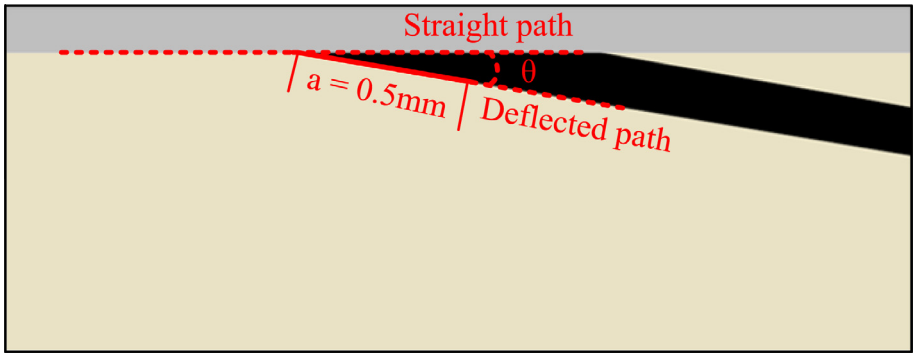

Fig. 19. Crack paths investigated around the tri-material junction.

path" for the crack deflecting at the peel stopper. The ability to achieve crack deflection wrt. the peel stopper angle θ was also investigated (see Fig. 19). The peel stopper angle, θ was varied from 5 to 30° with steps of 5°, and with a kinked crack length of 0.5 mm away from the corner as shown in Fig. 19. The 10° angle represents the tested configuration.

In Fig. 20, the predicted energy release rates (left) and mode-mixities (right) for the two different crack paths are plotted as functions of the peel stopper angle θ for configurations C1, C2 and C3. From Fig. 20 it is observed that the energy release rate for a crack propagating straight through the tri-material junction for C1 is not affected significantly by changing the peel stopper angle. For C2 and C3 though, the peel stopper angle influences the energy release rate significantly, as the protruding fibres (C2) and the inter fibre layer (C3) follow the changing value of θ. Thus, the value of the angle θ has an effect on the local stiffness around the crack tip, and this directly affects the energy release rate. For the deflected crack paths, it is seen that the change in energy release rate is very small for C1 and C2, but for C3 a large and nearly linear drop of the predicted energy release rate is observed with increasing angle θ.

Fig. 20 also shows that for all 3 peel stopper configurations only small changes of the mode mixities are predicted with increasing θ-value for the case of a crack propagating straight through the tri-material junction. For the deflected crack paths it is observed for all 3 configurations that the mode-mixity decreases with increasing θ. Further, for C1 and C2 the mode-mixity becomes negative for increasing θ, whereas it remains positive for every θ-angle for C3. Even though the mode-mixity changes for the deflected crack path with increasing θ, the shear component only increases significantly for very high deflection angles. For small deflection angles the mode-mixity is such that the crack experiences mode I dominant conditions for both the straight and the deflected crack paths.

The numerical results are used together with a criterion for crack kinking proposed in [17] to substantiate and explain the experimental observations. According to this criterion the condition for a crack to kink out of an interface can be expressed by the inequality [17]:

$$\frac{G_{straight}}{\Gamma(\psi)_{straight}} < \frac{G_{deflected}}{\Gamma(\psi)_{deflected}} \tag{10}$$

where $G_{straight}$ is the calculated energy release rate at the face sheet/core interface (i.e. for a crack growing along the straight path), and $G_{deflected}$ is the energy release rate corresponding to a given deflection angle θ which is identical to the peel stopper angle. $\Gamma(\psi)$ represents the interface fracture toughness values corresponding to the straight and deflected crack paths at a given mode-mixity angle ψ. Since the interface fracture toughness values are unknown, the considerations presented are qualitative rather than quantitative, and based on the calculated energy release rate and mode-mixity values alone.

Fig. 20 shows that for each peel stopper configuration and for every peel stopper angle the energy release rate of the deflected crack path is lower than the energy release rate for the straight crack path. Thus, for all configurations and peel stopper angles the following inequality hold true:

$$G_{straight} > G_{deflected} \tag{11}$$

Further, the criterion for crack deflection (kinking) given by the inequality (9), can be rearranged as follows:

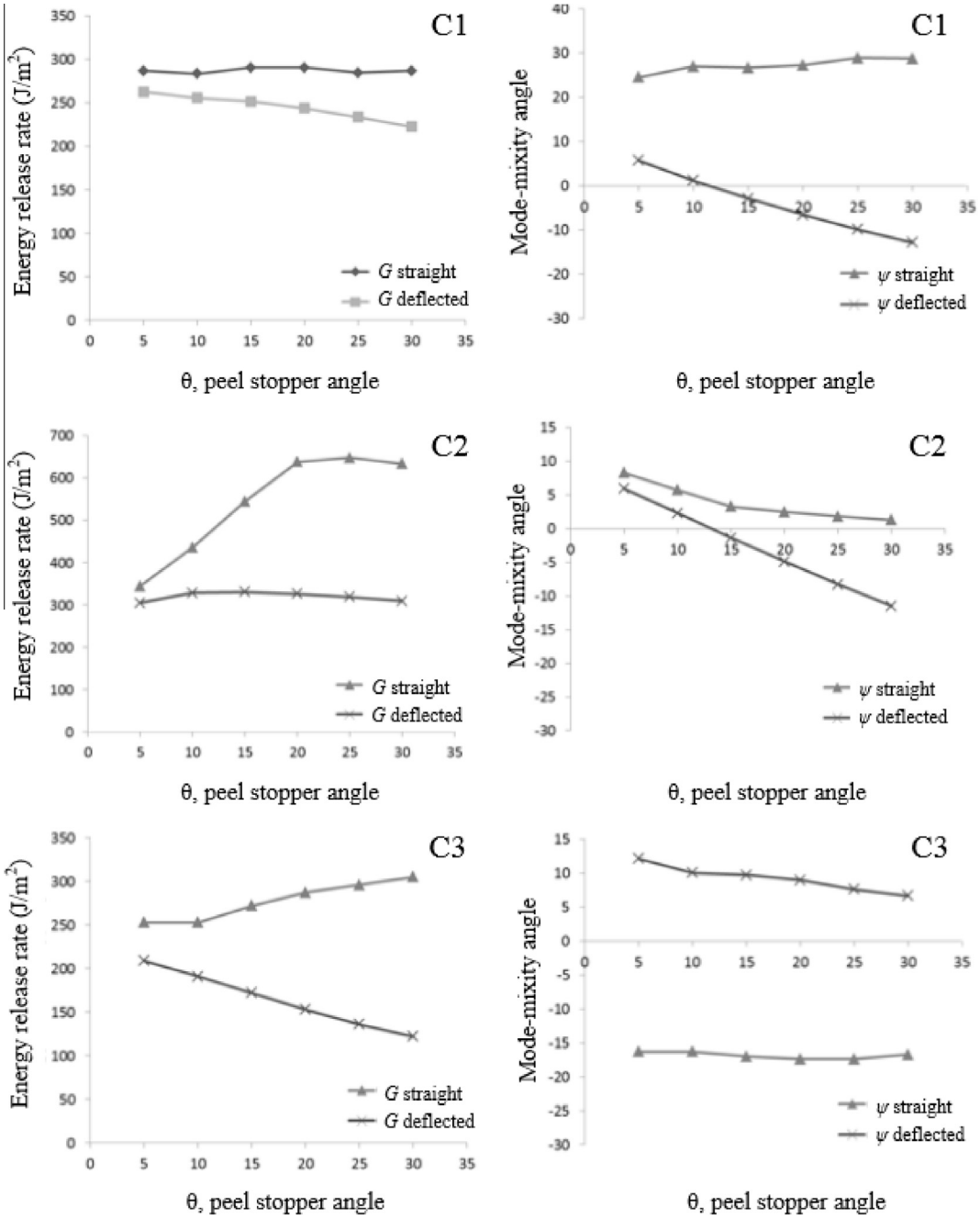

Fig. 20. Left: predicted energy release rate vs. peel stopper angle for the three peel stopper configurations. Right: predicted mode-mixity vs. peel stopper angle for the three peel stopper configurations.

$$\frac{G_{deflected}}{G_{straight}} > \frac{\Gamma(\psi)_{deflected}}{\Gamma(\psi)_{straight}} \tag{12}$$

The two inequalities (11) and (12) show that crack kinking is highly dependent on the ratio between the two interface fracture toughnesses $\Gamma(\psi)_{deflected}$ and $\Gamma(\psi)_{straight}$. It can further be deducted that a propagating crack will have a tendency to stay close to the straight interface where the energy release rate is higher, rather than to follow the deflected crack path.

From Fig. 20 it can also be observed that the mode-mixity remains highly mode I dominant which means that the interface fracture toughness of each path is close to its mode I fracture toughness [17,18].

Based on the numerical results presented in Fig. 20 the ratio $\frac{G_{deflected}}{G_{straight}}$ can be expressed for different crack deflection angles as shown in Fig. 21. Then it follows from Eq. (12), that for each peel stopper configuration the crack will kink when the fracture toughness ratio $\frac{\Gamma(\psi)_{deflected}}{\Gamma(\psi)_{straight}}$ is smaller than the energy release rate ratio $\frac{G_{deflected}}{G_{straight}}$ for a given peel stopper angle (in Fig. 21).

It can be seen that by increasing the peel stopper angle the crack kinking at the tri-material junction becomes more difficult, especially for C2 and C3. For the case tested in this study, at 10° the fracture toughness ratio needed to obtain crack deflection is

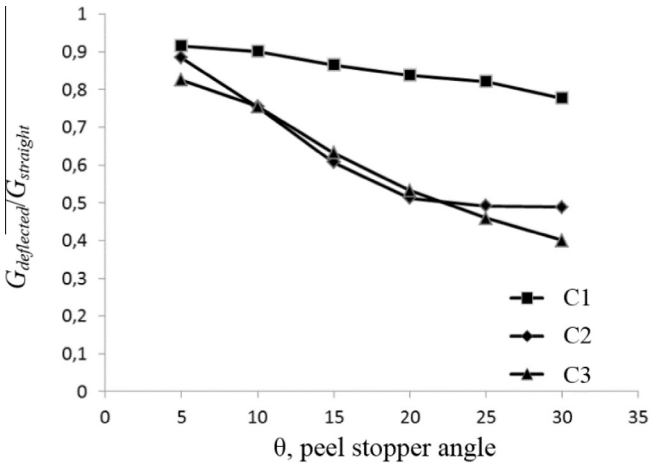

Fig. 21. $\frac{G_{deflected}}{G_{straight}}$ vs. peel stopper angle θ.

similar for C2 and C3, while for C1 the ratio is significantly higher. These observations agree well with results presented in [7] which considered the efficiency of peel stoppers to deflect and arrest propagating face-sheet/core interface cracks under mode II dominated stress fields in the vicinity of the tri-material junction.

Fig. 21 explains the behaviour observed for C1 (straight crack path followed in 2 of 3 cases). Since the required fracture toughness ratio must be below the energy release rate ratio, the straight path interface fracture toughness ($\Gamma(\psi)_{straight}$) must be larger than the interface fracture toughness at the deflected path. It may be assumed that the material systems at the two interfaces have comparatively similar interface fracture properties since the bonding is achieved by the infused epoxy resin and an epoxy glue respectively. The possibility of the fracture toughness ratio and the energy release ratio being both close to 1 explains why in one of the tests crack deflection was observed around the tri-material junction. Crack deflection may occur occasionally in C1 if the two ratios are close to being equal.

C2 and C3 represent an effort to increase the straight path interface fracture toughness by using glass fibres reinforced with resin and thus lowering the fracture toughness ratio. For a crack to propagate straight ahead it has first to break the fibres at the straight path interface. In both configurations the increase is local, only around the crack tip, where the fibres are "sticking out" or laid in front of the peel stopper. Even though in Fig. 21, the energy release rate ratio at 10° is $\frac{G_{deflected}}{G_{straight}} = 0.75$, the mode I fracture toughness of the fibres is several times higher than that of epoxy [24] thus explaining why C2 and C3 generally were shown to enable crack deflection as required.

10. Conclusions

The geometry and material composition of a previously proposed (original) peel stopper [5–7] was modified to a 'U' shape to reduce the volume and mass, and glass fibre layers were introduced into the peel stopper material (PU) to increase the fracture toughness. Using the new peel stopper concept, three different configurations of the peel stopper (C1, C2 and C3) were proposed. C1 has the same configuration at the tri-material junction as that of the original peel stopper (the peel stopper is directly bonded to the foam core). For C2 reinforcement fibres inside the peel stopper protrudes from the peel stopper tip and are attached to the face sheet by bonding through the infusion process. For C3 an inter-fibre layer glass fabric is placed along the peel stopper/core interface and the part of the fibre-layer extending from the peel stopper tip is bonded to the face sheet in the infusion process. The mechanisms controlling the crack propagation at the tri-material junction were studied using both TSA and FE analysis. The main findings can be summarised as:

1. The local effects induced near the peel stopper tip for the different peel stopper configurations were quantified using TSA. It was shown that the local effects induced near the peel stopper tip were significantly influenced by the type of peel stopper used.
2. When the interfacial crack reached the tri-material junction for the C1 specimens, large stresses were identified ahead of the peel stopper tip in the face sheet. However, an increase in the stresses at the peel stopper/core interface was observed for configurations C2 and C3. It has been demonstrated that the large stresses ahead of the peel stopper tip for C1 indicate the presence of significant interfacial peeling stresses which result in crack propagation along the face sheet/peel stopper interface. For C2 and C3 it was demonstrated that interfacial peeling stresses are primarily induced along the peel stopper/core interface, thus promoting crack deflection.
3. For specimens C1 and C3 an increase in face sheet stresses was induced ahead of the peel stopper tip when the crack had passed the tri-material junction. This indicates a weak bonding at the face sheet/peel stopper where debonding initiated.
4. The capability of achieving crack deflection of the 3 peel stopper configurations as a function of the peel stopper angle was investigated using FE analysis. The energy release rate and the mode-mixity associated with different peel stopper angles and crack paths were studied. It has been shown that by increasing the peel stopper angle, crack deflection at the tri-material junction becomes increasingly more difficult. In the study the 10° angle was the one tested since it represents the more practical solution.
5. For the tested 10° angle, the energy release rate for the two possible crack paths, crack propagating straight and crack deflecting at the peel stopper were used to derive results on the crack deflection ability of each configuration. It was shown that if the ratio of the energy release rates for the two crack paths is equal (or near equal) to the ratio of the interface fracture toughnesses of the two crack paths, then crack deflection at the peel stopper is unlikely to occur as observed for C1. To ensure crack deflection, it was found that the interface fracture toughness of the straight path must be large compared to the interface fracture toughness of the deflected crack path. By placing/embedding fibres in front of the peel stopper tip in C2 and C3 the desired behaviour was achieved and the crack is deflected every time, as was confirmed in the experiments.

Acknowledgements

The work presented was co-sponsored by the University of Southampton and the Danish Council for Independent Research Technology and Production Sciences (FTP), under the research project 'Enhanced Performance of Sandwich Structures by Improved Damage Tolerance' ('SANTOL'). The financial support received is gratefully acknowledged. DIAB AB Sweden is highly appreciated for the support for the foam material and supply of the PVC material.

References

[1] Zenkert D. An introduction to sandwich construction. London: EMAS; 1997.
[2] Hirose Y, Matsubara G, Hojo M, Matsuda M, Inamura F. Evaluation of modified crack arrester by fracture toughness tests under mode I type and mode II type loading for foam core sandwich panel. In: Proc. US–Japan conference on composite materials 2008, Tokyo, Japan; 2008.

[3] Hirose Y, Matsuda H, Matsubara G, Inamura F. Evaluation of new crack suppression method for foam core sandwich panel via fracture toughness tests and analyses under mode-I type loading. J Sandwich Struct Mater 2009;11(6):451–70.
[4] Rinker M, Zahlen PC, John M, Schäuble R. Investigation of sandwich crack stop elements under fatigue loading. J Sandwich Struct Mater 2012;14(1):55–73.
[5] Jakobsen J, Bozhevolnaya E, Thomsen OT. New peel stopper concept for sandwich structures. Compos Sci Technol 2007;67:3378–85.
[6] Bozhevolnaya E, Jakobsen J, Thomsen OT. Fatigue performance of sandwich beams with peel stoppers. Strain 2009;45(4):349–57.
[7] Jakobsen J, Andreasen JH, Thomsen OT. Crack deflection by core junctions in sandwich structures. Eng Fract Mech 2009;14:2135–47.
[8] Jakobsen J, Thomsen OT, Andreasen JH, Bozhevolnaya E. Crack deflection analyses of different peel stopper design for sandwich structure. Compos Sci Technol 2009;69(6):870–5.
[9] Dulieu-Barton JM, Stanley P. Development and applications of thermoelastic stress analysis. J Strain Anal 1998;33(2):93–104.
[10] Wang W, Fruehmann RK, Dulieu-Barton JM. Application of digital image correlation to address complex motions in thermoelastic stress analysis. Strain, accepted for publication.
[11] Pan B, Qian K, Xie H, Asundi A. Two-dimensional digital image correlation for in-plane displacement and strain measurement: a review. Meas Sci Technol 2009;20(6).
[12] Suo Z. Singularities, interfaces and cracks in dissimilar media. Proc Roy Soc Lond, Ser A, Meas Phys Sci 1990;427:331–58.
[13] Berggreen C. Damage tolerance of debonded sandwich structures [PhD thesis]. Technical University of Denmark, Department of Mechanical Engineering, Maritime Engineering; 2004.
[14] Berggreen C, Carlsson LA. A modified TSD specimen for fracture toughness characterization – fracture mechanics analysis and design. J Compos Mater 2010;44(15):1893–912.
[15] Zhang S, Dulieu-Barton JM, Fruehmann RK, Thomsen OT. A methodology for obtaining material properties of polymeric foam at elevated temperatures. Exp Mech 2012;52:3–15.
[16] Quispitupa A, Berggreen C, Carlsson LA. On the analysis of a mixed mode bending sandwich specimen for debond fracture characterization. Eng Fract Mech 2009;76:594–613.
[17] Hutchinson JW, Suo Z. Mixed mode cracking in layered materials. Adv Appl Mech 1992;29:63–191.
[18] He M, Hutchinson JW. Kinking of a crack out of an interface. J Appl Mech 1989;111:270–8.
[19] Wang TC. Kinking of an interface crack between two dissimilar anisotropic elastic solids. Int J Solids Struct 1994;31(5):629–41.
[20] <http://148.204.81.206/Ansys/readme.html>.
[21] Wang W, Dulieu-Barton JM, Thomsen OT. A methodology for characterizing the interfacial fracture toughness of sandwich structures using high speed infrared thermography. Exp Mech 2015. http://dx.doi.org/10.1007/s11340-015-0023-3.
[22] Manca M, Quispitupa A, Berggreen C, Carlsson LA. Face/core debond fatigue crack growth characterization using the sandwich mixed mode bending specimen. Compos A Appl Sci Manuf 2012;43(11):2120–7.
[23] Wang W. Infrared techniques for quantitative evaluation of interfacial fracture behavior and damage tolerance in sandwich structures [PhD thesis]. University of Southampton; 2015.
[24] Ashby MF. Materials selection in mechanical design. Butterworth-Heinemann; 2011.

PAPER #2

Experimental Investigation of Interfacial Crack Arrest in Sandwich Beams Subjected to Fatigue Loading using a Novel Crack Arresting Device

G. Martakos[1], J.H. Andreasen[1], C. Berggreen[2], O.T. Thomsen[3,1]

[1]Department of Mechanical and Manufacturing Engineering, Aalborg University

Fibigerstræde 16, DK-9220 Aalborg East, Denmark

Email: {gm,jha, ott}@aau.dk, web page: http://www.aau.dk

[3]Department of Mechanical Engineering, Technical University of Denmark

Nils Koppels Allé, Building 403, DK-2800 Kgs. Lyngby, Denmark

Email: cbe@mek.dtu.dk, web page: http://www.mek.dtu.dk

[3]Faculty of Engineering and the Environment,
University of Southampton, Highfield, Southampton, UK

Email: o.thomsen@soton.ac.uk , web page: http://www.soton.ac.uk/engineering/

The paper was submitted and accepted for publication in revised form to the Journal of Sandwich Structures and Materials, September 2016

Abstract

A recently proposed face-sheet/core interface crack arresting device is implemented in sandwich beams and tested using the Sandwich Tear Test (STT) configuration. Fatigue loading conditions are applied to propagate the crack and determine the effect of the crack stopper on the fatigue growth rate and arrest of the crack. Digital image correlation is used through the duration of the fatigue experiment to track the strain evolution as the crack tip advances. The measured strains are related to crack tip propagation, arrest, and re-initiation of the crack. A finite element model is used to calculate the energy release rate, mode mixity and to simulate crack propagation and arrest of the crack. Finally the effectiveness of the crack arresting device is demonstrated on composite sandwich beams subjected to fatigue loading conditions.

Keywords: Sandwich structures, Finite Element Analysis, Composites, Fracture Mechanics, Fatigue

1. Introduction

Sandwich structures represent a special form of laminated composites comprising stiff and thin face-sheets separated by and bonded to either side of a light and compliant core material. The resulting layered sandwich element or structure displays very high stiffness and strength to weight ratios [1]. Their structural attributes and the need for larger and ever lighter structures has led to the implementation of sandwich structures into many areas of industrial production, including aerospace, ship/marine, automotive and wind turbine blade structures to mention a few. Due to their extensive and increasing use, novel ways to further enhance the performance of sandwich structures are being pursued continuously. Consequently the wish to fully understand the behaviour of sandwich structures is increasing, as well as the need to control and predict the effect of limitations and weaknesses inherent in their nature. One of the main limitations of sandwich structures is their high sensitivity to separation or debonding between the core material and the face-sheets. Localized loadings like bolt mounts or momentary overloads like impact loads can be responsible for introducing such debond damages in the structure. Debonds or dry spots can also be introduced during manufacturing, especially for larger parts. The separated or debonded zones effectively act as inherent structural weaknesses that often have no direct connection to the baseline mechanical properties of the constituent materials that comprise the structure. This study concerns the quantitative evaluation of a recently proposed face-sheet / core interface crack arresting device to be embedded in the sandwich core material [2-4], and which has the potential of significantly enhancing the damage tolerance of the sandwich structure.

The phenomenon of face-sheet /core separation or debonding (sometimes also referred to as “disbonding” or delamination) is frequently occurring as a so called bi-material or interfacial crack. Several studies have addressed the bi-material crack propagation and characterization problems. The earlier works of Erdogan [5] and Dundur [6] provided the theoretical background for examining crack behaviour in

dissimilar materials. Later, Hutchinson and Suo [7], He and Hutchinson and Suo [8-9] and Wang [10] described the conditions for crack propagation and kinking of an interface crack for isotropic and orthotropic material constituents. Several works have being conducted using Finite Element Modelling to investigate interfacial crack initiation and propagation [11-13]. Berggreen [12] provided the theoretical background for the finite element analysis framework and introduced and implemented the Crack Surface Displacement Extrapolation method (CSDE) [14-15]. The method is used for calculating the energy release rate and mode mixity of a bi-material crack by using relative node displacements of the separated crack surfaces. Finally, Moslemian et al. [13, 16] developed a *cycle-jump* technique that together with the CSDE method was used to simulate fatigue crack growth in the face/core interfaces of sandwich structures.

Development of new testing methods to characterize face/core interface cracks in sandwich structures has been the focus of many studies. The Single Cantilever Beam test (SCB) [17-18], the Cracked Sandwich Beam test (CSB) [19], the Mixed Mode Bending test (MMB) [20-21] were used to apply different loading conditions to cracked sandwich beams. Most notably with the MMB test, the mode mixity applied can be constant and independent of the crack length making the test ideal for fatigue crack growth characterization [21-22]. Lastly Berggreen et al [14] introduced the Sandwich Tear Test (STT) to investigate crack propagation paths in different core materials. In this work, the STT configuration is used to examine the effect of the crack arresting device embedded in damaged composite sandwich beams.

Previous attempts to delay or arrest propagating face/core interface cracks by using special crack stopping core insert like devices have shown some promise, but they have been somewhat dependent on the applied loading conditions. Rinker et al [23] introduced two types of carbon fibre reinforced inserts loaded using the SCB and CSB tests for mode I and mode II loading conditions, respectively. It was shown that especially under mode II loading conditions the crack arresters could arrest the crack for a considerable number of loading cycles. This effect is mostly a consequence of the much higher fracture toughness of the CFRP arresters, in comparison with the core material, as well as of the specific geometry of the crack arresters. Hirose et al. [24-25] demonstrated that crack arrest can be achieved by using either a semi-circular CFRP rod glued on the face / core interface or a splice-type arrester connecting the two face-sheets of the sandwich beam through CFRP layers. In both cases a stress release from the crack tip was recorded as the crack approached the arresters. The reduction of stresses at the crack tip resulted in a reduction of the energy release rate and the deceleration of the crack. Despite the observed ability to arrest propagating interface cracks, major limitations arise from the inclusion of very high stiffness materials in the core structure of the sandwich component. As has been shown by Johannes at al. [26-27], core junctions in sandwich materials can lead to premature failure and crack initiations due to high stiffness differences.

In addition to core inserts, several techniques that utilize through thickness stitching of sandwich structures have been developed to enhance their face / core interface fracture properties. Kim et al [28] and Raju et al [29] investigated the effect of stitching in the strength and energy absorption capacity of sandwich composites. They demonstrated a considerable increase in the respective properties and damage

tolerance of the tested components. Wallace et al [30] showed that pin reinforced sandwich structures have significantly higher resistance to axial compression failure that initiates delamination due to buckling instabilities. Compared to core insert crack arresting devices stitching techniques such as z-pinning and tufting have the advantage of not introducing strain concentrations in the bulk of the core material. Even so stitching can often affect negatively the strength of the composite facesheets especially when unidirectional (UD) fiber facesheets are used. Pins that are stitched through the facesheet fabrics will alter the orientation of the fibers that are wrapped around them. This drastically decreases the axial in plane strength of UD facesheets that can lead to premature failure of the sandwich component.

An alternative approach aiming to impede interface crack propagation by using a material with stiffness properties close to those of sandwich core materials was introduced by Jakobsen et al. [2-3] and[31-35]. In this work the authors used a wedge shaped core insert made from Polyurethane (PU) resin, a low stiffness but highly ductile material, to deflect and arrest propagating interface cracks to the inner part of the sandwich core. The concept was successful as the required energy for a crack to penetrate the PU insert was relatively high due to the high ductility of the PU, while at the same time the similar stiffness properties of the core and the PU insert material and the low wedge angle adjacent to the face/core interface ensured that the locally induced stress concentrations were relatively modest. Jakobsen et al. [31-35] performed both static and fatigue tests with sandwich beams displaying mode II dominated interface crack propagation, and the ability of the crack arresting device (referred to as a peel stopper) to deflect a crack and arrest interface cracks was convincingly demonstrated under these conditions. It was also shown that the principle could only work with insert materials processing low stiffness. A drawback of the peel stopper is that it is rather bulky, thus indicating that a significant weight penalty will be imposed to structures in which the concept is adopted. Furthermore, the manufacturing costs of implementing the proposed peel stopper may be considerable, making the concept un-attractive for low-cost applications like wind turbine blades and marine structures, but likely still to be of potential interest for high-cost applications like e.g. composite aero structures.

In the present study an improved crack stopper based on the peel stopper concept of Jakobsen et al [2-3 and 32-35] embedded in composite sandwich beams subjected to fatigue loading is investigated. The new crack stopper has been investigated experimentally and numerically by Wei et al. [4] for its ability to deflect and arrest a propagating face /core interface crack under both static and fatigue loading. In their work the loading conditions at the interface crack tip were Mode I dominated, which for many applications is considered a more realistic scenario than mode II. It was shown that the ability to deflect a propagating face /core interface crack is enhanced by reinforcing the connection (joint) between the crack arresting device (the peel stopper) and the face-sheet with glass fibres extending into or bonded to the face-sheet. The principal difference between the novel peel stopper proposed in [4] and that presented by Jakobsen et al [2-3] and [31-35] is that it involves much less material usage, and thus provides a much smaller weight penalty.

The findings from [4] are used in this study to ensure crack deflection away from the face /core interface and into the core. Although [4] involved extensive studies of the

crack deflection capacity of the novel crack arrester (hereinafter referred to as a "peel stopper"), its overall capacity to contain a crack when subjected to a high number of loading cycles was not investigated. The reason is that the MBB test set-up used in [4] is ideal for highly controlled crack propagation tests [20-21], but does not allow for very large crack lengths. This prohibited the crack from advancing until (and beyond) the physical boundary of the peel stopper was reached. To circumvent this problem, in the research presented in this paper the STT set-up (Sandwich Tear Test [14]) is chosen due to its ability to allow for very large crack lengths. A drawback (or rather a validation challenge) of the STT test, when comparing with numerical simulation results, is that the physical crack propagation parameters, i.e. the energy release rate and mode mixity, cannot be specified independently during the testing. Thus, when using the STT test, the crack is allowed to propagate "freely" under fatigue loading conditions. The performance of the peel stopper is then evaluated based on its ability to deflect a propagating crack, as well as its ability to achieve crack arrest for a high number of loading cycles. The crack arrest behaviour is investigated by means of digital image correlation (DIC), where the strain distribution in the sandwich specimen surface around the crack arrest area is linked directly to the crack arresting performance.

2. Methods

2.1. Test specimen-peel stopper

The face-sheets of the sandwich beam specimens were manufactured using 3 layers of glass fibre mats; face-sheet quad-mat (0/45/90/-45) from Devold, AMT (DBLT-850), providing a face-sheet thickness of 2 mm. The resin system used was Huntsman Araldite LY 1564 SP/Hardener XB 3486. For the core material, DIVINYCELL H100 PVC foam from DIAB was used, having a nominal density of 100kg/m^3 [36].

The peel stopper was manufactured based on the novel design concept proposed in [4], and according to this its shape is chosen to be a thin strip of compliant Polyurethane (PU) reinforced with UD glass fibres as shown in Figure 1. The PU resin used for the peel stopper is Permalock 2K PU-9004. Using the PU/glass fibre hybrid material enables the peel stopper to display stiffness properties that are very similar to those of the foam core material, but at the same time having a higher fracture toughness. In accordance with [4], the fibres running along the peel stopper wedge (see Figure 1) are protruding from its tip. The goal of the new design is to improve the crack arresting ability without penalizing the overall structural weight.

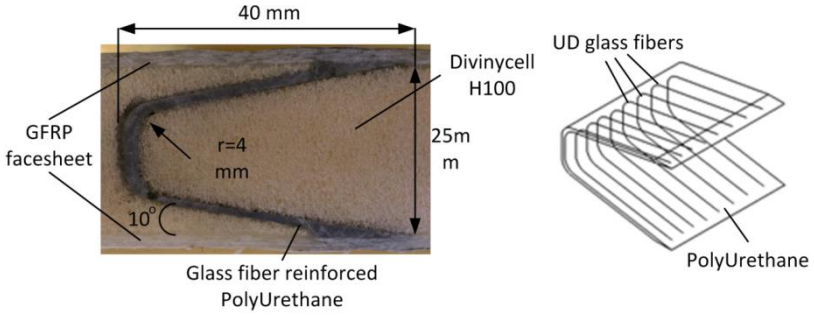

Figure 1. Peel stopper shape and material alignment

The peel stopper is fabricated into shape in one piece using a specially designed closed mould tool. First, the embedded glass fibres are inserted into the open mould. Then, the PU resin is injected in the mould in excess amount. Finally the mould is closed and the RVPU resin is pressed into the shape of the mould tool impregnating the glass fibres at the same time. Steel clamps are used to apply the needed pressure to close the mould, while the excess PU material is allowed to exit from holes drilled along the length of the mould. The mould is made from Polyprolylene, a material that forms neither mechanical nor chemical bonds with PU resin. Therefore no special release or demoulding agent is applied in the mould.

The sandwich beams were all cut from one sandwich panel which was fabricated in a two-step process. In the first step, the core of the sandwich panel including the peel stoppers was assembled. This process requires the PVC foam to be milled into the correct shape to include the peel stopper. Then, the peel stopper was bonded to the PVC foam using a two-component epoxy glue, Araldite 2000.

In the second step, the final assembly of the sandwich panel components is made. The face-sheet and assembled core structure are placed in the right order, while a 25 μm thickness Teflon foil is placed between them. The Teflon foil is used to introduce a pre-cracked region across half the span of the specimen. When the TEFLON foil is placed, the core and face-sheets are infused by the epoxy resin using Vacuum Assisted Resin Transfer Moulding (VARTM). At this point the glass fibres protruding from the peel stoppers are effectively bonded to the face-sheet glass reinforcement during the epoxy resin infusion. Finally, the sandwich panel is cut into sandwich beam specimens that contain the peel stopper in the core structure.

The material properties of the sandwich beam specimen components were measured, and the results are shown in table 1. The stiffness properties of the glass face sheet were obtained by conducting tension and V-notched shear tests using the facilities at the Technical University of Denmark (DTU). The Divinicell H100 foam stiffness properties were obtained by Taher et al. [37] in Aalborg University. The stiffness of the PU was obtained by Jakobsen [35] by conducting a simple tension test and deriving the full stress strain curve of the material until failure.

Table 1. Sandwich beams material properties.

Materials	In-plane Young's modulus (E_x)	Through thickness Young's modulus (E_y)	Shear modulus (G_{xy})	Poisson's ratio (ν_{xy})
DIVINYCELL H100	56 MPa	128 MPa	32 MPa	0.2
E-glass/epoxy	18.6 GPa	--	2.7 GPa	0.4
PU	100 MPa	100 MPa	--	--

2.2. STT setup

In the STT [14] test the energy release rate and mode mixity at the crack tip are not changing monotonically as the crack length increases. This behaviour makes the STT test especially interesting for this work, since the objective is to investigate the effect of the novel peel stoppers on the fatigue life of sandwich structural components under generalized loading conditions. In previous works from Berggreen and Moslemian [14],[22,38] testing and simulation of the behaviour of the STT setup were conducted by using FE models both for static and fatigue loading conditions. In those studies though, the propagation of the crack was made in only one predefined bi-material interface to avoid uneven and unpredictable loading of the specimen and generation of moments at the load introduction point, when two cracks are propagating in the specimen. In the present study the interface cracks can also propagate in only one interface. However, the embedded peel stoppers can diverge the initial face/core interface crack away from the face/core interface and thus initiate a new crack path into the core along the peel stopper surface

The STT specimen and setup is shown in Figure 2. The edges and middle of the sandwich specimen are clamped to the T-slot table of the testing machine, while the upper face-sheet is being pulled at mid-span by the testing machine piston. The Teflon foil introduced in manufacturing separates the core material from the pulled face-sheet allowing for only one crack to propagate towards the direction where the peel stopper is implemented in the core structure. The face-sheet on top of the debonded area is also clamped at its edge carrying high in-plane membrane forces, when the applied displacements are large.

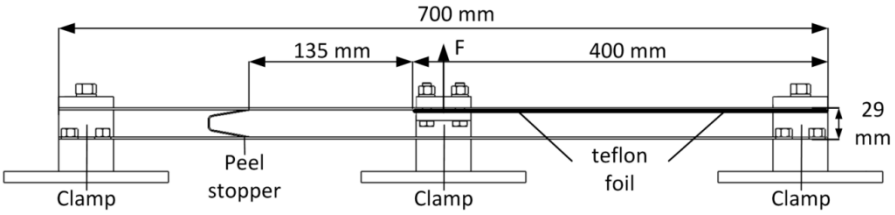

Figure 2. STT specimen dimensions and test setup.

A four-column 100 kN MTS 319.25 with a T-slot table operated by a MTS FlexTest 60 controller and equipped with a 10 kN load cell was used to mount and load the STT specimens for both quasi-static and fatigue load testing. The specimens have a length of 700 mm, a height of 29 mm and a width of 47-50 mm, see Figure 2. At the edges of the sandwich beams the DIVINYCELL H100 foam has been replaced by wooden inserts to enable the imposing of appropriate clamping conditions (Figure 3). In the middle of the sandwich specimens, the foam has been removed completely to allow for the clamping of the lower face-sheet (Figure 3).

2.3. Digital Image Correlation (DIC)

Two DIC cameras have been placed on one side of the STT beam specimens, monitoring the crack tip region of interest. The DIC system ARAMIS 4M from GOM Gmbh was utilized in this study to track crack propagation and strain evolution through the fatigue experiments. DIC [39] utilizes white light cameras to capture images of specimens before and after they have been deformed. The technique divides the images into subsets and tracks the deformation of each subset using correlation algorithms. By re-constructing all subsets into one image, the full field displacement of the specimen can be derived. In Figure 3, the STT setup and DIC system are shown. The two cameras are placed such that they focus only on the area where the crack is propagating. The two camera 3D-DIC set up is selected for this study instead of the simpler 2D DIC configuration that uses just one camera, in order to minimize the effect of out-of-plane effects such as out-of-plane movement of the specimen which can create blurring of the strain maps. This area of interest is selected such that it contains the area where the crack is free to propagate, i.e. the peel stopper area, and also the area behind the peel stopper (see Figure 4). Images of the area of interest were taken with an interval of 60s for the entire duration of the experiment. It will be shown later that the strain field induced in the vicinity of the peel stopper tip, when the crack is arrested can provide useful information about the peel stopper behaviour and performance. Table 2 summarizes all the DIC set-up and parameters used in this study.

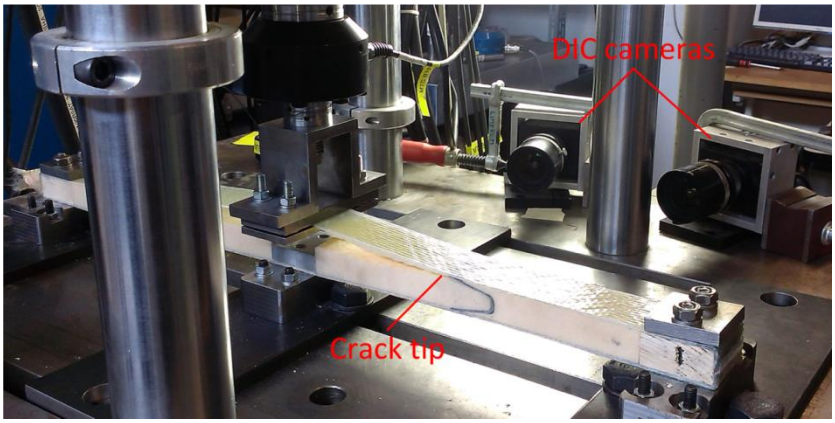

Figure 3. DIC camera set-up and STT test setup.

Table 2. DIC set-up and parameters.

Technique used	*3D digital image correlation*
Subset size	*25×25 pixel*^{2}
Subset step	*12 pixel*
Cameras	*8 bit, 2048×2048 ARAMIS 4M system*
Field of view	*190×29 mm*^{2}
Total number of Subsets	*4455*
Image resolution	*2048×2048 pixel*^{2}
Spatial resolution	*92×92 μm*^{2}
Strain	
Smoothing method	*Gaussian Average (3×3 subsets)*
Differentiation method	*Finite differences*

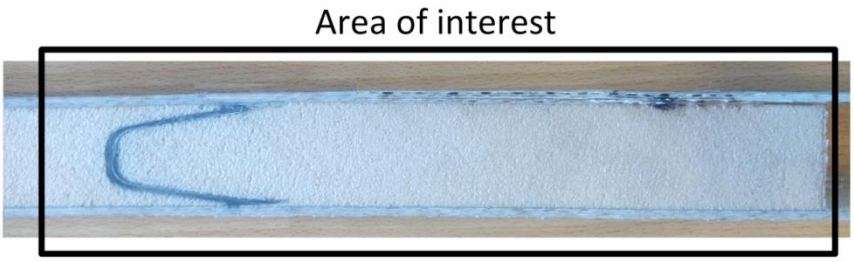

Figure 4. Region of interest for DIC measurements. The crack is propagating in the upper face/core interface from the right towards the peel stopper to the left.

2.3. Numerical modelling

A 2D Finite Element (FE) model has been developed using the commercial FE package ANSYS 15. The model is used to identify the crack loading conditions in the specimen in terms of the energy release rate and mode mixity angle as the crack length increases. The FE model represents the STT setup without including the parts that remain unloaded below the debonded face-sheet, see Figure 5. The peel stopper is meshed in the part of the sandwich core structure that shares nodes with the foam core elements. After crack propagation in the PU/foam interface has occurred, the re-meshing allows for the nodes to be separated. The mesh is created by using 8-node plane strain elements (PLANE 183) with a global element size of 1mm. The crack tip is meshed at the respective bi-material interfaces with an element size of 10 μm. The face-sheet and foam materials are modelled as being transverse orthotropic, while the PU/glass reinforced material used for the peel stopper is modelled as isotropic.

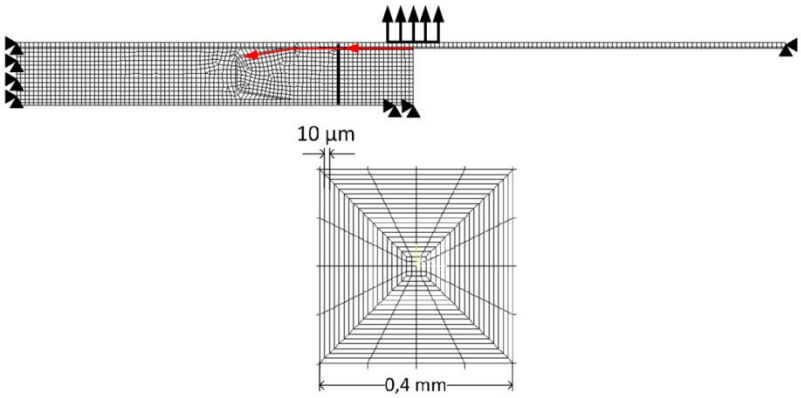

Figure 5. STT finite element model representation and near tip mesh geometry.

The CSDE method [14] was used to calculate the energy release rate and mode mixity phase angle at the crack tip using the reduced formulation [40] defined as:

$$\psi_K = \arctan\left[\frac{\Im(Kh^{i\varepsilon})}{\Re(Kh^{i\varepsilon})}\right] \quad (1)$$

$$G = \frac{H_{11}\,|K|^2}{4\cosh^2(\pi\varepsilon)} \quad (2)$$

where G represents the energy release rate and ψ the mode mixity angle of the crack tip. K is the complex form of the stress intensity factor, ε is the oscillation index, while H11 is an anisotropy parameter introduced by Suo [9]. Finally h is a characteristic length here equal to the facesheet thickness.
The CSDE method has been shown to perform well in bi-material interface problems avoiding the oscillating part of the singularities at the near crack tip region

[12]. The FE model is used to develop a thorough understanding of the crack propagation behaviour in the STT setup and the conditions under which the crack is deflected and arrested by the peel stopper. This will prove useful when the effect of the peel stopper on the fatigue life of the sandwich specimen is evaluated.

3. STT Testing

3.1. Identification of test specimen response and crack propagation behaviour

Quasi-static tests were conducted prior to the fatigue tests to identify the load/displacement curves as the crack increases in length. In total, three specimens were tested quasi-statically in displacement control at a rate of 1 mm/min. Figure 6 shows the load-displacement curves for the three STT specimens that were loaded quasi-statically. The face/core interface crack propagated just below the resin rich layer of the core below the face-sheet.

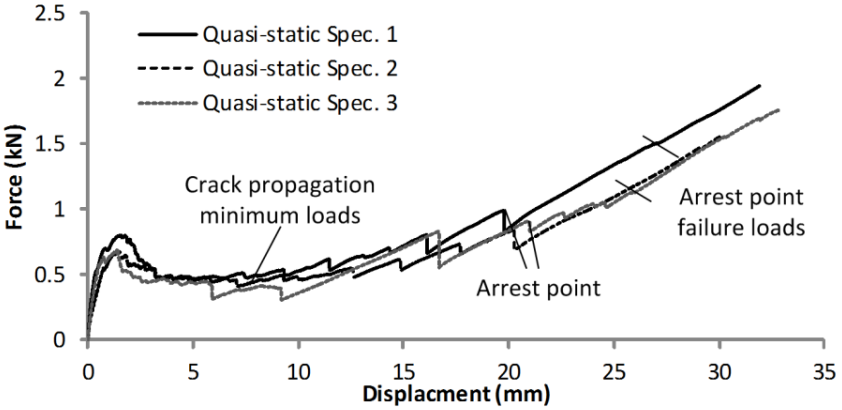

Figure 6. Force-displacement plots obtained from quasi-static tests conducted in displacement controlled loading of STT specimens.

The STT crack growth behaviour makes it cumbersome to test under displacement controlled fatigue loading conditions due to the large increase in displacement that occur as the crack length increases. Due to this, load control is chosen for the fatigue testing. Since the load needed to propagate the crack changes significantly during a test, the propagation of the crack in fatigue is promoted under two different fatigue load amplitudes. The initial fatigue load sequence (Sequence A) corresponds to the average minimum load needed to propagate the crack under quasi-static loading conditions. The second fatigue load sequence (sequence B) corresponds to the average load that causes initiation of a new (and second crack) behind the crack stopper when the initial crack has been arrested. The fatigue load sequences are chosen such that they represent approximately 80% of the imposed quasi-static loads through most of the duration of the experiments. The fatigue tests are conducted at a load ratio of $R=0.2$ and a frequency $f=2$ *Hz*. Table 3 summarizes the observed loads

from quasi-static tests and the chosen fatigue load amplitudes, load ratios and loading frequencies.

Table 3. Quasi-static test load results and fatigue loading magnitudes

Specimen	Crack propagation minimum load (N)	Arrest point failure load (N)
Quasi-static Specimen 1	437	1120
Quasi-static Specimen 2	457	1040
Quasi-static Specimen 3	452	1410
Static average	**448**	**1190**
Fatigue test data	Initial fatigue load Sequence (A)	Second fatigue load Sequence (B)
Fatigue maximum load	380	950
Fatigue minimum load	76	190
Load Ratio	0.2	0.2
Frequency	2 Hz	2 Hz

The initial fatigue load sequence (A), with a relatively small amplitude, was used to drive the crack growth up to the peel stopper tip, and subsequently the second fatigue load sequence (B) with a higher amplitude applied was imposed to guide the crack to the arrest point. It should be noted that if only a single fatigue load amplitude was chosen instead of two (as is done in this work), then a compromise would have to be made taking into account the two extremes. One extreme corresponding to imposing a low initial load amplitude from the beginning of the fatigue test and until the crack arrest point would result in an infinite arrest time. As the other extreme, a large load amplitude imposed from the beginning of the test would cause unstable crack propagation at the specimen face/foam interface.

3.2. Fatigue testing

Four STT specimens were subjected to fatigue loading conditions. During the fatigue experiments the load and displacements peaks were recorded for every 100 cycles. DIC images were taken starting from the unloaded state just before the loading of the specimen. The first fatigue load sequence (Sequence A) was applied until the crack reached the peel stopper tip, which happened at different numbers of loading cycles for each specimen. Subsequently the fatigue test was restarted imposing the second fatigue load sequence (Sequence B), until a second crack was initiated on the back side of the crack stopper or until the maximum allowable cycle limit set to 160,000 was reached.

3.3. Energy release rate and mode mixity vs. number of cycles

The STT crack propagation behaviour was also investigated using FE analysis. In Figure 7 the energy release rate (ERR) at the crack tip and the mode mixity angle are plotted against the crack length along the crack propagation path and for the two experimentally applied fatigue load amplitudes (Sequences A and B) as described in section 3.1. It is seen that the ERR changes drastically and non-monotonically with the crack length as mentioned above. The ERR under fatigue loading is seen to increase to almost the level of the ERR value for quasi-static loading at a crack length of 60 mm. At later stages of the crack propagation, the ERR decreases and almost approaches its initial value before it meets the peel stopper tip and the increase in fatigue loading amplitude (shifting from Sequence A to B) is imposed. The ERR rises suddenly as the loading amplitude is increased, but it then starts to drop again as the crack tip approaches the crack arrest point. It is observed that the mode mixity angle starts with a dominant mode I component that decreases (or increases negatively) as the crack length increases. For crack lengths up to 100 mm the crack is highly mode I dominant. As the crack tip approaches the peel stopper wedge tip the shear component increases and there is an abrupt change after the crack gets deflected by the peel stopper. The change and increase of the mode II component can be attributed to the change in propagation angle of the crack when the crack is forced to move downwards. The increase of the mode mixity angle has a decelerating effect on the propagation speed as mixed mode cracks propagate slower than mode I loaded cracks [40-41].

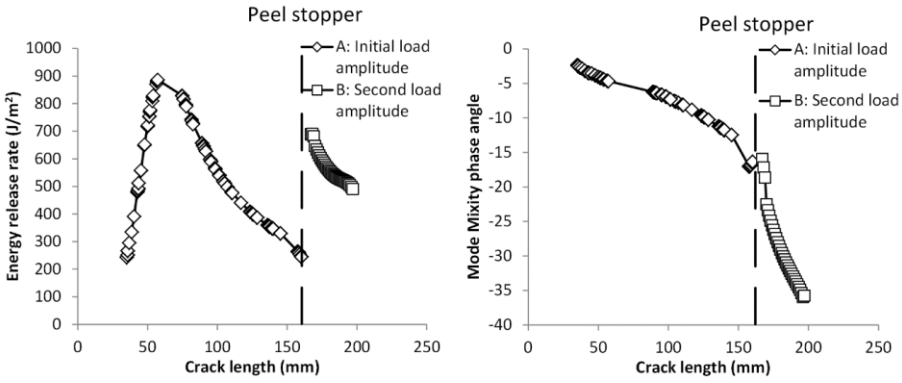

Figure 7. Energy release rate and mode mixity versus crack length load amplitudes A and B (the vertical broken line indicates the position of the tip of the peel stopper).

3.4. Observed crack paths during fatigue testing

The observed crack propagation path in the specimens is shown in Figure 8 (a-d). Similar to the quasi-static tests, the crack propagated along the face-sheet/foam core interface immediately below the resin rich layer of the core just below the face-sheet, until it reached the peel stopper tip, Figure 8 (c). After this point the crack continued to propagate in the PU/foam interface after it was deflected by the peel stopper. Finally the crack was arrested towards the end of the peel stopper, Figure 8 (d).

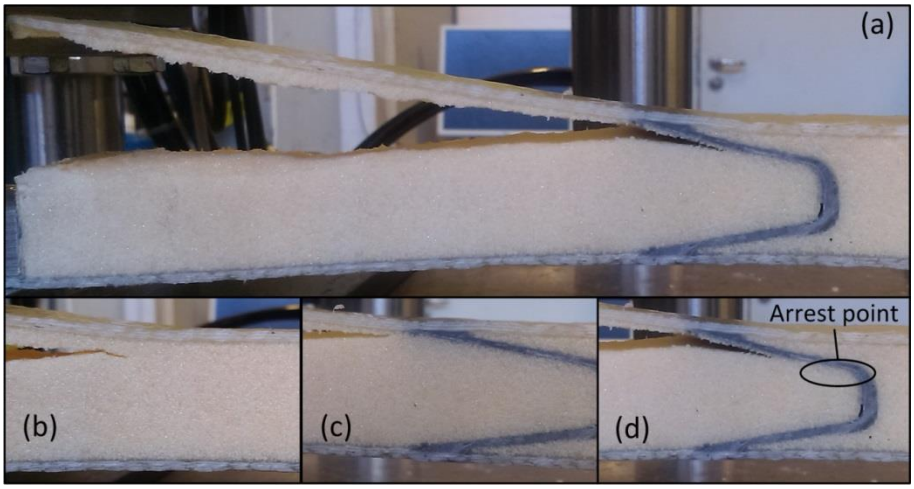

Figure 8. (a) Crack propagation in STT specimen and peel stopper. (b) Crack propagation in/near the face-sheet/foam core interface. (c) Crack propagation close to the peel stopper tip. (d) Crack propagation in the PU-foam interface near the crack arrest point.

4. Crack Arrest Effect

4.1. Number of cycles to crack arrest

In Figure 9, the vertical face-sheet displacement during the fatigue experiment is plotted against the number of loading cycles for all four specimens. When the crack meets the peel stopper tip the load is increased which leads to an abrupt change in displacement. The number of cycles until crack arrest occurs is identified from the recorded images (used for DIC) to assess the effect of the peel stopper. For specimen 3, re-initiation of the crack did not occur before the predefined maximum number of 160,000 loading cycles was reached. From the displacement vs. number of cycles plots shown in Figure 9 it is difficult to determine precisely when the crack meets the arrest point and stops propagating. Instead, the images captured by the cameras (for DIC) are used to identify the number of load cycles, see Figure 10, and the corresponding displacements where crack arrest and crack re-initiation (on the back side of the crack arrester) occurred (indicated in Figure 9).

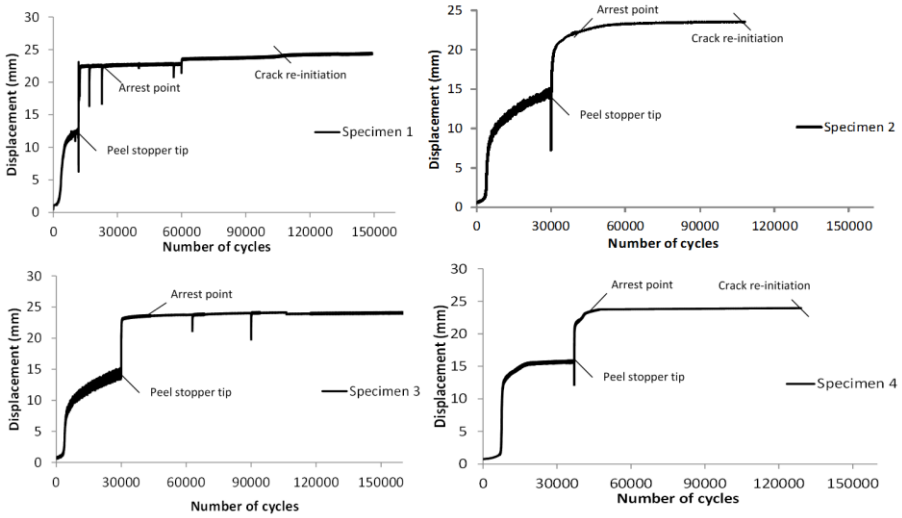

Figure 9. Vertical displacement-loading cycles curves for four specimens.

Table 4 summarizes the number of cycles to crack arrest for all specimens. In columns 2 and 3, the number of loading cycles to the crack arrest point is presented as along with the number of loading cycles the crack was trapped at the arrest point. The latter refers to the number of loading cycles the crack has spent without the occurrence of further crack propagation. This is counted as the interval between the number of cycles where the initial crack reached the arrest point, and until the number of cycles where a new crack was initiated on the back side of the crack stopper. The fourth column presents the total number of cycles, which refers to the duration of the whole experiment which is the sum of columns 2 and 3. To clarify what part of the total fatigue life of the specimen was due to the crack arrest, the ratio between the number of cycles to crack arrest and the total number of cycles is calculated and given in column 5 of Table 4.

Table 4. Observed number of cycles at the arrest point

Specimen	Number of cycles to crack arrest point	Number of cycles until crack reinitiation	Total number of cycles	$\frac{\text{Cycles to arrest}}{\text{Total life}}$ %
Specimen 1	22,136	81,432	103,568	78,62
Specimen 2	42,905	65,197	108,102	60,31
Specimen 3	46,000	< 114,000	160,000	< 71,25
Specimen 4	51,547	77,489	129,036	60,05

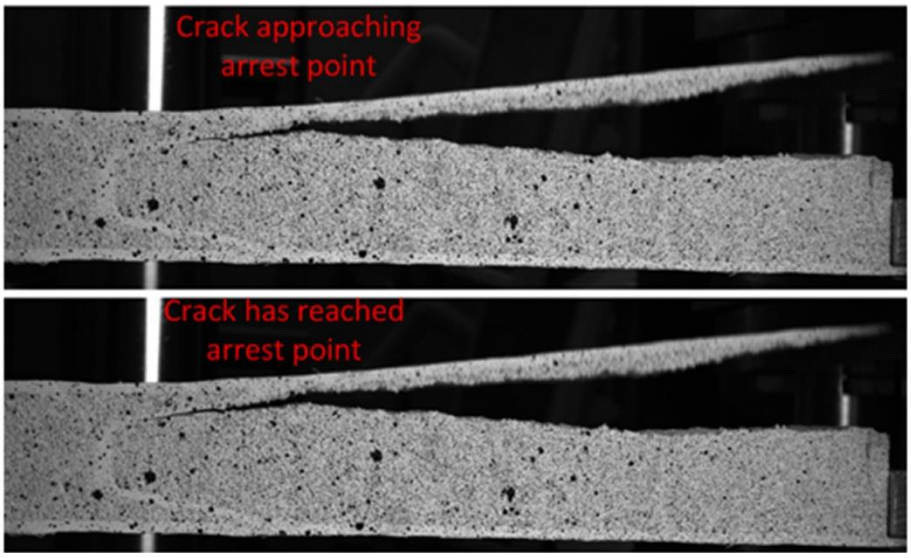

Figure 10. Images showing the crack approaching and reaching the arrest point. The recorded images were used in conjunction with test machine output data to identify the number of loading cycles the crack needed to reach the crack arrest point in each specimen.

From the 3rd column in Table 4 it is seen that the lowest number of loading cycles to crack arrest observed was 65,197. This represents at least 60% of the total test duration which includes propagation of the crack in the face-sheet/core and the PU/core interfaces. Thus, it is evident that the peel stopper increases the overall fatigue life of the tested sandwich beams significantly.
Moreover, Figure 7 shows that the crack energy release rate at the crack arrest point is significant. This demonstrates that the crack would be free to propagate at a comparatively high rate if the peel stopper was not present. The increased mode II component of the crack due to its change of direction (when crack deflection along the PU/core interface occurs when load sequence B is imposed**)** also has a significant effect on the crack propagation speed.

4.2. Strain distribution from DIC

The failure mechanisms that drive crack re-initiation can be identified using DIC to capture the strain fields on the surfaces of the tested specimens. In Figure 11, the major principal strain field is plotted for all four specimens at the loads and number of cycles corresponding to crack arrest after the crack has been deflected away from the face /core interface. The major principal strains are derived by the DIC software using the normal and shear in-plane strain components calculated on the surface of the specimen. The direction of the major strain varies considerably along the specimen due to the complex strain distribution introduced. It is observed that a strain localization appears on the back side of the crack arrester corresponding to the

arrest point in the core material. It is hypothesized that this strain localization (which is linked to a corresponding stress concentration) is causing the initiation of a new crack in the foam core material behind the crack arrester.

From Figure 11 it is further observed that the propagating crack in specimen 4 followed a slightly different path compared to the rest of the specimens. The crack kinked from the upper face-sheet/core interface into the foam, where it reached the lower interface and then kinked back to the upper interface to continue the propagation there. This behaviour may be attributed to the high mode I dominance in the mode mixity for small crack lengths, see Figure 7. Under mode I dominated loading conditions the crack may kink prematurely away from the initial path in any direction, due to the strongly heterogeneous nature of the foam core cell morphology, and even though positive mode II conditions do not occur. Opposed to this, the crack always propagates towards the upper face-sheet where it stays in the region of the face-sheet /core or PU/core interfaces when the crack experiences increased negative mode II component loading.

Specimen 4 shows a slightly different strain field than the other specimens. Due to a discontinuity between the peel stopper and the foam core induced in the manufacturing process, the strain concentration discussed above occurs at the PU/foam interface rather than in the foam behind the peel stopper. The apparent effect of this is that specimen 4 experienced fewer loading cycles before initiation of a new crack after arrest of the initial crack had occurred (see Table 4). Thus, the initial crack did not propagate into the peel stopper before a new crack initiated on the back side of the peel stopper. This is considered to be caused by core material fatigue failure rather than being a regular crack propagation problem, and the observed strains in the foam are associated with the onset of core material fatigue damage. Table 5 summarizes the major principal strains observed in each specimen during the fatigue loading, i.e. the largest values of the major principal strains observed when the peak fatigue load was applied to each specimen.

Table 5. Major principal strain as extracted from the DIC measurement.

Specimen	Major principal strain %
Specimen 1	4.037
Specimen 2	4.225
Specimen 3	1.91
Specimen 4	4.819

It is observed that the peak strain observed for specimen 3 is almost half of the values observed for the other specimens. A possible explanation for this could be a local increase in foam density in the area behind the peel stopper for specimen 3. The spatial variation of the density in PVC foams is a result of the manufacturing process. It has been shown that the foaming process leads to areas of higher or lower density compared to the nominal value which usually corresponds to the average

density of the foam. This would further explain why a new crack did not initiate during the duration of the fatiguing of specimen 3.

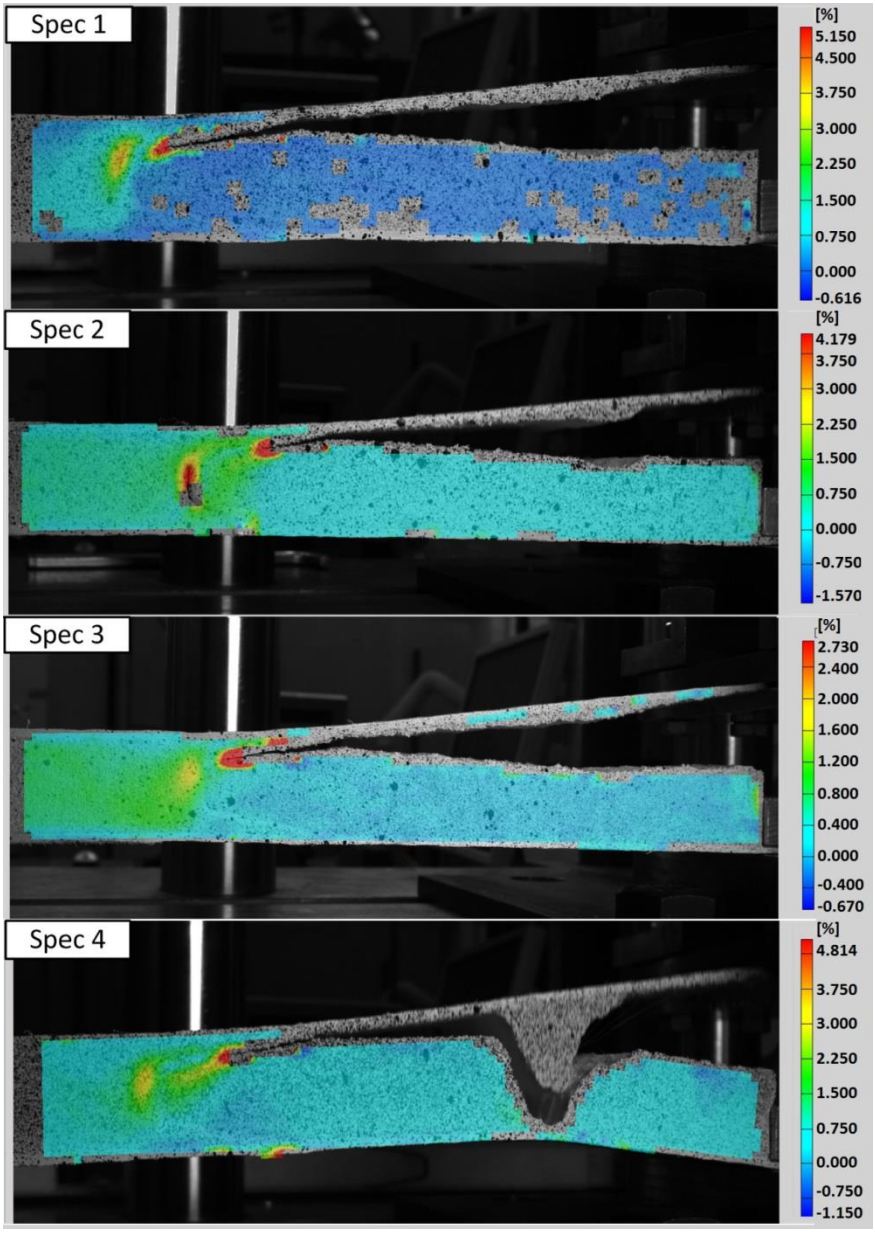

Figure 11. Major principal strain fields corresponding to crack arrest on STT specimen surfaces measured using DIC. In addition to the strain concentrations near the crack tip, a strain concentration appears behind the peel stopper.

4.3. Strain-fatigue data for foam/fatigue life correlation

In this section a comparison is made between the strains measured using DIC at the hot spot on the backside of the peel stopper, the observed number of cycles between the arrest of the initial crack and the initiation of a new crack behind the peel stopper taken from Tables 4 and 5, and fatigue data for the foam core material Divinycell® H100 provided by DIAB [36]. Figure 12 shows an S-N curve obtained from four-point bending of sandwich beam specimens investigating the shear strain fatigue behaviour of H100 PVC foam core material [42]. The core shear stress is the dominant stress between the supports and loading rollers component in the four-point bending test, and therefore it is chosen to compare this with the major principal strain captured by DIC on the back side of the peel stoppers in the tested sandwich beam specimens. For each test specimen the major principal strain is plotted against the number of loading cycles between the occurrence of arrest of the initial interface crack and initiation of a new crack behind the peel stopper (see Table 4) in Figure 12. It is seen that the interval of loading cycles where the crack remains arrested is higher than suggested by the pure shear fatigue data for the Divinycell® H100 foam for specimens 1, 2 and 4. For specimen 3, crack re-initiation was not observed at all, and therefore the interval of load cycles where the initial crack remained arrested before crack re-initiation is higher than observed for specimens 1, 2 and 4.

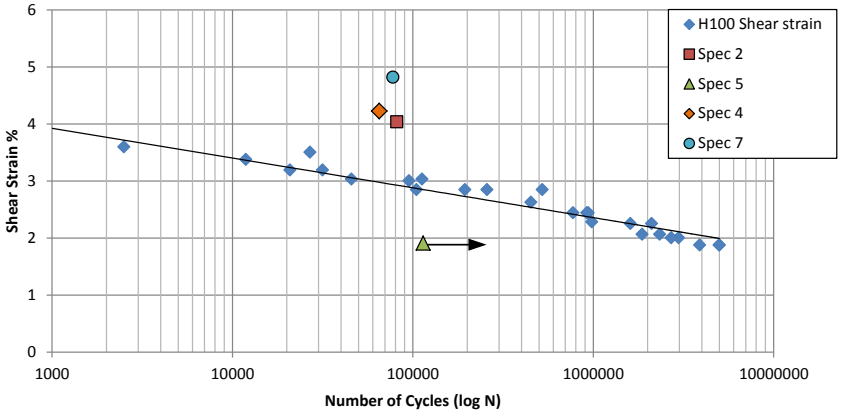

Figure 12. Fatigue data (shear strain vs. number of cycles) for Divinycell® H100 foam core material [36] and major principal strains vs. number of cycles when the crack was arrested before initiation of a new crack for sandwich beam specimens tested using the STT setup.

In the comparative discussion the initiation of a new crack behind the peel stopper does not seem to relate well with the fatigue properties of the foam core material. The reason is that the fatigue strain ratio, R is not taken into account in the comparison for neither the H100 shear strain data nor the crack initiation strains. The strain ratio of the shear strain data is reported to be $R=0.1$ [42] while the ratio of

the crack initiating principal strains could not be derived from the DIC data. An investigation using numerical simulation tools is made as a continuation of this work [43] in order to identify the strain range and strain ratio of the principal strains behind the peel stopper.
It is concluded that the performance of the peel stoppers is highly dependent on the strains in the core material on the back side of the peel stopper. More precisely, it is suggested that the core strain concentration observed behind the peel stopper may relate directly to the fatigue data of the core material, and this can be used for estimating the fatigue life of the sandwich beam specimens with embedded peel stoppers. This further suggests that minimizing the strains in the core material would lead to an increased fatigue arrest time. It should be noted though that the time of crack arrest (i.e. the load cycle interval between initial crack arrest and crack re-initiation) alone does not provide sufficient information for assessing the peel stopper performance. To properly assess the peel stopper performance, a comparison between the entire crack propagation and the re-initiation processes has to be made against the propagation time of an interface crack of similar length in a sandwich panel with no embedded peel stopper.

5. Conclusions

An experimental investigation of the fatigue loading performance of a novel interface crack arrester (or peel stopper) for foam cored sandwich structures has been presented. A PVC foam cored and GFRP composite face-sandwich specimen configuration with embedded peel stoppers was chosen for the investigation. In this configuration the energy release rate and mode mixity of the crack vary considerably with the crack length. The Sandwich Tear Test (STT) together with DIC was used to evaluate the crack arrest effect of the peel stopper as well as the identification of the mechanisms of crack reinitiation behind the peel stopper.
The new peel stopper was found to perform well under fatigue loading conditions. The observed crack propagation paths can be divided into 3 phases: (1) Firstly the propagating initial face-sheet/core interface crack was deflected away from the face-sheet/core interface when reaching the peel stopper tip; (2) the crack was arrested inside the peel stopper and remained arrested for than 67% of the total duration of the fatigue experiments; (3) finally a new crack was initiated in the core material behind the peel stopper. An investigation of the strain distribution in the vicinity of the crack arrest area suggests that the post-crack arrest behaviour is significantly influenced by the fatigue properties of the foam core material used in the sandwich beams. This further suggests that the effectiveness and overall performance of the peel stopper are highly dependent on the local strains developed in the core material on the back side of the peel stopper behind the arrest point.

Acknowledgements

The work was sponsored by the Danish Council for Independent Research | Technology & Production Sciences (FTP) under the research grant “Enhanced performance of sandwich structures by improved damage tolerance" (SANTOL)

(Grant 10082020). The Divinycell H100 material used in this study was provided by DIAB Group, Sweden. The work has been conducted in collaboration with and co-sponsored by the Technical University of Denmark, Aalborg University, Denmark, the University of Southampton, UK, Siemens Wind Power A/S, Denmark, and LM Wind Power Blades A/S, Denmark.

References

[1] Zenkert, D., "An introduction to sandwich construction" London: Chameleon Press Ltd, 1995

[2] Jakobsen, J., Bozhevolnaya, E., Thomsen, O.T., 2007. New peel stopper concept for sandwich structures. Compos Science Technology. 67:3378–85.

[3] Jakobsen, J., Andreasen, J.H., Bozhevolnaya, E., 2008. Crack kinking of a delamination at an inclined core junction interface in a sandwich beam. Engineering Fracture Mechechanics. 75(16):4759–73.

[4] Wang, W., Martakos, G., Dulieu-Barton, J. M., Andreasen, J. H., Thomsen, O. T., 2015. Fracture behaviour at tri-material junctions of crack stoppers in sandwich structures. Composite Structures 133, 818-833

[5] Erdogan, F., 1971. Bonded dissimilar materials containing cracks parallel to the interface, *Engineering Fracture Mechanics*, 3(3), 231-240.

[6] Dundurs, J. Edge-bonded dissimilar orthogonal elastic wedges. Journal of Applied Mechanics. 36. 650-652.(1969)

[7] Hutchinson, J.W., Suo, Z., 1992 . Mixed Mode Cracking in Layered Materials, *Advances in Applied Mechanics*, 29, 63-191.

[8] He, M.., Hutchinson, JW. 1989. Kinking of a Crack Out of an Interface. ASME. Journal of Applied Mechanics.;56(2):270-278

[9] Suo, Z., 1990. Singularities, interfaces and cracks in dissimilar anisotropic media. Proceedings of the Royal Society of London A: Mathematical, Physical and Engineering Sciences 427 (1873), 331-358.

[10] Wang, T. C., 1994. Kinking of an interface crack between two dissimilar anisotropic elastic solids. International Journal of Solids and Structures 31 (5), 629–641.

[11] Zenkert, D., 1991. Strength of sandwich beams with interface debondings. Composite Structures 17 (4), 331–350.

[12] Berggreen, C., 2004. Damage tolerance in debonded sandwich structures. PhD. Thesis. Department of Mechanical Engineering, Technical University of Denmark.

[13] Moslemian, R., Karlsson, A. M., Berggreen, C., 2011. Accelerated fatigue crack growth simulation in a bimaterial interface. International Journal of Fatigue 33 (12), 1526–1532.

[14] Berggreen, C., Simonsen, B. C., Borum, K. K., Feb. 2007. Experimental and numerical study of interface crack propagation in foam-cored sandwich beams. Journal of Composite Materials 41 (4), 493–520.

[15] Berggreen, C., Simonsen, B. C., 2005. Non-uniform compressive strength of debonded sandwich panels – II. Fracture mechanics investigation. Journal of Sandwich Structures and Materials 7 (6), 483-517.

[16] Moslemian, R., Berggreen, C., Jul. 2013. Interface fatigue crack propagation in sandwich x-joints – part II: Finite element modeling. Journal of Sandwich Structures and Materials 15 (4), 451-463

[17] Prasad, S., Carlsson, L. A., 1994. Debonding and crack kinking in foam core sandwich beams—I. analysis of fracture specimens. Engineering Fracture Mechanics 47 (6), 813–824.

[18] Prasad, S., Carls8son, L. A., 1994. Debonding and crack kinking in foam core sandwich beams—II. experimental investigation. Engineering Fracture Mechanics 47 (6), 825–841.

[19] Carlsson, L.A., Sendlein, L.S. and Merry, S.L., 2004. Characterization of face sheet/core shear fracture of composite sandwich beams. Journal of Composite Materials, 25: 101–116.

[20] Quispitupa, A., Berggreen, C., Carlsson, L. A., 2009. On the analysis of a mixed mode bending sandwich specimen for debond fracture characterization. Engineering Fracture Mechanics 76 (4), 594–613.

[21] Manca, M., Quispitupa, A., Berggreen, C., Carlsson, L. A., 2012. Face/core debond fatigue crack growth characterization using the sandwich mixed mode bending specimen. Composites Part A: Applied Science and Manufacturing 43 (11), 2120–2127.

[22] Manca, M., Berggreen, C., Carlsson, L. A., 2015. G-control fatigue testing for cyclic crack propagation in composite structures. Engineering Fracture Mechanics.

[23] Rinker, M., Zahlen, P. C., John, M., Schäuble, R., 2012. Investigation of sandwich crack stop elements under fatigue loading. Journal of Sandwich Structures and Materials 14 (1), 55–73.

[24] Hirose, Y., Matsubara, G., Hojo, M., Matsuda, H., Inamura, F., 2008. Evaluation of modified crack arrester by fracture toughness tests under mode I type and mode II type loading for foam core sandwich panel. In: Proc. US-Japan conference on composite materials 2008, Tokyo, Japan.

[25] Hirose, Y., Matsuda, H., Matsubara, G., Hojo, M., Inamura, F., 2012. Proposal of the concept of splice-type arrester for foam core sandwich panels. Composites Part A: Applied Science and Manufacturing 43 (8), 1318–1325.

[26] Johannes, M., Jakobsen, J., Thomsen, O. T., Bozhevolnaya, E., 2009. Examination of the failure of sandwich beams with core junctions subjected to in-plane tensile loading. Composites Science and Technology 69 (9), 1447-1457.

[27] Johannes, M., Thomsen, O. T., 2010. Examination of the failure of sandwich beams with core junctions subjected to transverse shear loading. Journal of Sandwich Structures and Materials 12 (2), 199–236.

[28] Kim J. H., Lee Y. S., Park B. J., Kim D. H. 1999. Evaluation of durability and strength of stitched foam-cored sandwich structures. Composite Structures, 47: 543-550

[29] Raju K. S., Tomblin. 1999.Energy absorption in stitched composite sandwich panels. Journal of Composite Materials, 33(8): 721-728

[30] Wallace B. T., Sankar B. V. and Ifju P. G. 2001. Pin reinforcement of delaminated sandwich beams under axial compression. Journal of Sandwich Structures and Materials, 3: 117-129

[31] Bozhevolnaya, E., Jakobsen, J., Thomsen, O.T., 2009. Performance of sandwich panels with peel stoppers, strain. Int J Exp Mech 45. 349–57.

[32] Bozhevolnaya, E., Jakobsen, J., Thomsen, O.T., 2009. Fatigue Performance of Sandwich Beams With Peel Stoppers, Strain, 45(4) 349-357.

[33] Jakobsen, J., Thomsen, O.T., Andreasen, J.H., Bozhevolnaya, E., 2009. Crack deflection analyses of different peel stopper design for sandwich structure. Compos Science Technology 69:870–5.

[34] Jakobsen, J., Andreasen, J.H., Thomsen, O.T., 2009. Crack deflection by core junctions in sandwich structures. Engineering Fracture Mechanics. 76(14):2135–47.

[35] Jakobsen, J., 2004. Local Effects and the Control of Face-Core Debond Failure in Sandwich Structures . PhD. Thesis. Department of Mechanical Engineering, Aalborg University.

[36] DIAB. Divinycell H-Grade Technical data, 2014. Laholm (Sweeden) (http://www.diabgroup.com).

[37] Taher, S.T., Thomsen, O.T., Dulieu-Barton, J.M. and Zhang, S., 2011. Determination of mechanical properties of PVC foam using a modified Arcan fixture. Composites Part A: Applied Science and Manufacturing, 43, 1678-1708. (doi:10.1016/j.compositesa.2011.11.010).

[38] Moslemian, R., 2011. Residual Strength and Fatigue lifetime of debonded damaged sandwich structures. PhD. Thesis. Department of Mechanical Engineering, Technical University of Denmark; September.

[39] Schreier H., Orteu J. J., Sutton M. A., 2009. "Image Correlation for Shape, Motion and Deformation Measurements" Springer US.

[40] Berggreen, C., Carlsson, L. A., 2010. A modified TSD specimen for fracture toughness characterization - fracture mechanics analysis and design. Journal of Composite Materials 44 (15), 1893-1912.

[41] Shipsha, A., Burman, M., Zenkert, D., 1999. Interfacial fatigue crack growth in foam core sandwich structures. Fatigue & Fracture of Engineering Materials & Structures 22 (2), 123–131.

[42] Burman, M., Magnusson, B., 2008. Fatigue testing of H60, H100 and H200. Technical report (DIAB), KTH (Sweeden).

[43] Martakos, G., Andreasen J.H., Berggreen C., Thomsen O.T.: Interfacial Crack Arrest in Sandwich Beams Subjected to Fatigue Loading using a Novel Crack Arresting Device - Numerical modelling. Submitted for publication.

PAPER #3

Interfacial Crack Arrest in Sandwich Beams Subjected to Fatigue Loading using a Novel Crack Arresting Device - Numerical Modelling

G. Martakos[1], J.H. Andreasen[1], C. Berggreen[2], O.T. Thomsen[1,3]

[1]Department of Mechanical and Manufacturing Engineering, Aalborg University

Fibigerstræde 16, DK-9220 Aalborg East, Denmark

Email: {gm,jha,ott}@m-tech.aau.dk, web page: http://www.m-tech.aau.dk

2Department of Mechanical Engineering, Technical University of Denmark

Email: cbe@mek.dtu.dk, web page: http://www.dtu.dk

[3]Faculty of Engineering and the Environment,
University of Southampton, Highfield, Southampton, UK

Email: o.thomsen@soton.ac.uk , web page: http://www.soton.ac.uk/engineering/

The paper was submitted and accepted for publication in revised form to the Journal of Sandwich Structures and Materials, September 2016

Abstract

A novel crack arresting device is implemented in foam cored composite sandwich beams and tested using the Sandwich Tear Test (STT) configuration. A Finite Element Model of the setup is developed, and the predictions are correlated with observations and results from a recently conducted experimental fatigue test study. Based on a linear elastic fracture mechanics approach, the developed FE model is utilized to simulate crack propagation and arrest in foam cored sandwich beam specimens subjected to fatigue loading conditions. The effect of the crack arresters on the fatigue life is analysed, and the predictive results are subsequently compared with the observations from the previously conducted fatigue tests. The FE model predicts the energy release rate and the mode mixity based on the derived crack surface displacements, utilizing algorithms for the prediction of accelerated fatigue crack growth as well as the strain field evolution in the vicinity of the crack tip on the surface of the sandwich specimens. It is further shown that the developed finite element analysis methodology can be used to gain a deeper insight onto the physics and behavioural characteristics of the novel peel stopper concept, as well as a design tool that can be used for the implementation of crack arresting devices in engineering applications of sandwich components and structures.

Keywords: Sandwich structures, Finite Element Analysis, Composites, Fracture Mechanics, Fatigue

1. Introduction

Sandwich structures represent a special form of laminated composites comprising stiff and thin face-sheets separated by and bonded to either side of a light and compliant core material. The resulting layered sandwich element or structure displays very high stiffness and strength to weight ratios [1]. Structurally, the face-sheets are responsible for carrying the in-plane stresses and the bending loads, while the core carries the out of plane shear stresses. Sandwich structures are notoriously sensitive to debonding or interfacial cracking of the adhesive bond layers that connect the face-sheets to the core material. When such interface cracks or debonds propagate this may lead to a significant loss (complete loss as a worst case scenario) of structural integrity, leading to premature structural failure or collapse. Such debonds may be caused by in-service loads such as local/concentrated external loads and impact loads, but may also be induced as defects during the manufacturing process (such as e.g. dry spots and resin voids). Ideally face-sheet/core debonds should not occur at all, but since this is impossible to achieve for real industrial scale sandwich structures which may also include safety critical applications, there is a need to develop and introduce design methodologies able to take account of the existence of such face-sheet/core interface debonds. Furthermore, and more importantly, there is a great need for the development of methodologies and design features that enable the mitigation of the effects of propagating interface cracks as described. This has led to an increased interest in the interfacial debond behaviour of

sandwich structures, which again has led to several research studies adopting both analytical/numerical and experimental approaches.
The framework of fracture mechanics has been commonly used to describe the conditions of interfacial debond/crack propagation and arrest [2-7], where numerical modelling has been used to simulate interface crack growth in the most recent studies. Several methods have been proposed based on Finite Element (FE) analysis to simulate interface crack propagation. Examples include the Virtual Crack Closing Technique (VCCT) [8-10] and the Crack Surface Displacement Extrapolation method (CSDE) [11-12] The cycle jump technique, developed by Moslemian [13-16], has been proposed and utilized to reduce the number of loading cycles that need to be analysed in fatigue simulations.
In a recent study of a proposed crack arresting device, a CZM [17] method was utilized to calculate the crack propagation and mitigation due to fibre bridging for an increasing crack length [18-20]. Other crack arrester concepts were proposed in [21-23], where FE analysis was used to demonstrate the efficiency of the crack arresting elements. In all studies [21-23] the energy release rate and the crack mode mixity angle were considered, since these physical measures are needed to quantitatively describe the conditions under which an interfacial crack will propagate. Yet another embedded sandwich crack arresting device (or peel stopper) utilizing a compliant core insert was discussed in [24], were analytical and FE methodologies were used to characterize the conditions for interface crack deflection at the tri-material junction present at the peel stopper tip. In [24] a "prediction surface" was proposed for different mode mixities and deflection angles, and based on this it was shown that crack deflection at the tri-material junction can be predicted. A common feature of the referenced research is that modelling of the entire fatigue load sequence including interface crack propagation, arrest and post arrest behaviour were not attempted.

In this study the CSDE method together with the cycle jump technique [13-16] is used to simulate interface crack propagation in foam cored sandwich beams with embedded interface crack devices (hereinafter referred to as peel stoppers) subjected to fatigue loading conditions. The emphasis is to investigate the effect of the embedded peel stopper, considering the conditions under which crack propagation, crack deflection as well as crack arrest can occur. The numerical results will be correlated with and compared against the results of a recent experimental study [25]. The aim is to demonstrate that numerical simulations can be used to assess and predict the behaviour of embedded peel stoppers and their effect on the fatigue life of sandwich structures. The peel stopper elements proposed in this work are based on the concept proposed in [24], but modified to enhance the crack deflection and arresting capabilities [26]. The models developed in this paper are used to predict the fatigue life of sandwich beams with embedded peel stoppers and are built to reflect the experimental observations made in [25] such as the crack propagation path. The numerical predictions are compared with the experimentally observed crack propagation and fatigue behaviour reported in [25]. In this paper, crack propagation and crack arrest are modelled based on a modification of Paris' law,

while the post crack arrest behaviour is predicted based on fatigue data (S-N curve) for the sandwich foam core material.

2. Experimental Results

2.1. Fatigue testing and crack propagation behaviour

A brief summary of the results of the experimental investigation conducted in [1] is given in this section. The novel peel stopper manufactured from pre-moulded Polyurethane (PU) resin [26], Figure 1, was implemented in foam cored sandwich beam specimens subjected to fatigue loading conditions using the Sandwich Tear Test (STT) setup, Figure 2. The sandwich specimens consisted of identical glass fibre reinforced (GFRP) face-sheets and a PVC foam core material (Divinycell® grade H100 with a density of 100 kg/m^3 from DIAB), and a total of four specimens were tested. The crack initiation and propagation was similar for all the tested specimens encompassing the following sequence of events, which is illustrated in Figure 3. The initial crack propagated in the face-sheet/foam interface, just below the resin rich area that is created between the face sheet and the core material, until it reached the peel stopper tip, where the crack was deflected by the peel stopper. The crack then continued propagating along the PU/foam interface until it reached the end of the peel stopper where the propagation was stopped at the crack arrest point. The fatigue loading level was subsequently increased and the fatigue test was continued until a new crack initiated on the back side of the peel stopper. The new crack then propagated into the undamaged part of the sandwich core leading to a complete failure. For each specimen, the peel stopper was evaluated with respect to the number of cycles where the crack stayed arrested at the arrest point before the re-initiation occurred (i.e. the number of cycles encountered between crack arrest and crack re-initiation), and this was compared with the overall fatigue life of the specimen. White light cameras were used to capture images during the fatigue experiments, and a digital image correlation (DIC) was established between the measured strains and the efficiency of the peel stopper.

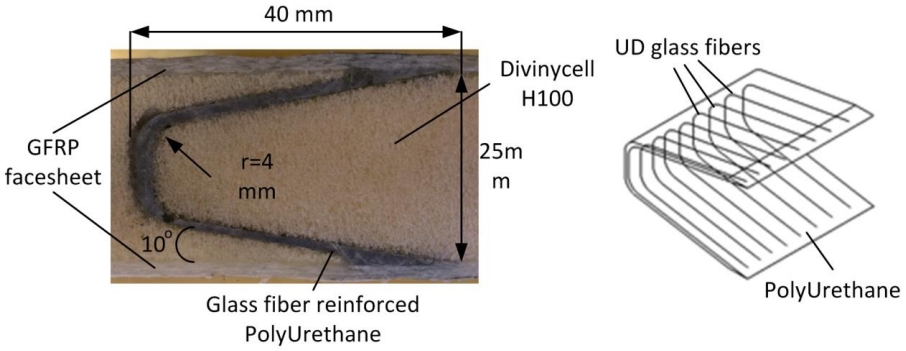

Figure 1. Peel stopper shape and material alignment.

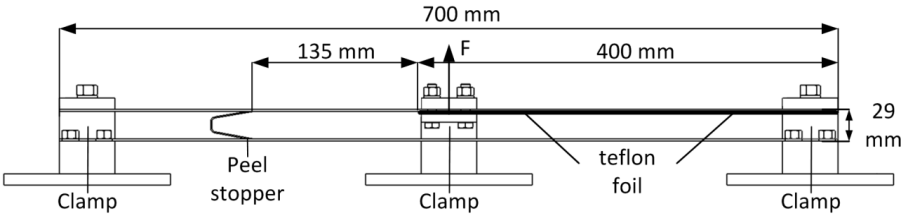

Figure 2. Sandwich Tear Test (STT) specimen dimensions and test setup.

The proposed peel stopper demonstrates an unsymmetrical shape that is able to deflect and arrest a propagating crack coming from only one direction (see Figure 3). This concept is highly practical only in applications where the location of damage initiation in the sandwich component can be predicted by the designer. In other cases two peel stoppers could be utilized and placed facing on opposite directions creating a dual faced peel stopper. In this manner cracks propagating from both directions can be arrested. In this study since the initial crack front is well defined by the specimen set-up and requirements only one peel stopper is embedded in the sandwich beams.

As mentioned above, the STT specimens were loaded in load controlled fatigue at two different loading amplitudes; the first driving the crack propagation along the face-sheet/core interface until the peel stopper tip is reached, referred as load sequence A, and the second higher loading amplitude imposed to propagate the crack along the PU (peel stopper)/foam interface until the crack arrest point is reached, referred to as load sequence B. Table 1 summarizes the two fatigue load sequences imposed, as well as the load ratio and frequency of the fatigue tests. The

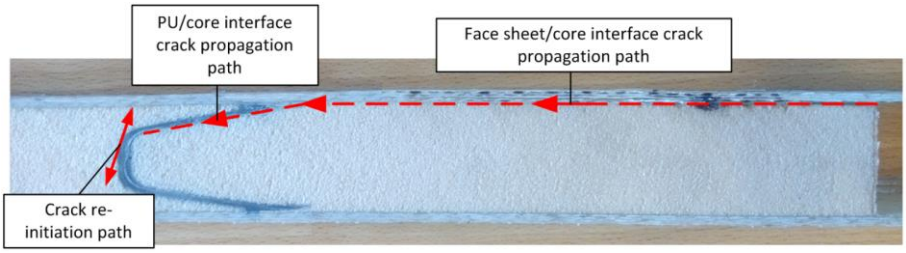

Figure 3. Crack propagation path in STT sandwich beam specimens imbedded with crack stoppers.

Table 1. Fatigue test load conditions

Fatigue test data	First fatigue load / Sequence A	Second fatigue load / Sequence B
Fatigue maximum load	380 N	950 N
Fatigue minimum load	76 N	190 N
Load Ratio	0.2	0.2
Frequency	2 Hz	2 Hz

3. Numerical Modelling

3.1. FE Model

The finite element model has been developed in the commercial FE package ANSYS 15.0 [27]. The model is used to identify the crack loading conditions including the energy release rate (ERR) and the mode mixity phase angle as functions of the crack length. To simulate fatigue crack growth in the face-sheet/foam and PU/foam interfaces a re-meshing algorithm is used. Since the crack in all the experiments [25] propagated along the face-sheet/core interface until it reached the peel stopper tip, after which the crack was deflected along the PU/core interface, the debonded area in the FE simulations follows the path of the peel stopper angle (see Figure 4 a). The FE model represents the STT setup without including the unloaded specimen region below the debonded face-sheet in the left side of the specimen, see Figure 4 a. The peel stopper is meshed in the core structure such that it shares nodes with the foam core elements. After crack propagation along the PU/foam interface has occurred the re-meshing allows for the nodes to be separated. In Figure 4 b-d the crack tip elements are shown at different states of crack propagation while in Figure 4 e-g the respective states are shown in the actual specimen.

The FE mesh is created using 8-noded plane strain elements (PLANE 183) with a global element size of 1 mm. The crack tip is meshed using element sizes down to 10 μm at the bi-material interfaces. The face-sheet and foam materials are modelled as orthotropic, while the PU/glass fibre reinforced material of the peel stopper is homogenised and modelled (approximated) as isotropic. Table 2 lists the mechanical properties of the constituent materials [25]. Geometric nonlinear behaviour is included in the FE-models to capture the in-plane membrane stresses developed in the face-sheet due to large vertical displacements.

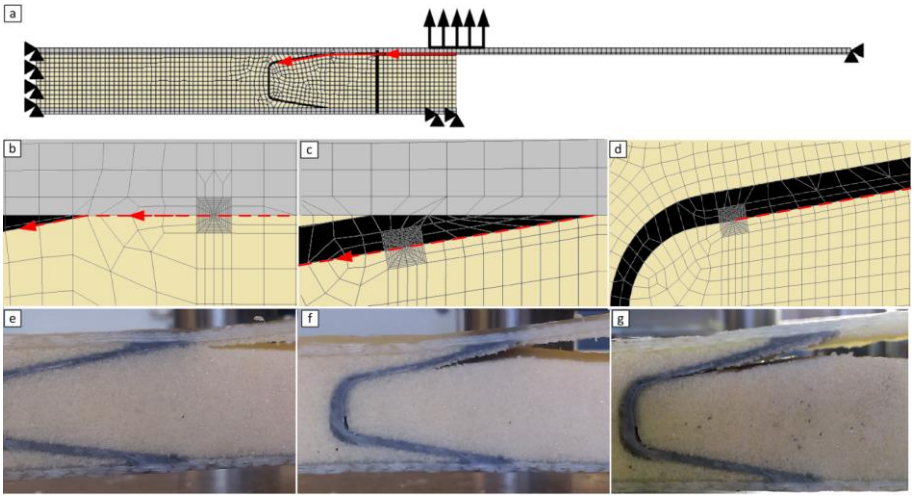

Figure 4. a) STT finite element model representation; b) and e) Crack propagating at face-sheet/foam interface; c) and f) Crack propagating at the PU/foam interface; d) and g) Crack at the arrest point.

Table 2. Material properties of the constituents of the test specimens

Materials	In-plane Young's modulus (E_x)	Through thickness Young's modulus (E_y)	Shear modulus (G_{xy})	Poisson's ratio (ν_{xy})
DIVINYCELL H100	56 MPa	128 MPa	32 MPa	0.2
E-glass/epoxy	18.6 GPa	9.2 GPa*	2.7 GPa	0.4
PU	100 MPa	100 MPa	34.2 MPa	0.45

*: Assumed value

The glass face-sheet stiffness properties were obtained by conducting a series of tension and V-notched shear tests in the facilities of Technical University of Denmark (DTU). E_y has not been measured and its' value is assumed based on properties of similar GFRP laminate composites. For the numerical analyses conducted in this study, variations of E_y have very little impact on the results. Siavash et al. [28] used an improved Arcan ficture developed in Aalborg University to derive the stiffness properties of the Divinicell H100 foam. The stiffness of the PU was obtained by Jakobsen [29] by conducting a simple tension test and deriving the full stress strain curve of the material until failure.

3.2 CSDE method/cycle jump technique

The Crack Surface Displacement Extrapolation (CSDE) mode mixity methodology [11-12] fits classical bi-material interface theory solutions [4,5] into a FE analysis framework to calculate directly the energy release rate (ERR) and mode mixity of a bi-material crack. In this study a special crack tip mesh is used to extract the relative nodal displacements behind the crack tip, and then use these to calculate the energy release rate (ERR) and mode mixity. The ERR and mode mixity equations for anisotropic materials are derived by using Suos formulation [6] of the COD where he introduced the H_{11} and H_{22} anisotropy parameters :

$$\sqrt{\frac{\boldsymbol{H_{11}}}{\boldsymbol{H_{22}}}}\boldsymbol{\delta_y} + \boldsymbol{i\delta_x} = \frac{\boldsymbol{2H_{11}(K_1 + iK_2)|x|^{\frac{1}{2}+i\varepsilon}}}{\boldsymbol{\sqrt{2\pi}(1 + 2i\varepsilon)cosh\pi\varepsilon}} \tag{1}$$

$$\sqrt{\frac{\boldsymbol{H_{11}}}{\boldsymbol{H_{22}}}}\boldsymbol{\sigma_{yy}} + \boldsymbol{i\sigma_{xy}} = \frac{\boldsymbol{K\, x^{i\varepsilon}}}{\boldsymbol{\sqrt{2\pi x}}} \tag{2}$$

where x represents the distance away from the crack tip and K the complex stress intensity factor K_1+iK_2. An oscillation in the solution is created by the $i\varepsilon$ term which acts as a power of the distance away from the tip.

From fracture mechanics the ERR and mode mixity can be calculated as:

$$\boldsymbol{\psi_K} = \mathbf{arctan}\left[\frac{\boldsymbol{\Im(Kh^{i\varepsilon})}}{\boldsymbol{\Re(Kh^{i\varepsilon})}}\right] \tag{3}$$

$$G = \frac{H_{11}\,|K|^2}{4\,\cosh^2(\pi\varepsilon)} \tag{4}$$

where G represents the energy release rate and ψ the mode mixity angle of the crack tip and can be solved with regards to the relative crack displacements by substituting equation 1 and 2 into equation 3 and 4,

$$\psi_K = \arctan\left(\sqrt{\frac{H_{22}}{H_{11}}}\frac{\delta_x}{\delta_y}\right) - \varepsilon\, ln\left(\frac{x}{h}\right) + \arctan(2\varepsilon) \tag{5}$$

$$G = \frac{\pi(1 + 4\varepsilon^2)}{8\,H_{11}|x|}\left(\frac{H_{11}}{H_{22}}\,\delta_y^2 + \delta_x^2\right) \tag{6}$$

where δ_x and δ_y are the relative shear and opening displacements of the crack tip nodes behind the crack tip, $|x|$ is the distance of the crack tip node pair from the crack tip, ε is the oscillation index, and h is the chosen characteristic length [13] which is usually and for the considered analysis case is set equal to the face-sheet thickness. The CSDE parameter values are given in Table 3.
Finally, the cycle jump technique [13-16] is used to simulate fatigue crack growth in combination with the CSDE method. The cycle jump technique is used to reduce the number of simulated cycles in the fatigue analysis. After simulating three or more consecutive loading cycles of crack propagation, the new crack length can be calculated by linear extrapolation for a "safe" number of cycles without running the respective simulations. This allows for saving considerable computation time when simulation of long fatigue sequences with a large number of loading cycles is needed. Previous investigations [16] have explored the sensitivity of the method to the "jump distance", and the suggestions presented are used in this study.

The propagation rate of the crack was calculated using the measured ERR, the mode mixity and a Paris' like law [30], based on energy release rate amplitude rather than stress intensity amplitude:

$$\frac{da}{dN} = m\,\Delta G^{c} \qquad (2)$$

where a is the crack length and da the crack length increment. N and dN are the loading cycles and the increment in loading cycles, respectively. Parameters m and c are fitting variables of the Paris' law curve. Finally, ΔG represents the ERR amplitude, thus the difference between the corresponding ERR levels relative to the imposed maximum and minimum fatigue load levels.

The input data for Paris' law were obtained by fatigue experiments conducted on the same bi-material interface configuration as considered in this paper using the Mixed Mode Bending test (MMB) and the G-control method developed and proposed by Manca et al. [31]. Parameters c and m are mode dependent meaning that they vary depending on the mode mixity applied. In this study the Paris law parameters were extracted for mode-I dominant crack loading conditions. It is assumed that small variations in mode mixity under general mode I loading do not affect the Paris law curve considerably. As it will be shown later, the crack propagating at the face-sheet/foam core interface (Sequence A) is highly mode I dominated. Unfortunately, fatigue data are not available for the PU/core interface over the wide range of mode mixities the crack tip is experiencing during a STT test. Alternatively, to simulate fatigue crack propagation, observations from the tested sandwich specimens are used to determine the crack growth rate along the PU/core interface, Table 3. The values of c and m were derived by determining the fatigue crack growth rate from the experimental results [25] and the energy release rate from the numerical tools developed for this study.

Table 3. CSDE and Paris' law parameters for the two interfaces.

	Face/core interface	PU/core interface
H_{11}	$1.68 \cdot 10^{-2} \left(\frac{1}{MPa}\right)$	$2.79 \cdot 10^{-2} \left(\frac{1}{MPa}\right)$
H_{22}	$1.56 \cdot 10^{-2} \left(\frac{1}{MPa}\right)$	$2.19 \cdot 10^{-2} \left(\frac{1}{MPa}\right)$
ε	$-7.066 \cdot 10^{-2}$	$-4.56 \cdot 10^{-2}$
h	2 mm	2 mm
c	$1.3758 \cdot 10^{-14}$	$0.9278 \cdot 10^{-14}$
m	4.55	4.486

4. FE-Model Results And Comparison With Experiments

4.1 Predicted crack propagation paths

As shown in Figure 4, the crack propagation and fatigue experiment is modelled in three separate stages:

a) Crack propagation along the face-sheet/foam core interface
b) Crack propagation along the PU (peel stopper)/foam core interface
c) Crack arrest

Figure 5 shows the test machine actuator piston displacement measured for all four STT specimens [25] and the respective FE model predictions corresponding to the load application point on the debonded face sheet plotted against number of cycles for the loading sequences A (F_{max}*=380 N)* and B (F_{max}*=950 N*) respectively (corresponding to crack propagation as indicated in Figure 4a and 4b). The first part of the plot (Sequence A) represents the fatigue response of the specimens during propagation in the face/core interface and the initial stage of the fatigue life of the specimens. The second part (Sequence B) represents the fatigue response after deflection of the crack to the PU/core interface.

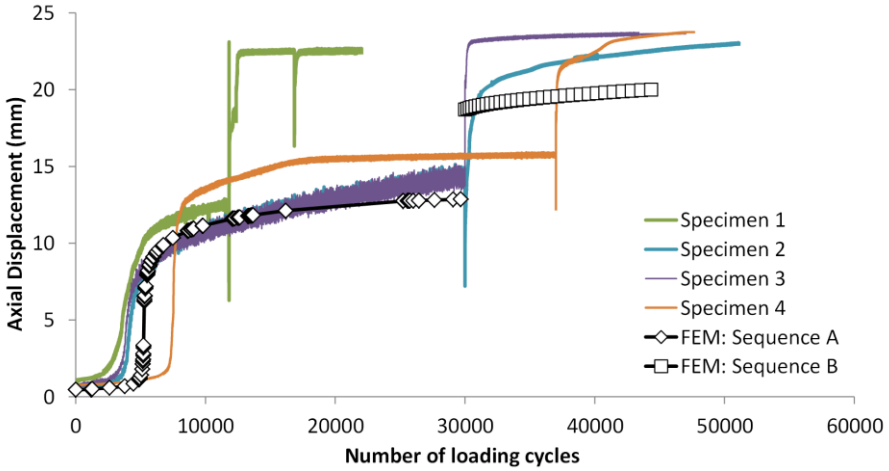

Figure 5. Vertical displacement (test machine actuator piston) vs. number of loading cycles; experimental data [1] and FE model predictions.

Figure 5 reveals an overall fair agreement between the measurements and the predictions for Specimen 2 and 3, but also that a significant variation (scatter) between the measurements for the four sandwich beam specimens exists. However, evaluating the data in Figure 5 more closely reveals that the finite element model generally under predicts the vertical displacements slightly despite the fact that geometrically nonlinear effects are included in the modelling. This is especially pronounced for the displacements corresponding to load sequence B. The most significant cause of this discrepancy is likely to be that the vertical displacements included in Figure 5 represent the test machine piston displacement rather than displacements measured directly from the specimen. However, for the sandwich beam specimens tested in this work, the overall response does not affect the crack tip loading conditions or the stress/strain distribution in the specimen significantly as will be shown in the following. The error of the piston measurements is investigated by a direct comparison with displacement measure from the images captured by the DIC system. Unfortunately since the images were captured at random points in time during the experiments the vast majority of the images is not taken during the maximum loading of the specimens. For this reason DIC data from the images could not be used to create the displacement vs loading cycle curves. Figure 6 shows plots that compare the displacement as recorded by the machine piston and as measured from the images of the DIC system. It can be seen that the error is very small for specimens 1 and 4 while quite significant for specimens 2 and 3. In all cases the piston measurements over predicts the actual displacement of the specimens.

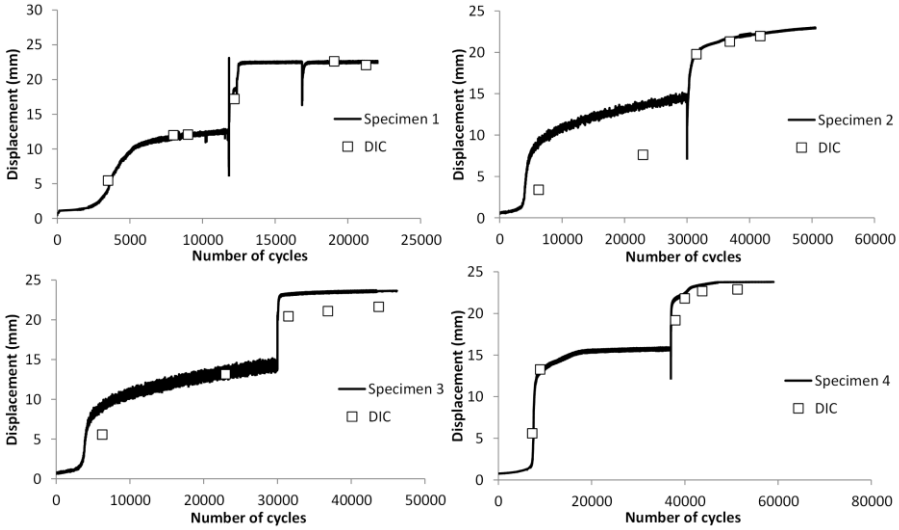

Figure 6. Comparison of displacement measured by hydraulic machines piston and images of DIC.

4.2 Energy release rate (ERR) / Mode mixity angle

Figure 7 and 8 show the evolution of the ERR and mode mixity phase angle as a function of the crack length (Figure 7) and number of loading cycles (Figure 8). The plots provide a good representation of the characteristic response of the STT sandwich beam specimen behaviour under load controlled fatigue testing. It is observed that the ERR rises considerably with increasing crack length until it reaches a maximum. Past this point the vertical displacements of the debonded face-sheet have become so large compared to its thickness so that the in-plane membrane forces in the face-sheet become dominating and thus affecting the load response. Effectively the induced membrane forces stiffen the face-sheet and specimen response significantly (geometrically nonlinear effect) and consume the majority of the strain energy in the specimen, and consequently reduce the resulting ERR at the crack tip. In effect this is the reason why it was chosen to increase the imposed load at stage b (cf. Figure 4 – corresponding to load Sequence B), when the crack propagates into and along the PU/foam interface [25]. The higher load counters the increased resistance to out of plane displacements of the facesheet due to the membrane forces. If the load amplitude was kept constant as per Sequence A, the crack would arrest due to the continuously decreasing ERR. The observed abrupt change in ERR, seen from both the FE results and the experimental observations, is a result of this sudden increase of the imposed load. It is further observed that the ERR decreases again until the crack arrest point is reached.

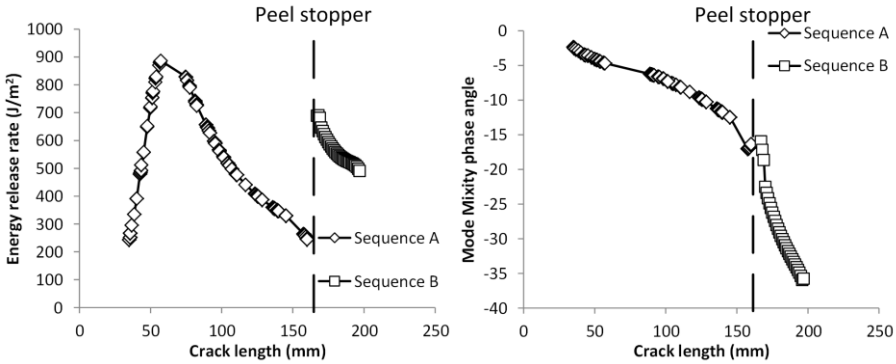

Figure 7. Energy release rate and mode mixity phase angle vs. Crack length for loading sequences A and B

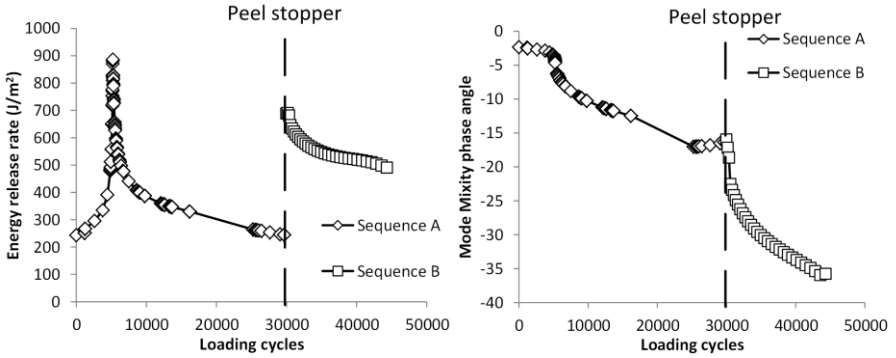

Figure 8. Energy release rate and mode mixity phase angle vs. Number of loading cycles for loading sequences A and B.

The mode mixity at the crack tip changes considerably as the crack length increases. The shear component (mode II) initially is small but increases fast. Especially at stage b (cf. Figure 4) or during Sequence B where the crack has already been deflected, the mode mixity increases negatively very rapidly, since the crack is propagating at a 10^{O} angle towards the inner part of the sandwich core material. This rapid change in mode mixity phase angle means that it is cumbersome to define the crack propagation rate to be expressed by Paris' law, since the crack propagation rate is highly dependent of both the ERR and the mode mixity. A large number of iterations of fatigue experiments are required to define the Paris Law parameters of an interface under a wide range of mode mixity phase angles. Finally, the observed increase of the negative mode-II component at the crack arrest point shows a distinct and very significant tendency of the crack to return to the upper face-sheet/core interface. Under such loading conditions the high fracture toughness of the PU/GFRP peel stopper, achieved by embedding glass fibre reinforcement in the PU material [26], is essential for the performance of the peel stopper. The peel stopper

itself is not displaying any sign of crack initiation, but a new crack is instead initiated in the core material on the back side of the peel stopper. That makes stage c (cf Figure 4) of the experiment last for a considerably longer period of cycles than stages a and b. That is because new cracks usually initiate a lot slower than they propagate under the same loading conditions. The main goal of embedding glass fibres in the PU material of the peel stoppers was to increase its fracture toughness and prohibit crack propagation at stage c.

5. FE Vs. Experimentally Captured Strains – Crack Re-Initiation And Lifetime Predictions

5.1. Comparison between FE model predictions and DIC measurements

The major principal strains in the core material behind the peel stopper are derived from the FE analysis of the sandwich specimen with the crack located at the arrest point, i.e. stage c (cf. Figure 4). Figure 9, shows the field of major principal strains obtained from the DIC measurements for specimens 1-4 during the conducted fatigue tests [25], and the corresponding field of major principal strains predicted using the FE model. It is observed that the characteristic strain concentration observed in the core material on the back side of the peel stopper in the experiments, is also observed from the FE simulation results. Moreover, the FE model predicts principal strain values that are close to the average of the values measured using DIC. It should be noted that the discrepancy between the strain fields observed for the physical specimens can be attributed to the slightly different propagation paths observed and experimental scatter [25]. The foam material exhibits local variations of mass density and therefore local stiffness variations, and this also contributes to explain the differences between the observed strains. In all cases the observed strain concentrations are caused by local bending of the peel stopper and are not the result of the stress concentrations at the crack tip. To predict the crack arrest time, i.e. the number of cycles between crack arrest and crack re-initiation behind the peel stopper (i.e. number of cycles where the crack remains at stage (c), cf. Figure 4), it is necessary to relate the peak strain values to the occurrence of crack re-initiation. Since the development of a crack re-initiation modelling algorithm was not part of this work, the estimation of the remaining fatigue life is conducted through the use of fatigue data obtained for the Divinycell® H100 PVC foam material [32,33].

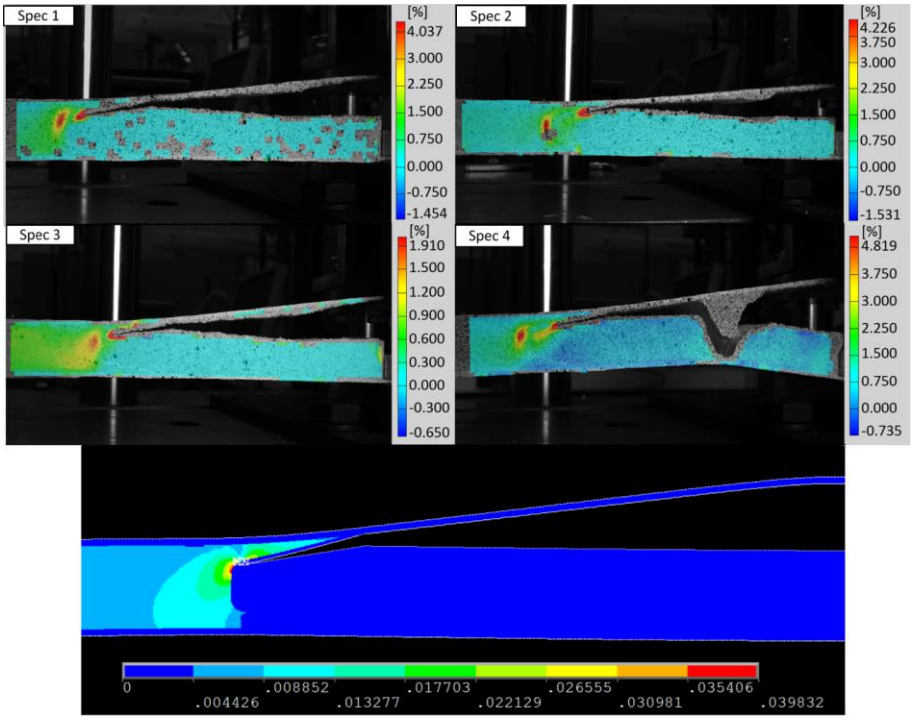

Figure 9. Comparison of FE predictions and measured major principal strain fields (DIC – [1]) at crack re-initiation behind the peel stopper.

5.2. Maximum strain

The FE model was used to predict the major principal strain field, as depicted in Figure 10, for several different crack lengths extending between the peel stopper tip and the crack arrest point. The maximum values of the major principal strain were recorded for both the maximum and minimum fatigue load values as defined by Table 1. This is not to be confused with the two different fatigue load amplitudes (load Sequences A and B) used during the testing in [25]. The maximum and minimum loads discussed here represent the fatigue load limits corresponding to the second fatigue load amplitude level (sequence B), i.e. F_{max}=950N, F_{min}=190N. In Figure 10a the maximum and minimum major principal strains, ε_{max} and ε_{min}, at the crack re-initiation point in the core are plotted against the number of loading cycles. In Figure 10b, the corresponding strain ratio $R_\varepsilon=\varepsilon_{min}/\varepsilon_{max}$ plotted against the number of loading cycles is shown.

It is observed that the strains at the crack re-initiation point increase when the crack approaches the crack arrest point. Since at stage (c) the crack is not propagating (it is arrested), the strain values remain constant for the remaining part of the arrest time, until a new crack initiates behind the peel stopper. As discussed previously, the

crack re-initiating behind the peel stopper can be associated with the major principal strain values. Accordingly, the strain ratio (defined as $R_\varepsilon=\varepsilon_{min}/\varepsilon_{max}$) at the re-initiation point is of high interest. It is seen that R_ε does not remain constant as the crack propagates along the peel stopper, and it reaches its maximum value at the crack arrest point where it is equal to R_ε=0.39. It should be noted that the applied load ratio in the experiments and also in the FE-model is constant at R_L=0.2.

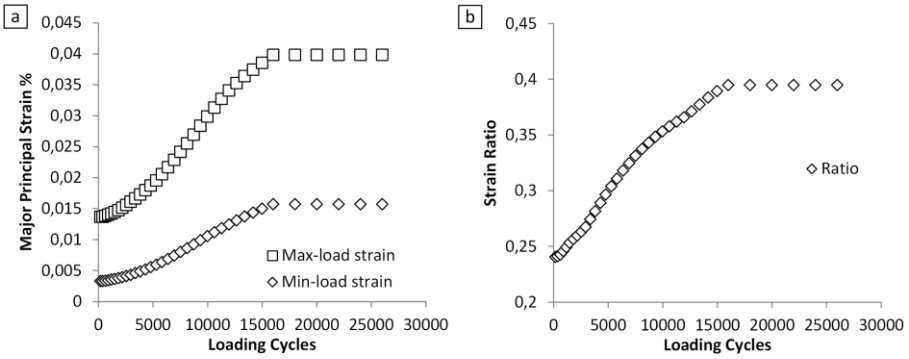

Figure 10. Major principal strains and the strain ratio at the crack re-initiation point corresponding to the maximum and minimum fatigue load levels during fatigue testing vs. number of load cycles.

5.3. Arrest time prediction

To estimate the total time of crack arrest (or the number of cycles between crack arrest and crack re-initiation) based on the calculated strains, shear strain fatigue data are considered according to [32] and [33]. The data correspond to shear strain fatigue tests of H100 Divinycell PVC foam material conducted on sandwich beams in four-point bending. The stress or equivalently the strain ratio during the fatigue tests was defined at R_s=0.1. To account for the effect of the strain ratio on the fatigue damage accumulation in the foam and to effectively compare the strains calculated from the FE analyses to the H100 fatigue data, the maximum to minimum strain difference (or strain range) is calculated:

$$\Delta\varepsilon = (1 - R) * \varepsilon_{max} \quad (3)$$

where ε represents the shear strain from the fatigue data as well as the major principal strains from the DIC measurements and the FE analyses. Figure 11 shows observed strain range vs. the number of cycles when the crack was arrested (between crack arrest and re-initiation) in comparison with the H100 shear fatigue data. The shear fatigue data curve in combination with the calculated FE model strain are used to predict the number of cycles before crack re-initiation and at the crack arrest point, and this is also shown in Figure 11 (orange circle).

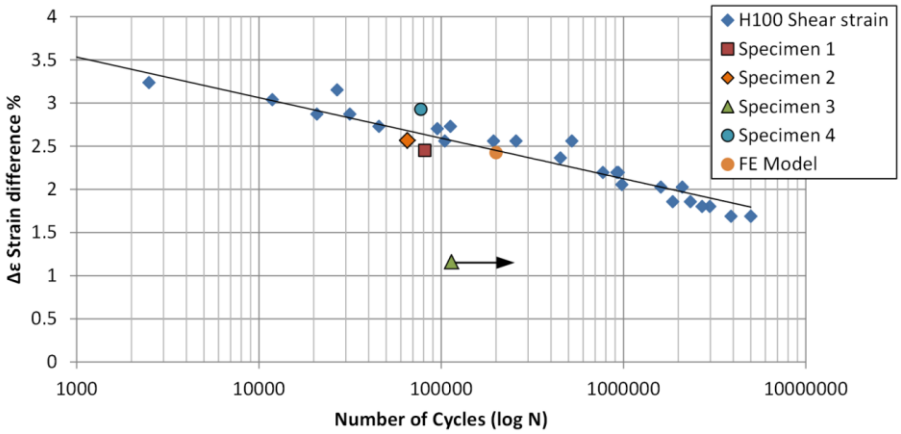

Figure 11. Strain range vs.-number of cycles while crack is arrested; measurements [1], FE model results and comparison with H100 shear fatigue data.

From Figure 11 it is observed that according to the FE model predictions for the average sandwich specimen can be expected to withstand a total of approximately 200,000 load cycles in arrested state before crack re-initiation occurs. This corresponds to almost 3 times the number of cycles to crack arrest, and this effectively implies that the embedded peel stopper has almost doubled the expected fatigue life of the specimens in comparison with sandwich specimens without embedded peel stoppers. The four sandwich beam specimens tested and reported in [1] experienced between approximately 65,000 and 114,000 load cycles at the arrested state, and this implies that FE-model in combination with the H100 fatigue data overestimates the number of load cycles to crack re-initiation. The likely reason for this is that the fatigue shear data for the H100 PVC that was used together with the FE model was obtained from a four-point shear test, and this test configuration does not provide an accurately representation of the stress/strain state at the crack re-initiation point behind the peel stopper. This demonstrates that the performance and efficiency of the peel stopper concept proposed is very sensitive to the actual strain state developing at the crack re-initiation point. Accordingly, a small change (reduction) of the peak strains developing behind the peel stopper, which can be achieved by careful design optimisation of the peel stopper geometry/configuration, has the potential of increasing the expected fatigue life considerably.

6. Conclusions

The basis and motivation for the research presented is a recent experimental study [25] concerning the performance of a novel peel stopper (crack arresting device) for foam cored composite sandwich structures. The principal findings of this investigation has formed the basis for the research presented in this paper, which encompasses the proposition of both a numerical modelling strategy, as well as a classification of the different stages of the crack initiation and propagation process for the foam cored sandwich beams with embedded peel stoppers. In particular, the

numerical simulation methodology developed in this research enables the prediction of the fatigue response and expected fatigue life of foam cored composite sandwich beams with embedded peel stoppers subjected to fatigue loading. The numerical modelling includes fatigue crack propagation simulation along two bi-material interfaces, crack kinking simulation as well as strain field extraction for the prediction of crack initiation. The experimental data obtained from the sandwich beam specimen tests conducted using the STT setup in [25] have been used to validate the FE models predictions. Overall the numerical predictive results compare well with the experimental observations. Moreover, it is demonstrated that the post crack arrest behaviour can be predicted. The results further suggests that there is a significant potential for improving the peel stopper design leading to increased efficiency (and thereby increased fatigue life expectancy) by optimisation of peel stopper geometry/configuration, since the results demonstrate that crack re-initiation behind the peel stopper depends very much on the local strain state.

The findings of this research are important for future development and application of peel stoppers (crack arrest devices) in more representative real application sandwich structures (like e.g. sandwich panels that may be flat or curved). The proposed modelling methodology can be very useful in achieving this, as it can be used for design evaluation as well as optimisation of the shape and position of peel stoppers embedded into complex sandwich components, sub-structures or larger assemblies.

Acknowledgements
The work was sponsored by the Danish Council for Independent Research | Technology & Production Sciences (FTP) under the research grant “Enhanced performance of sandwich structures by improved damage tolerance" (SANTOL) (Grant 10082020). The Divinycell H100 material used in this study was provided by DIAB Group, Sweden. The work has been conducted in collaboration with and co-sponsored by the Technical University of Denmark, Aalborg University, Denmark, the University of Southampton, UK, Siemens Wind Power A/S, Denmark, and LM Wind Power Blades A/S, Denmark.

References

[1] Zenkert, D., “An introduction to sandwich construction” London: Chameleon Press Ltd, 1995

[2] Erdogan, F., 1971. Bonded dissimilar materials containing cracks parallel to the interface, *Engineering Fracture Mechanics*, 3, 231-240.

[3] Dundurs, J., 1969. Edge-bonded dissimilar orthogonal elastic wedges. J.Appl.Mech. 36, 650-652.

[4] Hutchinson J.W., Suo Z., 1992. Mixed Mode Cracking in Layered Materials", Advances in Applied Mechanics, 29, 63-191.

[5] He M.Y., Hutchinson J.W., 1989. Kinking of a crack out of an interface, J. appl. Mech., 56, 270–278.

[6] Suo, Z., 1990. Singularities, interfaces and cracks in dissimilar anisotropic media. Proceedings of the Royal Society of London A: Mathematical, Physical and Engineering Sciences 427 (1873), 331-358.

[7] Wang, T. C., 1994. Kinking of an interface crack between two dissimilar anisotropic elastic solids. International Journal of Solids and Structures 31 (5), 629–641.

[8] M. Rinker, R. Krueger, J. Ratcliffe, 2013. Analysis of an Aircraft Honeycomb Sandwich Panel with Circular Facesheet/Core Disbond Subjected to Ground-Air Pressurization, NASA/CR-2013-217974, NIA report no. 2013-0116.

[9] Riccio, A., Damiano, M., Raimondo, A., Di Felice, G., Sellitto, A. 2016. A fast numerical procedure for the simulation of inter-laminar damage growth in stiffened composite panels. Composite Structures, 145, pp. 203-216

[10] Riccio, A., Raimondo, A., Scaramuzzino, F. 2015. A robust numerical approach for the simulation of skin-stringer debonding growth in stiffened composite panels under compression, Composites Part B: Engineering. 71, pp. 131-142

[11] Berggreen C., 2004. Damage tolerance in debonded sandwich structures. PhD. Thesis. Department of Mechanical Engineering, Technical University of Denmark.

[12] Berggreen, C., Simonsen, B. C., Borum, K. K., 2007. Experimental and numerical study of interface crack propagation in foam-cored sandwich beams. Journal of Composite Materials 41 (4), 493–520.

[13] Moslemian, R., Karlsson, A. M., Berggreen, C., 2011. Accelerated fatigue crack growth simulation in a bimaterial interface. International Journal of Fatigue 33 (12), 1526–1532.

[14] Moslemian, R., Berggreen, C., 2013. Interface fatigue crack propagation in sandwich X-joints – Part I: Experiments. Journal of Sandwich Structures and Materials, 15(4), 429-450.

[15] Moslemian, R., Berggreen, C., 2013. Interface fatigue crack propagation in sandwich x-joints – Part II: Finite element modeling. Journal of Sandwich Structures and Materials 15 (4), 451-463

[16] Moslemian, R., 2011. Damage Tolerance of Curved Sandwich Structures in Wind Turbine Blades. PhD. Thesis. Department of Mechanical Engineering, Technical University of Denmark.

[17] C. G. Dávila, P. P. Camanho, and A. Turon. "Effective Simulation of Delamination in Aeronautical Structures Using Shells and Cohesive Elements", Journal of Aircraft, Vol. 45, No. 2 (2008), pp. 663-672

[18] Lundsgaard-Larsen, C., Berggreen, C., Carlsson, L. A. 2010. Tailoring Sandwich Face/Core Interfaces for Improved Damage Tolerance: Part I: Finite Element Analysis. Applied Composite Materials, 17(6), 609-619.

[19] Lundsgaard-Larsen, C, Berggreen, C & Carlsson, LA 2010, 'Tailoring Sandwich Face/Core Interfaces for Improved Damage Tolerance: Part II: Experiments' Applied Composite Materials, vol 17, no. 6, pp. 621-637.

[20] Lundsgaard-Larsen, C., Berggreen, C., Carlsson, L. A. 2010. Tailoring Sandwich Face/Core Interfaces for Improved Damage Tolerance: Part II: Experiments. Applied Composite Materials, 17(6), 621-637.

[21] Rinker, M., Zahlen, P. C., John, M., Schäuble, R., 2012. Investigation of sandwich crack stop elements under fatigue loading. Journal of Sandwich Structures and Materials 14 (1), 55–73.

[22] Hirose Y, Matsubara G, Hojo M, Matsuda H, Inamura F., 2008. Evaluation of modified crack arrester by fracture toughness tests under mode I type and mode II type loading for foam core sandwich panel. In: Proc. US-Japan conference on composite materials 2008, Tokyo, Japan.

[23] Hirose, Y., Matsuda, H., Matsubara, G., Hojo, M., Inamura, F., 2012. Proposal of the concept of splice-type arrester for foam core sandwich panels. Composites Part A: Applied Science and Manufacturing 43 (8), 1318–1325.

[24] Jakobsen, J., Andreasen, J. H., Thomsen, O. T., Sep. 2009. Crack deflection by core junctions in sandwich structures. Engineering Fracture Mechanics 76 (14), 2135-2147.

[25] Martakos G., Andreasen, J. H., Berggreen C., Thomsen, O. T., Experimental Investigation of Interfacial Crack Arrest in Sandwich Beams Subjected to Fatigue Loading using a Novel Crack Arresting Device. Journal of Sandwich Structures and Materials.

[26] Wang, W., Martakos, G., Dulieu-Barton, J.M., Andreasen, J.H. and Thomsen, O.T., 2015. Fracture behaviour at tri-material junctions of crack stoppers in sandwich structures. Composite Structures, 133, 818-833. 10.1016/j.compstruct

[27] ANSYS® Academic Research, Release 15.0

[28] Taher, S.T., Thomsen, O.T., Dulieu-Barton, J.M. and Zhang, S., 2011. Determination of mechanical properties of PVC foam using a modified Arcan fixture. Composites Part A: Applied Science and Manufacturing, 43, 1678-1708. (doi:10.1016/j.compositesa.2011.11.010).

[29] Jakobsen, J., 2004. Local Effects and the Control of Face-Core Debond Failure in Sandwich Structures . PhD. Thesis. Department of Mechanical Engineering, Aalborg University.

[30] Paris P., Erdogan F., 1963, A critical analysis of crack propagation laws, J Basic Engng Trans ASME Ser D, 85 (4) 528–534.

[31] Manca, M., Berggreen, C., Carlsson, L. A., 2015. G-control fatigue testing for cyclic crack propagation in composite structures. Accepted for publication in Engineering Fracture Mechanics. DOI 10.1016/j.engfracmech

[32] Burman, M., Magnusson, B., 2008. Fatigue testing of H60, H100 and H200. Technical report (DIAB), KTH (Sweeden).

[33] DIAB. Divinycell H-Grade Technical data, 2014. Laholm (Sweeden) (http://www.diabgroup.com).

PAPER #4

Interfacial Crack Arrest in Sandwich Panels with Embedded Crack Stoppers Subjected to Fatigue Loading

G. Martakos[1], J.H. Andreasen[1], C. Berggreen[2], O.T. Thomsen[3,1]

[s1]Department of Mechanical and Manufacturing Engineering, Aalborg University

Fibigerstræde 16, DK-9220 Aalborg East, Denmark

Email: {gm,jha, ott}@m-tech.aau.dk, web page: http://www.m-tech.aau.dk

[3]Department of Mechanical Engineering, Technical University of Denmark

Nils Koppels Allé, Building 403, DK-2800 Kgs. Lyngby, Denmark

Email: cbe@mek.dtu.dk, web page: http://www.dtu.dk

[3]Faculty of Engineering and the Environment,
University of Southampton, Highfield, Southampton, UK

Email: o.thomsen@soton.ac.uk , web page: http://www.soton.ac.uk/engineering/

The paper was submitted and accepted for publication in the Journal of Applied Composite Materials, August 2016

DOI: 10.1007/s10443-016-9514-3

Abstract

A novel crack arresting device has been implemented in sandwich panels and tested using a special rig to apply out-of-plane loading on the sandwich panel face-sheets. Fatigue crack propagation was induced in the face-core interface of the sandwich panels which met the crack arrester. The effect of the embedded crack arresters was evaluated in terms of the achieved enhancement of the damage tolerance of the tested sandwich panels. A finite element (FE) model of the experimental setup was used for predicting propagation rates and direction of the crack growth. The FE simulation was based on the adoption of linear fracture mechanics and a fatigue propagation law (i.e. Paris law) to predict the residual fatigue life-time and behaviour of the test specimens. Finally, a comparison between the experimental results and the numerical simulations was made to validate the numerical predictions as well as the overall performance of the crack arresters.

Keywords: Sandwich structures, Composites, Finite Element Analysis, Fracture mechanics, Fatigue

1. Introduction

Sandwich structures represent a special form of laminated composites comprising stiff and thin face-sheets separated by and bonded to either side of a light and compliant core material. The resulting layered sandwich element or structure displays very high stiffness and strength to weight ratios [1,2]. Their structural attributes and the need for larger and ever lighter structures has led to the implementation of sandwich structures into many areas of industrial production, including aerospace, ship/marine, automotive and wind turbine blade structures to mention a few. Due to their extensive and increasing use, novel ways to further enhance the performance of sandwich structures are being pursued continuously. Consequently the wish to fully understand the behaviour of sandwich structures is increasing, as well as the need to control and predict the effect of limitations and weaknesses inherent in their nature. One of the main limitations of sandwich structures is their sensitivity to separation or debonding between the core material and the face-sheets. Moreover, debonds or dry spots can be introduced during manufacturing, especially for larger parts. The separated or debonded zones effectively act as inherent structural weak points/zones, which may lead to premature fracture in the core which is likely to develop into cracks separating the core and face-sheets. Such debonds may progressively expand under the action of external loading (quasi-static of fatigue), and may lead to a global failure that occur with little or no prior warning.

The increasing interest concerning interfacial debond behaviour of sandwich components and structures has led to several studies including analytical, experimental and numerical approaches. Interfacial debonds can be considered and

studied within the framework of fracture mechanics, since the conditions of debond progression and arrest can conveniently be described in terms of physical quantities defined through fracture mechanics. Several studies have discussed and applied the theoretical background for this [3-8] in describing bi-material and interface crack behaviour [3-6] and the conditions for crack kinking out of an interface [7-8]. However, it is only in the most recent studies that numerical tools have been successfully utilized to simulate interfacial crack growth in sandwich panels. Several methods have been proposed based on the Finite Element Method framework and have been used to simulate interface crack propagation convincingly. Recent examples include the Virtual Crack Closing Technique (VCCT) [9], the Crack Surface Displacement Extrapolation method (CSDE) [10-11] as well as cohesive zone modelling (CZM) [12]. Moreover, the CSDE method has been applied in conjunction with the cycle jump technique (CJT) [13-15] to reduce the calculated loading cycles of fatigue simulations. The mentioned methodologies have been applied for the simulation of interface fatigue crack growth in both sandwich beams and sandwich panels [15]. In this study the CSDE and CJT methods have been used to predict the interface crack propagation behaviour in foam cored sandwich panels with composite face-sheets. In addition, this study considers the conditions under which an embedded crack stopper device (in the form of a core insert) can promote crack deflection away from the face-sheet/core interface and into the sandwich core material following a pre-described propagation path along an interface between the crack stopper and the foam core material.

Previous attempts to delay or arrest propagating interfacial face-sheet core cracks by the use of special embedded crack stopping inserts (or devices) have been reported. In [16] two types of carbon fibre reinforced composite (CFRP) inserts loaded using the Sandwich Cantilever Beam (SCB) and Cracked Sandwich Specimen (CSB) tests were introduced to examine crack arrest under mode I and mode II loadings, respectively. It was shown that the embedded crack stopper devices/elements could arrest a propagating interface crack for a considerable amount of loading cycles, especially under mode II loading conditions. The reason for this effect is the much higher fracture toughness of the CFRP compared to conventional core materials as well as the geometry of the CFRP crack arresters. In [17-18] it was demonstrated that crack arrest can be achieved by using either a semi-circular CFRP rod glued onto face-sheet/core interface, or by using a splice-type crack arrester connecting the two face-sheets through CFRP layers. In both cases a stress release at the crack tip was observed as the crack approached the tip of the arresters. The reduction of stresses at the crack tip resulted in a reduction of the energy release rate and a deceleration of the crack. Finally, in [19-25] a new type of crack arrester (referred to as a peel stopper) was tested. The peel stopper, which is configured as a core insert made from a compliant/soft material bonded to both the face-sheets and sandwich core, is capable of re-directing propagating cracks away from the interface and subsequently arresting the cracks in the centre of the peel stopper. The peel stopper has been shown to be able to deflect and arrest propagating interface cracks in

sandwich beams subjected to both quasi-static and fatigue loading conditions, and where the stress field near the crack trip is Mode II dominated [21, 25].

Following on from and inspired by the work presented in [26-28], a new and significantly lighter design of the peel stopper was proposed and implemented in sandwich beams [26-28]. Initially, the conditions under which the novel peel stopper was able to deflect a propagating face-sheet/core interface crack were investigated in [26]. This included testing of sandwich beams made of glass reinforced composite face-sheets (GFRP) and PVC foam core with embedded peel stoppers subjected to fatigue loads using the Mixed Mode Bending test (MMB) [26]. Three design variations of the peel stopper were tested showing that a design with glass fibres extruding from the tip of the peel stopper and extending into either the face-sheets or the face-sheet/core interface improved the interface crack deflection capabilities. The new peel stopper was further tested in sandwich beams using the Sandwich Tear Test (STT) in [27]. The aim of the research presented in [27, 28] was to evaluate and validate the ability of the new lightweight peel stopper design to delay or hinder interface crack propagation, and ultimately achieving crack arrest in composite foam cored sandwich beams subjected to fatigue loading conditions. This was achieved and the underlying physical mechanisms were accounted for using both experimental and numerical approaches. It was further shown that the novel peel stopper design was capable of more than doubling the expected life time of sandwich beams.

This study concerns the fatigue testing of sandwich panels with GFRP face-sheet and PVC foam core that have been fitted with embedded peel stoppers of the improved design introduced in [26, 27, 28]. The ability of the peel stoppers to enhance the damage tolerance of sandwich panels, i.e. to delay or prevent interface crack propagation, has been investigated using both experimental observations and finite element (FE) analyses.

2. Methods

2.1. Specimens/Materials

The experimental study involves testing of quadratic sandwich panels by applying transverse loads as a concentrated force applied through a metallic insert in the centre of the panel. To simplify the test rig design, it was chosen to use quadratic sandwich panels that are simply supported along all four edges. Fatigue loading was applied to progress a predefined face-sheet/core debond located in the centre of the panel around the loading point. Two types of sandwich panel specimens were manufactured; one with embedded peel stoppers and another without peel stoppers.

The peel stoppers were manufactured in a circular shape, and subsequently embedded in the sandwich foam core with the peel stopper circle having its centre coinciding with the sandwich panel centre. Thus the peel stopper is configured as a circular “barrier” around the load introduction area in the plate centre. The

configuration with a central external load, and a concentric circular peel stopper was chosen to achieve a nearly axisymmetric strain and stress field in the vicinity of the plate centre and the peel stopper despite the fact that the sandwich panel specimens were in fact quadratic. The sandwich panel/plate dimensions were chosen such that edge effects from the four straight edges did not influence the strain and stress fields near the crack stopper.

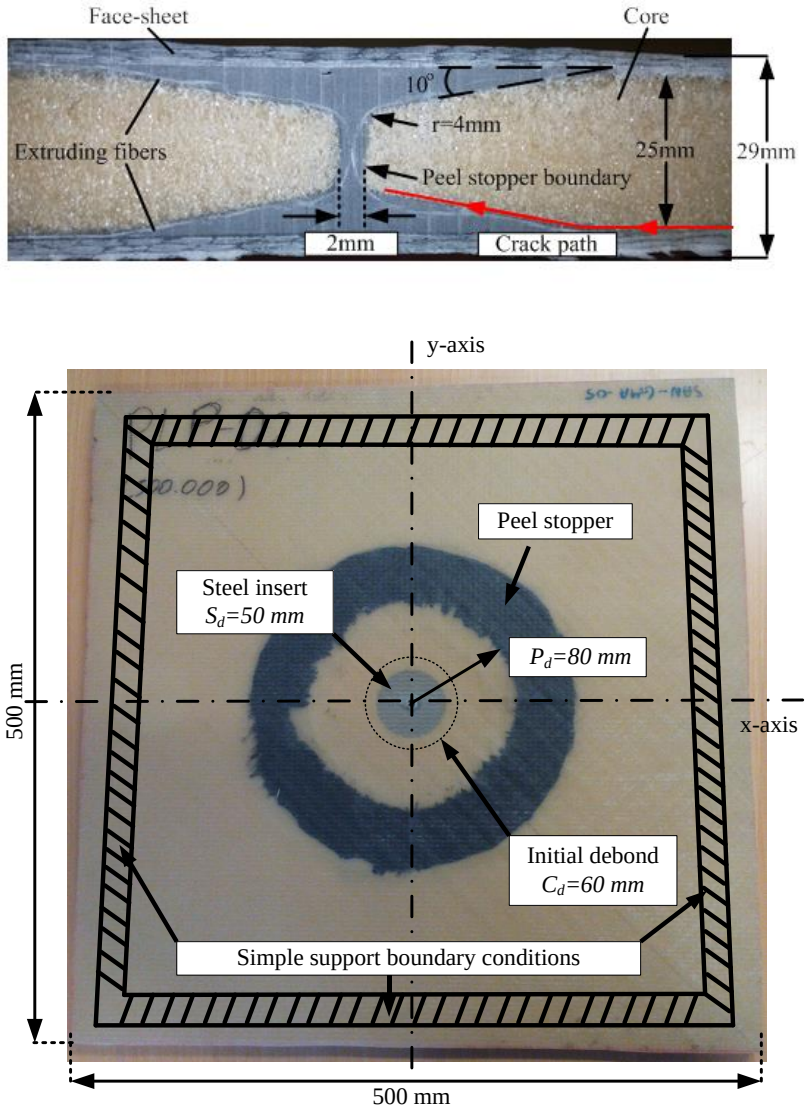

Figure 1. Layout and dimensions of foam cored sandwich panel test specimens with embedded PU peel stopper.

Figure 1 shows the sandwich panel dimensions, the sandwich panel boundary and loading conditions, and the peel stopper shape and dimensions. The peel stopper cross section was designed with a double U shape, thus enabling crack deflection of face-sheet/core interface cracks propagating from the centre of the plate towards the edge as well as cracks propagating from the edge towards the centre (if that was to occur). Once deflected, cracks from both sides were allowed to propagate only until the middle of the peel stopper where the crack was arrested at the physical boundary created by the geometry of the peel stopper.

The peel stoppers were manufactured using a special mould tool made from Polypropylene. The peel stopper was made using a two-component Polyurethane (PU) resin (PERMALOCK 2K PU-9004) which was reinforced by UD glass fibres along its length as devised in [26]. The use of Polypropylene for the mould tool allowed easy de-moulding of the cast PU peel stoppers without the need of a release agent. For practical reasons the circular peel stopper configuration was made from 4 quarter circle sections that were manufactured separately and then embedded into the PVC foam core material, see Figure 1. The glass reinforcement was first placed in the mould tool, and to reduce complexity during fabrication, the glass reinforcement was only extending from the side of the double U peel stopper shape (see Figure 1) facing towards the plate/panel centre. After this the PU resin was carefully poured into the mould tool, and subsequently the mould tool was closed to form the PU peel stopper. The PU peel stoppers were cured for 8 hours at room temperature.

The face-sheets of the sandwich panels consisted of 3 layers of glass reinforcement, quad-mat [0°/45°/90°/-45°] AMT (DBLT-850) from Devold, providing 2 mm thick face-sheets after the resin infusion. The resin system used was Huntsman Araldite LY 1564 SP/Hardener XB 3486. Divinycell H100 PVC foam from DIAB having a nominal density of 100 kg/m^3 [29] was used as the core material. This combination of composite face-sheets and core material was chosen, as it was used for the research presented in [27,28], from which the interface crack propagation properties are available. Table 1 summarizes the material properties of the sandwich panel specimens.

The sandwich panel specimens were fabricated in two steps. In the first step, the core structure comprising of the machined PVC foam material and the PU peel stoppers was assembled, and in the second step the glass reinforcement of the top and bottom face-sheets and the sandwich core were laid up into the mould tool. Finally, the entire assembly was infused using Vacuum Assisted Resin Transfer Moulding (VARTM).

The manufacturing of the sandwich panels without embedded peel stoppers was straightforward, as it only required cutting of the PVC H100 foam into the square shape of the sandwich panel, followed by milling of the cylindrical cut-out in the plate centre where a steel insert of diameter 50 mm and the same height as the foam core was placed in the succeeding process step.

For the sandwich panels with embedded peel stoppers, an additional extra milling process was conducted to shape the PVC foam to allow the assembly with the PU peel stoppers. Since the peel stopper appears as a "through thickness" core insert, the "inner" and "outer" areas of the foam were separated after milling. After the foam was milled, all the parts were bonded together using an epoxy adhesive, Araldite 2000. The core parts were pressed together using clamps while the adhesive was allowed to cure for one day at room temperature. After this the cylindrical steel insert was inserted in the centre of the square shaped core assembly, thus providing a means to apply the external loading into the sandwich specimens. The central steel insert was coated by a thin layer of Teflon to prevent bonding to the adjacent core and face-sheet components in the resin infusion process. This was chosen to assure that the desired crack was always initiated in the lower face-sheet/core interface of the panel specimens. Before the resin infusion an extra layer of Teflon foil of diameter 60 mm (see Figure 1) was inserted at the top face-sheet/core interface to induce an initial concentric crack front in the sandwich panel specimens. Finally, after following all the steps outlined above, the sandwich panel specimens were infused and cured at room temperature for 24 hours, followed by a post curing at 80^{o}C for an extra 12 hour period.

Table 1. Material properties of sandwich panel specimens [26-28]

Materials	In-plane Young's modulus (E_x)	Through thickness Young's modulus (E_y)	Shear modulus (G_{xy})	Poisson's ratio (v_{xy})
DIVINYCELL H100	56 MPa	128 MPa	32 MPa	0.3
E-glass/epoxy	18.6 GPa	9.2GPa	2.7 GPa	0.4
PU	100 MPa	100 MPa	34.2 MPa	0.45

2.2. Test set-up

The tests were conducted using a Schenck 400 kN servo-hydraulic test machine with an Instron 8800 controller. A 10 kN load cell was mounted in the machine to improve the load control accuracy during the tests. Figure 2 shows the testing set-up, including load application through a central insert and the square shaped steel test rig providing the simply supported boundary conditions imposed along the panel edges. As indicated in Figure 2, the sandwich panels were simply resting on the square shaped steel test rig, providing approximate simple support conditions along the four panel edges. Rubber strips were attached to the supporting flat steel surfaces of the test rig, and the specimens rested on these rubber strips to avoid indentation

damage during testing. The test rig was mounted to the cross-head of the test machine, hanging from the load cell attached to the load frame of the test machine. The mounted test rig was placed as high as possible to maximize the distance between the hydraulic actuator at the bottom of the test frame and the underside of the panel specimen. This was done to maximize the viewing area of the 2 digital cameras facing upwards towards the panel specimens and used for digital image correlation (DIC) measurements. To apply the loads from the actuator to the specimen, an extension rod was attached to the actuator. The rod was made from aluminium with a diameter of 25 mm to minimize the obscuring of the field of view for the 2 digital cameras.

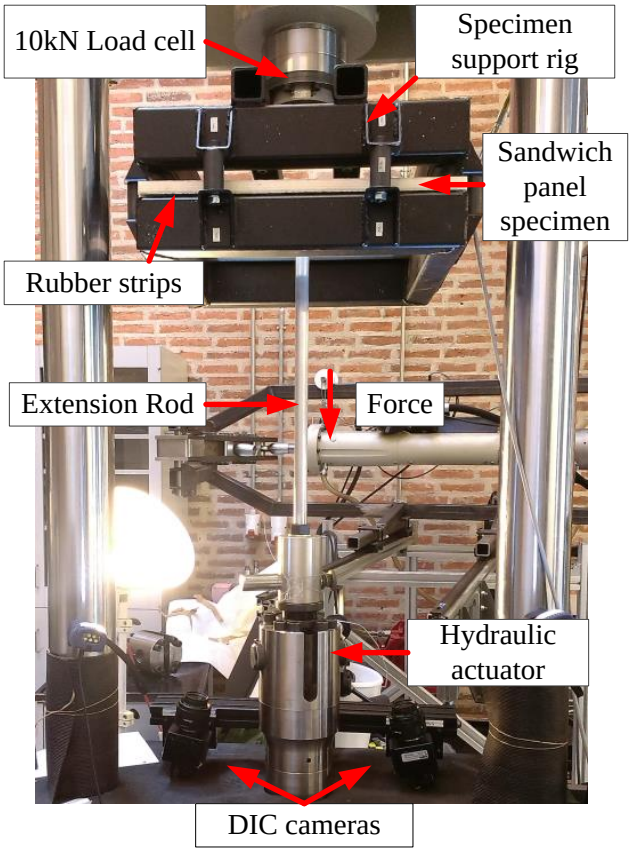

Figure 2. Sandwich panel testing setup and DIC setup of the tested sandwich panels.

As mentioned above, the sandwich panels were subjected to a central point load applied through the central loading insert. The test was designed to drive the face-sheet/core interface crack pre-initiated in the centre of the sandwich panels towards the peel stopper and outer panel boundary. The advantage of this test setup is that

the interface crack propagation is both predictable and easy to control as the crack propagates steadily under all load control schemes. The central force loading applied to the specimens led to a sub-interface crack propagation path without any occurrence of crack kinking into the foam material, as the mode mixity induced always drove the crack to propagate towards the debonded face-sheet rather than into the core. In fact, the crack tended to propagate on the core side just below the facesheet/core interface, The self-similar crack propagation behaviour in all tested specimens allowed for a high consistency and repeatability throughout the tests and thus reduced the number of test repetitions required. Three tests were conducted under load controlled fatigue loading conditions with an R-ratio of $R = 0.1$; two specimens with embedded peel stoppers, and one specimen without a peel stopper. In addition, one sandwich panel specimen was tested subject to quasi-static loading in order to derive the appropriate load amplitudes imposed in the fatigue tests. Figure 3 shows the force vs, cross-head displacement obtained from the quasi-static test, where the panel specimen was loaded in displacement control until the interface crack propagated two times before the test was stopped. The four sandwich panel specimens are presented in Table 2.

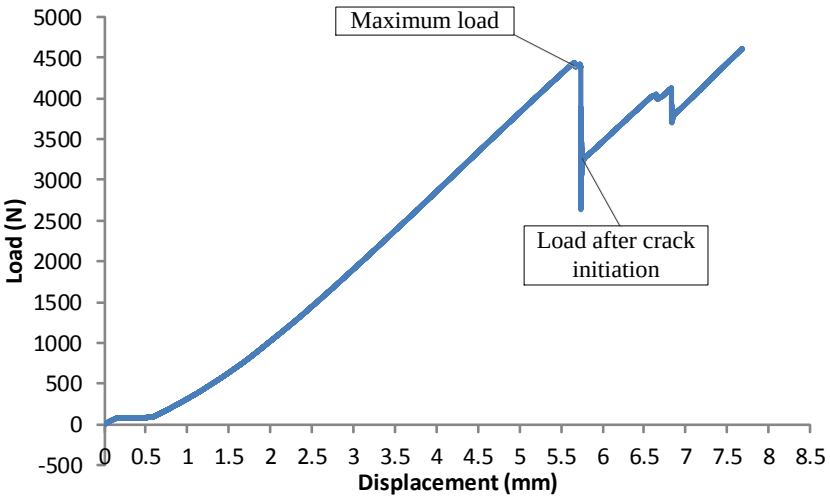

Figure 3. Load-displacement obtained from quasi-static testing of a sandwich panel without a peel stopper.

Table 2. Sandwich panel specimens used for fatigue and quasi-static load tests.

Specimen name	*Loading conditions*	*Specimen Type*
PLP 1	*Fatigue*	*with embedded peel stopper*
PLP 2	*Fatigue*	
PLT 1	*Quasi-static*	*Without peel stopper*
PLT 2	*Fatigue*	

The fatigue load applied to specimens PLT2 (without peel stopper) and PLP1, PLP2 (with embedded peel stoppers) was chosen to be about 80% of the maximum load obtained for PLT1 (quasi-static test), and equal to the load where interface crack propagation first occurred. As the interface crack front propagated from the centre of the panel, the load was distributed along a larger circumference as well as contributing to an increasing membrane force build-up in the debonded face-sheet, and thus the stresses as well as energy release rate at the crack tip reduced acordingly, with the important implication that the applied load amplitude needed to be increased to propagate the crack further. If the fatigue loading had been applied at a constant magnitude throughout the entire test, this would have resulted in a self arresting propagation mechanism, where the interface crack propagation would have deccelerated as the debonded interface crack area increased in size (diameter). Despite this fact, the fatigue load amplitude was chosen to remain contant throughout the entire test, since the initially chosen load amplitude was proven to be sufficiently high to propagate the crack far enough to assess the peel stopper performance.It is important to note here that the energy release rate of the crack is directly infuencing the performance of the peel stopper. Higher loads will effectively result in a reduced crack arrest time, while lower loads will enhance it. However, the effect of the load magnitude has been taken out in this study by testing also specimens without peel stoppers. The evaluation is based on a comparison of the fatigue life of specimens with and without crack stoppers loaded under the same load ampitude.

Since visual identification of the crack position was impossible, the duration of the tests could not be controlled based on visual inspection. The number of cycles to test completion was selected based on DIC observations, which gave an indication of the crack position inside the panels. This procedure required testing of the sandwich panels up to an initialy selected number of cycles, followed by post-processing of the images captured by the DIC system to identify the crack position. In cases where the crack had not propagated adequately, the test was continued. Initially a total of 250.000 load cycles were imposed for all panels. For the case of the panel without a peel stopper the number of cycles was found to be sufficient to propagate the crack at a radius of approximetaly 100 mm without the need to increase load magnitud. For the two panels with embedded peel stoppers 250.000 cycles resulted in a crack

propagation radius of 82 mm. This was found inadequate and an additional 250,000 loading cycles were imposed (thus reaching a total of 500,000 cycles for the 2 panels with embedded peel stoppers) to propagate the crack further. With the additional loading cycles the crack grew to a radius of approximetaly 85 mm. The experiements were terminated at this stage, as it was observed that the crack growth rate at the specified load magnitude was so low that further continuation would not result in a substantial increase of the crack radius. Table 3 summarizes the fatigue loading conditions applied to the 4 sandwich panel specimens.

Table 3. Fatigue loading configuration

Fatigue test data	*Fatigue load*
Fatigue maximum load	*3800 N*
Fatigue minimum load	*380 N*
Load Ratio	*0.1*
Frequency	*2 Hz*

2.3 Digital Image Correlation (DIC)

A two camera DIC system was used to capture the out-of-plane displacements of the lower face-sheet of the tested sandwich panels as the face/core debond propagated (see test setup in Figures 2 and 4). The DIC system used was an ARAMIS 4M system from GOM GmbH. The DIC software ARAMIS v6.2.0 was used to post-process and extract deformation data from the images. The digital cameras were placed below the specimen facing upwards at a distance of approximately 1 m from the sandwich specimen underside surface (lower face-sheet), see Figure 4. The observed area or the Region of Interest (RoI) covered an area of approximately 250 mm by 250 mm in the centre of the lower face-sheet, within the region of where the peel stoppers were positioned and the interface crack was expected to propagate. A random speckle pattern was sprayed onto the lower face-sheet covering the RoI. A thin strip of tape was placed on one side of the panel along the x-axis (see Figure 2). The strip created a thin line in the RoI, clear of the speckle pattern allowing the identification of the crack front location relative to the peel stopper, when the images were post-processed. This enabled the inspection of the crack front propagation radius which was used to control of the total duration of the tests, as explained in the previous section. Images of the RoI were automatically recorded every 60 seconds during the fatigue tests. The DIC setup and image processing details are given in table 4.

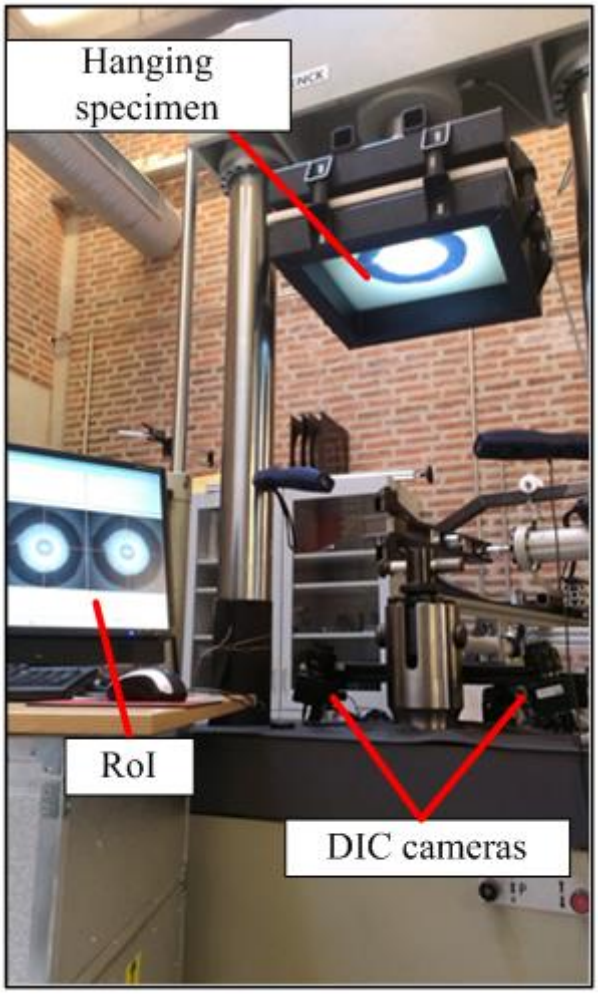

Figure 4. Dual camera DIC setup and Region of Interest (RoI) on the tested sandwich panels.

Table 4. Specification of DIC setup and processing

Technique used	*3D digital image correlation*
Subset size	*15×15 pixel*^{2}
Shift	*15 pixel*
Cameras	*8 bit, 2048×2048 ARAMIS 4M system*
Field of view	*250×250 mm*^{2}
Measurement points	*18769*

Displacement	
Spatial resolution	*1.83mm/15pixel*
Resolution	*122 μm*
Strain	
Smoothing method	*Gaussian Average (3×3)*
Differentiation method	*Finite differences*

3. Numerical Analyses

A three dimensional (3D) Finite Element (FE) model was developed in the commercial software package ANSYS 15.0 [30]. The model was developed to simulate crack growth in the sandwich panel specimens with and without peel stoppers subjected to fatigue loading conditions. To capture the 3D nature of the problem, the crack propagation in the face-sheet/core and core/PU interfaces was modelled by means of a 3D crack front. By using the mesh at the crack tip, the CSDE mode-mixity method [10-11] was used to extract the energy release rate and mode-mixity along the crack tip front. Each nodal point was able to move independently in a direction perpendicular to the crack front depending on the energy release rate and mode-mixity values, respectively. By the use of a re-meshing algorithm, the 3D crack propagation inside the sandwich panels was simulated.

Figure 5 and 6 show the detailed 3D FE models for both the specimens with and without peel stoppers. Only one quarter of the sandwich plate specimens were modelled due to double-symmetry of the test specimens. The main panel model consisting of 8.000-14.000 20-node solid elements, depending on the radius of the crack front modelled. Geometrical non-linear analyses were conducted to accurately account for the large displacements and rotations of the debonded face-sheet during the experiments, as well as membrane effects in the debonded face-sheet.

It is observed from Figure 6 that the peel stopper was not modelled in great detail, and that only the lower part facing towards the panel centre was included in the model. The reason being that the geometric complexity of the peel stopper created meshing instability issues in the crack simulation analyses. The fatigue crack propagation is simulated by repeated loops of defining the new crack position and then re-meshing the model accordingly without user intervention. This means that high geometric complexity is bound to lead to occasional errors in meshing that would stop the simulations. To avoid this, the geometric complexity of the model had to be reduced significantly. The cause derives from the choice to use 20-node cubic elements to mesh the entire geometry of the model. ANSYS requires a very structured division of the model geometry to enable automatically meshing with 20-node elements without errors. To avoid meshing errors as the crack front propagated radially in the panel along the face-sheet/core and core/PU interfaces, the FE model

was divided into volumes of more generic shapes. Since the crack propagation was modelled only in the face-sheet/core and core/PU interfaces, it was not necessary to develop a more detailed FE meshing of the peel stopper.

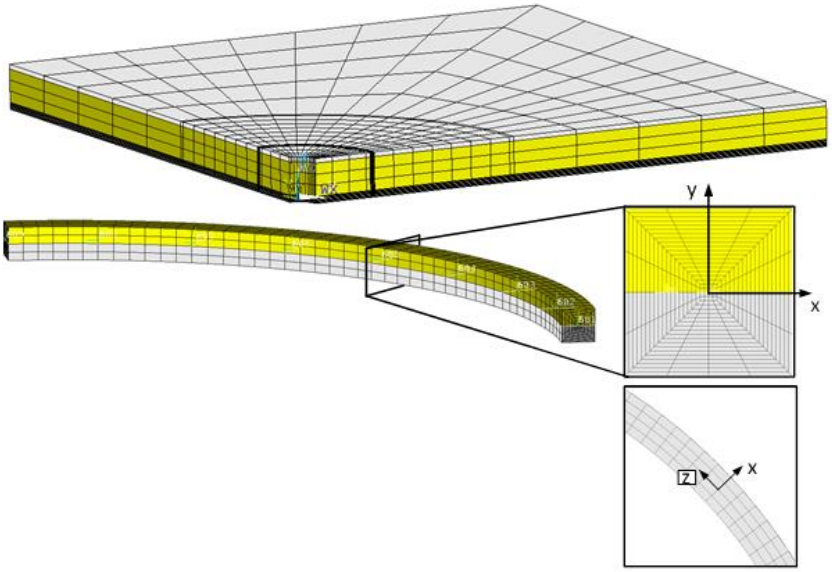

Figure 5. Global FE model of a sandwich panel specimen without a peel stopper (left), and FE sub-model and crack tip mesh along the crack front (right).

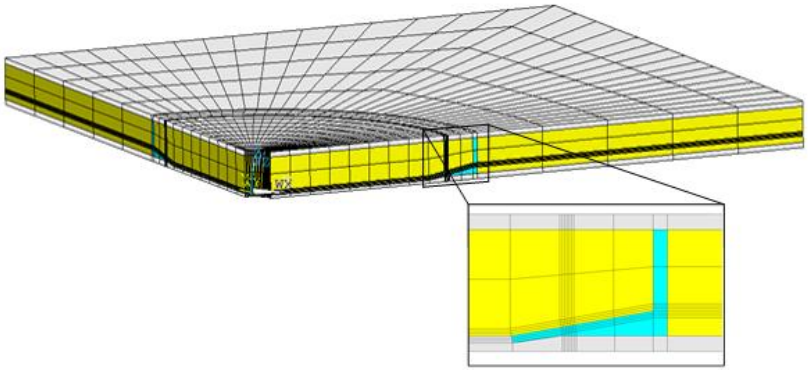

Figure 6. Global FE model of a sandwich panel specimen with an embedded peel stopper, and detailed meshing around the peel stopper, when the interface crack has been deflected.

3.1. Fatigue Crack growth analysis

As mentioned above the CSDE method [10-11] was used to derive the energy release rate and mode-mixity at the crack tip using relative displacements derived from the nodes in the crack tip wake from the FE model. For that purpose a dense crack tip mesh was used in the crack tip region and along the crack front of the debond, see Figure 5. Applying this mesh in the global FE model would result in very long computation times. Therefore, a sub-model containing only the crack tip elements was used for extracting the displacements, similar to applied in [13-15]. The sub-model routine is inherent in the ANSYS software, and works by transferring displacements from a coarse global model into a dense and more detailed sub-model in the form of boundary conditions. For this case, the detailed sub-model consisted only of the crack front and it was meshed by 20-node solid elements. The number of elements increased as the interface crack front propagated and increased in diameter. For the sake of simplicity, and also to save computation time, the sub-model was subject only to geometrically linear analyses. This was justified by the observation that the displacements and rotations at the crack tip are small, and thus there was no need for geometrically non-linear analysis on the sub-model scale. This simplification is important for the feasibility of the adopted approach, since the CSDE method is based on Linear Elastic Fracture Mechanics.

The crack front growth was controlled by nine independent control points along its length. Once the energy release rate and mode mixity were calculated they were used as input on the Paris law defining the crack growth rate in order to calculate the crack increment after one loading cycle. Each control point was then moved independently towards the individual crack growth direction. Once every control point position was updated, the new crack front was created.

After the displacements were extracted from the sub-model, they were used as input for the CSDE code that was implemented using the ANSYS APDL language. The energy release rate and mode-mixity equations used in the code are given by [10-11]:

$$\psi_K = \arctan\left(\sqrt{\frac{H_{22}}{H_{11}}}\frac{\delta_x}{\delta_y}\right) - \varepsilon\, ln\left(\frac{x}{h}\right) + \arctan(2\varepsilon) \tag{4}$$

$$G = \frac{\pi(1+4\varepsilon^2)}{8\,H_{11}|x|}\left(\frac{H_{11}}{H_{22}}\,\delta_y^2 + \delta_x^2\right) \tag{5}$$

where δ_x and δ_y are the crack shear and opening displacements of the crack tip nodes, ε is the oscillation index, and h is the characteristic length of the problem, which was set equal to the face-sheet thickness, i.e. *2* mm. H_{11} and H_{22} are the parameters that account for the anisotropic behaviour of both the face-sheet and the core, Table 5.

Every time the energy release rate and mode-mixity were calculated, the crack increment after one loading cycle was calculated by the use of Paris' Law [31]:

$$\frac{da}{dN} = m\,\Delta G^{c} \tag{6}$$

where a is the crack length, da is the crack length increment, and N and dN are the number of loading cycles and the increment in loading cycles, respectively. The parameters m and c are the fitting variables of the Paris' law curve. Finally ΔG represents the difference in energy release rate (ERR herinafter) between the maximum and minimum fatigue loads. In this study the ERR at the minimum fatigue load level was not specifically calculated. Instead it was considered to be equal to 10% of the ERR value corresponding to the maximum load, based on the load ratio $R=0.1$. The fitting parameters, m and c an were obtained from a previous study by Manca et. al. [32] in which fatigue crack growth tests were conducted for the face-sheet/core interface of sandwich MMB test specimens with the same face-sheet and core materials as in this study. The Paris law parameters for the PU/core interface were determined in [27] for similar crack growth conditions and are given in Table 5.

Table 5. CSDE and Paris' law parameters for the two interfaces.

	Face/core interface	PU/core interface
H_{11}	$1.68\cdot10^{-2}\left(\frac{1}{MPa}\right)$	$2.79\cdot10^{-2}\left(\frac{1}{MPa}\right)$
H_{22}	$1.56\cdot10^{-2}\left(\frac{1}{MPa}\right)$	$2.19\cdot10^{-2}\left(\frac{1}{MPa}\right)$
ε	$-7.066\cdot10^{-2}$	$-4.56\cdot10^{-2}$
h	2 mm	2 mm
c	$1.3758\cdot10^{-14}$	$0.9278\cdot10^{-14}$
m	4.55	4.486

After the crack increment was determined, the crack front was propagated by an increment corresponding to one loading cycle. Then the model was re-meshed and the analysis was repeated to derive the new interface crack front shape. To avoid repeating the process for all the loading cycles of the fatigue experiments, the Cycle Jump Technique [13-15] was applied. The technique requires at least three consecutive iterations of single cycle crack propagation simulations in order to predict the crack length after a larger number of non-simulated loading cycles. For further details on the CJT and the application in connection with fatigue propagation of a debond in a sandwich panel, see [13-15]. The fatigue crack growth simulation procedure outlined above enabled the seamless FE simulation of the entire fatigue

experiments for both sandwich specimen types (i.e. with and without embedded peel stoppers).

4. Results

The crack propagation process inside the sandwich panel specimens was difficult to monitor and evaluate during the actual experiments. Since the crack propagated inside the panels no in-situ visual confirmation of the debond front location was possible. Moreover, the DIC analyses required significant computation time during and after the experiments, before they could be used to evaluate the debond front location. As a result the only indication of the crack location during testing was the actuator piston displacement output measured at the peak loads by the test machine, see Figure 7. This is possible since the specimens compliance is directly linked to the debond radius. The displacements were recorded by the machine by measuring the actuator piston displacement under the constant load amplitude. . In this study, though, the displacements are not used for compliance calculations, but rather to demonstrate and evaluate the effect of the peel stopper. After the experiments were conducted, DIC was performed using the recorded images to obtain the displacement field of the facesheet around the panel centre.

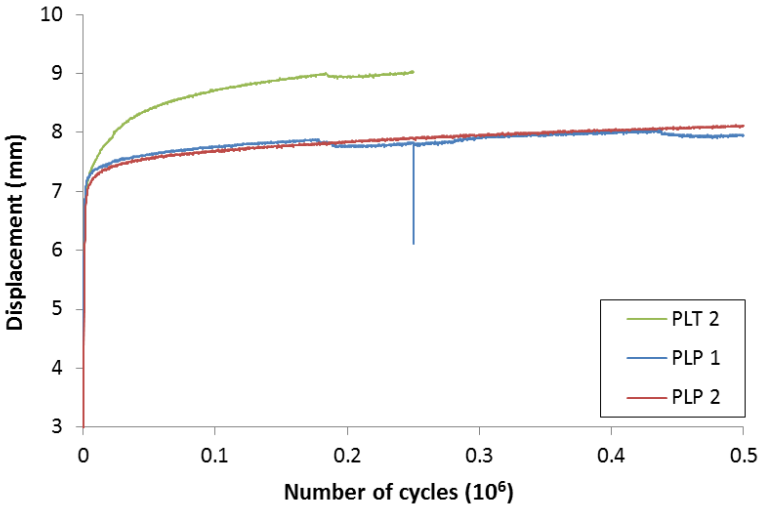

Figure 7. Measured piston displacement vs. number of cycles curves for the three fatigue tested sandwich specimens.

Figure 8 shows the vertical displacement field obtained from one of the tested panels (PLP1) containing a peel stopper next to the vertical displacement field obtained for the panel specimen without a peel stopper. The images correspond to the final stages of the two tests, i.e. 500,000 cycles for PLP1 (left), and 250,000 cycles for PLT2 (right). It is observed that the displacement field for specimen PLP1 with an

embedded peel stopper is concentrated in the centre of the panel. In contrast to this, the displacement field is more uniform over the entire observed area for specimen PLT2 (without a peel stopper) indicating a much larger debonded area, which again shows that the interface crack has propagated more extensively for the sandwich panel without a peel stopper. It should be further noted that for the panel with an embedded peel stopper (PLP1), the number of loading cycles were double that of the loading cycles observed for the panel without a peel stopper.

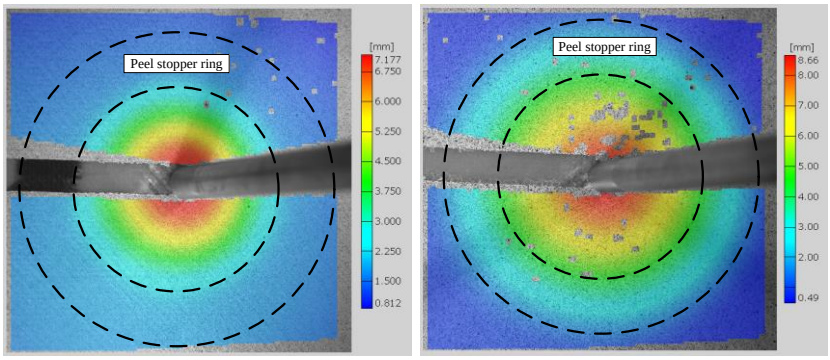

Figure 8. Sandwich panel specimens with (left – specimen PLP1) and without (right – specimen PLT2) embedded peel stoppers: DIC maps of vertical displacements at the end of the fatigue tests, corresponding to approx. 500,000 cycles for PLP1 (left) and approx. 250,000 cycles for PLT2 (right). The grey artifacts running horizontally through both images are the extension rod used for the application of the loading.

4.1. Tracking the crack

The post processed images from the digital cameras were used to extract the vertical displacement distribution along the axis of symmetry of the sandwich panel specimens. The displacement distributions were extracted from the DIC generated displacement data for all three sandwich panel specimens. These displacements were then used as input for a MatLab routine used for conducting numerical differentiation and smoothening to derive the first and second derivatives of the displacements along the x-symmetry axis (see Figure 1). The second derivative represents the curvature of the observed face-sheet. At the crack tip, an abrupt change of stiffness occurred due to the discontinuity caused by the debonded face-sheet. Since the face-sheet was responsible for carrying all of the transverse loading in the debonded area, a sudden increase of the curvature of the lower face-sheet was observed by DIC. Thus, it was hypothesized that the position of the crack tip corresponded to the local maximum of the second derivative of the displacement, as shown in, Figure 9. The vertical axes of the displacement and its two derivatives in Figure 9 have been “normalized” with respect to their peak value to demonstrate all three curves in one plot. Further, since the interface crack propagated axi-symmetrically away from the plate centre (see Figure 8), the crack front was traced

and positioned by using just one point along the symmetry axis (x axis – see Figure 1) of the panel.

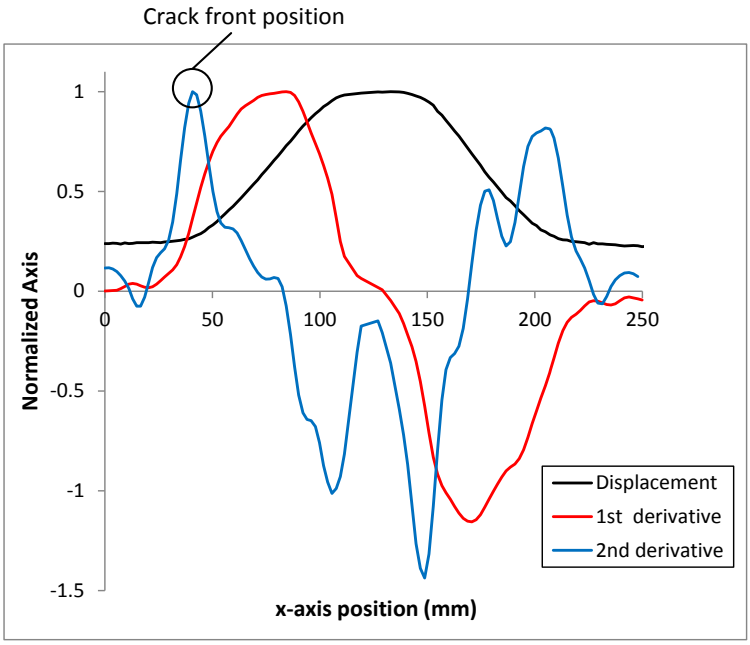

Figure 9. Normalised vertical displacement distribution for specimen PLP1 at 250,000 load cycles along the specimen x-axis (symmetry axis) derived from DIC, and the first and second derivatives of the displacement distribution.

The approach outlined above to track the crack front position is supported by the results of the FE analyses. Displacements from the nodes of the lower face-sheet were extracted from the FE model and used as input to the same MatLab algorithms. The algorithm was used to locate the crack tip, and this was then compared to the crack data input to the FE model. It was observed that the crack extension derived from the DIC data (Figure 9) consistently under-predicted the radial extension of the interface crack front by about 1-1.5 mm in comparison with the FE simulation results. The error could be partially due to the effect of the face-sheet thickness (2 mm) which was not taken into account in the MatLab algorithm. Since the differences observed between the FE simulated interface crack length and the experimentally derived results (shown in Figure 9) were consistent through all tests, the interface crack lengths derived using the DIC data were corrected by adding a 1 mm additional displacement (increase). The resulting "corrected" radial crack extension vs. number of loading cycles curve as obtained from the DIC calculated displacements is shown in Figure 10. An additional source of error could be the redirection of the crack front induced by the peel stopper. Therefore a loss of accuracy of the determination of the crack front position was therefore anticipated

for crack lengths larger than 80 mm for the sandwich panel specimens with embedded peel stoppers. The reason for this is that when crack deflection occurred at the peel stopper tip, the interface crack would propagate towards the inner part of the core, thus increasing the distance from the lower face-sheet.

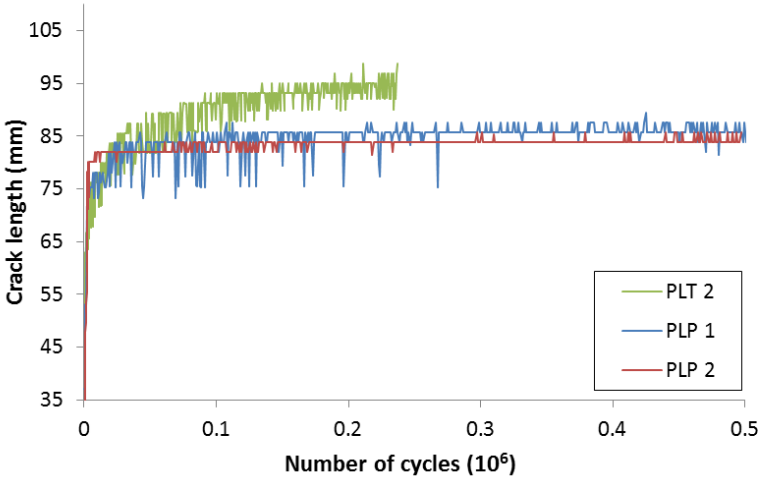

Figure 10. ”Corrected” interface crack length (radial direction) vs. number of load cycles.

4.2. Crack stopping effect

From Figures 7 and 10 it is observed that the interface crack growth was significantly influenced (delayed) by the presence of a peel stopper. To verify the experimental observations, the sandwich panel specimens were cut up after the tests to inspect the crack paths. Figure 11 shows two section cuts from specimens PLP2 (below - with peel stopper) and PLT2 (top - without peel stopper). The two cut sections are aligned so that the loading points of the two specimens are coinciding. For specimen PLT1 is observed that no crack deflection occurred, while it is observed that crack deflection occurred for specimen PLP2. The interface cracks in both specimens were measured and compared with the crack lengths extracted from the DIC data. For both cases the DIC measurements were very close to the crack lengths observed from the cut specimens. The crack in the panel without a peel stopper (PLT2) propagated up to about 100 mm during 250,000 loading cycles, thus exceeding the peel stopper boundaries (96 mm). For the panel with an embedded peel stopper (PLP2) the interface crack was measured to be about 87 mm long after a total of 500,000 loading cycles. Thus, it is concluded that the peel stoppers were successful in confining the propagating interface crack. From the post-mortem specimen images and crack lengths extracted from the DIC measurements it is observed that the interface crack propagation rate was slowed down considerably after crack deflection occurred for specimen PLP2.

Figure 11. Post mortem sections of sandwich panel specimens PLT2 (above – no peel stopper) and PLP2 (below - with embedded peel stopper).

In the next section the above observations will be further explained by examining the ERR and mode-mixity evolution at the crack tip after crack deflection occurred in the panels with embedded peel stoppers. Since the interface cracks did not reach the limits of the allowable growth area, i.e. peel stopper outer boundary, it was not possible to achieve complete crack arrest during the experiments. This suggests that the increase of the fatigue life of the sandwich panel with embedded peel stoppers is not fully demonstrated by the conducted experiments. Moreover, as described in previous research [27, 28], most of the load cycles endured while the crack is arrested occurs after the crack has reached the boundary of the area confined by the peel stopper

5. Numerical Simulation Results

The predicted loading point (vertical) displacement and the interface crack length evolution during the fatigue testing are shown in Figures 12 and 13 for sandwich panels with embedded peel stoppers and without peel stoppers. The crack length data are extracted from the FE model at the location of the crack front nodal points parallel to the x-axis (see Figure 1). The experimentally determined values are also shown in the figures. Figure 12 shows that the FE modelling was able to capture the initial steep rise in displacement as well as the plateau that was reached at the final stages of the fatigue experiment. In a similar manner it is observed from Figure 13 that the FE modelling accurately predicted the crack propagation rate during the entire fatigue experiment for the specimens with embedded peel stoppers. However, for the specimen without peel stoppers the FE model over-predicts the crack growth.

This can be attributed to the large geometrically non-linear effects that are not captured correctly at very large crack lengths (radial crack extensions). Despite the discrepancies found for the specimen without an embedded peel stopper, the results demonstrate that the developed 3D FE modelling approach was capable of accurately predicting the overall fatigue behaviour of the sandwich specimens with embedded peel stoppers.

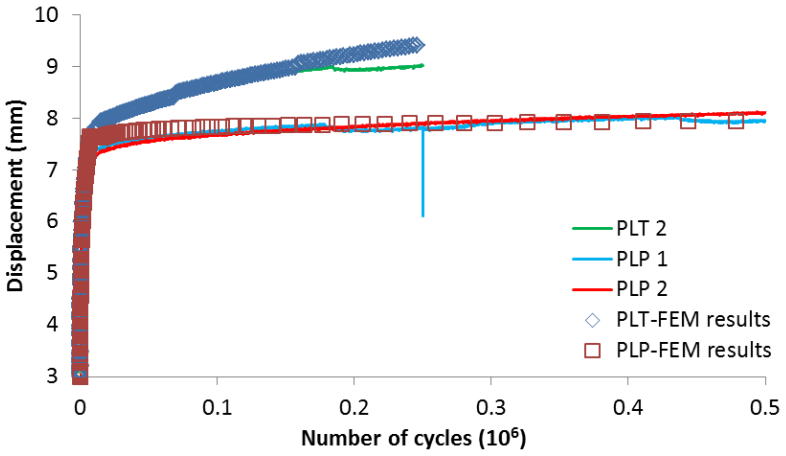

Figure 12. Central displacement for specimens PLP1, PLP2 (with embedded peel stoppers) and PLT2 (without peel stopper) vs. number of loading cycles; FE model predictions and experimental results (piston displacement of test machine).

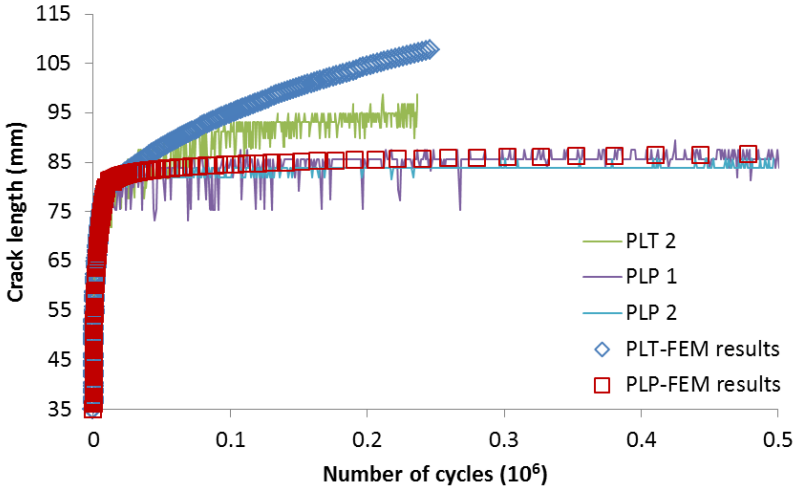

Figure 13. Interface crack length evolution vs. number of loading cycles; FE predictions and experimental results for specimens PLP1, PLP2 (with embedded peel stoppers) and PLT2 (without peel stopper).

The fatigue testing was limited to 500,000 loading cycles (for specimens PLP1 and PLP2 with embedded peel stoppers). To develop a further understanding of the effect and performance of the embedded peel stoppers, the FE simulation of the fatigue process together with the fatigue crack propagation algorithm has been used to extrapolate beyond 500,000 loading cycles. Figures 14 and 15 show the predicted ERR and mode-mixity against number of cycles and crack length, respectively. The fatigue experiments were simulated up to 2 million loading cycles, which is considered to be a realistic expected fatigue life for many foam cored composite sandwich structures.

From Figure 14 and 15 it is observed that the ERR drops significantly after the propagating interface crack has been deflected by the peel stopper, whereas the mode-mixity increases. Figure 14 shows that the ERR reaches a plateau which is associated with a drastic decrease in crack growth rate, when the propagating interface crack reaches the peel stopper (corresponding to approximately 25,000 cycles and a crack length of 80 mm). It is further seen that the mode-mixity increases continuously at a very low rate throughout the fatigue process. Figure 15 provides further information about the behaviour of the sandwich panel specimens in the earlier stages of the fatigue process. Thus, it is observed that the ERR is very high for small interface crack lengths, and that it decreases considerably as the crack propagates. This explains the very high propagation rate observed at the beginning of the fatigue process, as well as the crack arresting effect when the radial extension of the crack (the crack length) becomes larger. It is further observed that the mode-mixity increases slightly during crack propagation in the face-sheet/core interface, and that the mode-mixity increases significantly, when the interface crack deflects into the core at the peel stopper tip. This can be explained by the change in the angle of crack propagation, as the interface crack is forced to propagate at an angle of 10^{o} relative to the face-sheet. This increases the shear component (mode II) of the propagating crack front, since the crack naturally tends to propagate towards the lower face-sheet under such loading conditions.

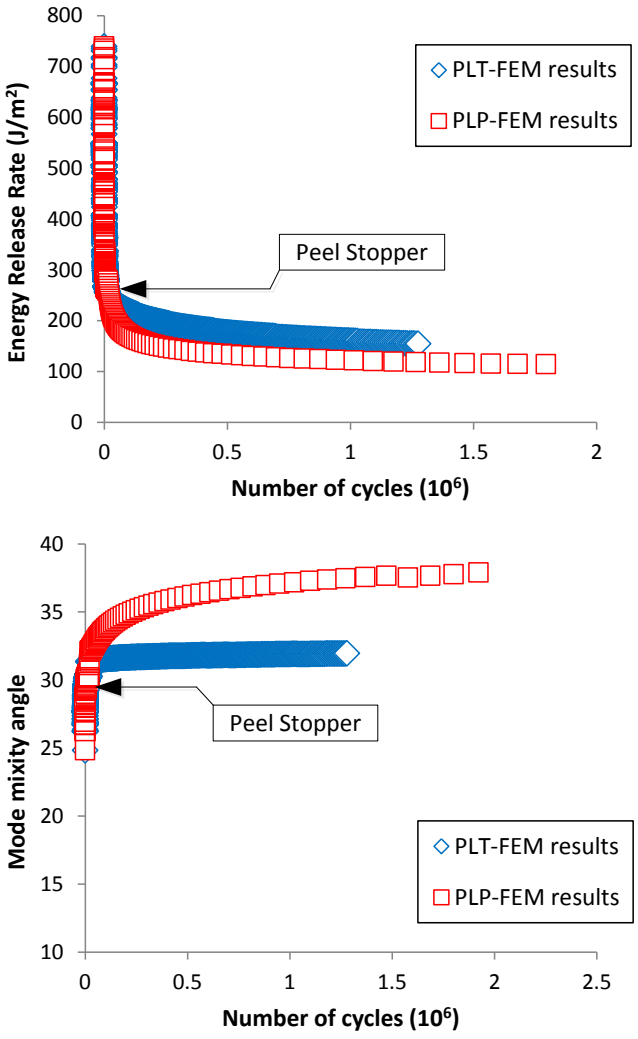

Figure 14. FE simulation of the fatigue process in the sandwich panel specimens with (PLP) and without peel stoppers (PLT): ERR and mode-mixity vs. number of loading cycles for up to 2×10^6 cycles

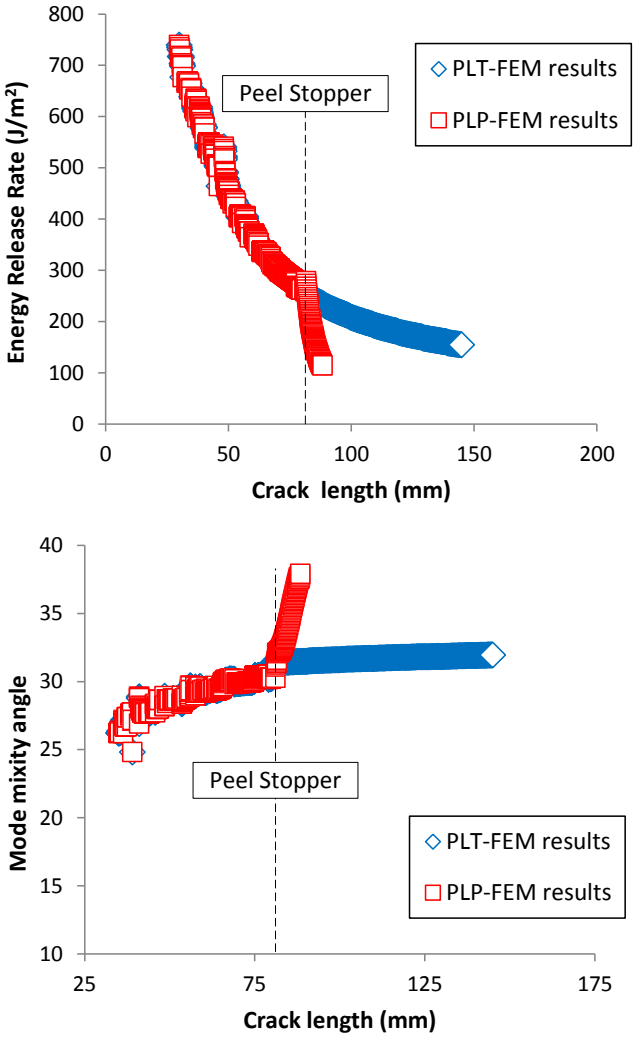

Figure 15. FE simulation of the fatigue process in the sandwich panel specimens with (PLP) and without peel stoppers (PLT): ERR and mode mixity vs. crack length.

From Figure 14 and 15 it is further seen that the crack growth conditions, imposed at the crack front after it has been deflected by the peel stopper, are such that the propagating crack is arrested inside the peel stopper. Moreover, the FE simulations predict that the propagating crack will not reach the physical boundary (radius of 98 mm) of the peel stopper even after 2 million cycles, Figure 15. Previous studies [27,28] have shown that most of the time (or loading cycles) to crack arrest is endured while the crack tip is located near the physical boundary of the peel stopper

(referred to as the arrest point). In the research conducted in [27, 28] concerning sandwich beams with embedded peel stoppers, it was observed that at this point the crack propagation stopped completely, and that a new crack was initiated on the opposite side (or behind) of the peel stopper. This behaviour (i.e. initiation of a new crack behind the peel stopper) was not observed in this study on sandwich panels (plate structures) with embedded peel stoppers, thus indicating that the potential advantage of peel stoppers (in terms of increased fatigue life and improved damage tolerance) is even higher for sandwich panels than for sandwich beams.

6. Discussion

Special crack stopping elements or devices, referred to as peel stoppers, have been introduced into composite face-sheet and foam cored sandwich panels that were tested under fatigue loading conditions. The main goal of the study was to demonstrate the feasibility and to quantify the effects on the fatigue life of such peel stoppers. The proposed peel stopper concept has previously been investigated and tested in foam cored sandwich beams, and it was shown that the fatigue life was improved considerably [27, 28].

The fatigue loading conditions were introduced into the sandwich panels through a central point force applied through a rigid insert. The loading and sandwich specimen layout were chosen and designed so as to propagate an initial face-sheet/core interface crack front away from the centre of a square sandwich panel and towards the panel edges. The damage evolution (interface crack propagation) was recorded using DIC on the loaded (and debonded) face-sheet, and the displacement of the loading point (assumed to be equal to the piston displacement of the test machine) was used to capture the evolution of the sandwich panel stiffness through the fatigue process.

The experimental results showed that for the sandwich panels with embedded peel stoppers the propagating face-sheet/core interface crack was deflected and re-directed into the core structure. As a result the propagating crack was decelerated considerably, and it was arrested completely inside the peel stopper. The testing of a foam cored sandwich panel without peel stoppers, and subjected to identical fatigue loading and boundary conditions, displayed a much faster interface crack growth and importantly no crack deflection occurred. The crack also slowed down and was arrested in the sandwich panel without an embedded peel stopper. This was anticipated as the crack tip stresses reduces with the radial distance from the load application point for the chosen panel test configuration. No quantitative criterion regarding the desired and/or expected performance of the sandwich panels with embedded peel stoppers was specified a priori. Because of this, and since the panel specimens were not completely delaminated after the fatigue testing, a quantitative analysis on the performance of the sandwich panels with embedded peel stoppers was not conducted. However, it is clear from the obtained results that the inclusion

of peel stoppers in foam cored sandwich panels significantly improves the resistance to interface crack propagation, and thereby also the damage tolerance.

To further substantiate and validate the findings of the conducted fatigue experiments, a numerical study was conducted to extract fatigue crack growth data for the face-sheet/core interface crack in the tested sandwich panel specimens. To achieve this, a finite element based analysis procedure was developed to simulate the complete fatigue process. The numerical predictions are in excellent agreement with the obtained experimental results when the crack radius extends within the peel stopper limits. For very large crack lengths outside of the peel stopper region the numerical and experimental observations begin to diverge considerably. Moreover, the numerical results explain the deceleration of crack growth when the propagating interface crack is deflected by the peel stopper. It is shown that the energy release rate (ERR) decreases considerably when the crack is deflected away from the face-sheet/core interface. The analysis results further show that the mode II component of the crack tip stress field increases significantly, especially when the crack reaches deep into the core structure following the peel stopper contour.

7. Conclusions

The proposed crack stopping device (or concept) has significant potential for practical use in critical load carrying sandwich structures, as it offers significant improvement of the damage tolerance. More specifically, the fatigue life of sandwich structures with embedded peel stoppers (as proposed) will be significantly improved, and the vision is that load carrying sandwich structures with embedded peel stoppers may be used in service even after face-sheet/core damage (debonds/delamination) has been detected inside. The proposed peel stopper concept enables the pre-specification of physical boundaries or borders through the embedding of a grid-work or system of peel stoppers, that will effectively confine debond/delamination damage to small pre-selected areas in the sandwich structural layout. Depending on the particular application and the desired limitations, internal interface damage propagation or global stiffness reduction could potentially be effectively controlled.

Acknowledgements

The work was sponsored by the Danish Council for Independent Research | Technology & Production Sciences (FTP) under the research grant “Enhanced Performance of Sandwich Structures by Improved Damage Tolerance" (SANTOL) (Grant 10082020). The Divinycell H100 material used in this study was provided for free by DIAB A/S. The work has been conducted in collaboration with and co-sponsored by the Technical University of Denmark, Aalborg University, Denmark, the University of Southampton, UK, Siemens Wind Power A/S, Denmark, and LM Wind Power Blades A/S, Denmark.

References

[1] Zenkert, D: An introduction to sandwich construction, London: Chameleon Press Ltd (1995)

[2] Shenoi, R.A, Groves, A, Rajapaske, Y.D.S.: Theory and Applications of Sandwich Structures, University of Southampton RGSE, ISBN-13: 978-0854328253 (2005)

[3] Erdogan, F.: Bonded dissimilar materials containing cracks parallel to the interface, *Engineering Fracture Mechanics*, 3:231-240 (1971)

[4] Dundurs, J.: Edge-bonded dissimilar orthogonal elastic wedges. J.Appl.Mech, 36:650-652 (1969)

[5] Hutchinson, J.W., Suo, Z.: Mixed Mode Cracking in Layered Materials, Advances in Applied Mechanics, 29:63-191 (1992)

[6] Suo, Z.: Singularities, interfaces and cracks in dissimilar media. Proc. R. Sot. Land, A427:331-358 (1990)

[7] He M., Hutchinson J.W.: Kinking of a Crack Out of an Interface. ASME. J. Appl. Mech. 56:270-278 (1989)

[8] Wang, T. C.: Kinking of an interface crack between two dissimilar anisotropic elastic solids. International Journal of Solids and Structures, 31:629–641 (1994)

[9] Krueger, R.: Virtual Crack Closure Technique: History, Approach and Applications," Applied Mechanics Reviews, 57:109-143 (2004)

[10] Jolma, P., Segercrantz, S., & Berggreen, C.: Ultimate Failure of Debond Damaged Sandwich Panels Loaded with Lateral Pressure: An Experimental and Fracture Mechanics Study. *Journal of Sandwich Structures and Materials*, *9*(2), 167-196 (2007)

[11] Berggreen, C. C., Simonsen, B. C., & Borum, K. K.: Experimental and Numerical Study of Interface Crack Propagation in Foam Cored Sandwich Beams. *Journal of Composite Materials*, *41*(4), 493-520 (2007)

[12] Bak, B. L. V., Turon, A., Lindgaard, E., Lund, E.: A simulation method for High-Cycle Fatigue-Driven delamination using a cohesive zone model. Int. J. Numer. Meth. Engng (2015)

[13] Moslemian, R., Karlsson, A. M., Berggreen, C.: Accelerated fatigue crack growth simulation in a bimaterial interface. International Journal of Fatigue, 33:1526–1532 (2011)

[14] Moslemian, R., Berggreen, C., & Karlsson, A. M.: Application of a Cycle Jump Technique for Acceleration of Fatigue Crack Growth Simulation. In *Proceedings — NAFEMS Nordic Seminar: Simulating Composite Materials and Structures, (2010)*

[15] Moslemian, R., Berggreen, C., Quispitupa, A., & Hayman, B.: Damage assessment of compression loaded debond damaged sandwich panels. In G. Ravichandran (Ed.), *ICSS 9* (2010)

[16] Rinker, M., Zahlen, P. C., John, M., Schäuble, R.: Investigation of sandwich crack stop elements under fatigue loading. Journal of Sandwich Structures and Materials, 14:55–73 (2012)

[17] Hirose, Y., Matsubara, G., Hojo, M., Matsuda, H., Inamura, F.: Evaluation of modified crack arrester by fracture toughness tests under mode I type and mode II type loading for foam core sandwich panel. In: Proc. US-Japan conference on composite materials 2008, Tokyo, Japan (2008)

[18] Hirose, Y., Matsuda, H., Matsubara, G., Hojo, M., Inamura, F.: Proposal of the concept of splice-type arrester for foam core sandwich panels. Composites Part A: Applied Science and Manufacturing, 43:1318–1325 (2012)

[19] Jakobsen, J., Bozhevolnaya, E., Thomsen, O.T.: New peel stopper concept for sandwich structures. Compos Sci Technol, 67:3378–85 (2007)

[20] Jakobsen, J., Andreasen, J.H., Bozhevolnaya, E.: Crack kinking of a delamination at an inclined core junction interface in a sandwich beam. Eng Fract Mech, 75(16):4759–73 (2008)

[21] Bozhevolnaya, E, Jakobsen, J & Thomsen, O.: Fatigue Performance of Sandwich Beams With Peel Stoppers, 45:349-357 (2009)

[22] Bozhevolnaya, E., Jakobsen. J., Thomsen, O.T.: Performance of sandwich panels with peel stoppers, strain. Int J Exp Mech, 45:349–57 (2009)

[23] Jakobsen, J., Thomsen, O.T., Andreasen, J.H., Bozhevolnaya, E.: Crack deflection analyses of different peel stopper design for sandwich structure. Compos SciTechnol, 69:870–5 (2009)

[24] Jakobsen, J, Andreasen JH, Thomsen OT.: Crack deflection by core junctions in sandwich structures. Eng Fract Mech 76(14):2135–47 (2009)

[25] Jakobsen, J., Johannes, M., Bozhevolnaya, E.: Failure prediction of in-plane loaded sandwich beams with core junctions. Composite Structures 82 (2), 194-200 (2008)

[26] Wang, W., Martakos, G., Dulieu-Barton, J. M., Andreasen, J. H., Thomsen, O. T.: Fracture behaviour at tri-material junctions of crack stoppers in sandwich structures. Composite Structures, 133, 818-833 (2015)

[27] Martakos, G., Andreasen J.H., Berggreen C., Thomsen O.T.: Experimental Investigation of Interfacial Crack Arrest in Sandwich Beams Subjected to Fatigue Loading using a Novel Crack Arresting Device. Submitted for publication.

[28] Martakos, G., Andreasen J.H., Berggreen C., Thomsen O.T.: Interfacial Crack Arrest in Sandwich Beams Subjected to Fatigue Loading using a

Novel Crack Arresting Device - Numerical modelling. Submitted for publication.

[29] DIAB. Divinycell H-Grade Technical data, Laholm (Sweeden), 2014. (http://www.diabgroup.com).

[30] ANSYS® Academic Research, Release 15.0

[31] Paris, P., Erdogan, F.: A critical analysis of crack propagation laws, J Basic Engng Trans ASME Ser D, 85:528–534 (1963)

[32] Manca, M., Berggreen, C., Carlsson, L. A.: G-control fatigue testing for cyclic crack propagation in composite structures. Engineering Fracture Mechanics (2015)

SUMMARY

The PhD thesis investigates the enhancement of the damage tolerance of sandwich structures by the embedding of a new type of core inserts that act as face/core interface crack stopping elements. The thesis presents series of experimental investigations where the new crack stopping elements are embedded in both sandwich beam and panel specimens. The experimental observations form the basis for evaluating the efficiency of the proposed crack stopping inserts. For the experiments, Digital Image Correlation (DIC) was used to characterize the measure the local strain fields and overall deformation behaviour around the new crack stopper elements. In support for the experimental investigations, a Finite Element (FE) analysis based methodology, including fracture mechanics analysis and the so-called 'cycle jump' technique, was developed to predict the progression of damage in sandwich specimens with embedded crack stoppers. The starting point for the research was is a new design for a crack stopper, referred to as a 'peel stopper', which is proposed for foam cored sandwich structures. Initially, the ability of the peel stopper to prolong the fatigue life of sandwich structures has been demonstrated through a series of three-point bending tests. During testing an initial crack front in the sandwich beams was arrested for a limited amount of cycles until a new crack initiated in the vicinity of the peel stopper. Subsequently, the study concentrated on investigating the main parameters that govern the performance of the proposed peel stopper, i.e. the crack deflection and crack arrest capability. The ability of the peel stopper to deflect a propagating face-sheet/core interface crack was investigated through a series of sandwich beam tests. Different configurations of the peel stopper were tested and the conditions for crack deflection for all configurations were identified by application of a fracture mechanics crack kinking criterion. From this research, the most promising peel stopper configurations were identified. Following this the crack arrest capacity of the peel stopper was investigated. Through the use of strain field measurements on the surface of sandwich beams with embedded peel stoppers using Digital Image Analysis (DIC), it was shown that the ability of the peel stopper to contain an arrested crack, or to prevent re-initiation of new cracks, is related to the inducement of strain concentrations in the foam core material on the back side of the peel stopper. By use of the developed numerical fracture mechanics based modelling tools, both fatigue crack growth and crack arrest in the specimens were simulated. It was shown that the strains responsible for crack re-initiation can be accurately calculated enabling the prediction of the fatigue life of the specimens. To demonstrate the beneficial overall effect on the damage tolerance of realistic sandwich structures, the peel stoppers were also embedded in sandwich plates (or panels). It was shown that peel stoppers in all cases were capable of effectively capturing and containing a propagating interface debond crack. The lateral displacements of the debonded face-sheet were measured using DIC and used to identify the crack tip location inside the sandwich panel specimens. To support and further explain the experimental findings, a three-dimensional FE model was developed and used to simulate the behaviour of the debonded sandwich panel specimens. The FE model was able to predict both the fatigue crack growth and crack arrest behaviour accurately. Due to time constraints, the sandwich panel fatigue experiments were only conducted up to about 200,000 load cycles, and to assess the effect of high cycle fatigue damage propagation was simulated up to about 2,000,000 load cycles. It was demonstrated that the developed computational methodology is capable of modelling the fatigue behaviour of sandwich structures with embedded peel stoppers, and that the overall enhancement of the damage tolerance can be predicted accurately.

ISSN (online): 2246-1248
ISBN (online): 978-87-7112-844-4

AALBORG **UNIVERSITETSFORLAG**